

# **EFFECT OF PARTICLE LOSS ON SOIL VOLUME, STRENGTH AND STIFFNESS**

By  
DARREN KELLY

June 2015

A thesis submitted in partial fulfilment of the requirements  
of Edinburgh Napier University, for the award of  
Doctor of Philosophy

## Abstract

Soil particle loss can occur through biodegradation, erosion and dissolution. Yet there is little understanding of the mechanical changes that accompany these phenomena, especially where the size of particle removed is concerned. This study investigated the influence of particle loss on the volumetric, strength and small-strain stiffness of analogue soils. These consisted of uniform Leighton Buzzard sand with selected salt particle sizes. Particle sizes chosen for experimental tests are representative of the fines that might be lost through an erosion process called suffusion in embankment dams or the various sizes that might be degraded and/or decomposed in landfill and mining wastes. A triaxial apparatus was modified to allow the in-situ dissolution of samples under triaxial stress states. This was achieved through the circulation of water through the pore-water pressure line with flow controlled by differential pressure using a peristaltic pump. Bender elements were installed to monitor changes in shear wave velocity before, during and after dissolution. Test results showed increases in void ratio in all dissolution tests. The influence of salt size and the stress under which tests were performed was found to have a limited impact on the magnitude of void ratio increase. Salt particle size did, however, affect the initial packing density of the sand-salt mixtures with fine salt sizes resulting in lower void ratios. Therefore, these tests showed lower post-dissolution void ratios. Coarse salt sizes initially densely prepared resulted in high post-dissolution void ratios close to the maximum void ratio for the Leighton Buzzard sand. Ultimately, post-dissolution void ratios determined the large-strain shearing behaviour. Therefore the fine salt tests, in which the post-dissolution void ratios were lowest, were the only tests to show minor peak strengths prior to the critical state with a shear behaviour described as strain-softening dilative. The comparatively high void ratios obtained in coarse salt tests showed no peak strength but a strain-hardening contractive behaviour. The structural role of salt particles within sand mixtures was continually assessed with evidence suggesting that salt particles maintained their structural integrity under the stresses applied through loading and subsequent shearing in this study. The influence of particle loss on the critical state was also probed. Post-dissolution samples consistently showed higher critical void ratios than sand-only samples not subjected to particle loss. Most of the findings might be explained in the context of strong force chains and their stability which is in turn influenced by the amount and size of soluble particles. Shear wave velocities were shown to decrease significantly with dissolution of 15% of weight of salt irrespective of size. Associated small-strain stiffness moduli were found to decrease even more substantially. The reported changes illustrate the significant influence that particle

removal has on the mechanical properties of soil and are discussed and analysed within this thesis.

## Acknowledgements

I would like to express my utmost gratitude to my supervisors Dr John McDougall and Dr Daniel Barreto for the assistance and support provided to enable the completion of this thesis. They have always made themselves available even while managing large workloads to offer encouragement and assistance. Professionally, I admire their dedication as teachers and researchers. Personally, I value their friendship and honesty. The financial support given by the School of Engineering and the Built Environment, Edinburgh Napier University made the fulfilment of this thesis possible.

My special thanks go to laboratory technician Mr. Willie Laing for his endless patience when assisting with the troubleshooting of the triaxial apparatus in the early stages, together with his continued support whenever it was requested throughout the duration of the experimental programme.

I would like to thank the Scottish Funding Council for the Post-Doctoral and Early-Career Researcher Award that allowed me to conduct a research trip to the University of Saskatchewan, Canada. Prof. Ian Fleming ensured that I experience the applications of our research at the industrial scale, together with all good things Canadian. Thanks also to Mr. David Parker who guided me around campus and Saskatoon during my stay.

Thanks to my parents for continually offering their help and encouragement. I was delighted to have them visit me in Edinburgh and their phone calls were very much appreciated.

Lastly, I am indebted to my partner, Megan, who has been the one to experience first hand the highs and lows of living with a student unable to disengage completely from his studies. She has often quelled my self-doubts and propelled me to the conclusion of this thesis. I think of her as my own personal teacher who helps me to see the things that really matter and I am truly privileged to have her in my company.

To my Parents and Megan.

# Contents

<b>Abstract</b>	<b>i</b>
<b>Acknowledgements</b>	<b>iii</b>
<b>1 Introduction</b>	<b>1</b>
1.1 Motivation . . . . .	1
1.2 Aim and objectives . . . . .	2
1.3 Layout of the thesis . . . . .	3
<b>2 Literature Review</b>	<b>5</b>
2.1 Traditional soil descriptors and their application to a soil experiencing particle loss . . . . .	5
2.1.1 Phase descriptors . . . . .	6
2.1.2 Intergranular void ratio and equivalent intergranular contact index . . . . .	7
2.1.3 Particle size distribution and shape parameters . . . . .	8
2.1.4 Particle packing of single sized spheres . . . . .	9
2.1.5 Particle packing in binary mixtures . . . . .	10
2.2 Decomposition-induced void change parameter . . . . .	12
2.3 The mechanical behaviour of sand . . . . .	14
2.3.1 Triaxial test stress states . . . . .	14
2.3.2 Compression . . . . .	14
2.3.3 Triaxial compression . . . . .	16

## CONTENTS

---

2.3.4	Triaxial compression of sand . . . . .	16
2.3.5	Stress paths in drained triaxial tests . . . . .	19
2.3.6	Critical state and critical state line . . . . .	22
2.3.7	Critical state line identification for sand at low stresses . . . . .	22
2.4	Particulate dissolution studies . . . . .	23
2.4.1	Dissolution of uncemented and cemented particulate materials . . . . .	24
2.4.2	Particle size relations in dissolution studies . . . . .	25
2.4.3	Sample strains with dissolution . . . . .	26
2.4.4	Void ratio change with dissolution . . . . .	28
2.4.5	Strength changes with particle loss . . . . .	37
2.4.6	Micromechanical insights using DEM . . . . .	42
2.4.7	Stiffness changes in dissolving soils . . . . .	49
2.5	Summary . . . . .	53
<b>3</b>	<b>Materials, Apparatus and Procedures</b>	<b>55</b>
3.1	Materials . . . . .	55
3.1.1	Selection of salt sizes and percentages . . . . .	56
3.1.2	Salt selection . . . . .	56
3.1.3	Salt crushing . . . . .	56
3.1.4	Salt sieving . . . . .	57
3.1.5	Sand preparation . . . . .	57
3.1.6	Sample density descriptors . . . . .	57
3.1.7	Mineral hardness . . . . .	58
3.1.8	Particle size distributions (PSDs) . . . . .	60
3.1.9	Sand and sand-salt mixture bulk moduli . . . . .	60
3.2	Triaxial apparatus . . . . .	64
3.2.1	Triaxial modifications overview . . . . .	64
3.2.2	Customised parts/modifications for sample preparation . . . . .	70

## CONTENTS

---

3.2.3	Triaxial test control and data acquisition . . . . .	71
3.2.4	Accuracy and resolution of transducers . . . . .	74
3.2.5	Equipment inventory . . . . .	74
3.3	Equipment development, commissioning and procedures . . . . .	75
3.3.1	Cell volume change (a) load ram displacement . . . . .	75
3.3.2	Cell volume change (b) distortion due to cell pressure . . . . .	76
3.3.3	Cell volume change (c) membrane penetration . . . . .	77
3.3.4	Difficulties encountered in commissioning . . . . .	81
3.3.5	Technical failures . . . . .	82
3.4	Triaxial test procedures including dissolution . . . . .	83
3.4.1	Cell preparation . . . . .	84
3.4.2	Sample preparation . . . . .	85
3.4.3	Cell pressure application . . . . .	87
3.4.4	Dissolution . . . . .	88
3.4.5	Post-dissolution shearing . . . . .	89
3.5	Sample volume measurement procedures and calculations . . . . .	89
3.5.1	Cell pressure application . . . . .	90
3.5.2	Dissolution . . . . .	94
3.5.3	Membrane penetration correction for dissolution stage . . . . .	94
3.5.4	Volume change comparison for each stage of dissolution tests . . . . .	97
3.5.5	Sample volume change prior to shearing - calculations example . . . . .	100
3.5.6	Post-dissolution shearing stage - stress-strain relations . . . . .	105
3.5.7	Membrane strength correction . . . . .	106
3.6	Bender element test procedures . . . . .	107
3.6.1	GDS BES Test Wizard . . . . .	107
3.6.2	Bender element test schedule . . . . .	108
3.7	Summary . . . . .	109



<b>4</b>	<b>Experimental results</b>	<b>110</b>
4.1	Test programme . . . . .	110
4.2	Dissolution strains . . . . .	111
4.3	Dissolution void ratio changes . . . . .	114
4.4	Dissolution induced lambda values . . . . .	116
4.5	Triaxial shear behaviour . . . . .	116
4.5.1	Sand only . . . . .	117
4.5.2	Sand-salt . . . . .	119
4.5.3	Post-dissolution . . . . .	121
4.6	Comparison of shear behaviours . . . . .	122
4.6.1	Sand vs. sand-salt . . . . .	122
4.6.2	Sand-salt vs. post-dissolution . . . . .	122
4.6.3	Sand-salt vs. post-dissolution shear behaviour with respect to salt size . . . . .	127
4.6.4	Sand vs. post-dissolution . . . . .	129
4.6.5	Effect of applied stress in shearing behaviour . . . . .	132
4.6.6	Shearing response of sand and sand-salt mixture with identical pre-shear void ratios . . . . .	132
4.7	Stress-ratio analysis of sand-salt and post-dissolution tests . . . . .	136
4.7.1	Maximum (peak) stress-ratio against pre-shear void ratio . . .	136
4.7.2	Peak stress-ratio shear strain . . . . .	139
4.7.3	End of shear stress-ratio with respect to salt particle size . . .	139
4.7.4	Volumetric shearing response of Leighton Buzzard sand . . . .	140
4.7.5	Influence of pre-shear void ratio on volumetric behaviour . . .	140
4.7.6	End of shear . . . . .	141
4.7.7	Stiffness evolution . . . . .	143
4.8	Chapter summary . . . . .	145

<b>5</b>	<b>Bender elements and waves</b>	<b>149</b>
5.1	Shear and pressure waves . . . . .	149
5.2	Bender elements . . . . .	150
5.3	Input wave - frequency . . . . .	150
5.3.1	Influence of input signal period on travel time determination . . . . .	151
5.4	Interpretation of wave travel time . . . . .	151
5.5	Near-field effect . . . . .	153
5.6	Time-domain method - shear wave arrival time determination . . . . .	154
5.6.1	First deflection . . . . .	154
5.6.2	First major peak-to-peak . . . . .	154
5.7	Frequency-domain method - shear wave travel time determination . . . . .	154
5.7.1	Cross-correlation . . . . .	154
5.8	Effective length of wave travel . . . . .	155
5.9	Degree of saturation effect on wave velocity . . . . .	156
5.10	State of stress . . . . .	156
5.11	Velocity-stress relations . . . . .	157
5.11.1	Interpretation of $\beta$ . . . . .	157
5.11.2	Interpretation of $\alpha$ . . . . .	157
5.12	Small-strain stiffness empirical relations . . . . .	158
5.12.1	Leighton Buzzard sand . . . . .	160
5.13	Summary . . . . .	161
<b>6</b>	<b>Shear wave and small-strain stiffness results</b>	<b>162</b>
6.1	Wave traces . . . . .	162
6.1.1	Wave traces - loading stage . . . . .	162
6.1.2	Wave traces - dissolution stage . . . . .	164
6.1.3	Wave traces - shearing stage . . . . .	164
6.2	Shear wave velocity with dissolution and shear . . . . .	164

## CONTENTS

---

6.3	Shear wave velocity with shear of Leighton Buzzard sand . . . . .	166
6.4	Velocity-stress relations in dissolution testing . . . . .	168
6.5	Velocity-stress relation comparison . . . . .	169
6.5.1	Sand tests . . . . .	170
6.5.2	Sand-salt tests . . . . .	171
6.6	Velocity-stress relations summary . . . . .	175
6.7	Velocity-stress relation constants . . . . .	176
6.8	Shear wave velocity versus void ratio in sand-salt mixtures . . . . .	178
6.8.1	Shear wave velocity versus void ratio - 42 kPa tests . . . . .	178
6.8.2	Shear wave velocity versus void ratio - 84 kPa tests . . . . .	180
6.8.3	Shear wave velocity versus void ratio - 168 kPa tests . . . . .	181
6.9	Small-strain stiffness . . . . .	181
6.10	Stiffness summary and comparison with the literature . . . . .	183
6.11	Chapter summary . . . . .	185
<b>7</b>	<b>Conclusions and recommendations for future work</b>	<b>187</b>
7.1	Conclusions . . . . .	187
7.1.1	From the literature . . . . .	187
7.1.2	Experimental tests and procedures . . . . .	189
7.1.3	Experimental results . . . . .	190
7.1.4	Bender elements . . . . .	193
7.1.5	Shear wave velocity results . . . . .	194
7.2	Recommendations for future work . . . . .	195
	<b>Appendices</b>	<b>197</b>
<b>A</b>	<b>Particle loss and volume change on dissolution: experimental re- sults and analysis of particle size and amount effects</b>	<b>198</b>
<b>B</b>	<b>Volumetric consequences of particle loss by grading entropy</b>	<b>208</b>

C Effect of particle loss on soil behaviour	214
References	223

# List of Tables

2.1	Relative density descriptors (Lambe & Whitman 1969) . . . . .	7
2.2	Key decomposition-induced $\Lambda$ parameter values (McDougall & Pyrah 2004) . . . . .	13
2.3	Shear wave velocity changes with dissolution (after Fam et al. (2002))	50
3.1	Mineral hardness values (Grabco et al. 2002, Gribble & McLean 2003, Vanders & Kerr 1967) . . . . .	58
3.2	Coefficients of curvature and uniformity of sand salt mixture PSDs .	62
3.3	Bulk moduli for 15% by weight of fine- and coarse-sized salt samples, and Leighton Buzzard sand for the applied pressure ranges . . . . .	63
3.4	Summary of capacity, accuracy, stability and resolution of transducers employed in the triaxial stress path cell . . . . .	74
3.5	Characteristics of sandy soils tested for membrane compliance amplitude (Nicholson et al. 1993) . . . . .	80
3.6	Grading characteristics of sand-salt mixtures . . . . .	80
3.7	Membrane penetration for sand-salt mixtures based on $D_{20}$ (Nicholson et al. (1993)) . . . . .	80
3.8	Void ratio change with cell pressure application based on bulk moduli values . . . . .	95
3.9	Membrane penetration by photographic method . . . . .	96
4.1	Triaxial test nomenclature . . . . .	112
4.2	Summary of void ratios and peak stress-ratios . . . . .	138
5.1	Pressure wave velocities and densities for solid and particulate salt and quartz . . . . .	157

5.2	Theoretical velocity-stress power-law $\beta$ exponents for solids and particulates . . . . .	158
6.1	Summary of velocity-stress relation constants . . . . .	178
6.2	Small-strain stiffness calculations for all triaxial tests . . . . .	182
6.3	Summary of shear wave velocity and void ratio changes with dissolution	184

# List of Figures

2.1	Theoretical packings of mono-sized spheres: (a) simple cubic, (b) single stagger, (c) double stagger, (d) face-centred cubic, and (e) rhombic. (Lade et al, 1998) . . . . .	9
2.2	Schematic diagram of theoretical variation of minimum void ratio in binary packings with percentage fines (Lade et al. 1998) . . . . .	11
2.3	Effect of percentage of fines and ratio of diameters of large and small spherical steel shot on minimum void ratios of binary mixtures (McGeary (1961); cited in Lade et al. (1998)) . . . . .	11
2.4	Minimum void ratios obtained for binary mixtures of steel shot plotted versus void ratio of large to small particle diameters (McGeary (1961); cited in Lade et al. (1998)) . . . . .	12
2.5	Phase diagram for decomposable soil, showing key phase changes and notation (McDougall & Pyrah 2004) . . . . .	13
2.6	Isotropic compression of Chattahoochee river sand (Vesic & Clough 1968) . . . . .	15
2.7	Triaxial shearing behaviour for drained tests on sand. Deviatoric stress and volumetric strain plotted against strain for (a) dense sand, (b) loose sand (Bishop & Henkel, 1962) . . . . .	17
2.8	Critical state identification using initially dense and loose samples (Roscoe et al. 1958) . . . . .	18
2.9	Idealised drained triaxial shear data (after Atkinson (2007)) . . . . .	19
2.10	Stress dependency of soil shear behaviour (Knappett & Craig 2012) . . . . .	20
2.11	Drained test paths in $q : p'$ and $v : p'$ space (Atkinson & Bransby 1978) . . . . .	21
2.12	Critical state line for Leighton Buzzard sand based on corrected data (Klotz & Coop 2002) . . . . .	23
2.13	Vertical strain with dissolution with (a) salt percentage by volume, and (b) vertical stress for 10% salt by volume tests . . . . .	27

2.14	Settlement strain with dissolution in oedometric tests varying with salt particle size and percentage (modified after McDougall et al. (2013))	29
2.15	Typical void ratio response to initial loading (pre-dissolution), dissolution and post-dissolution loading (after McDougall et al. (2013))	30
2.16	DEM simulation showing vertical strains at end of dissolution with respect to soluble volume fraction (Shin & Santamarina 2009)	31
2.17	Void ratio increase with dissolution for (a) 10% salt dissolution test performed at 160 kPa (b) 10% salt tests performed at various stresses, and (c) various salt percentages (Truong et al. 2010).	32
2.18	Void ratio versus soluble particle fraction pre-shear (post-dissolution) and post-shear (Tran et al. 2012)	33
2.19	Post-dissolution packing state and force chains simulated using DEM (Tran et al. 2012)	34
2.20	Vectorial depiction of void ratio increases due to dissolution of salt at various percentages and particle sizes. Tests performed under vertical stresses of 62 and 250 kPa (after McDougall et al. (2013))	36
2.21	Triaxial test shearing behaviour of post-dissolution sand-salt samples for (a) fine sand, and (b) coarse sand with salt percentages of 0, 2, 5, & 10 % (Fam et al. 2002)	38
2.22	Angle of shearing resistance against the state parameter for triaxial tests performed on post-dissolution coarse and fine sands (Fam et al. 2002)	39
2.23	Direct shear test results of post-dissolution samples varying with salt percentage under 100 kPa normal stress (Tran et al. 2012)	40
2.24	(a) Peak and critical shear strengths against soluble particle percentage removed through dissolution (b) Peak shear strength against pre-dissolution void ratio for confining stresses of 50, 100 & 150 kPa (Tran et al. 2012)	41
2.25	Triaxial shear behaviour of a specimen not subjected to erosion and three specimens for which erosion was performed under different stress conditions	43
2.26	DEM simulations of direct shear behaviour for post-dissolution samples varying with salt percentage in the shearbox apparatus under 100 kPa normal stress (Tran et al. 2012)	44
2.27	Polar distribution of contact normals	46
2.28	Polar distribution of normal contact forces	47



## LIST OF FIGURES

---

2.29	Polar distribution of shear contact forces . . . . .	48
2.30	Shear wave velocity-stress relations based on pre- and post-dissolution sand-salt mixtures using the resonant-column apparatus and bender elements (Fam et al. 2002) . . . . .	49
2.31	Pre- and post-dissolution velocity-stress relations for 10% by volume of salt in oedometer tests. Dissolution performed under 40, 80, 160 & 320 kPa (Truong et al. 2010) . . . . .	52
3.1	Leighton Buzzard sand-salt mixes showing relative sizes and shapes . . . . .	55
3.2	PSD of 1.0 mm salt for each increment of vertical stress in the oedometer . . . . .	59
3.3	PSD with load increments on Leighton Buzzard with 10% by weight of 1.0 mm salt, showing no crushing . . . . .	59
3.4	Particle size distributions for sand-salt mixtures with respect to salt percentage . . . . .	61
3.5	Secant bulk modulus for sand-salt mixtures . . . . .	63
3.6	Standard triaxial apparatus layout . . . . .	65
3.7	Modified triaxial apparatus schematic . . . . .	66
3.8	Modified triaxial apparatus layout . . . . .	67
3.9	GDS access ring . . . . .	68
3.10	Split-former seating ring in triaxial cell . . . . .	71
3.11	Modified split-former . . . . .	72
3.12	Drilled annular disc . . . . .	73
3.13	Ram volume calibration . . . . .	76
3.14	Cell volume change with pressure application . . . . .	77
3.15	Cell volume change with cell pressure cycling . . . . .	78
3.16	Axial force drift monitoring under two cell pressures . . . . .	83
3.17	Bulk moduli sample volume changes . . . . .	91
3.18	Triaxial volume change with pressure application in dummy sample tests . . . . .	92
3.19	Total measured volume change with pressure application . . . . .	93
3.20	Comparison of measured cell volume change against predicted cell volume change combined with bulk moduli for 3 sample types . . . . .	93

LIST OF FIGURES

---

3.21	Pre- and post-dissolution test performed with 0.063 mm salt @ 15% by mass confined at 168 kPa . . . . .	98
3.22	Pre- and post-dissolution test performed with 0.25 mm salt @ 15% by mass confined at 168 kPa . . . . .	98
3.23	Pre- and post-dissolution test performed with 0.5 mm salt @ 15% by mass confined at 168 kPa . . . . .	99
3.24	Pre- and post-dissolution test performed with 1.0 mm salt @ 20% by mass confined at 168 kPa . . . . .	99
3.25	Total volume changes and their constituents for compression, dissolution and shear stages of a typical triaxial dissolution test (Test no.7 0.5-15-42) . . . . .	101
3.26	Membrane strength correction . . . . .	106
4.1	Dissolution volumetric strain against salt particle size in triaxial tests	113
4.2	Dissolution vertical strain against salt particle size in oedometer tests (after McDougall et al. (2013)) . . . . .	114
4.4	Decomposition induced lambda parameter against salt particle size used in 15% salt by weight tests . . . . .	117
4.5	Shear behaviour of sand (a) $q/p'$ and $\varepsilon_{vol}$ , and (b) $e$ against $\varepsilon_s$ . . . . .	118
4.6	Shear behaviour of sand-salt (a) $q/p'$ and $\varepsilon_{vol}$ , and (b) $e$ against $\varepsilon_s$ . . . . .	120
4.7	Shear plane failure at 20% shear strain for (a) No. 26 (0.063 mm 15% 42 kPa) (b)No. 25 (0.063 mm 15% 168 kPa) . . . . .	121
4.8	Shear behaviour of post-dissolution tests (a) $q/p'$ and $\varepsilon_{vol}$ , and (b) $e$ against $\varepsilon_s$ . . . . .	123
4.9	Shear behaviour comparison of sand and sand-salt tests (a) $q/p'$ and $\varepsilon_{vol}$ , and (b) $e$ against $\varepsilon_s$ . . . . .	124
4.10	Shear behaviour comparison of sand-salt and post-dissolution tests (a) $q/p'$ and $\varepsilon_{vol}$ , and (b) $e$ against $\varepsilon_s$ . . . . .	126
4.11	Stress-ratio and volumetric strain against shear strain for sand-salt and post-dissolution tests (a) 0.063 mm (b) 0.25 mm (c) 0.5 mm and (d) 1.0 mm salt at 15% by weight tests . . . . .	130
4.12	Void ratio against shear strain for sand-salt and post-dissolution tests with (a) 0.063 mm (b) 0.25 mm (c) 0.5 mm and (d) 1.0 mm salt at 15% by weight . . . . .	131

LIST OF FIGURES

---

4.13 Shear behaviour comparison of sand-only and post-dissolution tests  
(a)  $q/p'$  and  $\varepsilon_{vol}$ , and (b)  $e$  against  $\varepsilon_s$  . . . . . 133

4.14 Void ratio against shear strain for sand-salt and post-dissolution tests  
for applied cell pressures of (a) 42 kPa, (b) 84 kPa, and (c) 168 kPa . 134

4.15 Shear behaviour for a sand and sand-salt test with identical pre-shear  
void ratios and gradings . . . . . 135

4.16 Maximum (peak) stress-ratio against pre-shear void ratio for sand-  
salt and post-dissolution tests . . . . . 137

4.17 Peak stress-ratios against (a) shear strain, and (b) void ratio at failure 139

4.18 End of shear (a) stress-ratio and (b) void ratio against salt particle size 140

4.19 Pre-shear void ratio against end of shear volumetric strain for sand  
tests . . . . . 141

4.20 Pre-shear void ratio against shear strain at dilation commencement  
in sand and post-dissolution tests . . . . . 142

4.21 End of shear/critical states for sand-salt tests . . . . . 142

4.22 End of shear/critical states for sand-only and post-dissolution tests  
tests . . . . . 143

4.23 Stiffness normalised by mean stress against shear strain . . . . . 144

4.24 Stiffness normalised by mean stress against shear strain in post-  
dissolution tests . . . . . 145

5.1 Influence of period input on travel-time based on points of similarity . 152

5.2 Small-strain stiffness based on the empirical formula by Hardin &  
Richart (1963) for  $e_{min}$  and  $e_{max}$  of Leighton Buzzard sand . . . . . 159

5.3 Small-strain stiffness based on empirical relations for Leighton Buz-  
zard sand by Bui (2009) . . . . . 160

6.1 Typical source and received pressure and shear waves during pre-  
dissolution cell pressure application . . . . . 163

6.2 Shear wave travel time during (a) dissolution and (b) shear . . . . . 165

6.3 Shear wave velocity with (a) time during dissolution and (b) axial  
strain during triaxial compression for 0.063 mm salt tests . . . . . 166

6.4 Shear wave velocity with (a) time during dissolution and (b) axial  
strain during triaxial compression for 0.25 mm salt tests . . . . . 167

6.5	Shear wave velocity with (a) time during dissolution and (b) axial strain during triaxial compression for 0.5 mm salt tests . . . . .	167
6.6	Shear wave velocity with (a) time during dissolution and (b) axial strain during triaxial compression for 1.0 mm salt tests . . . . .	168
6.7	Shear wave velocity during shear for dense Leighton Buzzard sand under confining stresses of 42, 84 and 168 kPa . . . . .	169
6.8	Shear wave velocity data and velocity-stress relation for Leighton Buzzard sand samples . . . . .	171
6.9	Shear wave velocity data and velocity-stress relation for 0.063 mm salt samples . . . . .	173
6.10	Shear wave velocity data and velocity-stress relation for 0.25 mm salt samples . . . . .	174
6.11	Shear wave velocity data and velocity-stress relation for 0.5 mm salt samples . . . . .	175
6.12	Shear wave velocity data and velocity-stress relation for 1.0 mm salt samples . . . . .	176
6.13	Summary of velocity-stress relations for pre- and post-dissolution tests	177
6.14	Shear wave velocity versus void ratio for confining pressures of 42, 84 & 168 kPa. . . . .	179
6.15	Shear wave velocity against void ratio for confining pressures of 42 kPa	180
6.16	Shear wave velocity against void ratio for confining pressures of 84 kPa	181
6.17	Shear wave velocity against void ratio for confining pressures of 168 kPa . . . . .	183
6.18	Small-strain stiffness for all tests . . . . .	185

# Chapter 1

## Introduction

### 1.1 Motivation

Processes that result in soil particle loss include biodegradation, erosion and dissolution. There follows a complex change in phase composition and grading. This in turn affects the mechanical properties resulting in damage to civil engineering infrastructure and loss of assets as highlighted by the following examples:

Landfill waste contains a biodegradable content that is lost due to microbial processes. Biodegradation occurs primarily through anaerobic digestion of the organic waste. Excessive settlement can result in landfill and mining waste containment capping barriers being breached resulting in the release of environmentally damaging contaminants such as leachate and landfill gas (Sharma & De 2007, Hester & Harrison 1995, Tchobanoglous et al. 1993).

Earthfill dams experience erosion through water seepage patterns and the consequent removal of fine material. Erosion has resulted in a loss of structural integrity in some cases (Muir Wood 2007). This can result in catastrophic failure with consequential loss of life and assets (Fell & Fry 2007, Kenney & Lau 1985). Similarly, piping erosion is a significant problem for rigid pavements. Removal of subgrade particles can produce failure/breakage of reinforced concrete slabs due to the loss of support (Menaar et al. 2009).

Sabkha soils are recognised for their high percentage of gypsiferous deposits which dissolve under the presence of water, producing settlements often with disastrous consequences on existing structures (Khan & Hasnain 1981). Mining waste often

contains a dissolvable fraction that is leached out of the waste with permeation of rainwater. At a larger scale, karst dissolution features can present subsidence issues and other significant problems to civil engineering infrastructure (Cooper 1998).

All these processes are the result of mass loss albeit by differing mechanical processes. The previous examples work to highlight the challenges faced by geotechnical engineers working in situations where soil particle loss impacts on design and remediation considerations.

### 1.2 Aim and objectives

The implications of inadequate knowledge on soil behaviour with particle loss can present dangerous situations. This study seeks to address the current lack of understanding of the factors controlling the volumetric, strength and stiffness changes that accompany particle loss.

Although dissolution tests focused on the amount of soluble material have been carried out previously, the role of particle size has received little attention. Hence, the volumetric and mechanical consequences of dissolution, taking particle size and amount of soluble material into account, are the subject of this research.

The objectives of this study were to:

1. Commission a new triaxial test configuration to allow dissolution tests to be performed under triaxial test conditions.
2. Produce an experimental database of triaxial dissolution tests.
3. Assess the changes in total volume and void ratio with dissolution of different salt particle sizes from Leighton buzzard sand in the triaxial apparatus.
4. Determine the influence of particle removal, specifically with respect to particle size, on the shearing behaviour of soil by contrasting intact sand-salt and post-dissolution sand-salt samples.
5. Examine if the critical states of the intact dry sand-salt, the pure sand, and the sand after salt has been removed by dissolution are the same.

6. Evaluate the structural role of salt particles in the sand, i.e. do they represent solids similar to sand particles, do they merely occupy void space between the sand particles, or do they have an intermediate role?
7. Assess how shear wave velocity is affected by particle removal and what can be learnt about the accompanying micro-mechanical changes.

### 1.3 Layout of the thesis

Chapter 1 provides an introduction to the subject of this thesis in the wider context of mass loss for biodegradation, erosion and dissolution. It also presents the aims and objectives while also describing the layout of all chapters in this document.

A literature review is presented in Chapter 2. Existing experimental and numerical research dealing with dissolving soils and its main findings are highlighted. This is preceded by a discussion of the validity of traditional phase relationships and soil descriptors to classify soils and to interpret changes induced by mass loss. Typical soil behaviour within the classical critical state soil mechanics framework is also described to provide a scope for comparison of the experimental findings in later chapters.

For the successful development of experimental tests involving dissolution a new tri-axial apparatus with several customised additions had to be commissioned. Chapter 3 describes the materials and the apparatus used, including planned changes, unexpected but required changes, as well as a detailed description of the technical failures and how they were dealt with. A description of the calculation procedures, particularly in relation to volume changes, is also presented in this chapter.

Chapter 4 interprets and describes the results of three different sets of triaxial tests including (i) sand, (ii) sand-salt mixtures, and (iii) post-dissolution (sand) samples. These three different tests are compared against each other in turn to provide further insight into the mechanical consequences of mass loss on the volumetric and stress-strain behaviour of dissolving soils. Analyses in the context of critical state soil mechanics as an attempt to interpret the experimental observations are also presented.

Since shear wave velocities were measured pre-, during and post-dissolution using bender elements, Chapter 5 presents existing research findings that help to interpret

and analyse these experimental measurements. Velocity-stress relations, void ratio functions and power functions that establish the likely limits of experimental findings are presented in Chapter 6.

Chapter 6 presents a detailed discussion of the shear wave velocities measured pre-, during and post-dissolution in dissolving soils subjected to triaxial stress states. Small-strain stiffness derived from the shear wave velocity and sample mass density are then presented.

Finally Chapter 7 presents a summary of conclusions and discusses recommendations for further research which can help to enhance our understanding of soil particle loss on the mechanical properties and engineering behaviour of granular materials.



# Chapter 2

## Literature Review

This chapter starts by introducing traditional phase relationships in soils while discussing their ability to describe mass loss. In this context existing proposals to characterise binary mixtures are presented. The decomposition-induced void change parameter  $\Lambda$  defined to describe complex phase changes in soils and to gain further insight on existing dissolution studies is presented to allow analyse of the experimental results. With the aim of presenting the experimental findings of this thesis in a general context, the typical stress-strain shear behaviour of coarse-grained materials is presented within the classical critical state soil mechanics framework. Finally, a selection of significant studies related to dissolution are critically reviewed; the influence of particle size and amount of soluble material on volumetric and stress-strain response of soils is discussed in detail, while some micro-mechanical studies and experimental observations on the small-strain behaviour of dissolving soils are also highlighted.

### **2.1 Traditional soil descriptors and their application to a soil experiencing particle loss**

This section sets out basic soil classifications that constitute the primary tools in analyses of the experimental tests performed as part of this research.

### 2.1.1 Phase descriptors

Soil is an assembly of particles with void spaces between particles containing fluids (usually liquid, gas, or a mixture of both). Phase relationships enable the proportions of solid, liquid and gas in a soil to be quantified. These proportions allow the definition of a number of descriptors such as porosity  $n$ , void ratio  $e$ , or specific volume  $v$ . These phase relation parameters can all be calculated provided the volume of voids  $V_v$  and volume of solids  $V_s$ , are known, e.g.

$$n = V_v/V_t \quad (2.1)$$

$$e = V_v/V_s \quad (2.2)$$

$$v = V_t/V_s = (V_s + V_v)/V_s = 1 + e \quad (2.3)$$

where  $V_t$  is the total volume of the soil ( $V_s$  and  $V_v$  combined). These volumetric parameters are indicators of the packing density of particles within the soil. Conventionally, bulk soil volume change is associated with void volume change only since soil particles and pore-water are regarded as incompressible in comparison with the soil skeleton. However, in soils that experience mass loss, the solid volume is also subject to change. In essence, any of these three volumetric phase relations can be adopted but void ratio is the most commonly used.

The relative density  $R_D$  indicates the current density of the soil relative to its minimum and maximum densities in terms of void ratio, where  $e_{min}$  and  $e_{max}$  are the minimum and maximum void ratios respectively:

$$R_D = [(e_{max} - e)/(e_{max} - e_{min})] 100 \quad (2.4)$$

Table 2.1 presents relative density ranges associated with various descriptors of soil density or packing as suggested by Lambe & Whitman (1969).

Table 2.1: Relative density descriptors (Lambe &amp; Whitman 1969)

Description	Relative density(%)
Very loose	0-15
Loose	15-35
Medium	35-65
Dense	65-85
Very dense	85-100

\* The limits of intervals are taken approximately

### 2.1.2 Intergranular void ratio and equivalent intergranular contact index

Alternatives to void ratio have been sought, especially in the description of coarse-grained soils with plastic or non-plastic fines since void ratio has been found to be inadequate as a state variable in soils of this nature. For example, Thevanayagam (1998) found that the undrained shear behaviour of sand with clay fines was better described by the intergranular void ratio. The percentage of fines by weight are discounted when calculating the intergranular void ratio. It assumes no structural participation (force/stress loading capacity) of fines within the soil as a first order approximation. However, Thevanayagam & Mohan (2000) found fines did participate even at low percentages. Ovando-Shelley & Perez (1997) also found that low fines content promoted the formation of looser structures due to the separation of the coarse-grain points of contact. To address this Thevanayagam & Mohan (2000) developed the equivalent intergranular contact index that takes account of the portion of fines engaging structurally with the coarse-grained matrix.

However, interpretation using intergranular void ratio and the equivalent intergranular contact index is only applicable to the mechanical behaviour of coarse-grained soil with fines. Furthermore, they are ‘static’ measures that do not consider ‘dynamic’ phase changes. This study focuses on the sample volume changes that accompany the removal of a range of particle sizes from coarse sand. Subsequently, it concerns the shearing behaviour of the remaining coarse-grained sand, meaning that the initial intergranular void ratio and the equivalent intergranular contact index are no longer applicable since only the coarse-grained sand particles remain. In this case the void ratio can be used. ‘Dynamic’ void ratio quantifiers are required to account for changes that accompany particle loss during the dissolution stage.

### 2.1.3 Particle size distribution and shape parameters

Particle size distributions (PSDs) are used to define the grading of a soil. Using the PSD curve, shape parameters such as the coefficient of uniformity  $C_u$  and the coefficient of curvature  $C_c$  can be obtained.

Muir Wood & Maeda (2008) considered a grading state index to account for changes to the critical state line with an evolving PSD. In this case grading changes were attributed to the erosion of particles or the effects of particle crushing. However, the index does not take account of the dynamic phase volume changes that might occur with particle loss processes.

Therefore, the diameter ratio defined by Lade et al. (1998) was used to describe the size relations of the sand/salt mixtures comprising single sized sand ( $D_{50} = 0.85$  mm) and single sized salt ( $D_{50} = 0.093, 0.375, 0.75$  or  $1.5$  mm) with  $D_{50}$  taken as the midpoint between the sieve mesh sizes that particles were retained on.

$$D_r = D_{50,sand}/D_{50,salt} \quad (2.5)$$

The sand/salt mixtures were effectively binary, i.e. comprised of two particle sizes.

In well-graded or gap-graded soil the opportunity exists for sufficiently small salt particles to occupy the interparticle voids of the larger sized sand. Provided the percentage of the small sized salt is low enough it is possible that they do not significantly disrupt the point-to-point contacts of the sand particles which constitute the coarse-grained skeleton. In a more uniform soil the sand and salt particles are closer in size and the same opportunity for the salt particles to occupy the interparticle voids of the sand particles without disruption does not exist. The salt might now assume a structural role in the soil. Particle size relations, such as  $D_r$ , therefore have implications for particulates, not only in terms of achievable packing density, as demonstrated by Lade et al. (1998) and McDougall et al. (2013), but in terms of understanding the structural role of the particles in a soil mixture. The  $D_r$  is used to describe these size relationships but is only used in the context of binary mixtures.

The diameter ratio is useful to dissolution studies in two ways. Firstly, it helps explain the initial packing densities achievable during sample preparation of the effectively binary sized sand and salt particulate mixtures. For example, a high diameter ratio indicates a soil that can be compacted to achieve a low initial void

ratio. As the diameter ratio decreases, the minimum achievable void ratio also increases. Secondly, it helps to explain the changes that occur with the removal of the salt fractions with dissolution. A high diameter ratio where the smaller salt particles can fit between the interparticle voids of the sand are unlikely to result in much rearrangement of the sand upon dissolution of the salt. A lower diameter ratio means that the salt is likely to actively participate in the load bearing soil skeleton resulting in the rearrangement of sand particles upon dissolution. Diameter ratios are thus useful in the discussion of volume changes accompanying dissolution of various salt particle sizes and amounts from uniform sand (see for example McDougall et al. (2013)).

#### 2.1.4 Particle packing of single sized spheres

Idealising granular materials as spheres has formed the basis for studies on void ratios. Using this method it was found that spherical grains of uniform size could be arranged in five idealised packings resulting in five different void ratios (Lade et al. 1998). Figure 2.1 illustrates the five grain configurations in order of decreasing void ratio. The simple cube configuration in Figure 2.1 (a) gave a  $e_{max}$  value of 0.90986 and was calculated using three-dimensional geometry (White & Walton (1937); cited in Lade et al. (1998)). The rhombic configuration in Figure 2.1(e) gave a  $e_{min}$  value of 0.35047. This theoretical framework gives an indication of the void ratios expected for loose and dense packing arrangements.

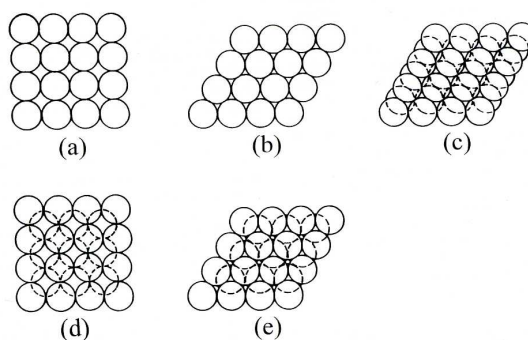


Figure 2.1: Theoretical packings of mono-sized spheres: (a) simple cubic, (b) single stagger, (c) double stagger, (d) face-centred cubic, and (e) rhombic. (Lade et al, 1998)

### 2.1.5 Particle packing in binary mixtures

Lade et al. (1998) considered the densities of binary mixtures of spherical particles in terms of void ratio. Figure 2.2 illustrates how the void ratio changes with percentage addition of fine particles. The sequence of void ratio change can be considered as follows:

1. At 100% large particles by volume, the soil has visibly large voids (Figure 2.2 point A).
2. As the fine particles are added to the soil, they begin to occupy the interparticle voids of the larger particles. This increases the soil density while decreasing the void ratio.
3. Fine particles are added to the soil until all interparticle voids of the large particles have been completely filled by the fine particles corresponding to the densest packing arrangement and therefore the lowest void ratio for the binary mix (Figure 2.2 point B).
4. If further additions of fine particles are made such that the large particles are no longer in contact, the void ratio now begins to increase again.
5. As the proportion of fine particles increases to 100% by volume, the highest theoretical void ratio occurs at point C.

McGeary (1961) performed tests on binary materials to achieve minimum void ratios through the addition of fines. Figure 2.3 shows experimental data obtained by McGeary (1961) for binary mixes with varying sizes of smaller particles and their associated minimum void ratios with percentage addition. The lines AB and BC show the minimum theoretical void ratios for each percentage addition fines as calculated by Lade et al. (1998). All experimental data by McGeary (1961) were found to be above these lines with deviation and related to the size increments of the added particles. The experimental results match Lade's hypothesis.

Figure 2.4 presents the minimum void ratios for each of the particle sizes found in Figure 2.3 where they are plotted against their respective diameter ratios. A change of behaviour is observed at a diameter ratio value  $\approx 7$ , the ratio marking the maximum diameter of a small nestling particle that can be accommodated without disruption of the large particle network.

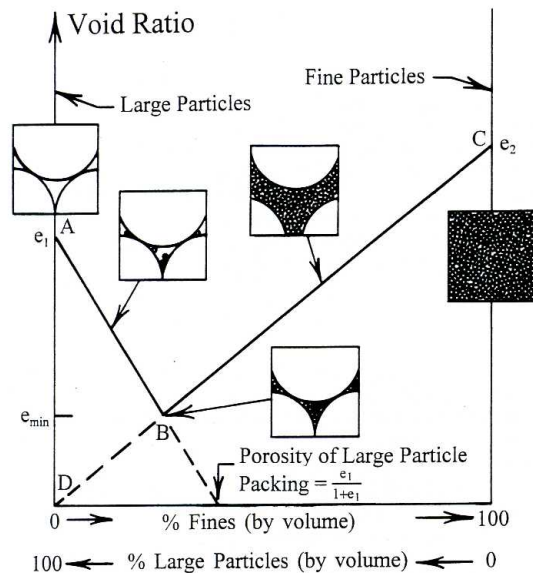


Figure 2.2: Schematic diagram of theoretical variation of minimum void ratio in binary packings with percentage fines (Lade et al. 1998)

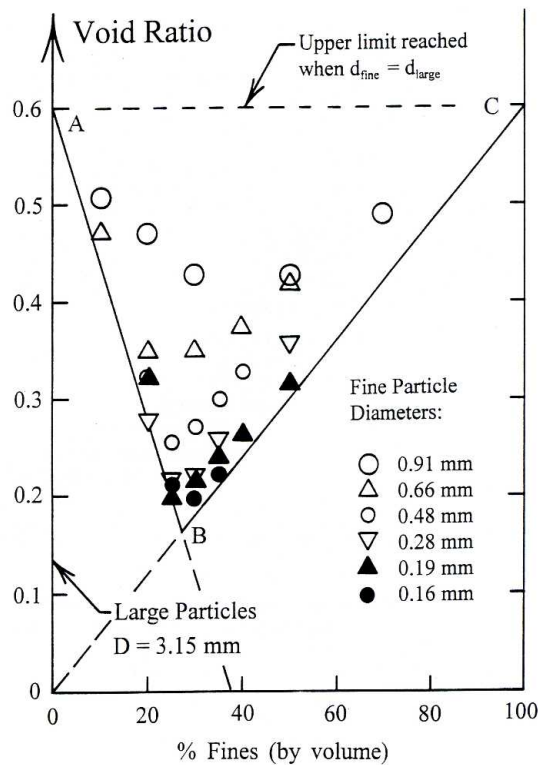


Figure 2.3: Effect of percentage of fines and ratio of diameters of large and small spherical steel shot on minimum void ratios of binary mixtures (McGeary (1961); cited in Lade et al. (1998))

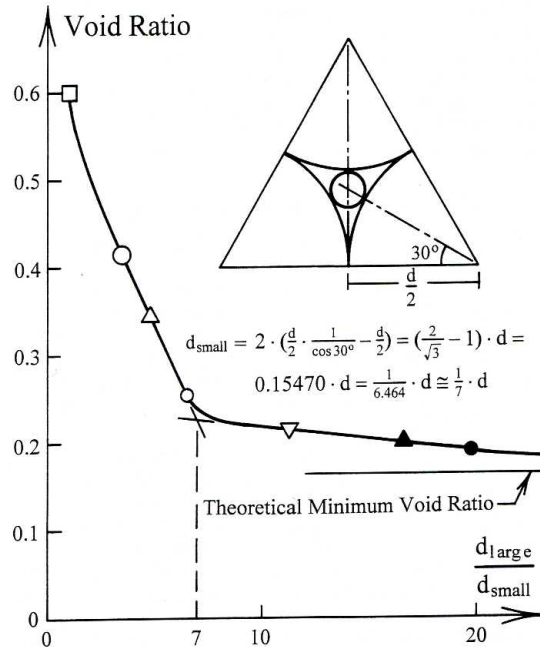


Figure 2.4: Minimum void ratios obtained for binary mixtures of steel shot plotted versus void ratio of large to small particle diameters (McGeary (1961); cited in Lade et al. (1998))

## 2.2 Decomposition-induced void change parameter

Changing phase relations of decomposable soils can be described using the decomposition induced void change parameter,  $\Lambda$ , proposed by McDougall & Pyrah (2004) that differentiates the inert and decomposable solid volumes (detailed in Figure 2.5):

$$\Lambda = \frac{dV_v}{dV_s} \quad (2.6)$$

Its prime role is to normalise the change in void volume for any given change in solid volume from which changes in void ratio can be deduced. Key values of  $\Lambda$  can be identified (and are summarised in Table 2.2). For example, a value of  $\Lambda = -1$  is indicative of a loss of the decomposable solid volume that does not contribute to total volume change because of an equivalent void phase volume increase. The resulting soil has become less dense while maintaining its original total volume, thereby resulting in maximum increases in void ratio.  $\Lambda = -1$  represents a limiting condition since the total volume of the soil cannot increase with decomposition.

The next landmark condition is represented by  $\Lambda = 0$ . Here, the loss of the decom-



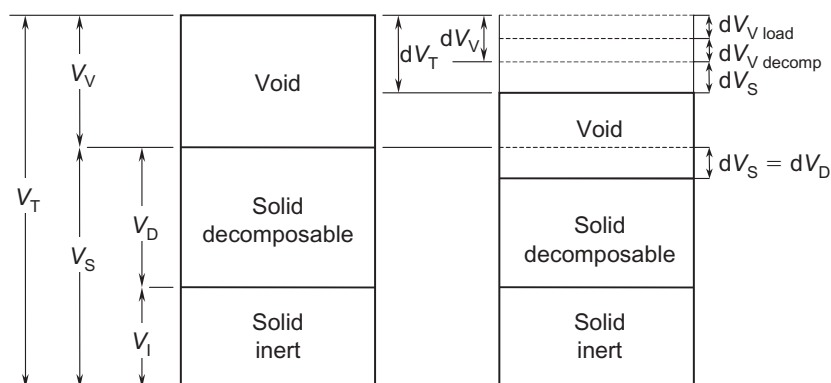


Figure 2.5: Phase diagram for decomposable soil, showing key phase changes and notation (McDougall & Pyrah 2004)

possible fraction contributes to the decrease in the total volume while the volume of voids remains constant. Since the volume of voids remains constant, and the volume of solids is decreasing with decomposition, the void ratio still increases but by a lower magnitude than when  $\Lambda = -1$ .

A value of  $\Lambda = e$ , indicates a switch from density decrease with decomposition to no density change at all; now the soil maintains a constant void ratio. In an inert soil this would indicate a mechanically stable soil. However large total volume decreases now accompany the decomposition described by  $\Lambda = e$ .

A value of  $\Lambda > e$  indicates densification of the soil. Void volume decrease has accompanied solid volume decrease and the total volume has decreased markedly. In an inert soil the resulting reduction in void ratio associated with this value of  $\Lambda$  would indicate a more mechanically stable soil.

Reference values of $d\Lambda$	Void inert ratio	Void ratio	Volumetric response
$d\Lambda \gg e$	Decreasing significantly	Decreasing	Collapse
$d\Lambda = e$	Decreasing	Constant	Contemporaneous rearrangement
$d\Lambda = 0$	Constant	Increasing	Pure void enlargement
$d\Lambda = -1$	Increasing	Increasing significantly	

Table 2.2: Key decomposition-induced  $\Lambda$  parameter values (McDougall & Pyrah 2004)

## 2.3 The mechanical behaviour of sand

The mechanical behaviour of sand and triaxial test variants are described in most standard soil mechanics textbooks, i.e. Powrie (2014). The current study focused on drained triaxial tests and are discussed in the following sections.

### 2.3.1 Triaxial test stress states

This section describes common triaxial stress states and descriptors, together with the stress state imposed on drained triaxial samples during shear. The triaxial apparatus allows an element of soil to be subjected to shear stresses and allows the measurement of strength and volumetric responses. The element of soil is first subjected to isotropic stress before an axial load  $F_a$  is applied. The deviatoric stress  $q$  is:

$$q = \sigma'_1 - \sigma'_3 \quad (2.7)$$

where  $\sigma'_1$  is the effective major principal stress and  $\sigma'_3$  is the effective minor principal stress since the axial and radial stresses constitute the principal stresses. The effective intermediate principal stress  $\sigma'_2$  and effective minor principal stress  $\sigma'_3$  in the triaxial test are equal. Another three dimensional stress invariant used in the analysis of triaxial tests is the mean effective stress  $p'$  and is defined as:

$$p' = (\sigma'_1 + \sigma'_2 + \sigma'_3)/3 \quad (2.8)$$

### 2.3.2 Compression

While some compression occurs due to stress application in the initial isotropic loading of sand, typical compression and swelling models such as those used for clay do not apply at low stresses (Atkinson & Bransby 1978). If loaded slowly enough under drained conditions, a normally consolidated clay will compress along a virgin compression line in  $v : \ln p'$  space. There is no common compression line for sands at low stresses. This only occurs for sand at high stress levels and is dictated by particle crushing. However, the stress levels applied in the current research are much lower than those required for crushing.

The isotropic compression of Chattahoochee sand was studied by Vesic & Clough (1968) (Figure 2.6). The study demonstrated that the particle crushing stage on the limiting isotropic compression line ( $B_1$ ,  $B_2$ ) was not reached for the loose sample until the application of a mean effective stress of 3 MPa, while a substantially higher stress of 40 MPa was required for initially dense sand.<sup>1</sup> Similar behaviour might be expected for Leighton Buzzard and other quartzitic sands. This indicates that Leighton Buzzard sand, which is similar to Chattahoochee sand, is not subject to significant compression during the application of isotropic stress.

An interesting feature of dissolution tests performed at constant mean effective stress is the ability of the soil to move up vertically in  $v : p'$  space due to void ratio increases as evidenced in studies by Fam et al. (2002), Shin & Santamarina (2009), Truong et al. (2010), McDougall et al. (2013), Kelly et al. (2012) (see Figures 2.15 and 2.17 presented later). This process can potentially leave the soil in a loose state.

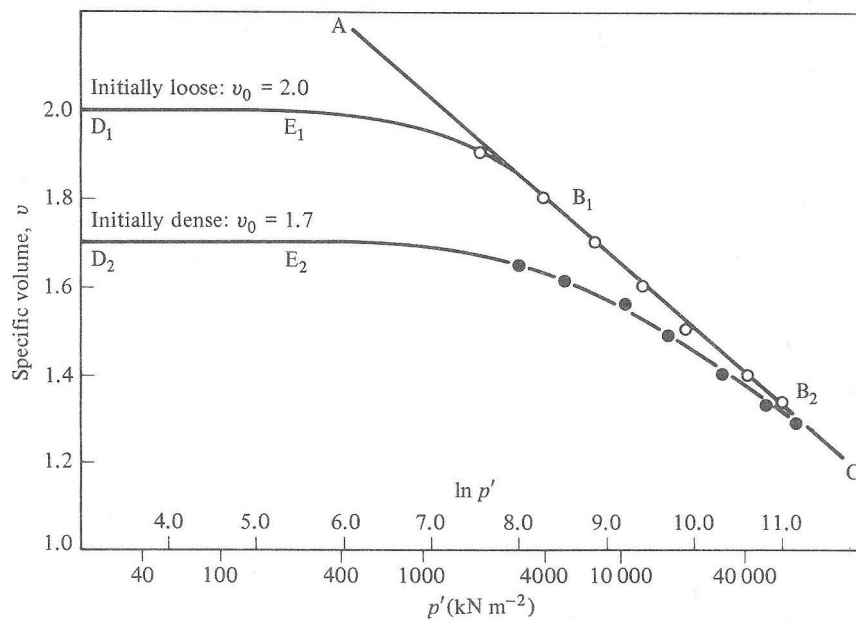


Figure 2.6: Isotropic compression of Chattahoochee river sand (Vesic & Clough 1968)

<sup>1</sup>The limiting isotropic compression line was named by Russell & Khalili (2004) in the context of sand compression in  $v : \ln p'$  space.

### 2.3.3 Triaxial compression

According to classical critical state soil mechanics, initially loose granular materials will contract during shear and will also experience a lower mobilised shear strength than dense granular materials. In contrast, dense soils may initially contract but then dilate. In both dense and loose soils the volumetric changes will eventually cease. While dense materials are inherently stronger, they also present a strain-softening response in contrast to the strain-hardening response of loose soils. However, at the critical state, loose and dense sands share a common shear stress and void ratio thereby enabling the critical state line (CSL) to be identified.

### 2.3.4 Triaxial compression of sand

The following sections review typical sand shearing behaviour to provide a benchmark for comparison with intact (pre-dissolution) and dissolved (post-dissolution) sand-salt tests performed in the current study and presented later. Furthermore, the analytical framework outlined in the following sections is later used to assess the shearing behaviour of the pre- and post-dissolution sand-salt tests.

Typical drained triaxial test behaviours for dense and loose sand under equal applied stresses (205 kPa) were presented by Bishop & Henkel (1962) in  $q : \varepsilon_a$  and  $\varepsilon_v : \varepsilon_a$  space where  $\varepsilon_a$  and  $\varepsilon_v$  are axial and volumetric strains, respectively (Figure 2.7). The initial void ratios were 0.64 for the dense sample and 0.84 for the loose sample. Strength behaviour for the dense sample is characterised by a high initial stiffness leading to a peak (failure) at low axial strains. The strength then decreases as the sample strain-softens to a constant value. The associated volumetric behaviour shows a small initial compression prior to dilation in which the soil increases in volume to large strains. The characteristics of the strength and volume behaviour graphs are inextricably linked. The maximum rate of dilation always coincides with the peak in the strength plot. Indeed, the peak strength is dependent on dilation (Bolton 1986), which in turn is dependent on the initial volumetric condition of the soil (Casagrande 1936).

The strength behaviour of the loose sand has a lower initial stiffness and gradually approaches constant (critical) strength at large strains of approximately 20%, a behaviour known as strain-hardening. The asymptotic strength for loose and dense sand at large strains approaches a unique value: the critical strength. This is inde-

pendent of the initial void ratio but dependent on the frictional strength of the soil and the mean effective stress  $p'$ .

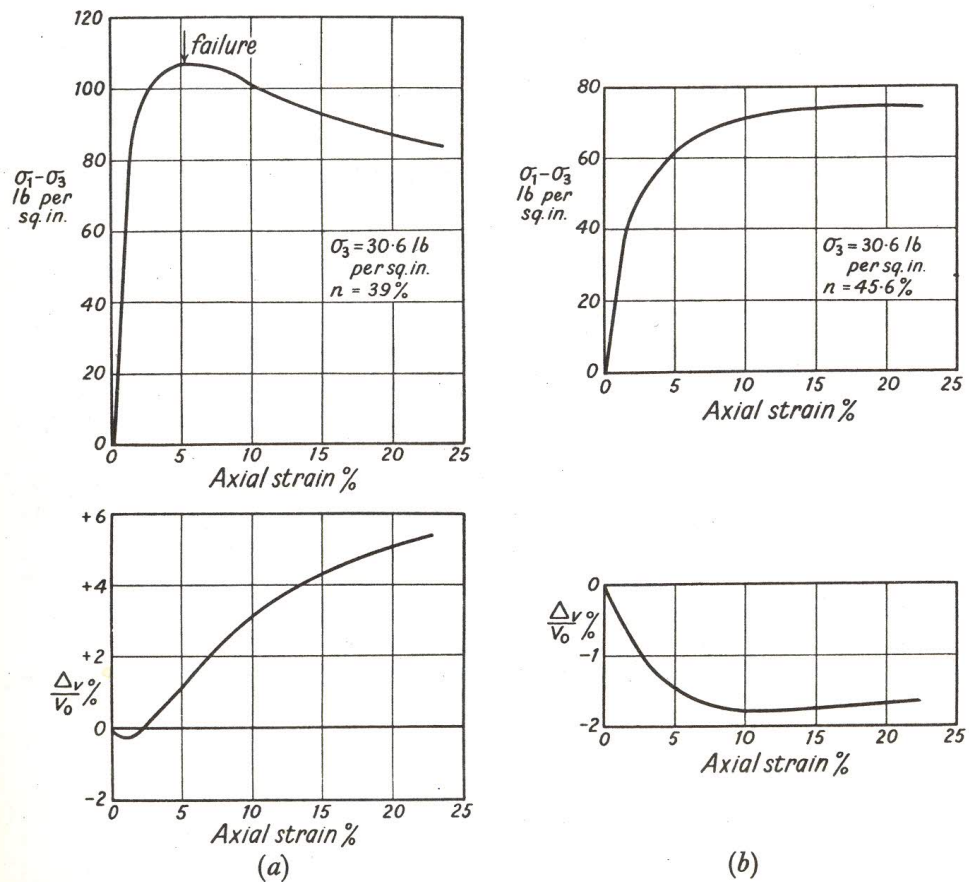


Figure 2.7: Triaxial shearing behaviour for drained tests on sand. Deviatoric stress and volumetric strain plotted against strain for (a) dense sand, (b) loose sand (Bishop & Henkel, 1962)

The associated volumetric strain is significantly different to that of the dense soil. The volumetric behaviour of the loose sand does not dilate. Instead the soil contracts until a constant volumetric strain with axial strain is reached. Another point is that the cumulative volumetric strain required for the sand to reach a constant value with axial strain is considerably less than that for a dense sample, in this case by approximately 4%. Furthermore the loose sample has reached the critical state condition at the end of the test, since the sample will continue to shear without further stress increments or volume changes. This is in contrast to the dense sample that has also been sheared to 22% axial strain but has not yet reached the critical state. Loose sand can reach the critical state within axial strains of 20% without experiencing the excessive volumetric strains that can lead to non-uniform deformations (Klotz & Coop 2002).

The difficulty with the application of large axial strains to triaxial samples are the induced non-uniform strains in the form of barrelling, as acknowledged by Klotz & Coop (2002), causing cross-sectional areas throughout the sample to vary and lead to errors in the calculation of stresses and volumetric strains. Atkinson & Bransby (1978) stated that because the sample usually lays on the dry side of the critical state line, that considerable sample deformations through dilation are required to arrive at the critical state. This resulted in the non-uniform stresses and strains in triaxial tests performed on Leighton Buzzard sand in the study by Klotz & Coop (2002). Therefore such large axial strains are deemed unreliable leading to difficulty in the identification of the critical state. This is illustrated by the stress paths in Figure 2.8 for initially loose and dense sands (Roscoe et al. 1958). The dense sample shows no prospect of reaching the critical void ratio line and will provide a false account of the critical state at the end of shear.

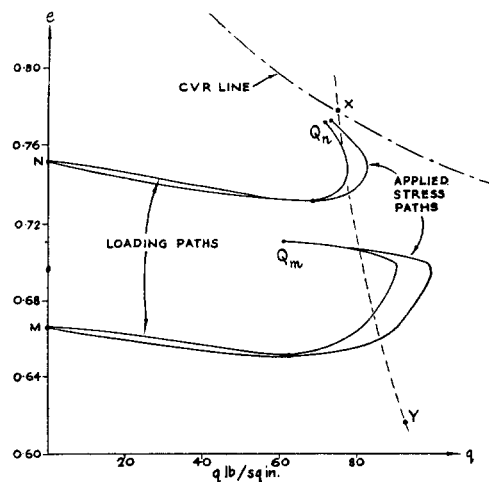


Figure 2.8: Critical state identification using initially dense and loose samples (Roscoe et al. 1958)

Idealised drained shearing behaviours are presented in Figure 2.9. This shows that at large strains both loose and dense soils converge towards critical state strength  $q_{crit}$  and the critical void ratio  $e_{crit}$ , respectively.

Applied stress has a significant influence on the strength and shearing characteristics of soil (Lee & Seed 1967). The critical strength increases proportionally to the mean applied stress as illustrated by the CSL in  $q : p'$  space in Figure 2.10c. Therefore tests performed at various applied stresses can be assessed using the stress ratio  $q/p'$  and analysed independently of confining pressures (Figure 2.10a). The idealised plots in  $q/p' : \varepsilon_s$  space show that for soils with initially identical void ratios a range of

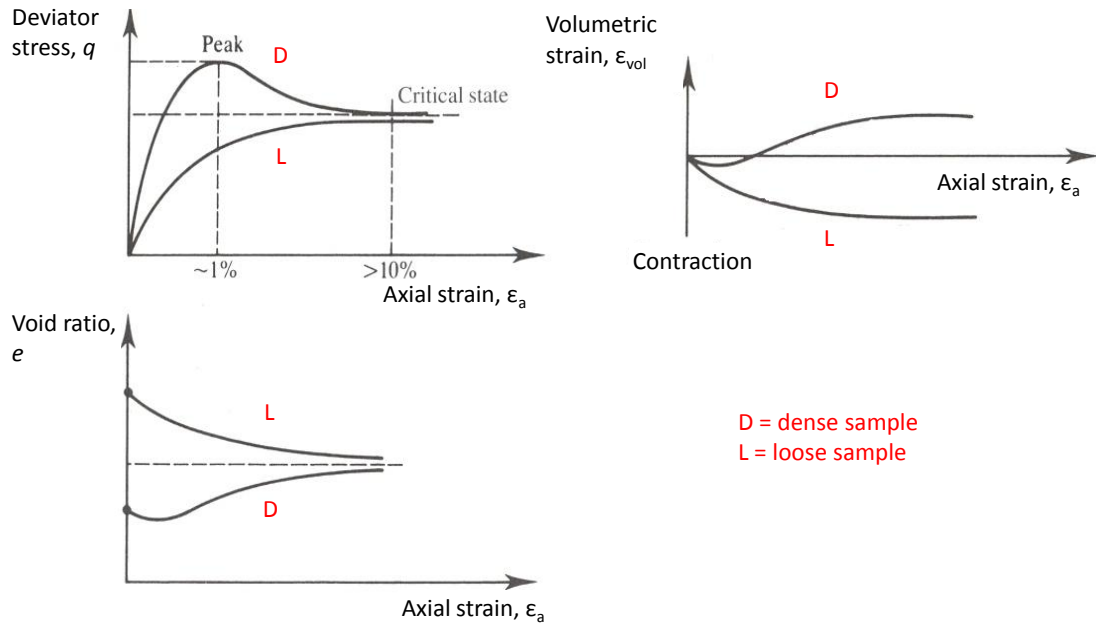


Figure 2.9: Idealised drained triaxial shear data (after Atkinson (2007))

stress-strain behaviours is possible. Increments in  $p'$  result in a change from strain-softening to strain-hardening behaviour. Hence, a sample with the same initial void ratio may illustrate dense behaviour at low stresses and loose behaviour at higher stresses. The level of dilation is suppressed as the applied mean effective stress increases as illustrated by the peak failure envelope in Figure 2.10c.

The volumetric behaviour is affected in a similar way (Figure 2.10b). The low stress test illustrates dilative behaviour but as the applied stress increases the behaviour becomes increasingly compressive.

### 2.3.5 Stress paths in drained triaxial tests

In addition to peak and critical stress states, the current stress state of soil in the triaxial can be described by stress paths in terms of deviatoric stress  $q$  and the mean effective stress  $p'$ . Figure 2.11a shows a typical stress path followed by a dense sample during drained shear in  $q : p'$  space. First the sample was isotropically compressed to 37 kPa. As the deviatoric stress is applied to the sample the stress path extends along a line at a gradient  $dq/dp' = 3$ . In a strain softening sample the peak (failure) is reached before returning along the line to the end of the test.

The path may also be tracked in  $v : p'$  space as shown in Figure 2.11b. The specific volume in  $v : p'$  must fall on the line projected from  $q : p'$  space as governed by the

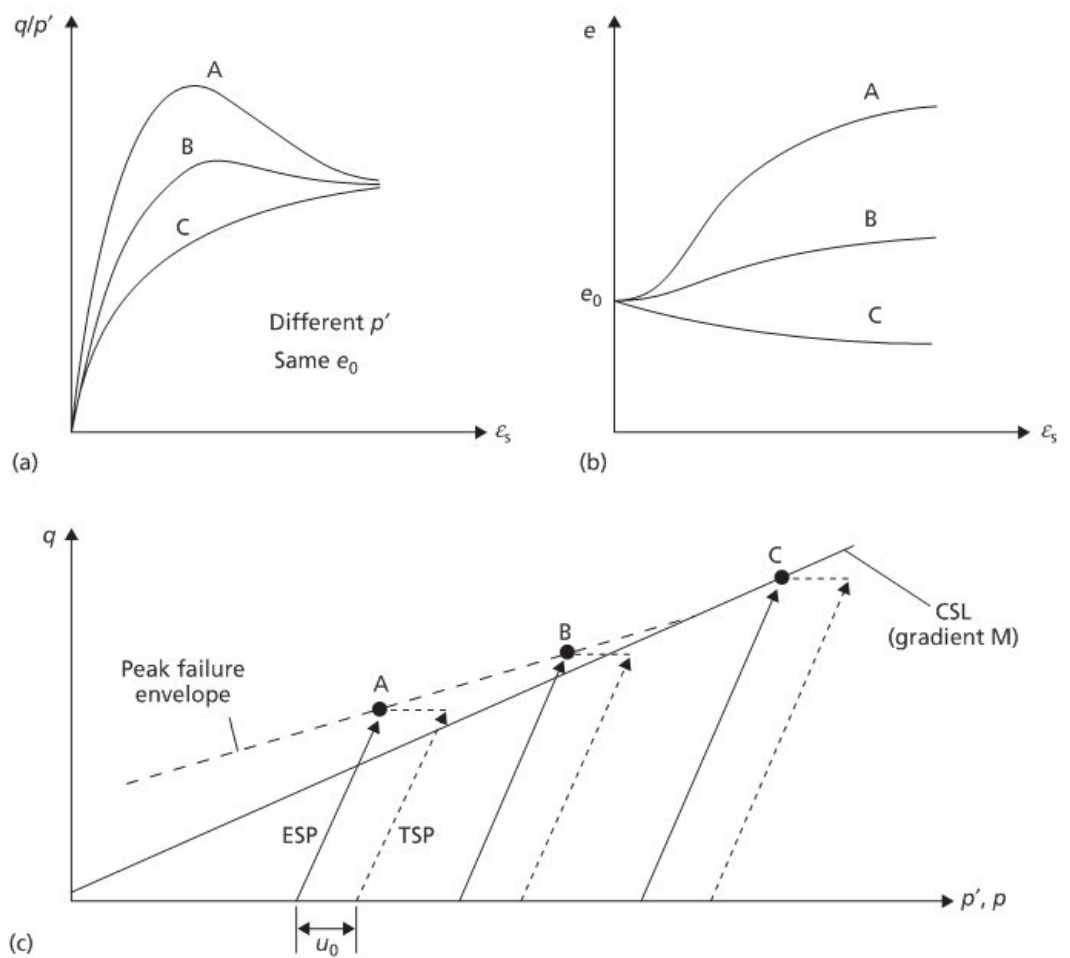


Figure 2.10: Stress dependency of soil shear behaviour (Knappett & Craig 2012)



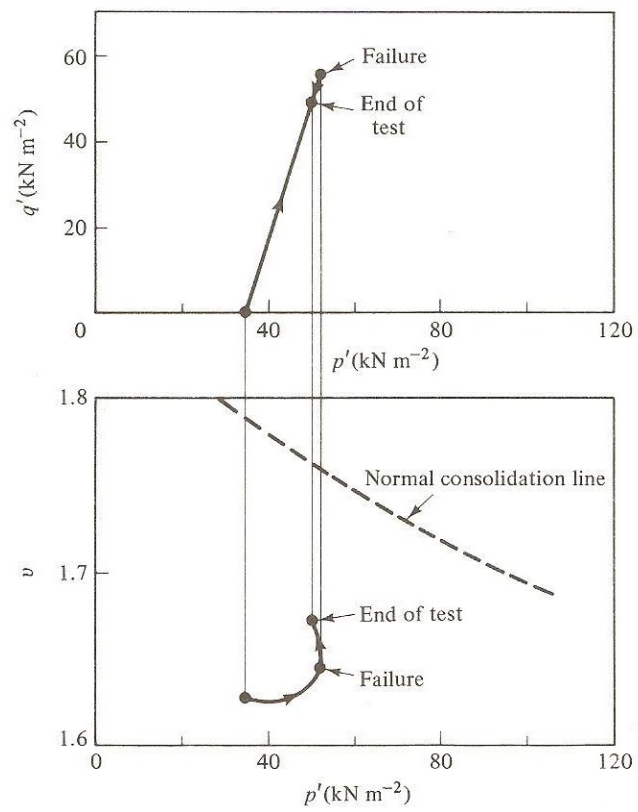


Figure 2.11: Drained test paths in  $q : p'$  and  $v : p'$  space (Atkinson & Bransby 1978)

common mean effective stress  $p'$ .

### 2.3.6 Critical state and critical state line

The critical state in shear tests occurs when soil continues to shear indefinitely without change in void ratio or shear stress (Roscoe et al. 1958). The critical state is unique to a given soil and is therefore independent of the initial density (Casagrande 1936) and is typically found through the application of large shear strains.

The critical state of a soil can be plotted in  $q : p'$  and  $v : p'$  space marking out the critical state line (CSL) in both planes. In  $q : p'$  space the CSL is described by:

$$q = M p' \quad (2.9)$$

where  $M$  is the gradient. The CSL is to the left and parallel to the NCL in  $v : p'$  space. It is described as follows:

$$v = \Gamma - \lambda \ln p' \quad (2.10)$$

where  $\Gamma$  is equal to the specific volume at a mean effective stress equal to 1 kPa and  $M$  and  $\Gamma$  are soil constants. Equations (2.9) and (2.10) therefore define the position of the CSL in  $q : p' : v$  three dimensional space.

### 2.3.7 Critical state line identification for sand at low stresses

Performing triaxial tests on sand, Verdugo & Ishihara (1996) and Klotz & Coop (2002) have found the CSL to be close to horizontal at low mean effective stresses before curving toward a straight CSL at high pressures in  $v : \ln p'$  space (e.g. see Figure 2.12).

Nevertheless, Klotz & Coop (2002) encountered difficulty identifying the near horizontal part of the CSL for Leighton Buzzard sand at low mean effective stresses. All test data showed dilation with no indication of cessation to large shear strains. Therefore, in  $v : \ln p'$  space the CSL always appeared to be approached from below. To overcome this Klotz & Coop (2002) applied corrections to the localised strain measurements meaning there was better convergence of end of shear data points and

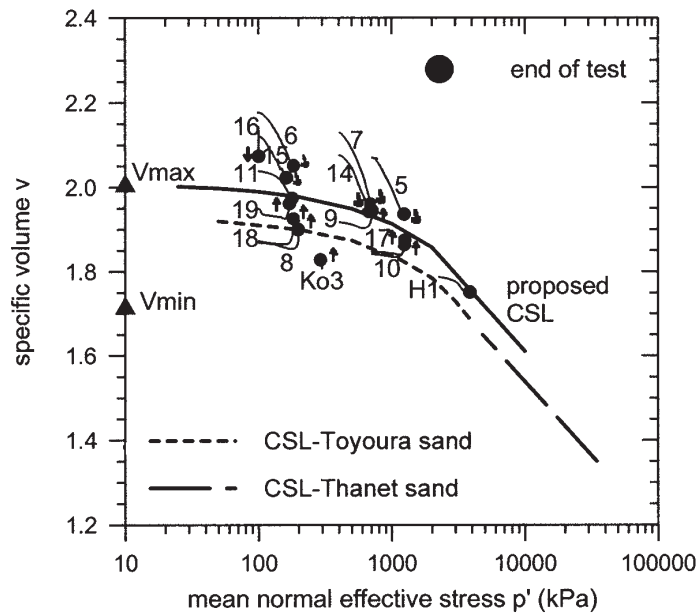


Figure 2.12: Critical state line for Leighton Buzzard sand based on corrected data (Klotz & Coop 2002)

a number of loose tests were portrayed as exhibiting contractive behaviour only. In this way the CSL was approached from above and below to give greater confidence in the positioning of the CSL. However, decisive positioning of the CSL was still not allowable and to further aid this the maximum achievable density at atmospheric pressure was taken as the start point of the CSL as suggested by Herle (1997) and an exponential function proposed in the hypo-plastic model of Gudehus (1996). The proposed CSL is presented in Figure 2.12. It is therefore evident that the identification of the critical state line in shearing tests performed on sand at low stresses is difficult even when using specialist measurement techniques. As the mean effective stress increases the CSL is more easily identified and curves until it forms a line parallel to the NCL in  $v : \ln p'$  space.

## 2.4 Particulate dissolution studies

Dissolving salt from coarse grained particulate (sand or glass beads) has recently received attention in order to reveal the volumetric and mechanical effects of particle loss (Fam et al. 2002, Shin & Santamarina 2009, Truong et al. 2010, Tran et al. 2012, Kelly et al. 2012, McDougall et al. 2013). Fam et al. (2002) were first to investigate the large- and small-strain properties of post-dissolution sand-salt mixtures using

triaxial, resonant column and bender element tests, while Truong et al. (2010) assessed the small-strain stiffness changes accompanying dissolution in an oedometer. Changes to the lateral earth pressure coefficient  $K_0$  with dissolution of salt from glass beads in a thin-walled oedometer were investigated by Shin & Santamarina (2009), while the mechanical strengths of post-dissolution sand-salt mixtures were tested by Tran et al. (2012) in the direct shear box. Then to assess the effect of particle size and percentage on the volumetric changes accompanying dissolution, McDougall et al. (2013) conducted numerous tests in a modified oedometer. Subsequently, and as part of the current study, Kelly et al. (2012) assessed the influence of salt particle size on the volumetric and small-strain stiffness changes with dissolution followed by the determination of the large strain response of the post-dissolution samples. The current study is an extension of the work presented by Kelly et al. (2012).

### **2.4.1 Dissolution of uncemented and cemented particulate materials**

Distinction needs to be made between studies concerning particulate dissolution within particulate mixtures and degradation of cemented bonds between particles. The response of cemented soil to dissolution is governed largely by the strength of the bonds.

Studying artificially cemented soils Castellanza & Nova (2004) showed the consequences of induced weathering in terms of axial strain and lateral stress changes in a thin-walled type oedometer. Lateral stresses were found to increase significantly, and with complete weathering resulted in earth pressure coefficients  $K_0$  of 0.45, resembling those expected for loose sand. The reported low initial  $K_0$  of 0.1 was a result of the cement bonds preventing vertical stress transfer to the lateral dimension. In contrast, Shin & Santamarina (2009) studied the  $K_0$  changes with dissolution of particulate mixtures consisting of glass beads and salt particles with no bonding. Typically, pre-dissolution  $K_0$  values were close to 0.6. During dissolution  $K_0$  dropped to a value close to 0.4 before recovering to its pre-dissolution value with dissolution complete. The current study focuses on un-bonded particulate soils experiencing particle loss.

### 2.4.2 Particle size relations in dissolution studies

Lade et al. (1998) demonstrated how particle size dictates the achievable packing densities in binary mixtures as discussed in Sections 2.1.4 & 2.1.5. An important aspect of the work performed by McDougall et al. (2013), Kelly et al. (2012) and in the present study is the attention given to the influence of the size of the dissolvable particles in terms of initial packing densities, and changes in total volume, void ratio, strength and small-strain stiffness with dissolution. The mixtures tested in all other dissolution studies consisted of a single sized inert fraction and a single sized dissolvable fraction at percentages by mass (or volume) ranging 0-15% (Fam et al. 2002, Shin & Santamarina 2009, Truong et al. 2010, Tran et al. 2012). The diameter ratios for the mixtures tested had a limited range of 1.0 - 2.3, effectively constituting uniformly graded mixtures. The only study where more than one combination of particle sizes was studied was by Fam et al. (2002) where uniformly graded coarse ( $D_{50} = 0.82$  mm) and fine ( $D_{50} = 0.55$  mm) sand formed the inert fractions with the dissolvable fraction consisting of single sized salt ( $D_{50} = 0.35$  mm). The coarse- and fine-sand mixtures had similar sand-salt diameter ratios of 2.34 and 1.57, respectively. Percentage salt additions of 0, 2, 5 and 10% by weight to coarse- and fine-sand, respectively, had a limited influence on the range of initial void ratios (0.63-0.65 for coarse-sand and 0.65-0.72 for fine-sand mixtures). This highlighted the limited influence of the diameter ratios on initial densities in the study, and the limited attention afforded to particle size in general.

Furthermore, Fam et al. (2002) did not attempt to assess the influence of particle size on the total volumetric changes with dissolution. Instead they stated that the salt particle size was chosen to minimise total volume changes and contribute to void volume increase only. They attempted to justify their selection by stating that smaller particles are subjected to smaller contact forces and therefore their removal through dissolution result in proportionately less total volume change. In dissolution tests performed in the triaxial apparatus, Fam et al. (2002) made the assumption that the dissolvable volume loss resulted in equivalent void volume increase by assuming that the total volume remained constant throughout (corresponding to the condition defined by a decomposition-induced parameter  $\Lambda$  value = -1 in Section 2.2 ). Applying this rationale, the influence of diameter ratios on settlement with dissolution was overlooked, and post-dissolution void ratios were not measured but calculated based on the volume of salt, more than likely resulting in errors. Similar diameter ratios of 1.1 and 2.3 for salt percentages of 10% by mass resulted in vertical settlements of 2.4-3.8% in oedometric tests performed by McDougall et al.

(2013), which meant that void ratio increase was not proportional to the volume of particulate lost as suggested by Fam et al. (2002).

McDougall et al. (2013) showed that the void ratio change was independent of the soluble particle size removed, and instead dependent on the percentage by weight removed. Therefore, since the fine-sized salt mixtures resulted in the lowest initial void ratios, the post-dissolution void ratios for the fine particles were also the lowest. In this way, soluble particle size can influence post-dissolution shearing behaviour since this is dependent on the void ratio (Roscoe et al. 1958, Lee & Seed 1967, Bolton 1986, Been et al. 1991). Furthermore, the small-strain stiffness is influenced by the void ratio (Hardin 1978).

### 2.4.3 Sample strains with dissolution

As discussed earlier, Fam et al. (2002) assumed that no sample strain would occur with dissolution in the triaxial specimens tested in their study, and that the volume of solids lost resulted in an equivalent volume of voids increase, corresponding to the condition defined by a decomposition-induced  $\Lambda$  value = -1. This assumption was convenient since the traditional method of measuring sample volume change in drained triaxial tests is through the pore-water line but this approach was not available since sand-salt mixtures were prepared dry and dissolution occurred during the saturation stage. Therefore the measurement of dissolution strains were not deemed necessary in their triaxial tests. In the resonant column apparatus only one dissolution test was performed on fine sand with 5% by weight of salt. However, for this test the axial strain with dissolution was measured but volumetric strain was calculated based on the assumption of isotropic deformation, which may not necessarily have been true. Additionally, one dissolution test was insufficient to learn much concerning the volumetric strains with dissolution. Fam et al. (2002) reported an axial strain of 0.05% with dissolution and used this to affirm their earlier assumption that salt dissolution had a negligible effect on total sample volume change. Based on this information it is reasonable to suggest that sample volume measurements were not sufficiently accurate to merit a study based on void ratios which were used in the analysis of post-dissolution large-strain and small-strain data.

Shin & Santamarina (2009) performed oedometer tests on glass beads ( $D_{50} = 0.7$  mm) and salt ( $D_{50} = 0.3$  mm;  $D_r = 2.3$ ) at percentages of 0, 5, 10, and 15% by volume. They demonstrated that inert-salt mixture diameter ratios approximately equal to those used by Fam et al. (2002) did result in significant vertical strains,

contradicting the  $\Lambda = -1$  conditions assumed by Fam et al. (2002). The relationship between the volume of salt lost and the vertical strain with dissolution in the study by Shin & Santamarina (2009) is presented in Figure 2.13a. These oedometer tests were performed under a single stress (37 kPa) and used a single salt particle size.

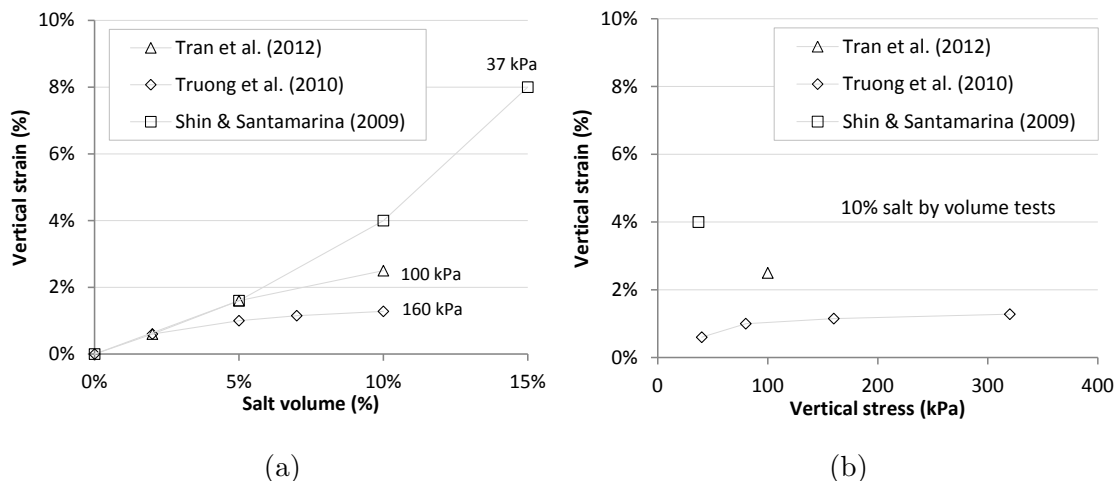


Figure 2.13: Vertical strain with dissolution with (a) salt percentage by volume, and (b) vertical stress for 10% salt by volume tests

The influence of salt percentage on vertical strain in sand-salt mixtures from studies by Tran et al. (2012) and Truong et al. (2010) are also presented in Figure 2.13a. The inert material used was medium angular Jumunjin sand, with sand/salt diameter ratios of 1.0 and 1.44 assessed in the respective studies. The vertical strains observed in these studies were considerably less than those found by Shin & Santamarina (2009) even though diameter ratios were lower. This may have been due to the interlocking ability of the medium angular sand used in contrast to the spherical glass beads used by Shin & Santamarina (2009). According to Figure 2.13a, the vertical stress appears to have an influence with higher stresses resulting in lower vertical strains. However, data by Truong et al. (2010) presented in 2.13b offers evidence to the contrary, with vertical strains increasing with vertical stress in identical mixtures. Additionally, no obvious relationship with respect to vertical stress for 10% by volume salt tests is apparent between the studies in Figure 2.13b.

Reported vertical strains with dissolution vary (Shin & Santamarina 2009, Truong et al. 2010, Tran et al. 2012) but they demonstrate that sample strains accompany dissolution, even for the diameter ratios and percentages tested by Fam et al. (2002) in the triaxial and resonant column apparatuses. This raises uncertainty in the assumption of zero strain with dissolution used by Fam et al. (2002).

McDougall et al. (2013) were first to assess the effect of particle size on dissolution strain. They presented the results of oedometric dissolution tests on sand-salt mixtures at 2, 5, 10 and 15% by weight of salt for particle sizes of 0.063, 0.125, 0.25, 0.5 and 1.0 mm. Diameter ratios were 0.6, 1.1, 2.3, 4.5 and 9.1. This range far exceeded that previously analysed in other dissolution studies (1.0 - 2.3). For samples prepared with equal compactive effort, it was found that the smallest particles (0.063 mm) resulted in the least settlement with dissolution for each percentage by weight tested. This was explained in terms of the ability of fine sized salt to exist in the interparticle voids of the coarse sand without interfering with the strong load bearing force chains. Hence, upon removal, there was minimal settlement. There followed a trend of increasing settlement with increasing salt particle size. Again, this was explained in terms of salt particle participation in the strong load bearing force chains. As the salt size increased, so too did its likelihood of participation in strong force chains since it could no longer simply exist in the sand voids but now began to perform a structural role within the soil. Therefore upon removal there followed disruption or rearrangement to the strong force chains resulting in buckling and collapse. This was translated as settlement at the macro scale. As the salt percentage increased, the influence of salt size was found to become less predictable (see Figure 2.14).

The data by Shin & Santamarina (2009) in Figure 2.14 is adjusted to take account of specific gravity values typical of glass beads ( $G_s = 2.48$ ) and salt ( $G_s = 2.16$ ). Dissolution test data from McDougall et al. (2013) and Shin & Santamarina (2009) show settlement strains less than that required to maintain a constant void ratio. In Figure 2.14 this condition is satisfied if dissolution strains for each salt percentage fall on the constant void ratio line (referred to as the ‘theoretical upper bound’ by Shin & Santamarina (2009)), marking the condition defined by  $\Lambda = e$  by McDougall & Pyrah (2004). This line demonstrates that dissolution always resulted in void ratio increase in the studies presented.

### 2.4.4 Void ratio change with dissolution

As shown in the previous section, dissolution tests result in a change in phase composition. This is a more complicated phenomenon than in inert soils because of the change in solid phase volume. It has consistently been shown that dissolution strains are not proportional to the percentage of material lost (Shin & Santamarina 2009, Fam et al. 2002, Truong et al. 2010, Tran et al. 2012, Kelly et al. 2012,



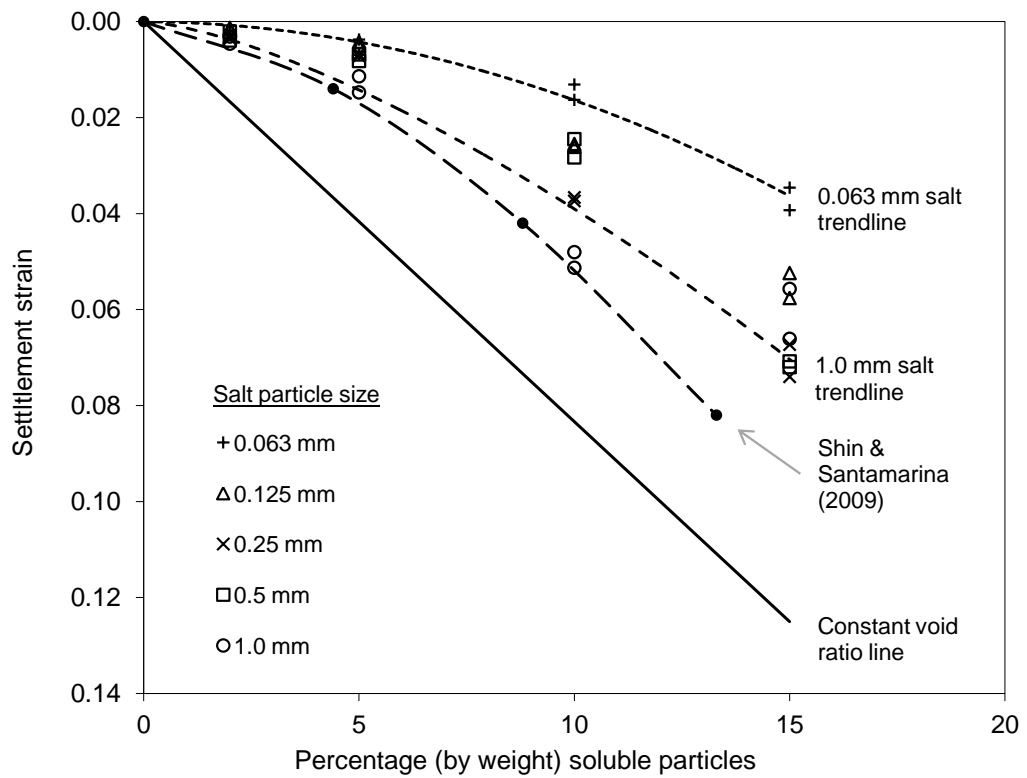


Figure 2.14: Settlement strain with dissolution in oedometric tests varying with salt particle size and percentage (after McDougall et al. (2013)). Data from dissolution tests by Shin & Santamarina (2009) included.

McDougall et al. 2013). Instead, dissolution results in a combination of settlement strain and phase composition change. Void ratio increase accompanied dissolution in each study.

A typical example of void ratio change for a dissolution test during initial loading, dissolution and post-dissolution is shown in Figure 2.15 (McDougall et al. 2013). Dissolution occurred at 62 kPa as indicated by the vertical step in void ratio. Subsequent loading did not result in soil collapse suggesting that the new looser soil sample was capable of supporting high vertical stresses.

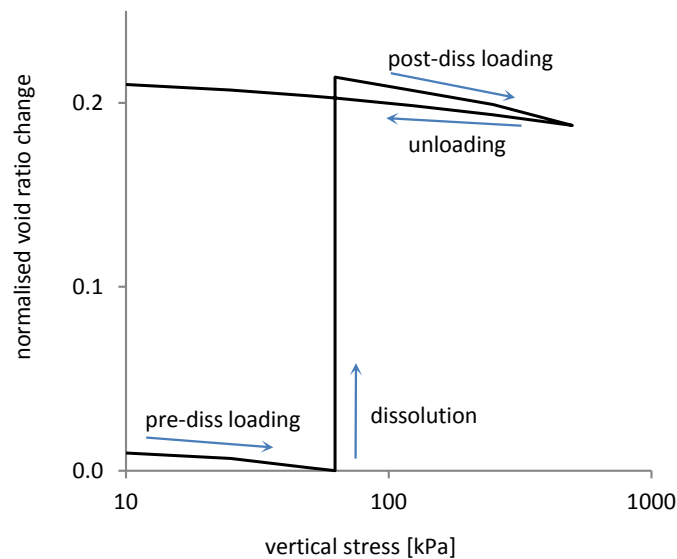


Figure 2.15: Typical void ratio response to initial loading (pre-dissolution), dissolution and post-dissolution loading (after McDougall et al. (2013))

Shin & Santamarina (2009) described the phenomenon in terms of load-bearing arches forming around the dissolving particles resulting in a honeycomb fabric, although this seems highly speculative and unqualified. They performed 2-dimensional DEM ‘dissolution’ simulations by gradually decreasing the soluble particle size. They suggested the presence of a terminal density for dissolvable volume fractions over 20%. This was defined as a condition in which further dissolution resulted in settlement only. It was assumed that this occurred when the maximum void ratio was achieved and any additional volume loss resulted in sample settlement. This is indicated in Figure 2.16 by a linear relationship between  $V_s/V_t$  and vertical strain at soluble volume percentages  $> 20\%$ .

Truong et al. (2010) also showed an increase in void ratio with dissolution in tests performed to assess the influence of salt percentage (0, 2, 5, 7 & 10% by volume) and applied stress (40, 80, 160 and 320 kPa). Figure 2.17a compares loading paths

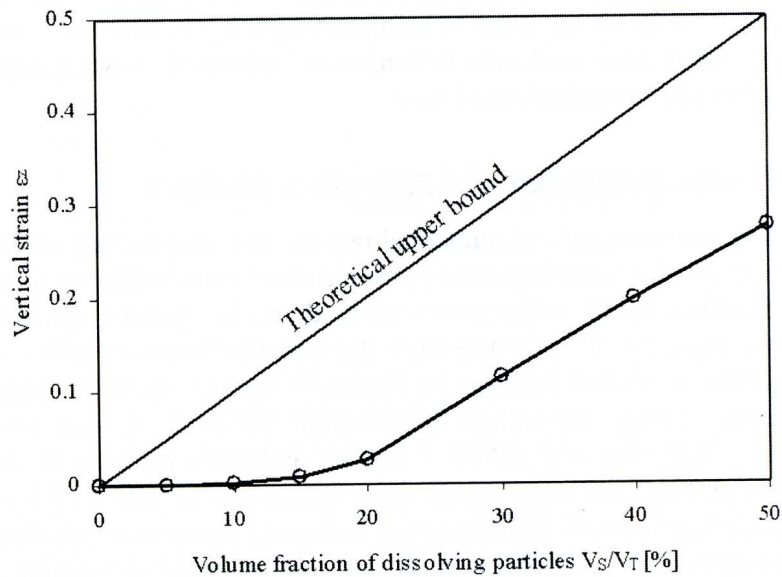


Figure 2.16: DEM simulation showing vertical strains at end of dissolution with respect to soluble volume fraction (Shin & Santamarina 2009)

for two 10% salt samples. Both were loaded in their dry state to a vertical stress of 160 kPa. One sample was dissolved showing a significant increase in void ratio. Subsequently, the dry and dissolved samples were loaded and unloaded. Although the void ratio for the dissolved sample was significantly higher, its loading paths were similar to those of the dry sample.

In Figure 2.17b, dissolution was performed at various vertical stresses. Truong et al. (2010) stated that dissolution tests performed at lower stresses showed greater void ratio increases, although this effect does not appear to be very significant. Subsequent loading paths showed near identical changes in void ratio.

The influence of various salt percentages dissolved at 160 kPa vertical stress were shown in Figure 2.17c. Void ratio was shown to increase with the percentage of salt dissolved. Subsequently, loading paths for all tests showed similar vertical strain responses although void ratios were significantly different.

The loading of dissolved mixtures ( $R_D = 0.29 - 0.38$ ) all resulted in similar loading paths, or void ratio changes, replicating those of the dry medium-dense sample ( $R_D = 0.67$ ). This agrees with the hypothesis put forward by Shin & Santamarina (2009) that resilient load-carrying grain arches can develop around the cavities formed by the dissolving salt particles.

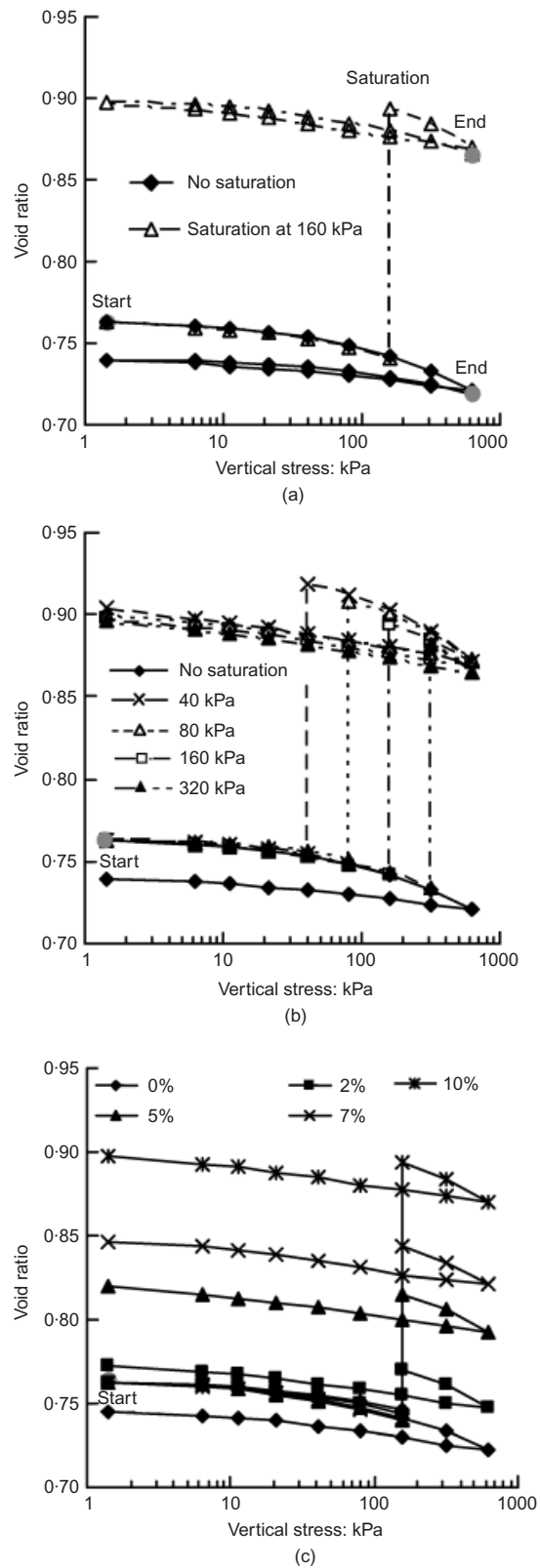


Figure 2.17: Void ratio increase with dissolution for (a) 10% salt dissolution test performed at 160 kPa (b) 10% salt tests performed at various stresses, and (c) various salt percentages (Truong et al. 2010).

The study by Truong et al. (2010) demonstrates that modest percentage removal (2-10% of salt by volume) for diameter ratios of 1.5 has little influence on the one-dimensional compressibility of the sand. Tran et al. (2012) did not take account of the sample settlement with pressure application. This may have been the reason for the reported higher post-dissolution void ratios for lower applied stresses. Tran et al. (2012) showed that the soluble particle fraction influenced the post-dissolution (pre-shear) void ratio in Figure 2.18 in the following ways:

- Higher soluble fractions resulted in higher post-dissolution void ratios
- Lower applied normal stress resulted in higher post-dissolution void ratios

The variation in void ratio after shear with respect to the soluble particle fraction indicates sample non-uniformity issues in the shear box apparatus (Figure 2.18).

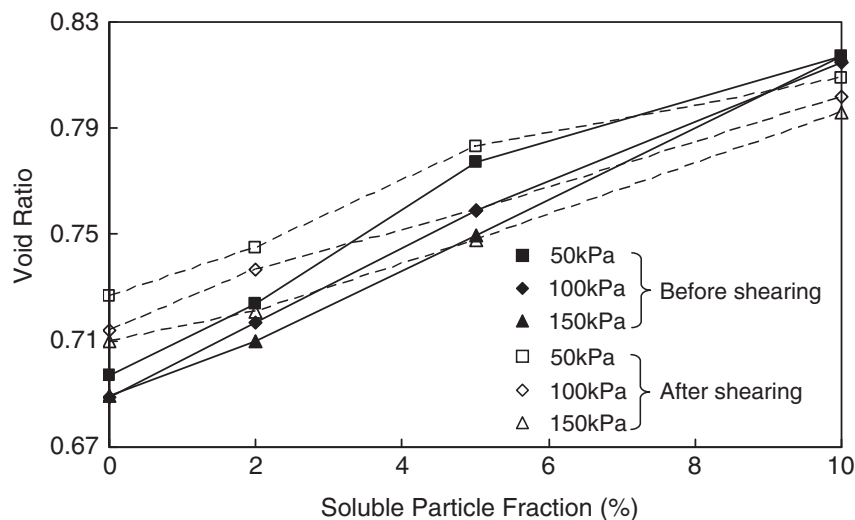


Figure 2.18: Void ratio versus soluble particle fraction pre-shear (post-dissolution) and post-shear (Tran et al. 2012)

Tran et al. (2012) used a two-dimensional DEM programme (PFC2D) to simulate dissolution tests performed in the shear box. Simulation results were qualitatively similar to experimental results. The void ratio increased with the soluble particle fraction. Tran et al. (2012) stated that void ratio increase was proportional to the initial soluble particle fraction in agreement with the findings of Truong et al. (2010). The coordination number was used to evaluate the changes in dissolution simulations.<sup>2</sup> The simulations by Tran et al. (2012) showed that higher soluble particle fractions resulted in lower post-dissolution coordination numbers. Interestingly,

<sup>2</sup>The coordination number is the average number of contacts per particle and defined as  $Z = 2C/N$  where  $C$  is the number of contacts and  $N$  is the number of particles (Thornton 2000).

Tran et al. (2012) showed that the coordination number after dissolution of 10% soluble particle fraction was lower than that for a simple cubic packing shown by Lade et al. (1998) demonstrating that the post-dissolution fabric might be unstable. There was discrepancy between the relative densities of experiments and simulations. Simulations showed much higher relative densities than experiments, e.g. the 10% soluble particle tests had values of 19 and 34% for simulations and experiments, respectively. This was as a result of the limitations of the DEM simulations. They were two-dimensional and therefore did not represent the three-dimensional reality of the soil tests. Furthermore, particles were represented by discs thereby simplifying the variability of shape in soil particles in real soils. Therefore, quantitatively the DEM simulations with real tests did not agree, yet qualitatively they were found to be similar. Using the packing state and contact force chains, it was shown that as the soluble fraction increases, so too does the void ratio and the contact force anisotropy (Figure 2.19).

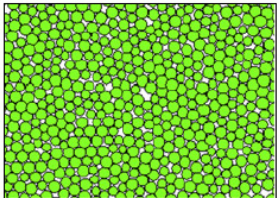
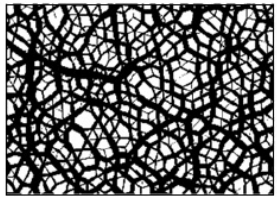
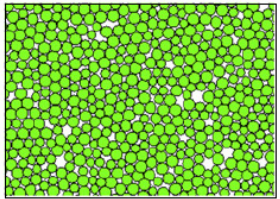
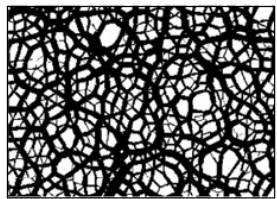
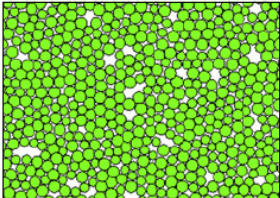
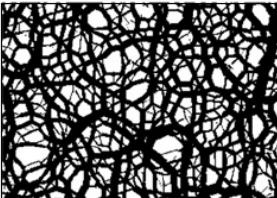
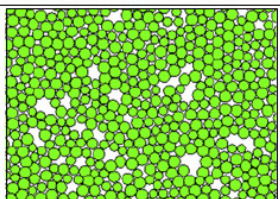
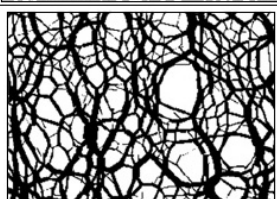
Soluble particle fraction	Packing state	Contact force chains
0 %		
2 %		
5 %		
10 %		

Figure 2.19: Post-dissolution packing state and force chains simulated using DEM (Tran et al. 2012)

Tran et al. (2012) then presented the polar distributions of contact normals, normal contact forces, and shear contact forces for the post-dissolution tests.<sup>3</sup> The 0% soluble fraction test was taken as the reference pre-dissolution sample for comparison with the post-dissolution samples with soluble percentages of 2, 5 and 10%. It was shown that the number of post-dissolution shear contact forces increase in proportion to the soluble particle percentage, creating a less stable fabric. Additionally, increasing anisotropy was indicated by increasing anisotropy coefficients with the soluble particle fraction removed, specifically with respect to contact normals, normal contact forces and shear contact forces.

McDougall et al. (2013) found that the void ratio always increased with dissolution (Figure 2.20). Salt percentage exerted the greatest influence on void ratio. Particle size did not appear to have an effect since the minor differences in void ratio change with respect to particle size appeared to be random. Figure 2.20 presents data from 32 dissolution tests. The graphs are separated according to salt particle size. The vertical stresses of 62 and 250 kPa are presented together allowing direct comparison. The pre-dissolution void ratio was always the lower of the two points defining the vector. The initial void ratios of the 0.063 mm salt tests were generally less than  $e_{min,LB}$ . This corresponded to the research on binary mixtures by Lade et al. (1998). Void ratio change did not appear to be affected by the vertical stress in the 62-250 kPa range since the void ratio changes for both stresses are similar. However, initial void ratios for the 250 kPa tests tend to be lower than the 62 kPa tests suggesting that the mixture is denser because of the greater applied stress, but the void ratio change with dissolution is not less as a consequence. The initial void ratio is not related to  $e_{min,LB}$  and  $e_{max,LB}$  since the soils have a different grading due to the range of salt additions varying in particle size and percentage. It is only the post-dissolution void ratios that can be meaningfully compared with  $e_{min,LB}$  and  $e_{max,LB}$  values. This point helps to illustrate that the soil structure evolves as dissolution progresses; the salt particles are shrinking thereby changing the grading of the soil. The general trend is an increase in post-dissolution void ratio with increasing percentage of salt. Post-dissolution void ratios were shown to approach the  $e_{max,LB}$  for the 10 and 15% additions in the 0.25, 0.5 and 1.0 mm salt sizes.

---

<sup>3</sup>The polar distributions for contact normals, normal contact forces, and shear contact forces are presented in Figures 2.27, 2.28, and 2.29 in the context of fabric changes during shear. The 'before shearing' relates to the post-dissolution state of interest here.

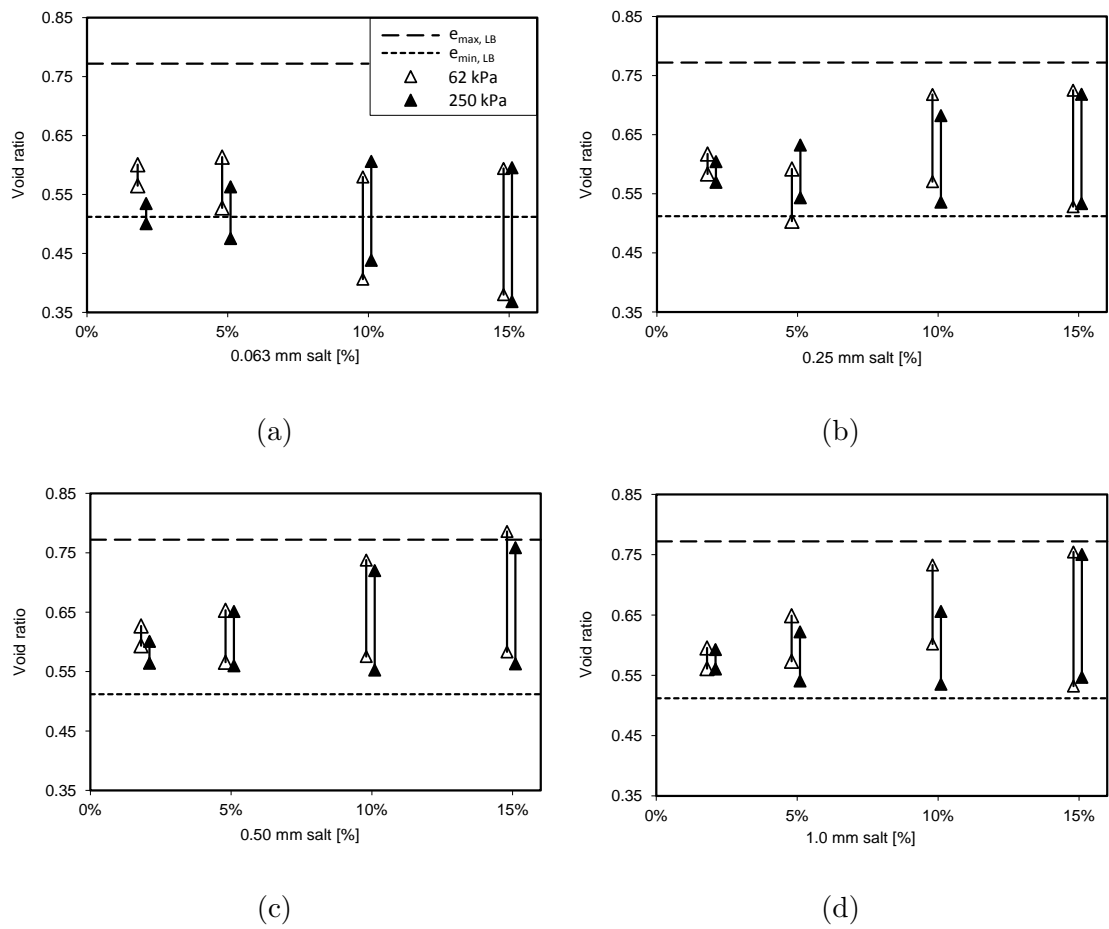


Figure 2.20: Vectorial depiction of void ratio increases due to dissolution of salt at various percentages and particle sizes. Tests performed under vertical stresses of 62 and 250 kPa (after McDougall et al. (2013))



### 2.4.5 Strength changes with particle loss

Fam et al. (2002) were first to investigate the large strain behaviour of post-dissolution samples in drained triaxial tests. Samples consisted of coarse or fine sand with 0, 2, 5 and 10% by weight of salt resulting in 8 tests in total, 6 with dissolution. In both fine and coarse sand tests (Figures 2.21a & 2.21b, respectively), results were similar, with sand-only samples showing higher strength than post-dissolution sand-salt samples. The change from strain-softening behaviour for sand to increasingly strain-hardening behaviour for higher salt percentages in post-dissolution tests was noted. Peak strengths were shown to decrease with percentage of salt particles removed. In fact, some higher salt percentage tests never developed a peak even after shearing to axial strains of approximately 10% (Tests FS-10%, CS-5% and CS-10%). Accordingly, volumetric strain with shear showed dilative behaviour for sand with mildly dilative behaviour for higher salt percentages in post-dissolution tests.<sup>4</sup> This was illustrated by large volumetric increases with shear in sand-only tests, with volumetric strains decreasing with increasing percentage of salt removed.

The angle of shearing resistance at failure was shown to vary widely between the sand-only and post-dissolution tests. For the coarse sand batch the sand-only test had a value of 41° while post-dissolution samples for 2, 5 and 10% had values of 40°, 36° and 30°, respectively. This points to the influence of particle loss, through void ratio increase, on shearing resistance.

Fam et al. (2002) plotted the peak angle of shearing resistance against the state parameter  $\psi$  ( $\psi = e - e_{ss}$ ; where  $e$  is the void ratio before shearing, and  $e_{ss}$  is the void ratio at the steady state condition (Been & Jefferies 1985)) showing a reasonable interdependent relationship (Figure 2.22).<sup>5</sup> However, the post-dissolution void ratios were based on the assumption of no total volume change with dissolution possibly leading to significant errors in the void ratio calculation and subsequent state parameter calculation. Furthermore the steady state void ratio  $e_{ss}$  was determined by the volumetric strain at large axial strains but plots of volumetric strain with shear did not show the attainment of the steady state. Fam et al. (2002) acknowledged this as a possible source of error leading to inconsistencies in the calculation of the

---

<sup>4</sup>In soil mechanics, it is conventional to take compression as positive, contrary to the approach adopted by Fam et al. (2002) in Figures 2.21a & 2.21b

<sup>5</sup>In basic terms, the terms *critical state* and *steady state* refer to a condition in which a soil continues to deform without a change in stress or void ratio. They are generally used to describe drained and undrained behaviour, respectively. It is now believed that the steady state and critical state define the same condition and that the critical state line and steady state line are coincident (Been et al. 1991, Verdugo & Ishihara 1996).

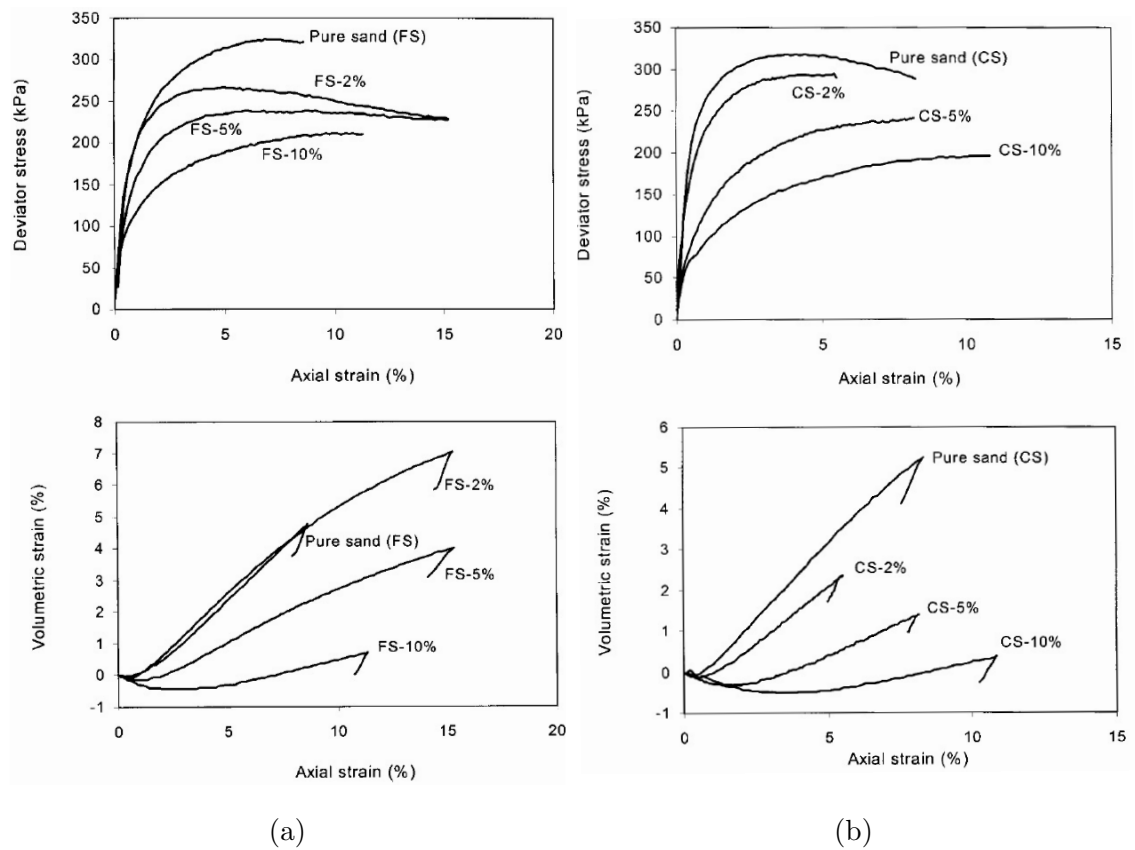


Figure 2.21: Triaxial test shearing behaviour of post-dissolution sand-salt samples for (a) fine sand (FS), and (b) coarse sand (CS) with salt percentages of 0, 2, 5, & 10 % (Fam et al. 2002)

steady state parameter. Recent researches have shown that void ratio increase is related to the percentage of salt removed (Shin & Santamarina 2009, Truong et al. 2010, Tran et al. 2012, McDougall et al. 2013) and that this was the likely reason for the changes in post-dissolution shear behaviour in the study by Fam et al. (2002).

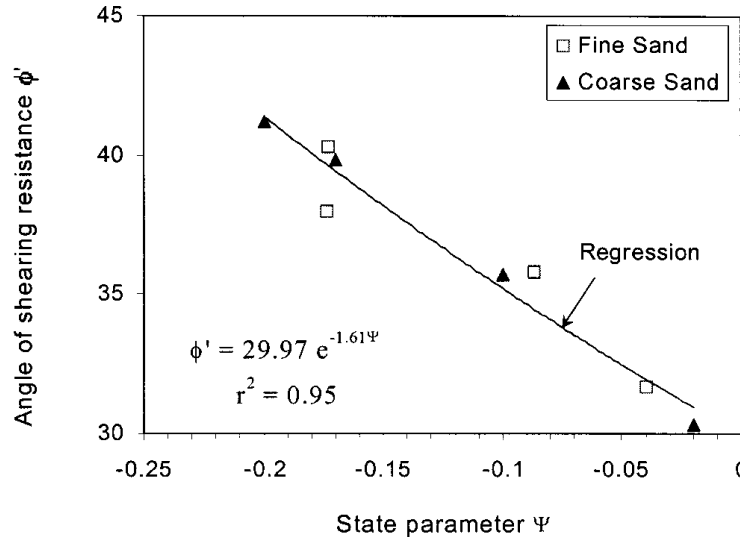


Figure 2.22: Angle of shearing resistance against the state parameter for triaxial tests performed on post-dissolution coarse and fine sands (Fam et al. 2002)

Having a more accurate measure of volume change during each stage of testing, Tran et al. (2012) assessed the strength changes with dissolution in the shear box. Again a sand-only test and post-dissolution samples having contained 2, 5 and 10% by volume salt were assessed. In agreement with the study by Fam et al. (2002) the sand-only sample showed the highest shear strength with each salt percentage increase showing a decrease in strength. The sand-only test also showed dilative behaviour with shear while post-dissolution tests showed increasingly contractive behaviour with increasing percentage of salt (Figure 2.23). For these tests, accurate void ratios prior to the shearing stage were available and provided more credible data on the effect of void ratio on shear behaviour than the study by Fam et al. (2002). Despite this, in order to define the state of the soil during shear, the presentation of the void ratio state variable would have been advantageous (Figure 2.23a). Furthermore, it is preferable to present horizontal displacement of the shear box as shear strain (Figure 2.23b). Lastly, the limitations of data obtained from direct shear tests are well known, e.g. the predefined failure surface and non-uniform stress conditions.

Although critical stress-ratios calculated based on the data presented in Figure 2.23a suggest that critical strength was not equal for all salt percentages in the 100 kPa

tests (0.6-0.73), the author claimed that critical strengths were almost the same. However the presented data suggests that higher salt percentages result in lower critical stress ratios. It may be that the identification of the critical state is difficult at low stresses as found by Klotz & Coop (2002). Regardless, later in the paper the author claimed that the critical strength was independent of the salt content.

For the interpretation of critical states from shearbox data in Figure 2.23b, it would have been preferable to present the volumetric data in terms of the void ratio state variable. Furthermore, vertical and horizontal displacements in the shear box would better be presented in terms of strain (Figures 2.23a & 2.23b).

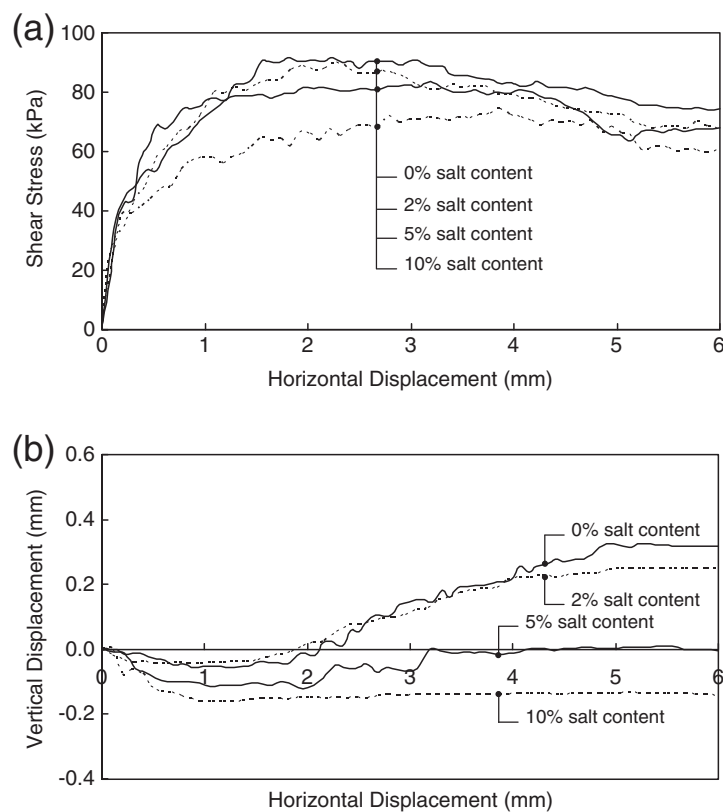


Figure 2.23: Direct shear test results of post-dissolution samples varying with salt percentage under 100 kPa normal stress (Tran et al. 2012)

Tran et al. (2012) presented the peak and critical shear strength for all tests varying with salt percentage (2, 5 & 10%) and applied stress (50, 100, 150 kPa) (Figure 2.24a). The tests showed that peak strength decreased with salt percentage in post-dissolution tests while the maximum stress was coincident with the critical stress in tests with 10% salt by volume.<sup>6</sup> The plot of peak shear strength versus void ratio

<sup>6</sup>Note that Tran et al. (2012) refer to the *critical shear strength* as the *residual shear strength*.

before shear showed a decrease in peak strength with void ratio increase (Figure 2.24b).

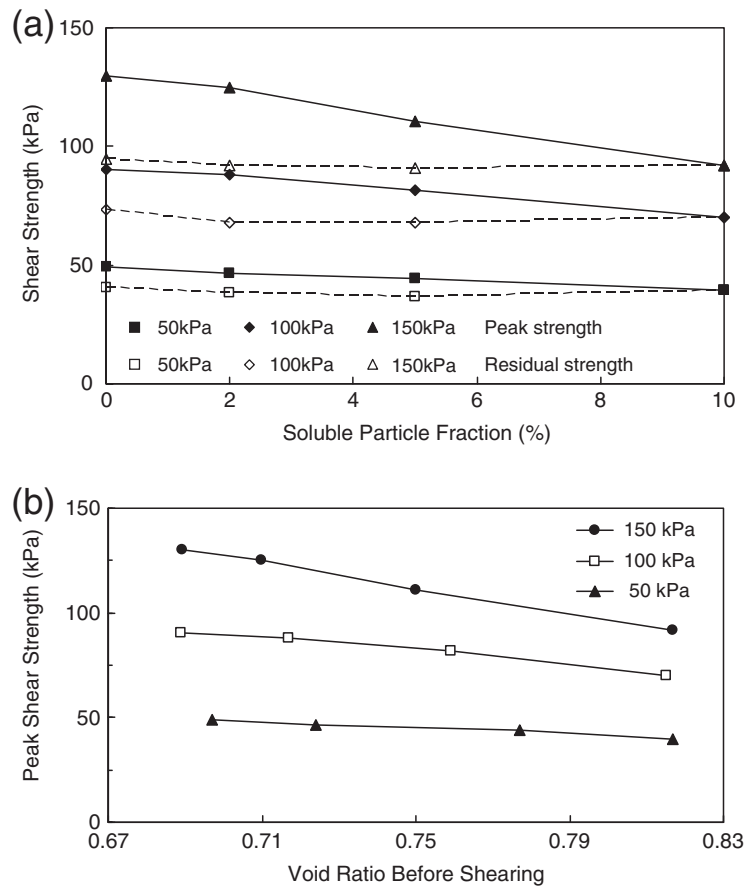


Figure 2.24: (a) Peak and critical shear strengths against soluble particle percentage removed through dissolution (b) Peak shear strength against pre-dissolution void ratio for confining stresses of 50, 100 & 150 kPa (Tran et al. 2012)

### Internal erosion - case study

Studying the effects of internal erosion, Chang & Zhang (2011) performed drained triaxial tests on an intact specimen not subjected to erosion, and three samples subjected to erosion under different stress states. Shearing was performed under a confining stress of 50 kPa in all tests and samples consisted of Leighton Buzzard sand (fraction E) and completely decomposed granite.

The intact sample showed strain-softening and an overall contractive response with

However, the residual shear strength is specific to clay soils and occurs subsequent to the critical state after large displacements along the rupture zone.

a tendency towards dilation, while the post-erosion samples demonstrated strain-hardening and contractive behaviours (Figure 2.25). The total mass eroded from the soil was 34 g, constituting a 2.5% loss by volume. Chang & Zhang (2011) attributed the change in shearing response to a change in void ratio. The intact sample was reported to have a void ratio of 0.479 prior to erosion while the post-erosion sample void ratio was calculated as 0.516 based on the reported volumetric strain and mass lost.

Although the mechanism of particle loss in the erosion study by Chang & Zhang (2011) is different to that of the dissolution study by Fam et al. (2002), the trend in shear behaviour change with particle loss is similar. Intact samples show strain-softening dilative behaviour while samples subjected to particle loss tend towards a more strain-hardening compressive behaviour. Crucially, both studies cited an increase in void ratio with particle loss.

### 2.4.6 Micromechanical insights using DEM

In addition to Shin & Santamarina (2009), Tran et al. (2012) also performed a study on dissolution using a two-dimensional DEM program (PFC2D). Simulating dissolution tests in a shear box apparatus the volumetric consequences could be analysed, but this also allowed the opportunity to study the shear behaviour of the post-dissolution tests. These were designed to replicate the mixtures performed in the experiments. However the simulation of two-dimensional discs do not represent the true behaviour of real soil. Another potential limitation in the DEM tests performed was the use of identical normal and shear stiffness for both sand and salt particles. Furthermore, a common frictional coefficient for both sand and salt particles was used. In agreement with experimental tests, the DEM simulations showed that peak strengths were observed for sand-only, and 2 and 5% salt by volume dissolution tests (Figure 2.26a). The 10% test showed no peak strength prior to critical strength development. The simulation showed decreases in peak strength and critical strength with increasing soluble particle fraction in agreement with experimental results presented earlier in Figure 2.23 .

The reductions in the peak shear strength and the peak friction angle resulted from the increase in void ratios with soluble particle fractions. The loss of strength with dissolution void ratio increase was explained in terms of the coordination number. For the sample with no soluble particle fraction a coordination number of 4.6 was computed. A near proportional decrease in coordination number with increase in

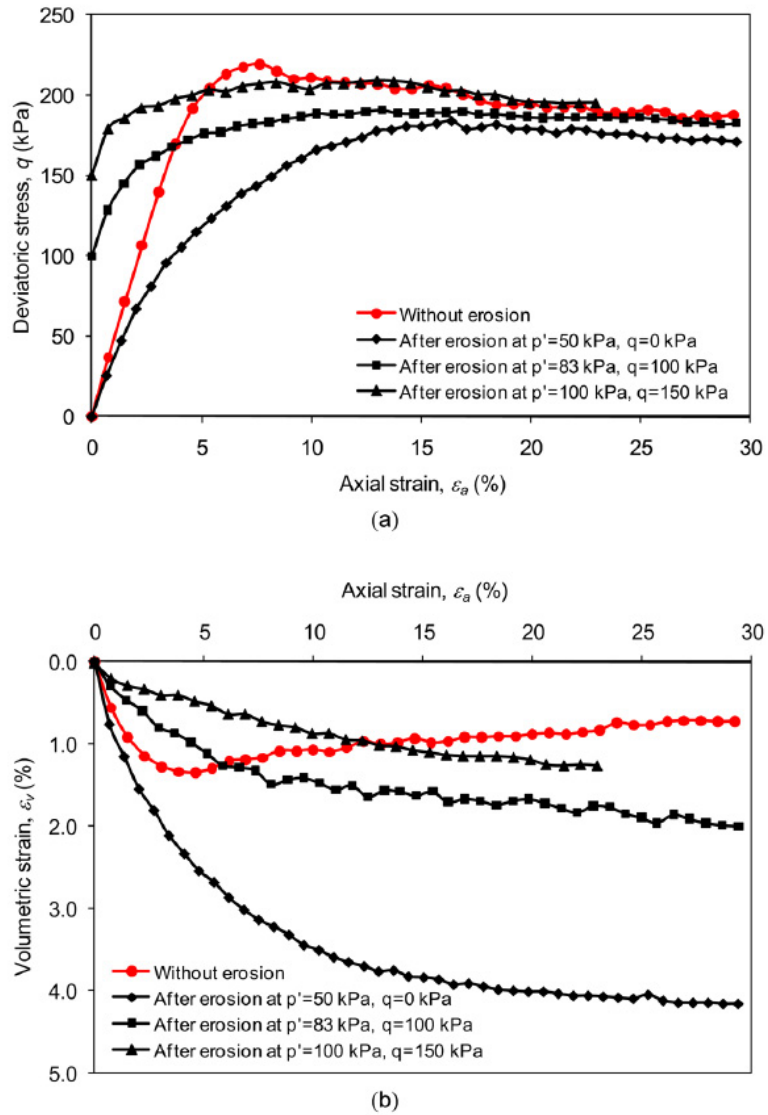


Figure 2.25: Triaxial shear behaviour of a specimen not subjected to erosion and three specimens for which erosion was performed under different stress conditions (a) deviatoric stress and (b) volumetric strain against axial strain. Shear was performed under 50 kPa confining stress in all tests (Chang & Zhang 2011)

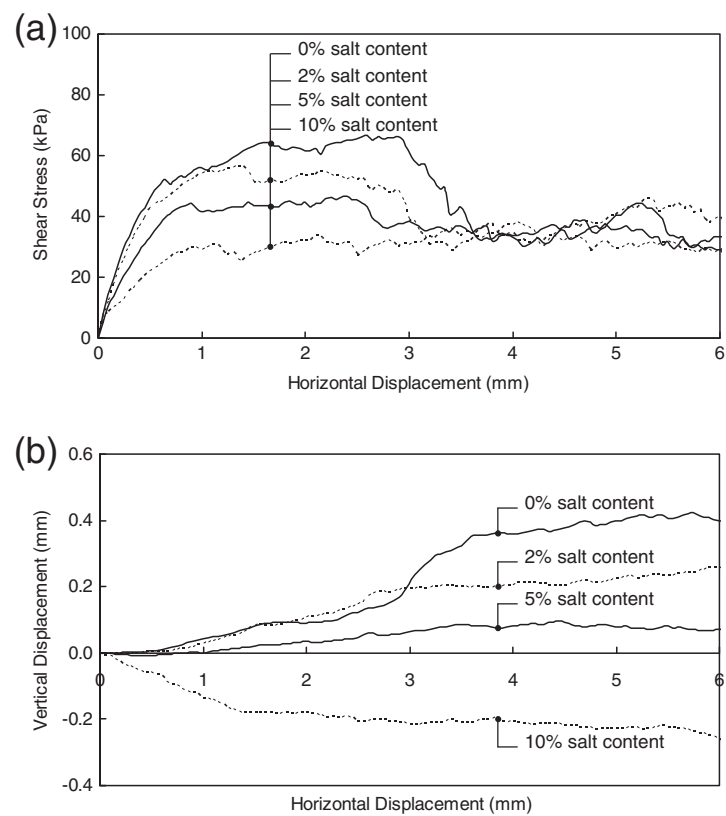


Figure 2.26: DEM simulations of direct shear behaviour for post-dissolution samples varying with salt percentage in the shearbox apparatus under 100 kPa normal stress (Tran et al. 2012)



soluble fraction dissolved culminated with a coordination number of 3.9 for the 10% soluble particle fraction.

Tran et al. (2012) computed the polar distributions of the contact normals, the normal contact forces and the shear contact forces at three stages in the simulation, and presented the results as histograms (Figures 2.27, 2.28 & 2.29, respectively). The three stages were after dissolution, the peak shear strength and the residual shear strength. The size of the polar distributions signify the number of contacts, the total normal contact forces and the total shear contact forces. Therefore assessing the polar distributions for the after dissolution stage, it can be seen that contact normals (Figure 2.27) and normal contact forces (Figure 2.28) decrease while shear contact forces increase (Figure 2.29) with the soluble particle fraction dissolved. Tran et al. (2012) noted that the preferential orientation of contact normals and normal contact forces was  $0^\circ$  from the vertical showing increased anisotropy with soluble fraction increase at the after dissolution stage. The preferential orientation of contact normals and normal contact forces changed to  $45^\circ$  from the vertical axis for peak and residual strength stages. This was found to be independent of the soluble fraction removed.

The polar distributions for the shear contact forces were greatest at the peak strength stage, and were greatest for the non-dissolution sample. Decreases in the shear contact forces with peak shear strength development were found with increasing soluble fraction. For the 10% sample, peak shear strength was the same as the critical strength, showing consistency with the stress-strain plots for experimental results.

Tran et al. (2012) used anisotropy coefficients to define the anisotropy of a sample where higher coefficients indicated greater anisotropy (shown on Figures 2.27, 2.28 & 2.29). Anisotropy coefficients were shown to increase with the soluble particle fraction at the post-dissolution stage in the simulations. Comparing post-dissolution, peak shear strength and residual shear strength stages, the coefficients indicate that anisotropy is always greatest at the peak shear strength stage. Then the anisotropy of the residual (or critical) shear strength stage is always greater than that at the post-dissolution stage. Tran et al. (2012) concluded that their finding agreed with the finding of Rothenburg & Bathurst (1989) in that the ability of a particulate assembly to develop anisotropic fabric determines the shear strength of the fabric. Anisotropy at peak stress was shown to decrease with soluble particle fraction, the level of which corresponded to the peak shear strength developed.

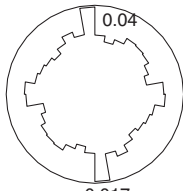
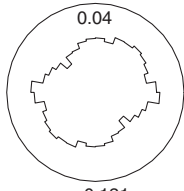
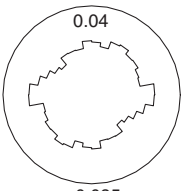
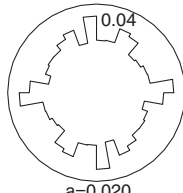
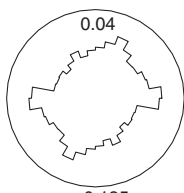
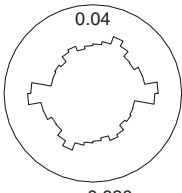
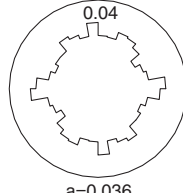
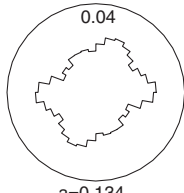
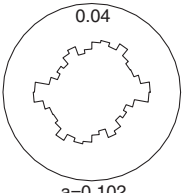
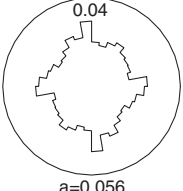
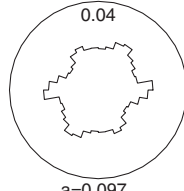
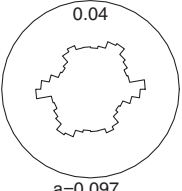
Soluble particle fraction	Before shearing (After dissolution)	Peak shear strength	Residual shear strength
0 %	 a=0.017	 a=0.121	 a=0.085
2 %	 a=0.020	 a=0.135	 a=0.090
5 %	 a=0.036	 a=0.134	 a=0.102
10 %	 a=0.056	 a=0.097	 a=0.097

Figure 2.27: Polar distribution of contact normals: The number 0.04 denotes the radius of the boundary circle, and the “a” denotes the anisotropy coefficient of the contact normals (Tran et al. 2012)

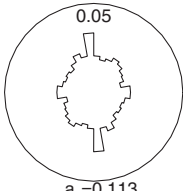
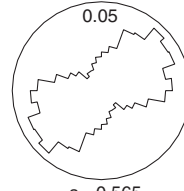
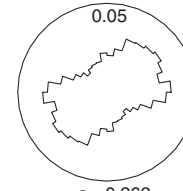
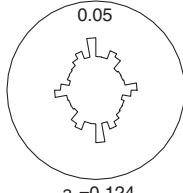
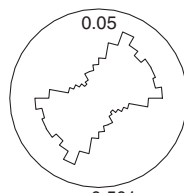
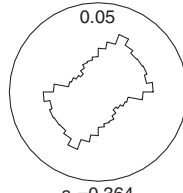
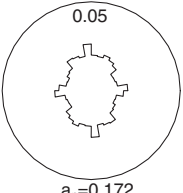
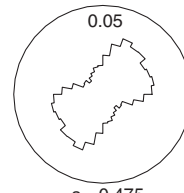
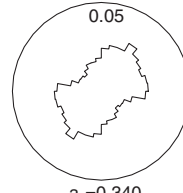
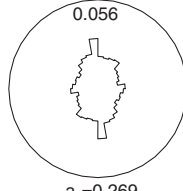
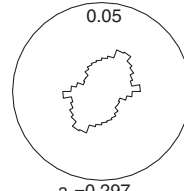
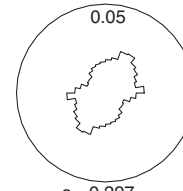
Soluble particle fraction	Before shearing (After dissolution)	Peak shear strength	Residual shear strength
0 %	 <p>0.05 <math>a_n=0.113</math></p>	 <p>0.05 <math>a_n=0.565</math></p>	 <p>0.05 <math>a_n=0.363</math></p>
2 %	 <p>0.05 <math>a_n=0.124</math></p>	 <p>0.05 <math>a_n=0.501</math></p>	 <p>0.05 <math>a_n=0.364</math></p>
5 %	 <p>0.05 <math>a_n=0.172</math></p>	 <p>0.05 <math>a_n=0.475</math></p>	 <p>0.05 <math>a_n=0.340</math></p>
10 %	 <p>0.056 <math>a_n=0.269</math></p>	 <p>0.05 <math>a_n=0.297</math></p>	 <p>0.05 <math>a_n=0.297</math></p>

Figure 2.28: Polar distribution of normal contact forces: The number 0.05 denotes the radius of the boundary circle, and the “a” denotes the anisotropy coefficient of the normal contact forces (Tran et al. 2012)

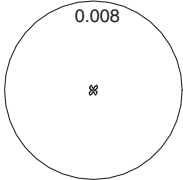
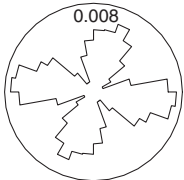
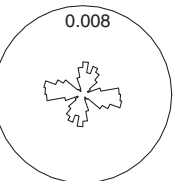
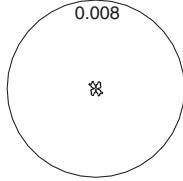
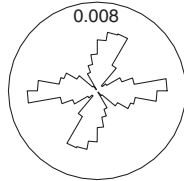
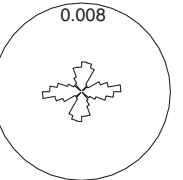
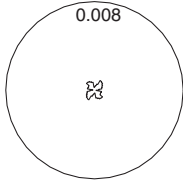
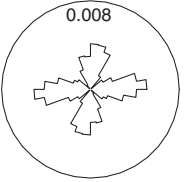
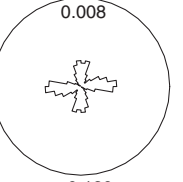
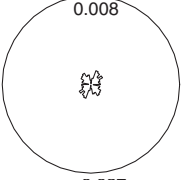
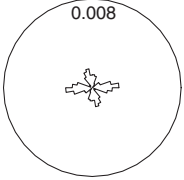
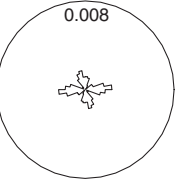
Soluble particle fraction	Before shearing (After dissolution)	Peak shear strength	Residual shear strength
0 %	<p>0.008</p>  <p><math>a_t=0.012</math></p>	<p>0.008</p>  <p><math>a_t=0.231</math></p>	<p>0.008</p>  <p><math>a_t=0.123</math></p>
2 %	<p>0.008</p>  <p><math>a_t=0.018</math></p>	<p>0.008</p>  <p><math>a_t=0.209</math></p>	<p>0.008</p>  <p><math>a_t=0.129</math></p>
5 %	<p>0.008</p>  <p><math>a_t=0.026</math></p>	<p>0.008</p>  <p><math>a_t=0.201</math></p>	<p>0.008</p>  <p><math>a_t=0.120</math></p>
10 %	<p>0.008</p>  <p><math>a_t=0.037</math></p>	<p>0.008</p>  <p><math>a_t=0.097</math></p>	<p>0.008</p>  <p><math>a_t=0.097</math></p>

Figure 2.29: Polar distribution of shear contact forces: The number 0.08 denotes the radius of the boundary circle, and the “a” denotes the anisotropy coefficient of the shear contact forces (Tran et al. 2012)

### 2.4.7 Stiffness changes in dissolving soils

Whilst shear strength data points to a looser particle structure following particle loss (by dissolution), it is illuminating to consider changes in stiffness as recorded during dissolution by shear wave velocity measurements.

The small-strain ( $\gamma < 10^{-6}$ ) properties of a sand-salt sample (5% by weight salt) were assessed using a resonant column with bender elements located in the top and bottom platens (Fam et al. 2002). The bender elements were used to obtain shear wave velocity change during the salt dissolution stage. In an alternative approach, bender elements were used to compare the shear wave velocity with confining stress for the dry sand-salt and the post-dissolution sample. This was achieved by isotropically loading and unloading the samples taking shear wave velocity measurements at stress increments. This provided the shear wave velocity  $V_s$  against mean confining stress  $\sigma'_0$  data in Figure 2.30. To fit the data, a standard shear wave velocity-stress  $V_s - \sigma'_0$  relation proposed by Hardin & Drnevich (1972) has been applied:

$$V_s = a \sigma'_0{}^b \quad (2.11)$$

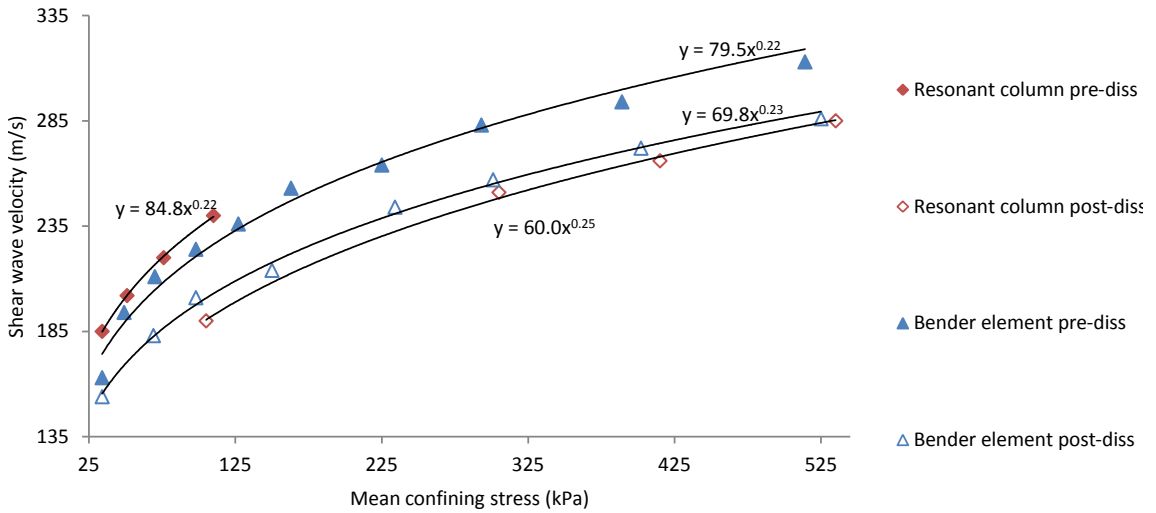


Figure 2.30: Shear wave velocity-stress relations based on pre- and post-dissolution sand-salt mixtures using the resonant-column apparatus and bender elements (Fam et al. 2002)

where  $a$  and  $b$  are material constants and  $\sigma'_0$  is the effective confining stress. The equations in Figure 2.30 indicate the value of the constants for each  $V_s - \sigma'_0$  relation.

The  $V_s - \sigma'_0$  exponent for the dry sand-salt “pre-diss” sample was found to be  $b = 0.22$ . Upon dissolution this increases to  $b = 0.23$ . At a confining stress of 100 kPa the  $V_s - \sigma'_0$  bender element relations represent an approximate 8% drop in shear wave velocity with dissolution. Figure 2.30 also shows the variation in shear wave velocities measured using the bender element and resonant column approaches. For comparison, a 19% decrease at 100 kPa was found using resonant column data.

The mineralogical difference between sand-salt and post-dissolution remaining sand were not considered by Fam et al. (2002). The relative stiffness of the salt means the surface area of the sand-salt interparticle contacts is likely to be larger than that of a sand-only sample. This large contact area could facilitate the transmission of shear waves through the sand-salt mixtures. This is qualified in data presented by Santamarina et al. (2001) showing that density determines wave velocity in solids. For example, quartz is denser than halite (salt) and therefore wave transmission in quartz is approximately 25% faster. However, in particulate form, wave velocities are higher in salt. This emphasises the importance of contact effects on wave travel in particulate media (Santamarina et al. 2001).

Table 2.3 shows the void ratio and shear wave velocities at 90 kPa for 3 tests presented by Fam et al. (2002). The post-dissolution test shows the lowest velocity as might be expected. However care must be taken in the interpretation of this data since Fam et al. (2002) calculated void ratios based on the assumption of zero total volume change with dissolution. This approach undermines the analysis of shear wave velocity in terms of sample fabric and density changes.

Table 2.3: Shear wave velocity changes with dissolution (after Fam et al. (2002))

	Void ratio	Shear wave velocity at 90 kPa confining stress (m/s)
Sand	0.77	222
Sand-salt (dry)	0.67	243
Sand-salt (post-dissolution)	0.77	192

Using Equation 2.12, Fam et al. (2002) attempted to predict the shear wave velocity of the post-dissolution sample based on changes in mass density.

$$V_s = (\text{shear modulus}/\text{mass density})^{0.5} \quad (2.12)$$

This approach predicted a 6.5% decrease in shear wave velocity with dissolution based on mass density changes. However it was not made clear how the shear modulus was calculated. Then, to address the shear wave velocity decreases due to void ratio change with dissolution, void ratio functions by Hardin & Drnevich (1972) (Equation 2.13) and Chang et al. (1991) (Equation 2.14) predicted a decrease of 8 and 6% respectively.

$$f(e) = (2.97 - e)/\sqrt{1 + e} \quad (2.13)$$

$$f(e) = (13.28 - 8e)/(1 + e)^{1/3} \quad (2.14)$$

Combining the mass density and void ratio predictions, total velocity decreases of 14.5 or 12.5% would be found. Taking the larger value, Fam et al. (2002) argued that 10% of the measured decrease in shear wave velocity with dissolution in the sand-salt test could not be attributed to density or void ratio changes. However assessing a constant fabric scenario where particle loss did not result in sample mineralogy change (i.e. sand-only before and after particle loss) a lower discrepancy of 7% between the predicted and measured velocity was found. Therefore Fam et al. (2002) concluded that the shear wave velocity decreases that occurred with dissolution could not be accounted for through changes in mass density or void ratio, and attributed this to a change in fabric. In this context, Fam et al. (2002) proposed that the reduction in coordination number with dissolution had a strong influence on shear wave velocity and this was not compensated for with increasing interparticle contact forces. Finally, the authors acknowledged that one dissolution test was insufficient to draw quantifiable conclusions and called for further research on the topic.

Truong et al. (2010) performed dissolution tests on sand-salt samples with various salt percentages (0, 2, 5, 10%) under different vertical stresses (40, 80, 160, 320 kPa). For dissolution tests performed at a vertical stress of 160 kPa, Truong et al. (2010) found that the decrease in shear wave velocity was proportional to the salt percentage removed. The 10% salt test resulted in a drop of 33% (approximately 240 to 160 m/s) as illustrated in Figure 2.31. An analytical approach by Santamarina et al. (2001) that accounted for non-isotropic loading associated with one-dimensional loading, and incorporating the void ratio function by Hardin & Drnevich (1972) to assess the micromechanical changes accompanying dissolution was used:

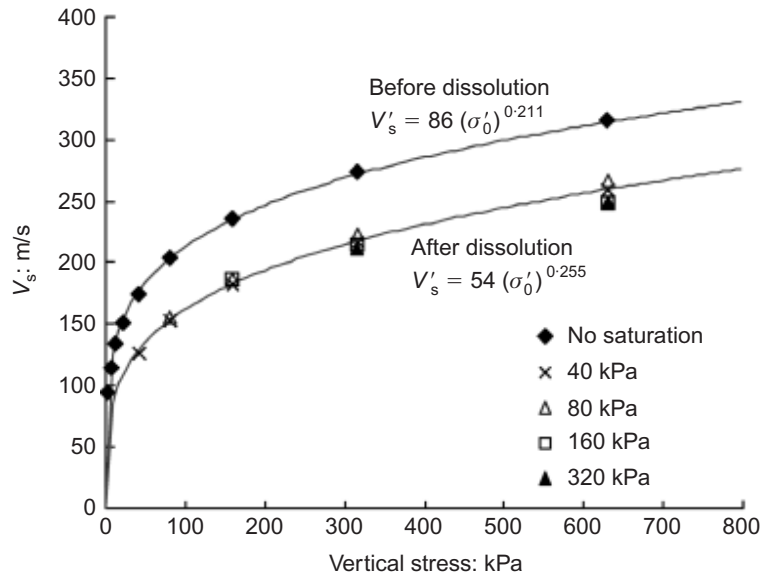


Figure 2.31: Pre- and post-dissolution velocity-stress relations for 10% by volume of salt in oedometer tests. Dissolution performed under 40, 80, 160 & 320 kPa (Truong et al. 2010)

$$V_s = \alpha \sigma_0'^{\beta} = \alpha \left( \frac{\sigma'_p + \sigma'_m}{2kPa} \right)^{\beta} = Af(e) \left( \frac{\sigma'_p + \sigma'_m}{2kPa} \right)^{\beta} \quad (2.15)$$

where  $(\sigma'_p + \sigma'_m)/2$  is the average effective stress on the polarization plane, and  $\sigma'_p$  and  $\sigma'_m$  are the effective stresses in the direction of wave propagation and particle motion, respectively. The  $\alpha$  coefficient and the  $\beta$  exponent were determined using the power law curve fitting procedure used by Fam et al. (2002). Santamarina et al. (2001) stated that the  $\beta$  exponent is related to the contact behaviour of the particles. This included the size, structure and shape of the particulate material. The  $\alpha$  coefficient represented the type of packing, particulate material properties, contact behaviour and fabric changes.

The key findings of this approach were that the  $\alpha$  coefficient decreased and the  $\beta$  exponent increased with dissolution. Truong et al. (2010) stated that this indicated that the sample becomes loose with dissolution, although this was already apparent through reported void ratio increases. They stated that shear wave velocity was sensitive to vertical stress with dissolution of 10% salt at 10 and 320 kPa showing decreases of 26 and 19%, respectively. In contrast, the void ratio increment with dissolution was approximately 21% for each 10% salt dissolution test irrespective of applied stress. Since the increment in void ratio was constant with dissolution, the void ratio function returned a constant change of 11%. This indicated that



the velocity change due to void ratio was nearly constant, but the  $\alpha$  coefficient decreased from 86 to 54 with dissolution. This meant a decrease in 30% for the A factor implying a loss of particle contact after dissolution. This is in agreement with the conclusions drawn by Fam et al. (2002) who proposed that dissolution resulted in a decrease in coordination number.

### 2.5 Summary

This chapter introduced traditional phase relationships in soils and presented the decomposition induced void change parameter  $\Lambda$ , as a useful alternative to analyse and interpret dissolution studies. The typical volumetric and shear behaviour of coarse-grained materials was presented within the critical state soil mechanics framework. Finally, a selection of significant studies related to dissolution was critically reviewed. The major issues that need to be highlighted from this chapter are as follows:

- Standard phase relationships in soils are not able to capture the mechanics involved during mass loss. This is a consequence of changes in both the void and solid phases which also have a “dynamic” nature dependent on the amount and size of soluble or degradable material.
- There is a complex interaction between soluble and inert materials which is highly dependent on their size and relative amounts. Small particles (in large quantities) are able to fill or rest within the voids of larger particles. As the amount (and size) of soluble material increases the probability of these particles being part of the load-bearing soil structure either as part of strong force chains or supporting elements increases. Hence upon dissolution different volumetric and stress-strain responses can be expected.
- The decomposition-induced void change parameter  $\Lambda$  is useful to capture the complexity of various phase volume changes associated with decomposable/dissolving soils.
- The identification of the CSL at low stresses is problematic due to the effect of non-uniform deformations, the difficulty in preparing loose samples of granular materials, as well as complexities related to the calculation of volumetric changes in experimental tests.

- Existing dissolution studies consider (at most) two different sand/salt diameter ratios with various amounts of salt. In this study a wide range of sand/salt diameter ratios are investigated by changing the salt particle size added.
- Evidence suggests that during dissolution there are changes in the shear wave velocity as measured in bender element testing, but the influence of void ratio and internal fabric/structure is not well understood.
- Existing studies show that  $K_0$  initially reduces during dissolution only to recover at the end of the dissolution process.
- Strength decreases have been observed for soils subject to particle loss, whether the mechanism is dissolution or erosion, or performed in the triaxial apparatus, shear box, or as a simulation using DEM. In general, there is a trend of changing behaviour from strain-softening dilative for intact samples, to strain-hardening contractive for samples subjected to particle loss. The change in behaviour has been shown to be dependent on the percentage of material removed. However, little is known about the influence of particle size removed. The determination of the role of the particle size removed in the mechanical behaviour of the soil is a key objective of this study.
- The state parameter has been applied to triaxial dissolution tests. However, calculation of void ratios were based on an assumption of no total volume strain with dissolution. Furthermore, the presented data did not indicate the conclusive determination of a critical void ratio for the sand.
- DEM simulations have offered micromechanical insights into the changes accompanying the removal of various percentages of soluble particles from a soil. These show that soil fabric becomes increasingly anisotropic with the percentage of soluble particles removed, with contact normals and normal contact forces becoming increasingly aligned in the direction of the major principal stress (vertical direction in the shear box). This is accompanied by an increase in the shear contact forces, indicating the development of a less stable soil fabric. Subsequent shearing simulations performed on the post-dissolution soil have shown qualitative agreement with experimental tests. That is, shear strength decrease and a change from strain-softening dilative to strain-hardening contractive behaviour with increasing percentages of particles dissolved.

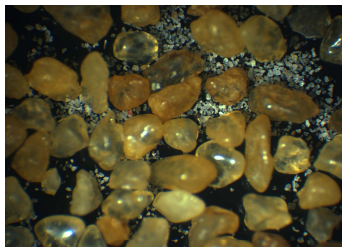
# Chapter 3

## Materials, Apparatus and Procedures

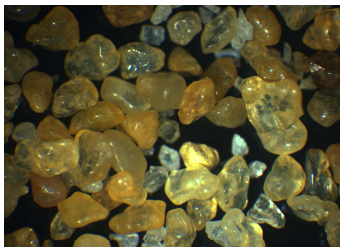
### 3.1 Materials

Testing material consisted of sand/salt mixtures. The sand was coarse uniform rounded Leighton Buzzard sand ( $D_{50} = 0.85$  mm;  $C_u = 1.4$ ;  $G_s = 2.65$ ) referred to as LB. The salt was sodium chloride ( $\text{NaCl}$ ;  $G_s = 2.165$ ) and had a more angular form. Salt particle sizes were defined by the sieve size on which they were retained with sieve sizes increasing by a factor of 2, i.e. 0.063, 0.125, 0.25, 0.5 and 1.0 mm.

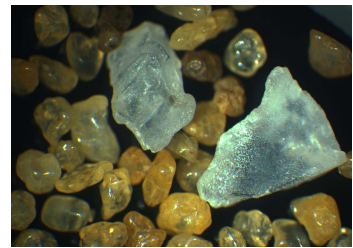
Figure 3.1 illustrates the relative sizes of sand and salt particles used in the mixtures with different diameter ratios of inert/soluble particles.



(a) Leighton Buzzard sand and 0.063-0.125 mm salt



(b) Leighton Buzzard sand and 0.25-0.5 mm salt



(c) Leighton Buzzard sand and 1.0-2.0 mm salt

Figure 3.1: Leighton Buzzard sand-salt mixes showing relative sizes and shapes

Salt was selected as the removable material since it can be easily crushed to the required dimensions, and is readily soluble in water allowing for quick dissolution. The use of salt and water as solute and solvent respectively made the testing procedure

uncomplicated since both are readily available and pose no safety concerns. Some concerns over the salt particle strength were anticipated but these are discussed later.

#### 3.1.1 Selection of salt sizes and percentages

The Leighton Buzzard sand is a uniform sized sand with a  $D_{50}$  of 0.85 mm. The salt particle sizes added to the sand were chosen to allow analysis of the removal of various particle sizes from the uniform sized sand. In terms of sand/salt particle size relations the  $D_{50}$  of the salt was taken as the value midway between the sieve on which particles were retained and that above it. Hence the  $D_{50}$  of the salt particle sizes tested were 0.095, 0.188, 0.375, 0.75 and 1.5 mm. In terms of diameter ratio ( $D_r$ ) of the sand and salt particle sizes, this corresponds to values of 9, 4.5, 2.3, 1.1 and 0.57, respectively. This range of diameter ratios allowed an investigation into the effect of particle size in soils experiencing particle loss.

#### 3.1.2 Salt selection

Initially, commercially sourced rock salt was used. It was sieved to remove dust and then sorted with any particles not clear or whitish in colour removed. While rock salt particles can vary in colour, darker shades were discarded in favour of clear coloured particles to prevent impurities. However, the use of rock salt was abandoned due to the blockages forming in the drainage lines that were thought to be caused by anti-caking agents and dust particles. To prevent future blockages the type of salt was changed to Tidman's natural rock salt which is a pure salt.

#### 3.1.3 Salt crushing

Several salt crushing techniques were attempted but could not produce the desired sizes efficiently. A mortar and pestle was used but this was time consuming and returned little of the 0.063 mm size due to the salt being ground below the required size. Other methods were tried out, but were not efficient in terms of the salt quantities required.

Salt particle crushing using a hand-held cylindrical piece of steel that was designed to allow compaction of the sample in layers within the confines of the split-former

was found to be most effective. The dimensions of the steel cylinder were 40 mm in diameter and 100 mm in height. The control provided by this hand held cylinder was crucial in obtaining the required salt sizes. For example, using a hammer on the rock salt particles was effective to provide particle sizes of 0.25, 0.5 and 1.0 mm salt particles. However, using the hammer to obtain sizes of 0.063 and 0.125 mm resulted in the pulverisation of the salt to the extent that it passed the 0.063 mm sieve and was of no use to the experiments. The hand held cylinder approach, although time consuming, allowed the production of the 0.063 and 0.125 mm salt.

#### 3.1.4 Salt sieving

The crushed salt was sieved on a sieve stack consisting of the following mesh sizes: 0.063, 0.125, 0.25, 0.5 and 1.0 mm. These sizes were chosen to facilitate analysis in terms of statistical entropy which requires a logarithmic distribution of sizes (Lőrincz et al. 2005). Sieving was performed in accordance with BS 1377-2:1990. A mechanical sieve shaker was used to sieve the sample for 30 minutes with intervals of vigorous hand shaking to unclog the sieve mesh apertures. The quantity of salt sieved during each sieving procedure was kept less than 500 g to enable a more effective sieving of particles. The sieved salt was then heated in the oven to 80° Celsius before being cooled to room temperature and bagged according to size in air tight plastic bags.

#### 3.1.5 Sand preparation

The Leighton Buzzard sand was allowed to soak in water before being rinsed with running water on the mesh of a 0.5 mm sieve. The sand was then oven dried at 80° Celsius in the oven until dry. It was then allowed to cool at room temperature.

#### 3.1.6 Sample density descriptors

Relative density was not necessary for the current study since all samples were initially prepared to achieve a dense packing. Post-dissolution, only the uniform Leighton Buzzard sand common to all dissolution tests remained. The Leighton Buzzard minimum and maximum void ratios ( $e_{min, LB}$  and  $e_{max, LB}$ ) were found to be 0.55 and 0.84, respectively. Therefore post-dissolution void ratios were not difficult

to interpret and were used to describe the volumetric state of the post-dissolution samples throughout the study. The  $e_{max, LB}$  was determined using the gas jar procedure whereby the sand in the gas jar is quickly inverted to achieve loose packing (Head 1982). The  $e_{min, LB}$  was determined by tamping layers of sand in a graduated cylinder before placing a weight on the sand surface and vibrating on a mechanical sieve shaker.

#### 3.1.7 Mineral hardness

The two minerals used are of quite different hardness.<sup>1</sup> On Moh's scale salt is c. 2.5, quartz is 7.0 (Grabco et al. 2002, Gribble & McLean 2003, Vanders & Kerr 1967). In terms of absolute hardness these values correspond to c. 8 and 100. At the outset of the test programme, there was a concern that the relative hardness/softness of the salt particles might allow for more deformation (or fracture) and hence greater volumetric strain under load than would occur for Leighton Buzzard sand alone.

Table 3.1: Mineral hardness values (Grabco et al. 2002, Gribble & McLean 2003, Vanders & Kerr 1967)

Mineral	Chemical formula	Hardness in Mohs scale	Absolute hardness
Salt (Halite)	NaCl	2.0-2.5	c. 8.0
Quartz	SiCO <sub>2</sub>	7.0	100.0

The structural integrity of salt particles was investigated by applying increments of vertical stress to a sample of 1.0 mm salt particles under oedometric conditions with particle-size distributions (PSDs) performed after each stress increment (Figure 3.2). First signs of particle breakage occurred at 880 kPa, with 1.5% passing the 1.0 mm sieve, rising to 2.3% passing at 1760 kPa. This breakage occurred at stresses far in excess of the stresses applied in the test programme (42, 84 and 168 kPa) suggesting that salt particles maintained their structural integrity in the tests prior to the wetting/dissolution stage.

Crushing tests were also performed on sand-salt mixtures to investigate if the presence of harder sand influenced the crushing of salt particles, and also since sand-salt mixtures were representative of the actual dissolution test samples. A mixture including 10% of 1.0 mm salt by weight was loaded in increments. Figure 3.3 shows

---

<sup>1</sup>Hardness is the resistance of a mineral to abrasion or scratching

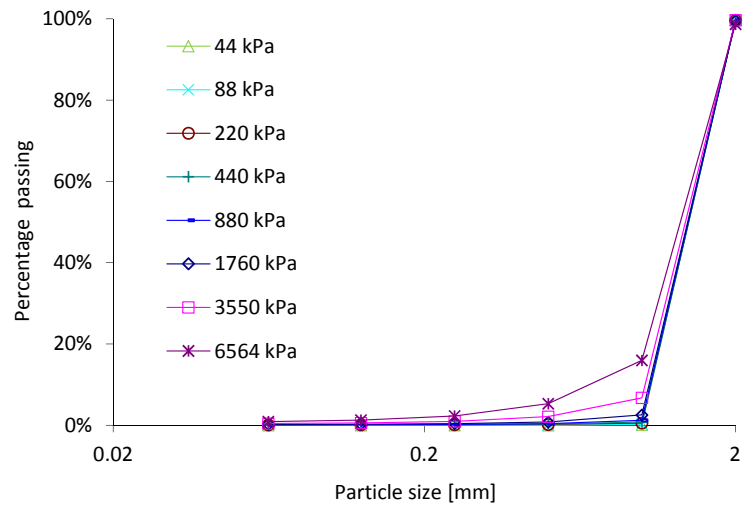


Figure 3.2: PSD of 1.0 mm salt for each increment of vertical stress in the oedometer

that the PSD remained virtually unchanged with loads up to 1760 kPa. The increase in the percentage passing the 1.0 mm sieve after application of the 880 kPa loading was 1.26% while approximately 0.5% of this was accounted for after the initial application of 44 kPa.

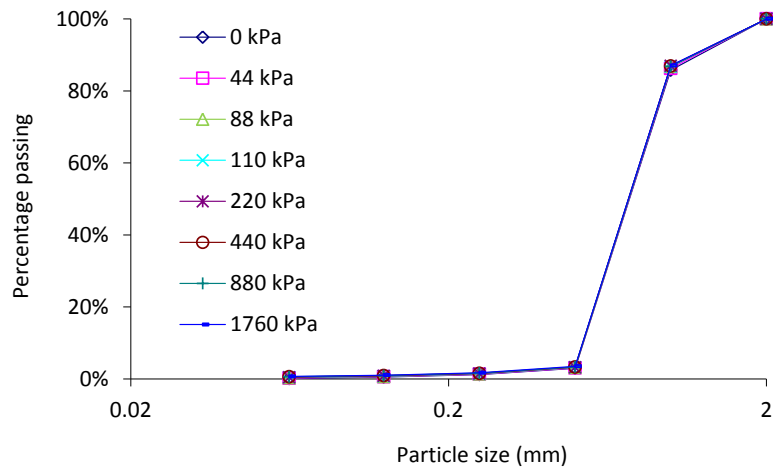


Figure 3.3: PSD with load increments on Leighton Buzzard with 10% by weight of 1.0 mm salt, showing no crushing

A crushing test was also performed on a sand-salt mixture with 10% of 0.5 mm salt particles with only one loading increment of 1760 kPa applied. The pre- and post-loading PSD curves were again indistinguishable with an additional 0.16% passing the 0.5 mm sieve post-loading.

#### 3.1.8 Particle size distributions (PSDs)

For a laboratory programme focussed on particle loss some measure of PSD is important to track the changes occurring with dissolution. The similarity in size of the median diameter of the Leighton Buzzard sand and the salt retained on the 0.5 mm samples of 0.85 and 0.75 mm, respectively, meant that the addition or removal of this particle size resulted in no change to the PSD (Figure 3.4). In dissolution tests where the salt particles are lost, the grading of the soil naturally returns to that of the Leighton Buzzard sand. The minor deviations from the Leighton Buzzard sand PSD with additions of salt of various percentages and sizes perhaps demonstrate the ineffectiveness of the PSD in soil characterization. Furthermore, commonly used grading coefficients derived from the PSD curve generally do not capture the changes of the PSD with the addition of the salt particles for various sizes and percentages as demonstrated in Table 3.2. The  $C_c$  and  $C_u$  grading coefficients remained practically the same for all salt particle size additions of 2 and 5%. The fine-salt sizes (0.063 and 0.125 mm) only began to have an influence at percentages of 10 and 15%. Therefore the  $C_c$  and  $C_u$  grading coefficients proved ineffective due to their incapacity to register the grading changes for the majority of mixtures.

#### 3.1.9 Sand and sand-salt mixture bulk moduli

Bulk moduli for the sample mixtures used in the study were estimated from oedometric tests. Jaky's equation for normally consolidated soil was used to estimate the lateral earth pressure and therefore the mean effective stress imposed during oedometric loading of sand and sand-salt mixtures. Here it is used based on an angle of shearing resistance of  $30^\circ$ . The resulting secant bulk modulus values are presented in Figure 3.5. This presents five loading tests performed to 168 kPa mean effective stress on sand with 15% by weight of salt for 0.063, 0.125, 0.25, 0.5 and 1.0 mm particle sizes. (The full test nomenclature is given in Section 4.1 but is briefly explained here, e.g., a test defined as 1.0-15-168 means 1.0 mm salt at 15% by weight with 168 kPa applied stress. The values of void ratio  $e$  indicated for each sample shown in Figure 3.5 is that at the beginning of loading). The fine-salt particle sizes of 0.063 and 0.125 mm are shown to have lower bulk moduli than coarse sized 0.25, 0.5 and 1.0 mm salt, and there is a clear change in secant bulk modulus according to the stress increments imposed.

Based on Figure 3.5, secant bulk moduli of 2.5, 3.5 and 5.5 MPa were obtained from



### 3. Materials, Apparatus and Procedures

---

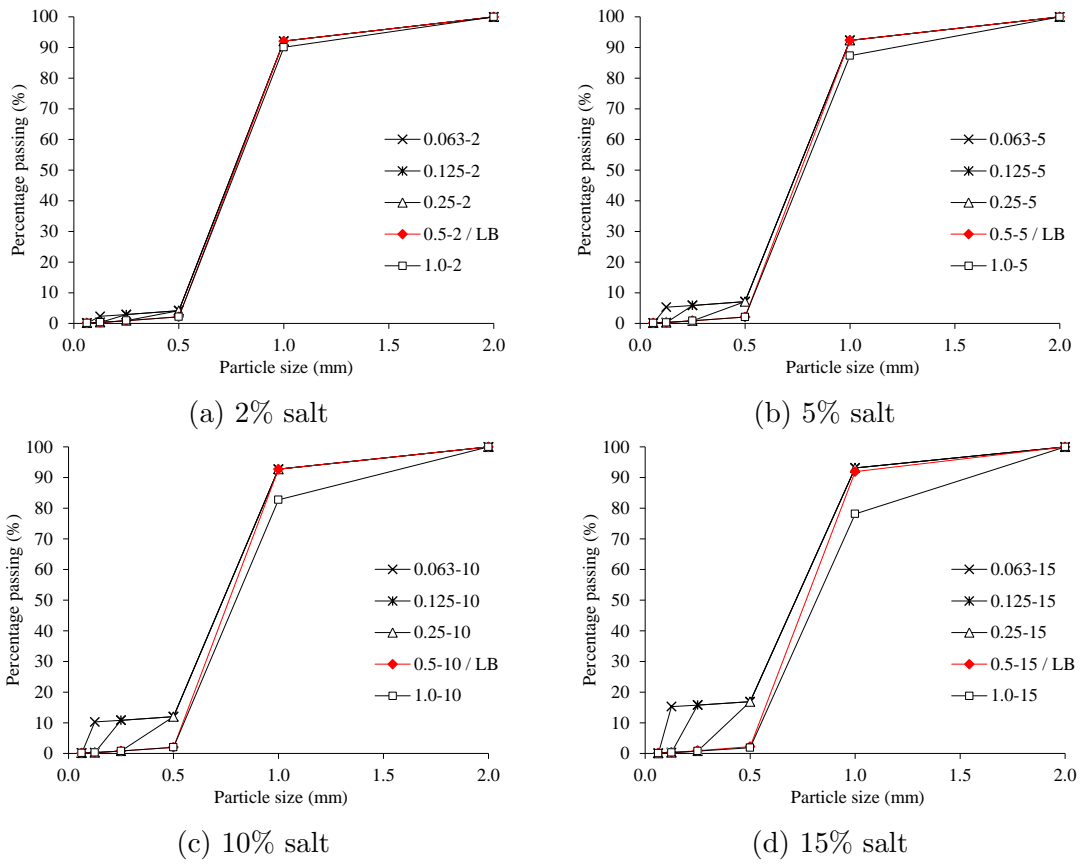


Figure 3.4: Particle size distributions for sand-salt mixtures with respect to salt percentage

Table 3.2: Coefficients of curvature and uniformity of sand salt mixture PSDs

Salt percentage	Salt size	D <sub>10</sub>	D <sub>30</sub>	D <sub>60</sub>	C <sub>c</sub>	C <sub>u</sub>
2%	0.063	0.53	0.65	0.82	1.5	1.0
"	0.125	0.53	0.65	0.82	1.5	1.0
"	0.25	0.53	0.65	0.82	1.5	1.0
"	0.5	0.55	0.66	0.82	1.5	1.0
"	1.0	0.55	0.66	0.83	1.5	1.0
5%	0.063	0.51	0.63	0.81	1.6	1.0
"	0.125	0.51	0.63	0.81	1.6	1.0
"	0.25	0.51	0.63	0.81	1.6	1.0
"	0.5	0.55	0.65	0.82	1.5	0.9
"	1.0	0.54	0.66	0.84	1.6	1.0
10%	0.063	0.13	0.61	0.80	6.2	3.6
"	0.125	0.24	0.61	0.80	3.3	1.9
"	0.25	0.45	0.61	0.80	1.8	1.0
"	0.5	0.55	0.65	0.82	1.5	0.9
"	1.0	0.55	0.67	0.86	1.6	0.9
15%	0.063	0.1	0.58	0.78	7.8	4.3
"	0.125	0.2	0.58	0.78	3.9	2.2
"	0.25	0.39	0.58	0.78	2.0	1.0
"	0.5	0.54	0.65	0.83	1.5	0.9
"	1.0	0.55	0.68	0.88	1.6	1.0

### 3. Materials, Apparatus and Procedures

the fine-sized salt samples for stress applications of 42, 84 and 168 kPa, respectively. Higher values of 4.5, 6.5 and 9 MPa were obtained for the coarse-sized salt samples for stress applications of 42, 84 and 168 kPa, respectively.

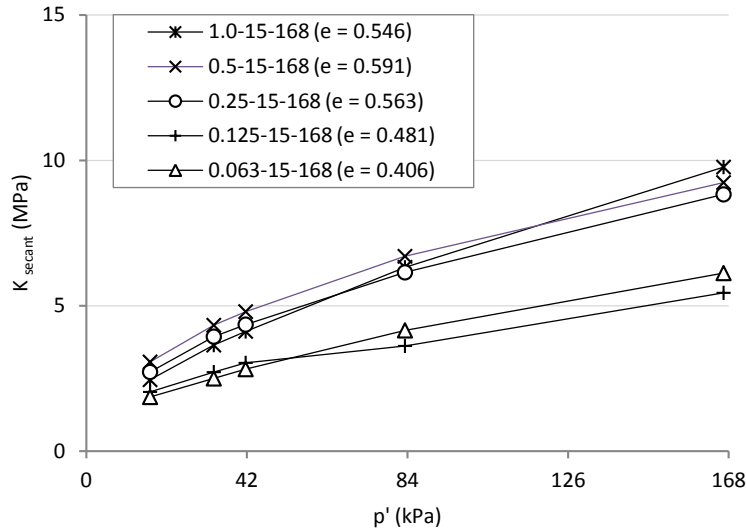


Figure 3.5: Secant bulk modulus for sand-salt mixtures

Secant bulk moduli values based on oedometric tests performed on Leighton Buzzard were found to be 7, 9 & 14 MPa for applications of 42, 84 and 168 kPa, respectively. Stress applications of 42 and 84 kPa yielded low secant bulk moduli values. However, the tangent bulk modulus based on the 84-168 kPa stress increment yielded a value of 28 MPa, a value much closer to that expected for a quartzitic sand.

Table 3.3 summarises the bulk moduli applied to Leighton Buzzard, fine-sized salt and coarse-sized salt triaxial samples.

Table 3.3: Bulk moduli for 15% by weight of fine- and coarse-sized salt samples, and Leighton Buzzard sand for the applied pressure ranges

Pressure range (kPa)	Bulk modulus (MPa)		
	Fine-salt/sand	Coarse-salt/sand	Leighton Buzzard
0-42	2.5	4.5	7.0
0-84	3.5	6.5	9.0
0-168	5.5	9.0	14.0

## 3.2 Triaxial apparatus

Triaxial dissolution tests are a follow-on from oedometer dissolution tests performed at an earlier stage of this research program, and on which the triaxial experimental set-up is based. The oedometer experiments are described in McDougall et al. (2013). The original triaxial system was supplied by ELE International with a schematic presented in Figure 3.6. The system conformed with the requirements of BS 1377:1990 for standard triaxial tests and a detailed description of such an apparatus and associated test procedures is given by Head (1986) and many standard soil mechanics textbooks. The original triaxial system consisted of:

- Triaxial cell (100 mm)
- Submersible load cell
- Axial strain transducer
- Pressure transducers (3 no.)
- Digital Tritest 50 load frame
- Pneumatic compressor
- Pressure control system consisting of pressure regulators with stepper motor control (2 no.) and bladder-type air\water pressure assembly (2 no.)
- Volume change transducer
- De-aired water apparatus
- Stress Path Control System with Autonomous Data Acquisition Unit (ADU)
- (TriPath) Tritest 50 Stress Path software

### 3.2.1 Triaxial modifications overview

The key modifications to the original triaxial system to allow the performance of dissolution tests and monitor stiffness before, during and after dissolution are summarised here:

### 3. Materials, Apparatus and Procedures

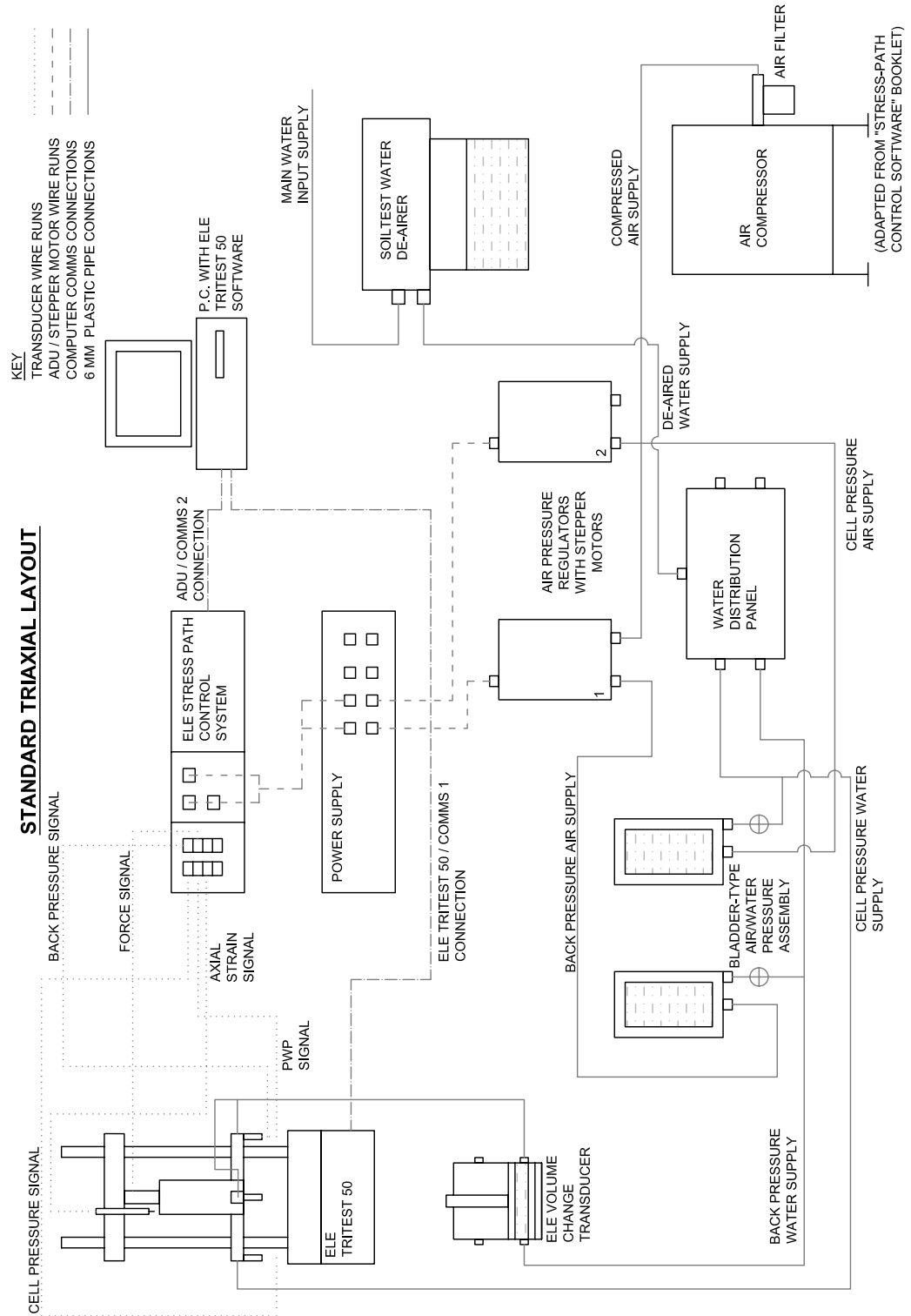


Figure 3.6: Standard triaxial apparatus layout

### 3. Materials, Apparatus and Procedures

---

- Custom-built access ring deployed with additional ports for drainage and instrumentation wiring
- Bender elements installed
- Pore-water circulation system installed
- Pressure control system replaced
- Customisation of sample preparation accessories
- Test control and data acquisition

The modified triaxial apparatus schematic and equipment layout are shown in Figures 3.7 and 3.8, respectively.

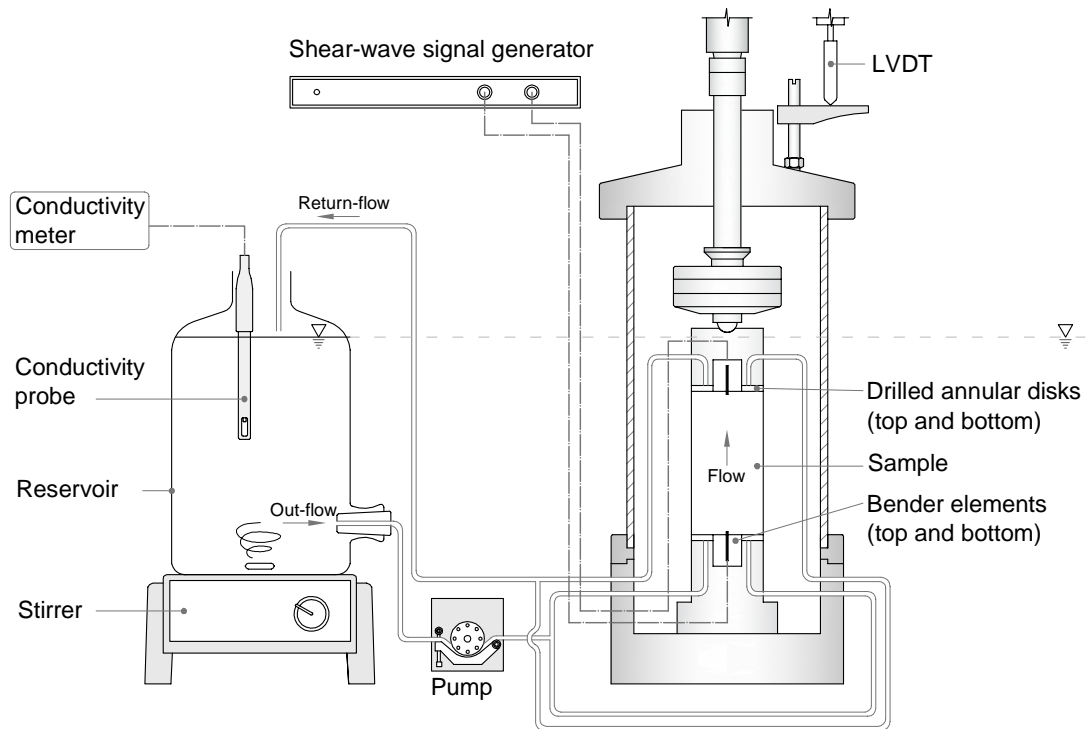


Figure 3.7: Modified triaxial apparatus schematic

#### Custom-built access ring

The access ring acted as an extension ring to provide additional height to allow the inclusion of a 100 mm x 50 mm sample, bender element inserts, and additional ports

### 3. Materials, Apparatus and Procedures

#### TRIAxIAL/ BES LAYOUT

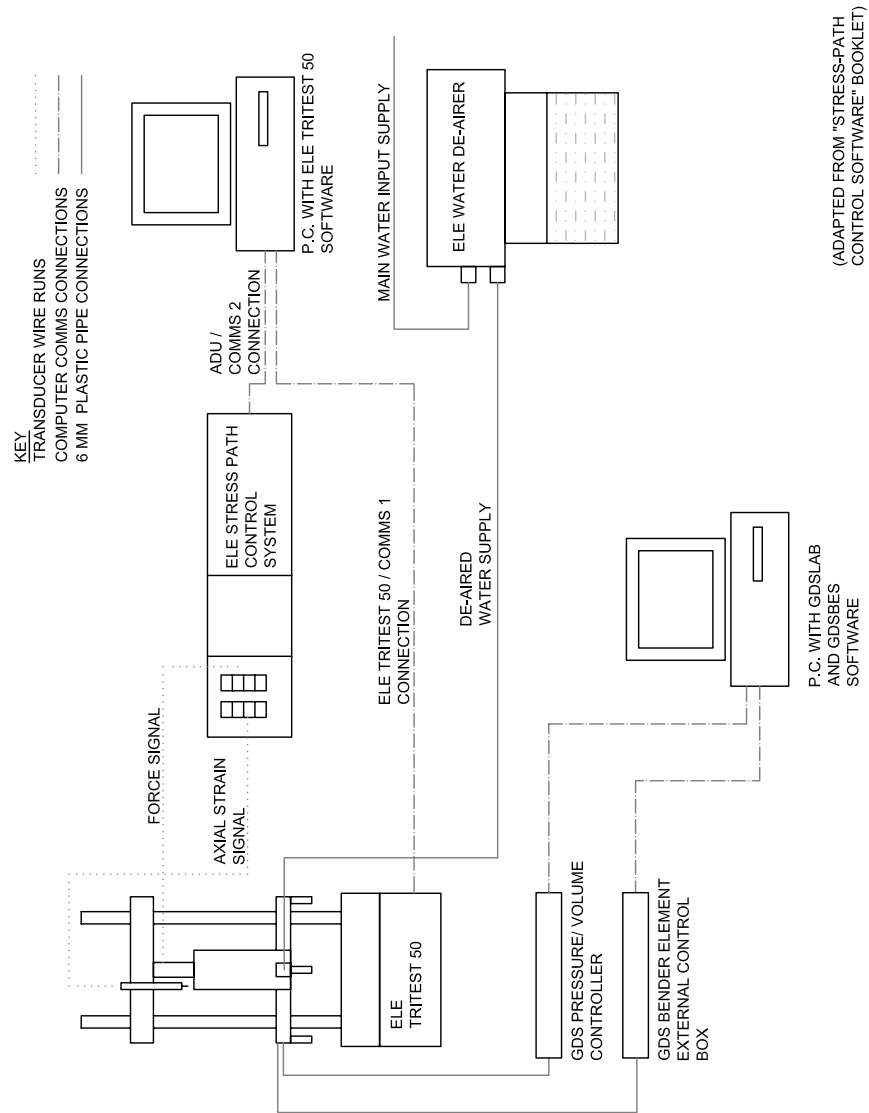


Figure 3.8: Modified triaxial apparatus layout

### 3. Materials, Apparatus and Procedures

---

(Figure 3.9). The pore-fluid circulation system required four ports while the bender elements required two ports for electrical wiring.



Figure 3.9: GDS access ring

#### **Bender elements**

A customised base-pedestal and top-cap with bender element inserts were supplied by GDS Instruments Limited<sup>®</sup> to fit the existing the ELE triaxial cell allowing the testing of 50 mm  $\varnothing$  samples. The customised base-pedestal and top-cap housed the bender elements, bender element signal wiring and two drainage ports on the top and base to facilitate the pore-water circulation system (see Figure 3.7). The base-pedestal and top-cap were originally equipped with annular porous disks to



accommodate the bender elements but these were replaced with drilled annular HDPE disks for dissolution tests as discussed before.

#### **Pore-water circulation system**

A circulation system for the dissolution stage replaced the standard pore-water pressure function and consisted of a reservoir, stirrer and peristaltic pump and custom triaxial access ring (see Figure 3.7). A standalone pressure/volume controller replaced the original pneumatic pressure control and volume change transducer to improve volume measure accuracy (resolution:  $\pm 0.001 \text{ cm}^3$ ).

The additional drainage tubing facilitated complete saturation and therefore dissolution of salt samples. The internal tubing used in the triaxial cell was Legris semi-rigid polyamide. The bore of the tubing within the triaxial cell was 0.09 inch  $\phi$ . A second drainage path allowed more uniform flow through the sample and prevented pressure build ups associated with air locking. The water-level was maintained at a height to allow for (gravity-driven) permeation of water through the sample (see Figure 3.7), by adjusting the height of the reservoir.

#### **Pore-water pressure control**

The ELE stress-path pore-water pressure control of the original triaxial apparatus was not used for the following reasons:

- Samples were prepared and isotropically confined in the dry state to prevent dissolution of salt particles prior to the dissolution stage
- The dissolution stage required the circulation of the pore-water

Therefore the cell water was required to measure sample volume changes during testing. Sample volume measurement procedures are detailed in Section 3.5.

#### **Cell pressure control**

Initially, in an effort to reduce costs, attempts were made to use the existing ELE stress-path cell pressure control and the ELE volume change apparatus for the research programme. The cell pressure control was adequate; however, the volume

change apparatus was found to be insufficiently accurate. The change in direction of travel required for the volume change apparatus to continually monitor volume change showed poor compliance. A GDS standalone pressure-controller with a volume measurement function was acquired to replace both the ELE cell pressure system and ELE volume change transducer. For all stages during sample testing the sample pore-water pressure line was open to atmosphere.

#### **3.2.2 Customised parts/modifications for sample preparation**

##### **Split-former seating ring**

The split-former seating ring (Figure 3.10) was necessary to provide a stable base for the split-former which otherwise would be resting on the wiring associated with the bender elements and the drainage lines entering the base pedestal when preparing the sample in-situ. The height of the split-former seating ring was chosen to allow a sample height of 100 mm. The split-former seating ring was drilled to coincide with the existing holding screws securing the base pedestal to the base of the cell to allow it also to be secured in place. It was manufactured from HDPE and made in two halves to allow placement around the existing base pedestal and sections were cut out to accommodate the wiring associated with the bender elements and drainage lines when in position. The sections that were cut out were sufficient in size to allow tightening of drainage fittings to the base pedestal without disassembly of the pedestal.

##### **Modified split-former**

Three slots were cut at the base to allow for the two drainage lines and electric cable entering the base pedestal. A rebate was cored at the bottom inner surface of the split-former to allow space for the o-rings to secure the membrane to the bottom pedestal. The modified split-former is shown in Figure 3.11.

##### **Drilled annular disc**

To prevent the blockages discussed earlier a HDPE drilled annular disc was devised to replace the original porous annular stone. The HDPE annular disc was drilled

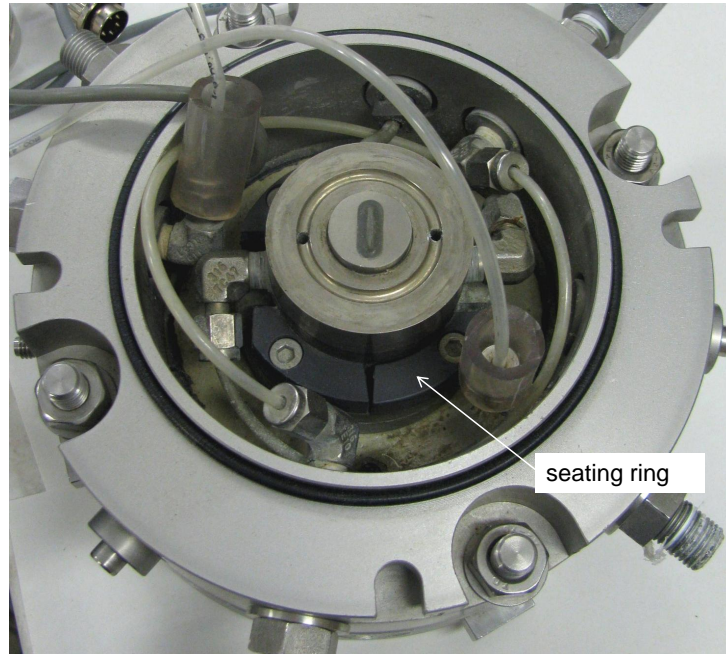


Figure 3.10: Split-former seating ring in triaxial cell

with a 1 mm drill bit as shown in Figure 3.12.

#### 3.2.3 Triaxial test control and data acquisition

The original triaxial system was controlled by TriPath software. This allowed the control of the Tritest50 loading frame and the cell and back pressures. The TriPath software also provided real-time readings of axial displacement, cell pressure, back pressure, pore-water pressure and axial load. Data acquisition was available but had a limitation in that only 80 readings per data-logging session were permissible.

For the modified triaxial system the TriPath software controlled the Tritest loading frame only. As stated, the original cell pressure, back pressure and pore water pressure functions of the ELE system were not used. Therefore the TriPath software was used to monitor and perform data logging on axial force and axial displacement readings only. The cell pressure was controlled by a GDS system comprising GDSLAB control and data acquisition software and a GDS pressure controller. The GDSLAB software offered continual data logging capabilities during initial cell pressure application, dissolution and shearing stages together with real time cell pressure and volume change measurements presented graphically.



Figure 3.11: Modified split-former

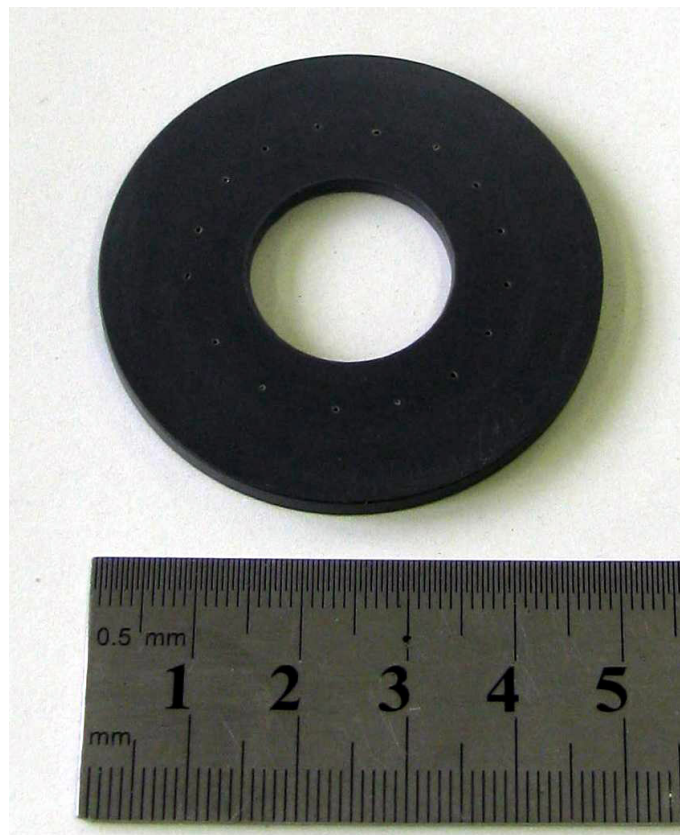


Figure 3.12: Drilled annular disc (HDPE)

### 3.2.4 Accuracy and resolution of transducers

The instrumentation used for the measurement of stress and strain in the triaxial apparatus are presented in Table 3.4 with details on the accuracy, stability and resolution of the transducers as provided by the manufacturers.

Transducer Type	Capacity	Accuracy	Stability	Resolution
Load Cell	±5.0 kN	±0.016 kN	0.002 kN	-
Pressure Transducer	1.0 MPa	±2.5 kPa	-	1.0 kPa
External Displacement	50 mm	±0.052 mm	0.005 mm	-
Volume Gauge	200 cm <sup>3</sup>	±0.8 cm <sup>3</sup>	-	0.001 cm <sup>3</sup>

Table 3.4: Summary of capacity, accuracy, stability and resolution of transducers employed in the triaxial stress path cell

### 3.2.5 Equipment inventory

- Specially modified GDS access ring
- GDS Bender Element system
- Legris nylon tubing ( $\frac{1}{8}$  inch diameter, clear (Part no. 1094P53 00))
- Swagelok: SS ferrule sets for connection to 4 no.  $\frac{1}{8}$  inch Swagelok fittings (Part no. SS-200-SET)
- Silex: 4.8 ID (mm) x 1.6 Wall (mm) quality silicone tubing
- Matlow peristaltic pump
- GDS feedthrough system (4 no.)
- Membrane placing tool
- Rubber membrane (50 mm diameter)
- Membrane sealing rings (50 mm diameter)
- Riffle box (7 mm slots complete with 3 no. receptacles)
- Two-way split former (50 mm diameter)

### **3.3 Equipment development, commissioning and procedures**

This section gives an account of the planned equipment development, difficulties encountered in commissioning and other technical failures. Key stages involved in equipment development and commissioning included:

- Scoping the modifications required for the dissolution testing procedure
- Apparatus modification
- Sourcing of equipment and accessories
- Modification of accessories
- Calibration of apparatus
- Bender element testing implementation and experimentation
- Refinement of sample preparation technique

#### **3.3.1 Cell volume change (a) load ram displacement**

The volume of cell water displaced by the ram was of importance to the calculation of sample volume change during shear. A calibration test was performed at the end of a shearing test with cell pressure maintained at 42 kPa. This cell pressure was maintained throughout the calibration test. The ram was moved away from the sample so that its subsequent displacements would not affect sample volume change. Therefore measured volume changes were associated with ram displacement only. The ram displacement was measured by the external axial displacement LVDT while the volume change was measured by the GDS pressure controller. The ram was pushed into the cell at 5 mm increments over a total of 30 mm and the displaced cell water volume was recorded. The ram was then withdrawn from the cell again at 5 mm increments over 30 mm with cell water volume recorded. The results of measured volume change against ram displacement are presented in Figure 3.13, showing good agreement.

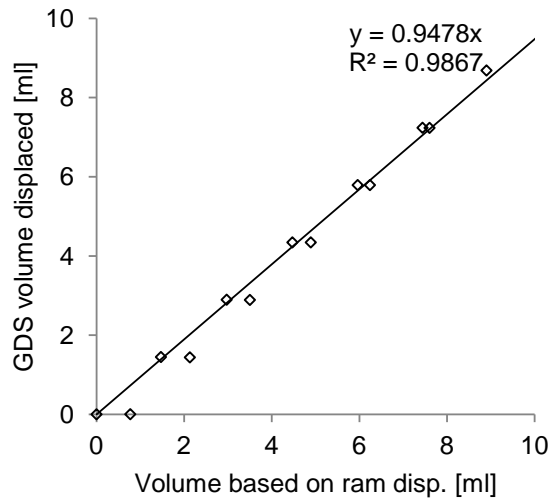


Figure 3.13: Ram volume calibration

### 3.3.2 Cell volume change (b) distortion due to cell pressure

Cell characterisation was performed to assess the cell water volume changes that occurred with cell pressure application with an incompressible dummy sample in place of a soil sample. The purpose of the test was to quantify the immediate and long term cell water volume changes with the application of cell pressure from 0 kPa to the cell pressures of 42, 84 and 168 kPa applied in the testing programme, and independent of sample volume changes. The cell water volume changes as measured by the GDS pressure controller are presented in Figure 3.14.

Four tests were performed, one for each of the 42, 84 and 168 kPa cell pressures applied in the testing programme, and a repeat of the 42 kPa test that appeared to be subject to leakage due to the constant rate of volume change occurring over 4 days and at a rate higher than any of the other 3 tests. Each test was performed over approximately 1 week.

Figure 3.14 demonstrates that significant cell volume changes associated with cell pressure application occurred within 1 day. Hereafter, 2nd order rates of volume change accounted for minimal volume changes during the relatively short time of 2 hours required for the dissolution stage, and 80 minutes for the dissolution stage. Furthermore volume changes during these stages dwarfed any volume changes associated with cell volume equilibration post cell pressure application. Figure 3.14 prompted the adoption of a 24-hour cell equilibration period post cell pressure application prior to performing testing stages that required the cell water volume changes



for the monitoring of sample volume change.

Further tests were done to assess the consistency of the cell volume change with pressure application by cycling the cell pressure between 0, 42, 84 & 168 kPa and are presented in Figure 3.15. The test was performed after the last long term 168 kPa volume change assessment.

Figure 3.15 indicates the consistency of the immediate cell volume changes accompanying cell pressure change. Also, it should be noted that the volume change associated with the 168 kPa cycles return to the volume measurement achieved after a period of 6 days under pressure. Volume changes with cell pressure changes of 0-42 kPa, 0-84 kPa and 0-168 kPa were 1.1, 1.9 and 3.4 ml respectively.

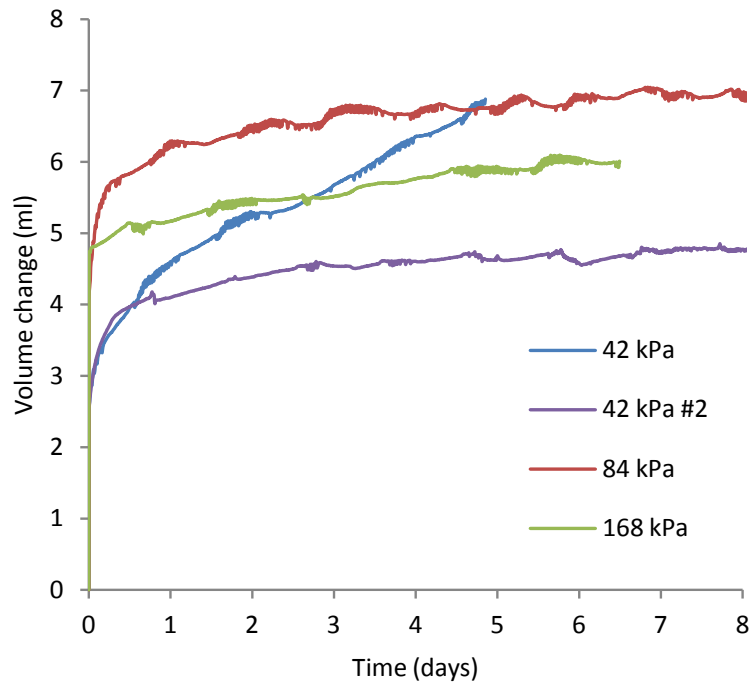


Figure 3.14: Cell volume change with pressure application

#### 3.3.3 Cell volume change (c) membrane penetration

An experimental approach to determine membrane penetration was outwith the scope of the current research, especially since pore water volume or local strain measurements were unavailable. Membrane penetration corrections by Nicholson et al. (1993) were assessed for application to samples in the current study. Firstly, membrane penetration corrections for two real sands comparable in grading to the

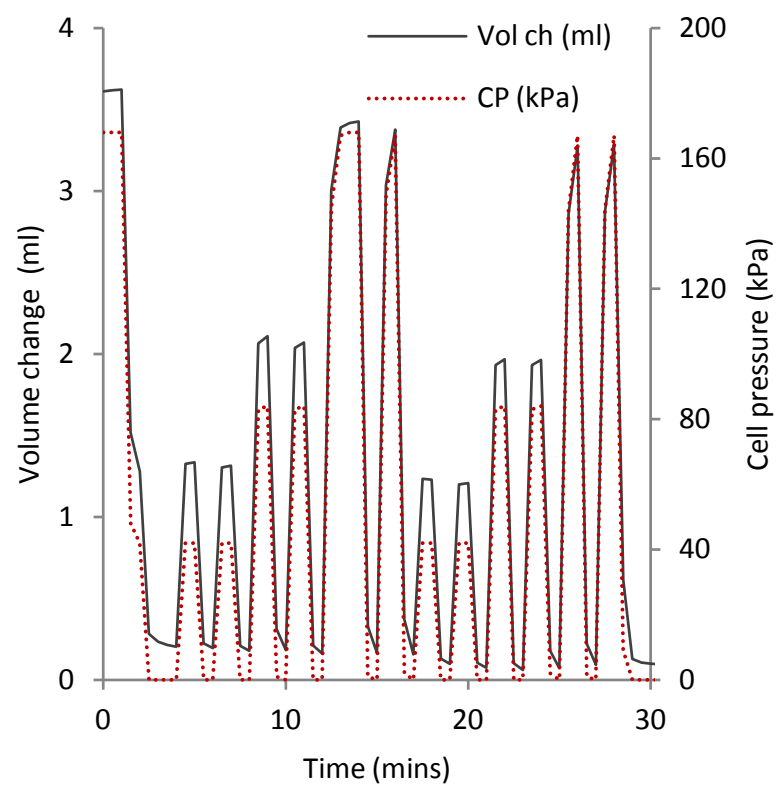


Figure 3.15: Cell volume change with cell pressure cycling

samples in the current study were assessed for comparison with results from the generalised equation proposed by Nicholson et al. (1993). The generalised equation was not immediately accepted since it relied solely on the  $D_{20}$  of the soil and, as shown earlier, grading coefficients did not sufficiently detect grading differences between samples in this study.

Table 3.5 presents the grading characteristics for the two sandy soils, one poorly-graded and one well-graded, together with their respective normalised membrane penetration  $S$  defined as:

$$S = \frac{\Delta v_m}{\Delta \log \sigma'_3} \text{ [mm}/\Delta \log \sigma'_3] \quad (3.1)$$

where  $v_m$  is the unit membrane penetration in mm. The Ottawa 20-30 sample in Table 3.5 is closest in grading to the coarse-sized salt samples with 0.25, 0.5, 1.0 mm salt at 15% by weight in the current study (see Table 3.6). Therefore  $S = 0.093 \text{ mm}/\Delta \log \sigma'_3$  was applied. Based on Equation 3.1, effective cell pressures of 42, 84 and 168 kPa resulted in  $v_m$  values of 0.151, 0.179 and 0.207 mm, respectively. Then, applying this to the sample surface area in contact with the membrane, membrane penetrations of 2.36, 2.8 and 3.25 cm<sup>3</sup> were found based on cell pressure applications of 0-42, 0-84 and 0-168 kPa, respectively.

Similarly the ‘well graded 2’ sand is closest in grading to the fine-sized 0.063 mm salt samples. Therefore  $S = 0.018 \text{ mm}/\Delta \log \sigma'_3$  was applied resulting in membrane penetration predictions of 0.046, 0.054 and 0.063 cm<sup>3</sup> for pressure applications of 0-42, 0-84 and 0-168 kPa, respectively. The difference in membrane penetration with respect to sample grading is apparent, with the well graded sample resulting in approximately 1/3 that of the uniform/poorly graded sample based on  $S$  values provided in Table 3.5.

Nicholson et al. (1993) proposed the following generalised equation to determine  $S$ :

$$S = 0.0019 + 0.0095 x - (0.0000157 x^2) \text{ [ml}/\text{cm}^2] \quad (3.2)$$

where  $x$  is the  $D_{20}$  grain size (in mm) of a soil. Table 3.7 presents the associated total membrane penetrations for the sample gradings used in the current research and the effective cell pressures applied. These were not significantly different to those calculated using normalised membrane penetrations for the specific sand types, and were therefore used to estimate membrane penetration in the current study.

### 3. Materials, Apparatus and Procedures

---

Table 3.5: Characteristics of sandy soils tested for membrane compliance amplitude (Nicholson et al. 1993)

Soil name <sup>a</sup>	Unified soil classification system	D <sub>10</sub> (mm)	D <sub>20</sub> (mm)	D <sub>50</sub> (mm)	S <sup>b</sup> (mm/ $\Delta \log \sigma'_3$ )
Ottawa 20-30	SP	0.605	0.63	0.72	0.093
Well graded 2	SW	0.13	0.2	0.6	0.018

<sup>a</sup> Well graded 2 : Monterey sands with some gravel and 5% silt.

<sup>b</sup> Change in volume per unit membrane area per log-cycle change in effective confining stress.

Table 3.6: Grading characteristics of sand-salt mixtures

Salt [%]	Salt [mm]	D <sub>10</sub>	D <sub>20</sub>	D <sub>50</sub>	C <sub>c</sub>	C <sub>u</sub>
15	0.063	0.1	0.52	0.72	7.2	3.8
	0.25	0.39	0.52	0.72	1.8	1.0
	0.5	0.54	0.60	0.77	1.4	0.9
	1.0	0.55	0.62	0.82	1.5	0.9

Table 3.7: Membrane penetration for sand-salt mixtures based on D<sub>20</sub> (Nicholson et al. (1993))

15 % by salt tests	S	M.P. [ml]	M.P. [ml] with $\sigma'_3$
Salt size [mm]	D <sub>20</sub>	ml/ cm <sup>2</sup>	ml/ $\Delta \log \sigma'_3$
0.063	0.52	0.00684	1.073
0.25	0.52	0.00684	1.073
0.5	0.60	0.00759	1.192
1	0.62	0.00778	1.222

#### 3.3.4 Difficulties encountered in commissioning

Leakage was a recurring problem during the commissioning of the triaxial dissolution test program. This included leakage of cell water out of the cell and also the leakage of cell water into the sample.

In standard triaxial testing where the sample pore water is used to measure sample volume change, cell water losses that do not impinge on the ability of the system to maintain the appropriate cell pressure may be tolerated. However, leakage from the cell was unacceptable as part of the dissolution triaxial procedure since the cell water was used to measure sample volume change. Therefore it was essential to ensure a watertight triaxial cell. Leakage of cell water out of the cell occurred due to a poor seal between the screw cap and cell top. This was solved by introducing new fiber washers that had been soaked in vacuum grease. Leakage still sometimes occurred when applying the cell pressure but this could be stopped by further tightening the screw cap with a vice-grips.

Leakage of cell water into the sample is never acceptable and in the current study frequently resulted in failed tests in the early stages. This occurred in the following ways:

The 37.5 mm o-rings ensured a watertight seal and were used after numerous attempts to ensure a watertight seal using purposely manufactured o-rings for 50 mm diameter samples from ELE<sup>®</sup>. The cause for leakage was not known until the 37.5 mm o-rings were used but a number of approaches were attempted prior to finding this solution. Approaches included:

- Changing the o-ring/ membrane set-up configuration
- Using silicon vacuum grease to improve the seal between the membrane and the base pedestal at o-ring locations.

Leakage also occurred at the insufficiently tightened Legris fittings at the base of the apparatus. Tightening was hindered by the seating-ring (see Section 3.2.2), electrical wiring and drainage lines. This issue was solved by increasing the size of the cuts in the o-ring to facilitate greater flexibility in the tightening of fittings.

Lastly, examination of membranes after failed tests occasionally showed weaknesses or pinholes. Subsequently, membranes were scrutinised thoroughly prior to use and

were painted with liquid latex to strengthen. A new batch of rubber membranes were of higher quality and the liquid latex approach was stopped.

#### 3.3.5 Technical failures

This section gives an account of technical failures encountered during the commissioning of apparatus and subsequently during the testing program. Troubleshooting these issues took considerable time during the project:

- Drifting load readings in the submersible load cell
- Erratic and erroneous load readings from the submersible load cell after a period of operation
- Leakage of water from the sleeve housing for the submersible load transducer ram in the triaxial cell head
- Replacement of inaccurate or malfunctioning equipment, such as the volume change apparatus and pressure control system

#### Submersible load cell difficulties

During the commissioning of the triaxial apparatus it was found that the submersible load cell readings were subject to drift. The load cell was subjected to cell pressures of 42 kPa and 84 kPa to assess the possible drift occurring during testing procedures. Figure 3.16 demonstrates the considerable drift occurring over a 5 day period for applied cell pressures of 42 and 84 kPa. As can be seen, the drift occurring over the duration of 80 minutes required for the shearing stage was relatively little. Only after 3 days drift became significant.

Subsequently, leakage of cell water was detected at the sleeve housing for the submersible load cell ram at the top of the cell head. This was not permissible as the cell water was required for sample volume change measurement. A new sleeve was fitted by ELE. Lastly the load cell began to produce over-range readings meaning that the load cell could no longer be used. ELE supplied a cell that was incompatible with the ELE data acquisition unit and ultimately were unable to provide a replacement.

Finally, a Stalc 9 (5 kN) load cell was sourced from Applied Measurements Limited for the latter part of the testing program (Test nos. 16-26) resulting in no further issues relating to drift.

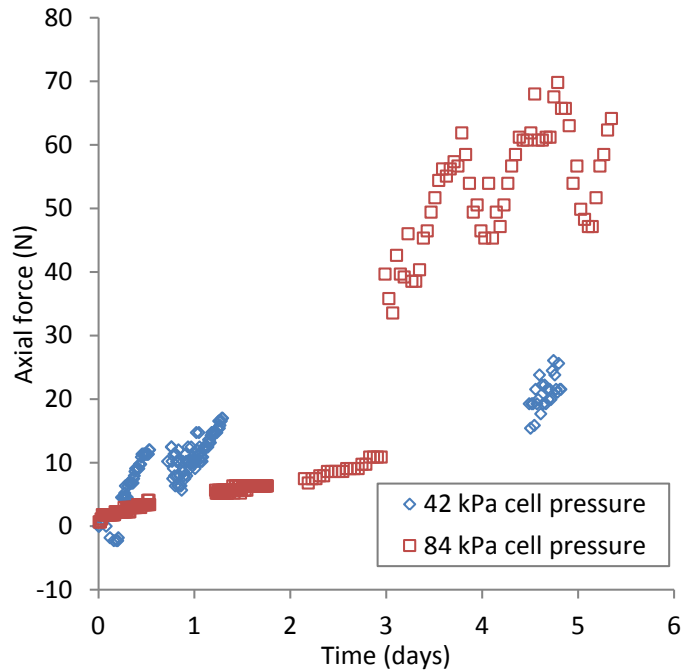


Figure 3.16: Axial force drift monitoring under two cell pressures

The duration over which the submersible load cell presented difficulties was  $33 \frac{1}{2}$  months. This period of time was not lost completely but was used for the overall commissioning of the cell.

## 3.4 Triaxial test procedures including dissolution

The triaxial test procedures outlined in this section allow the performance of the following key stages in dissolution tests:

1. Compression (Dry)
2. Dissolution
3. Shearing

#### 3.4.1 Cell preparation

1. The Legris<sup>®</sup> tubing providing sample pore-fluid circulation within the cell was rinsed out by applying the nozzle of a wash bottle to the drainage ports of the top and base-pedestal. The water was allowed to discharge at the external ports of the triaxial cell to a beaker thereby removing sand particles that may have lodged in the lines during the disassembly of the previous test. Free drainage at the ports indicated clear drainage lines. In the case of poor flow, copper wire was inserted at the ports to dislodge materials together with flushing using a wash bottle until flow was satisfactory.
2. Residual fluid in the Legris<sup>®</sup> tubing and associated drainage system after the rinsing process was blown out by applying the nozzle of an empty wash bottle to the sample drainage ports of the base-pedestal and squeezing the bottle to blow the residual fluid contents of the drainage lines to the external ports of the triaxial cell where it was collected with a beaker. The top-cap and base-pedestal of the sample were dried with paper towel in advance of sample preparation.
3. The GDS<sup>®</sup> pressure-controller was disconnected from the triaxial cell and emptied. It was refilled by submerging the water supply tube in a beaker of de-aired water with the controller emptied and refilled to its extremities of travel a number of times to ensure no air bubbles were present in the apparatus in accordance with the guidelines issued by the suppliers.
4. On reconnection of the pressure controller, the base of the cell was filled with de-aired water to a level that did not interfere with sample preparation. The pressure controller was used to expel any air in the port connection to the triaxial base by selecting the fast emptying option. The filling of the base of the cell with de-aired water prevented cell seals from drying during sample preparation stage thereby preventing the adhering of air bubbles to the seals at the base of the cell during filling. Additionally any bubbles visible at this stage could be removed by agitation prior to sample placement thereby removing the need to agitate the cell post sample set-up.
5. The acrylic cell body and cell head were maintained in a wet condition throughout cell and sample preparation by preventing inner surfaces from drying. This is of importance when using cell water for sample volume measurement. Incoming cell water was found to adhere to wet internal surfaces more readily thereby preventing or restricting air bubble adhesion. Acrylic water absorption



was limited by keeping the cell filled with water when not in use as suggested by Wheeler (1988). The cell water was drained prior to sample set-up with efforts made to ensure internal surfaces did not dry completely to limit air-bubble adherence to internal cell surfaces, especially at cell seals and fittings. The apparatus was then primed by applying the test cell-pressure for 24 hours prior to the dissolution test stage to allow any changes in volume change measurements due to the effects detailed earlier reach an acceptable value.

#### 3.4.2 Sample preparation

1. The triaxial cell was seated on the loading frame for sample preparation to avoid disturbance caused by relocation post sample preparation.
2. The HDPE drilled annular disk was placed on the base-pedestal.
3. Silicon vacuum grease was applied around the base-pedestal using a finger in advance of the placement of the membrane and o-rings to help ensure a watertight seal.
4. The rubber membrane was soaked in de-aired water overnight prior to use in accordance with BS 1377-8:1990. The membrane was allowed to become surface dry prior to use to prevent premature dissolution of the salt particles. A paper towel was threaded through the inside of the membrane to facilitate the drying of the inner surfaces and the membrane was left to air-dry for a period of approximately 1 hour or until surface dry.
5. It proved imperative to scrutinize the membrane for weaknesses prior to use by stretching it and holding it to a light source to identify any imperfections. The membrane was cut to a length of 150 mm to prevent excess membrane gathering at the drainage and wiring outlets from the top-cap.
6. The membrane was placed on the base-pedestal and verticality was ensured before the placing of the o-rings.
7. Using an o-ring placer two 37.5 mm o-rings were placed over the membrane on the base-pedestal.
8. A two-part split sample former was placed ensuring the membrane was not snagged during closure of the sample former. This was achieved by holding the membrane at the top and twisting once before closing the former. The

### 3. Materials, Apparatus and Procedures

---

split former was then fastened together using a jubilee clip. Two 37.5 mm o-rings were placed over the top of the former to allow them to be rolled onto the top-cap when in position and with the membrane in place.

9. The membrane was carefully folded over the former at the top ensuring no creases formed on the inner surface of the former. Suction was applied to the sample former through a vacuum pump applying a pressure of 6.7 kPa to draw the membrane against the inside wall of the former. Sample preparation could then commence.
10. Samples were prepared dry to prevent the dissolution of salt particles prior to the dissolution stage. The dry sand-salt particles were mixed and riffled into eight parts. Each part was deposited in the sample-former using a funnel to minimise drop height and avoid segregation of sand and salt particles, especially in samples with 0.063 mm salt. Each part was compacted by placing a steel cylindrical weight into the sample former before vibrating it using an electric engraver for 10 seconds to produce a medium-dense packing. Any remainder of the sand-salt sample was weighed. The salt component from this was removed by placing it in a beaker of water and decanting the water until the conductivity of the water was negligible as indicated by a hand-held conductivity meter. The sand was then oven dried to determine the weight of the sand and salt components. This allowed the calculation of the exact weight and proportions of each sample mixture.
11. The HDPE annular disk was placed on the top flattened surface of the sample mixture and gently pressed to ensure uniform contact and a smooth sample surface. The bender element insert was placed in the annular void of the disk ensuring to align top and bottom bender elements correctly. The GDS<sup>®</sup> bender element alignment was correct when the electrical wiring from the top-cap and base-pedestal were vertically aligned. Alignment of top-cap and base-pedestal was facilitated by etching a vertical line on the split former as a guide.
12. The membrane was unfolded from the split former onto the top-cap with the membrane secured by rolling the two o-rings previously placed on top of the former to the top-cap of the sample.
13. Three of four external drainage valves located on the access ring were closed. The vacuum pressure tube was disconnected from the sample former and applied to the remaining open drainage port. A vacuum pressure of 6.7 kPa was

applied to maintain the form of the sample during the removal of the sample former and subsequent cell filling.

14. The jubilee clip fastening was removed and the former was carefully prised apart using a screwdriver. This was facilitated by two slots that were machined on the external surface along the line of sample former separation. Prior to modification a sharp object such as a knife was used to prise the former apart putting the membrane in danger of being perforated.
15. Sample dimensions were measured and recorded.

#### **3.4.3 Cell pressure application**

The cell pressures applied to the dry sample were chosen to allow comparison with previously conducted oedometric dissolution tests. Oedometric tests consisted of 40 salt dissolution tests performed at two vertical stresses of 62 and 250 kPa, with salt particle sizes of 0.063, 0.125, 0.25, 0.5 and 1.0 mm at percentage mass additions of 2, 5, 10 and 15 %.

1. Prior to cell placement adequate clearance was ensured between the top of the sample and the crosshead of the loading frame to allow the cell to be placed without damaging the sample.
2. The cell o-ring seal and reveal were cleaned with a cloth to ensure an effective seal between the cell and the cell base.
3. The submersible load cell was fixed in position at an appropriate height using a timber spacer to prevent damage of the sample during cell placement. The timber spacer was placed between the top-cap of the cell and the screw at the top of the piston forming the load cell.
4. The water de-aerer was allowed to run for a minimum of 15 minutes prior to cell filling to reduce the dissolved oxygen content.
5. The cell was filled with de-aired water. Any visible air bubbles adhering to the inner surfaces of the cell were removed by lowering the level of the cell water and refilling until air bubbles were dislodged and removed. Air bubbles accumulating at the top of the cell after filling were removed by tilting the cell slightly to allow their exit through the open screw cap port.

6. The submersible load cell was lowered to make contact with the top of the sample and fixed in position before the cell was closed at the screw cap. Contact was verified visually and through 1-2 Newtons of load registered through the load cell on the TriPath software visual interface. The TriPath software displayed the axial force and axial displacement allowing written records to be noted.
7. The axial displacement LVDT was set in position and zeroed.
8. The appropriate cell pressure was applied through GDSLAB and maintained by the GDS pressure controller for a period of 24 hours to allow for cell volume equalization. The pressure controller continued to maintain the applied pressure for the remainder of the experiment, while recording volume changes at 10 second intervals.
9. Sample vertical displacement due to cell pressure application was measured at the end of this period by lowering the loading ram using the crosshead screws until contact was again made with the sample as indicated through 1-2 Newtons of loading registered through the load cell.

#### 3.4.4 Dissolution

This stage involved the removal of the salt particles from the sand-salt mixtures through dissolution. It involved the following:

1. The outlet from the aspirator bottle (reservoir) was plugged using a rubber stopper perforated to allow the silicon tubing deliver the solution to the inlet points on the custom-built access ring. The tubing branched out into two lines to service the two inlets to the base of the sample.
2. The aspirator bottle was maintained at a height to allow the solution level within the bottle to coincide with the top of the sample allowing the sample to become saturated under gravity flow.
3. Salt-solution (0.5 litre) was added to the reservoir.
4. The stirrer ensured uniform salt concentration in the aspirator bottle to encourage consistent conductivity measurements.

5. The peristaltic pump slowly circulated the salt-solution to saturate the sample initially to allow a more gradual and uniform dissolution. This marked the beginning of the dissolution stage.
6. Shear-wave measurements were taken at time intervals from the beginning of the dissolution stage.
7. One litre increments of water were added to the reservoir (4 litres in total) to allow complete dissolution.
8. The high solubility of sodium chloride salt in water ensured complete dissolution, indicated by the stabilisation of conductivity measurements and simultaneous cessation of sample volume strain after a period of approximately 1 hour similar to the oedometric tests detailed in McDougall et al. (2013).
9. Post-dissolution the loading ram was lowered to make contact with the sample to measure sample vertical displacement during dissolution as explained in the sample preparation stage.

#### **3.4.5 Post-dissolution shearing**

1. The TriPath data logger was programmed to log at one minute intervals.
2. The triaxial control was started at exactly one minute of logging.
3. Axial displacement was applied at 0.25 mm/min to 20% axial strain.
4. The TriPath software recorded the axial load, axial displacement and time of shearing.

### **3.5 Sample volume measurement procedures and calculations**

Expulsion or uptake of pore-water is the usual method for measuring sample volume change during triaxial testing. However, such an approach was not possible in the current testing procedure. Since the sample was initially dry, then wetted and subsequently flushed, it was not possible to use sample pore-water volume change to determine sample volume change. Therefore a procedure to measure sample

volume change through cell volume changes was required for each of the following stages:

- Cell pressure application (compression)
- Dissolution
- Post-dissolution shear

The approach applied for each of the three stages and the calculations applied are presented below.

#### **3.5.1 Cell pressure application**

The measurement of sample volume change during initial (dry) compression was not possible using the cell water volume since this included volume changes due to the following:

- Distortion of triaxial cell due to pressure application
- Membrane penetration
- System losses, e.g. absorption by perspex, leakage

Therefore bulk moduli values for the sand, fine salt-sand mixtures and coarse salt-sand mixtures were used to calculate sample volume change with cell pressure application. This approach is verified below.

#### **Predicted sample compression based on bulk moduli**

Figure 3.17 presents volume changes for a standard sized sample based on the bulk moduli for coarse salt-sand mixtures, fine salt-sand mixtures and sand based on values presented in Table 3.3. The x-axis represents the cell pressure applied from an initial pressure of 0 kPa.

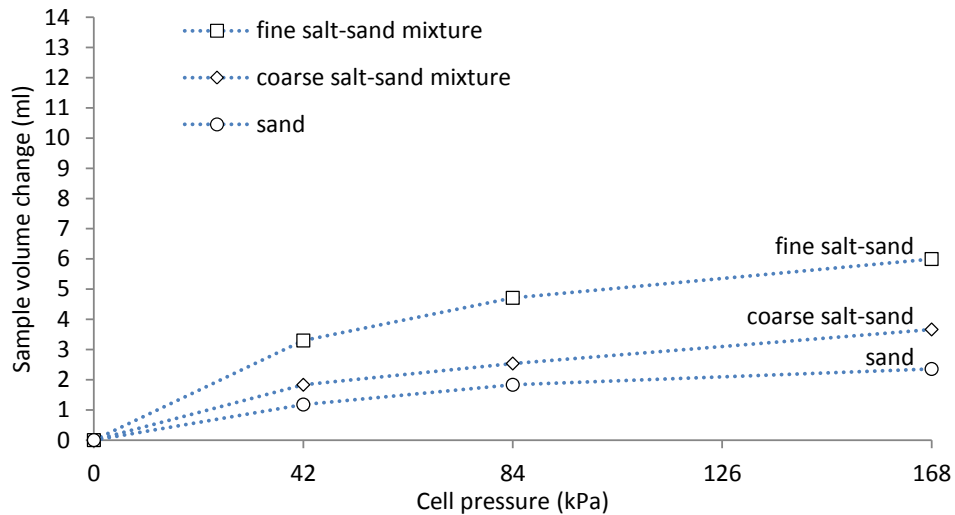


Figure 3.17: Bulk moduli sample volume changes

### Predicted distortion of cell with pressure application

The cell water volume changes  $\delta V_{cell}$  that occurred with pressure application in HDPE dummy sample tests are presented in Figure 3.18. Again, the x-axis represents the pressure applied from an initial pressure of 0 kPa. Data from two types of test are presented in Figure 3.18; the cell water volume changes associated with cell pressure cycling of 0-42, 0-84 and 0-168 kPa at the end of the 168 kPa dummy sample test, and the cell water volume changes recorded at time intervals post cell pressure application in dummy sample tests performed at 42, 84 and 168 kPa. The instantaneous volume change with pressure cycling resulted in the lowest values of volume changes. These are considered to show the least cell water volume change with cell pressure changes of 0-42, 0-84 and 0-168 kPa. Additional data sets relate to the cell water volume changes after one hour and after one day with cell pressure application to a newly prepared cell with a dummy sample.

The greater instantaneous volume change with pressure application in the newly prepared cell points to the initial compliance in the triaxial cell at the beginning of a test. The volume change after one day is of particular importance since this was the time required for the majority of volume change to occur as shown in Figure 3.14 and was therefore the time allowed for triaxial cell volume equilibration prior to the use of cell water for sample volume measurement purposes during the dissolution stage. The cell water volume changes after one day were 4.1, 6.3, 5.2 ml for 0-42, 0-84 and 0-168 kPa tests, respectively. Through assessment of dummy sample tests it is evident that cell distortion adds to the overall measured volume change with

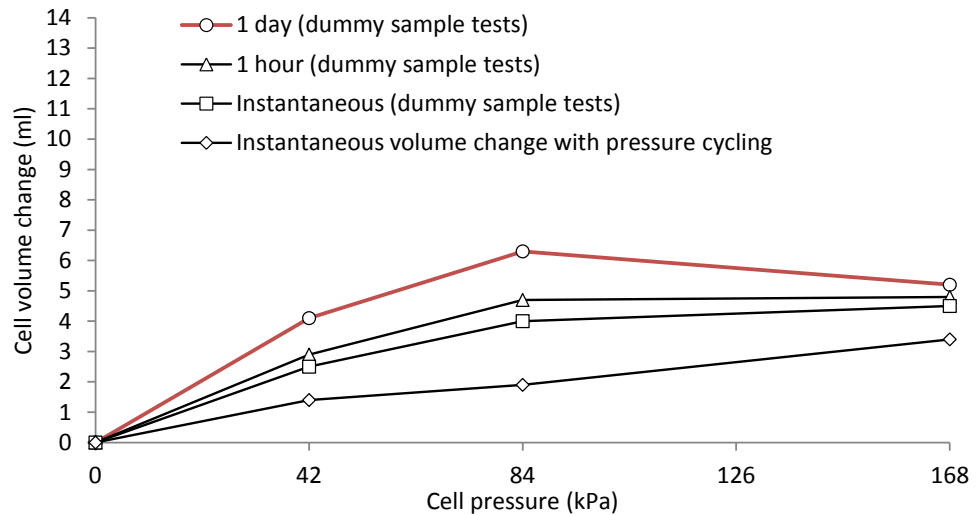


Figure 3.18: Triaxial volume change with pressure application in dummy sample tests

cell pressure application. An apparent anomaly occurred for the 0-84 kPa test. This shows the possible variability of cell distortion with pressure application. The ‘one day’ measurements represent the predicted cell distortion (cell volume change) in the current experiments.

#### Measured volume change with samples in place

Figure 3.19 shows the cell water volume changes measured for Leighton Buzzard sand, fine salt-sand mixtures and coarse salt-sand mixtures with the application of cell pressure. Tests where leakage occurred at the top screw cap during cell pressure application are omitted. Therefore this data accounts for a combination of sample volume change, cell distortion and membrane penetration.

#### Comparison of measured against predicted cell volume changes

Figure 3.20 presents the predicted and measured sample volume changes associated with cell pressure application. The predicted values are based on the ‘1 day’ volume change (taken from Figure 3.18) combined with the sample volume change associated with each sample type (taken from Figure 3.19). As can be seen, the agreement between predicted and measured volume changes is good. This validates the use of the bulk moduli corrections applied to the triaxial sample mixtures to account for compression with cell pressure application.



### 3. Materials, Apparatus and Procedures

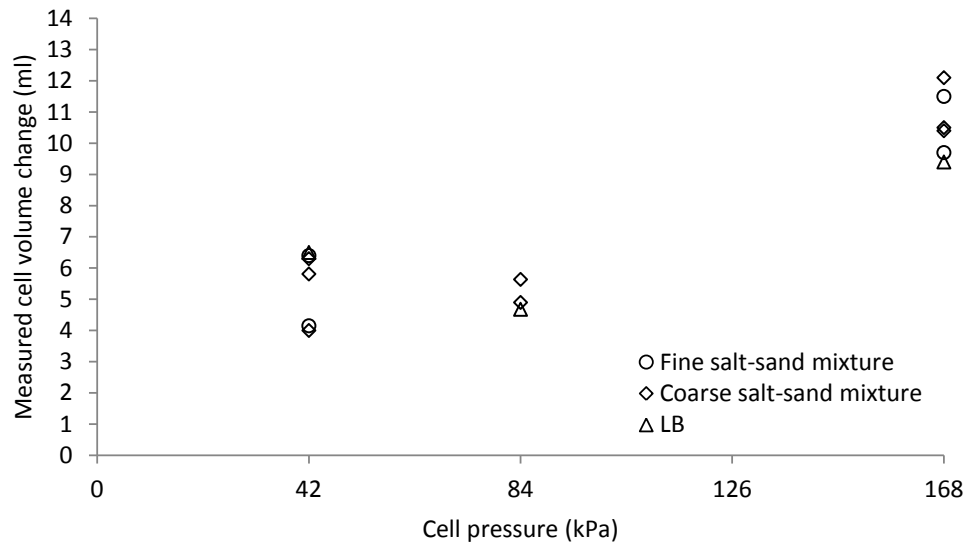


Figure 3.19: Total measured volume change with pressure application

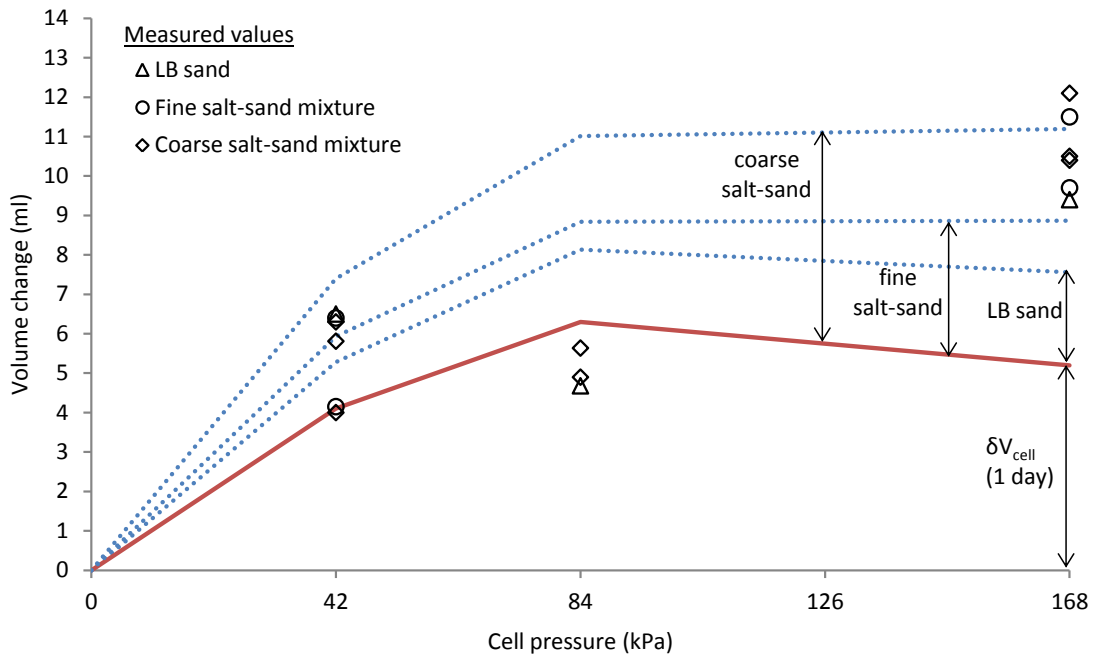


Figure 3.20: Comparison of measured cell volume change against predicted cell volume change combined with bulk moduli for 3 sample types

Table 3.8 presents the volumetric changes associated with the application of bulk moduli corrections for all tests. It shows that the void ratio is marginally affected by cell pressure application. Cell pressure application resulted in volumetric strains of 0.6-3.1%.

#### **3.5.2 Dissolution**

The dissolution stage was performed under constant cell pressure after a period of 24 hours was allowed for volume changes associated with cell pressure application to equilibrate. Sample volume changes during dissolution were therefore registered by cell water volume changes as measured by the GDS pressure controller placed on the cell pressure line. The sample height at the start of dissolution was known and the post-dissolution sample height was found by lowering the ram to the sample, with ram displacements measured by the external LVDT.

#### **3.5.3 Membrane penetration correction for dissolution stage**

Membrane penetration is typically calculated to compensate for the sample pore-water volume displaced from the interparticle voids of granular soils adjacent to the membrane during the application of cell pressure. However, as detailed previously, the volume changes associated with cell pressure application included membrane penetration effects.

The dissolution stage also resulted in membrane penetration due to an alternative mechanism where salt particles in contact with the membrane dissolved. However, there is no membrane penetration correction available in the literature to address this particular problem. Therefore a photographic method was devised to assist in the quantification of membrane penetration where pre- and post-dissolution photos were compared.

Firstly, a 1 cm vertical strip was selected in the middle of the sample. This was chosen to minimise issues relating to refraction of light through the water and acrylic cell wall. The membrane within this 1 cm strip was visually assessed with locations of membrane penetration identified by the drawing of circles. Figures 3.21, 3.22, 3.23 & 3.24 present the pre- and post-dissolution photographs of the 0.063, 0.25, 0.5 and 1.0 mm salt tests. Circle sizes of 0.5, 0.5, 0.75 and 1.5 mm were used to mark

### 3. Materials, Apparatus and Procedures

---

Table 3.8: Void ratio change with cell pressure application based on bulk moduli values

Test	Pre-compression void ratio	Bulk modulus (MPa)	Sample compression (ml)	Volumetric strain with cell pressure application	Post-compression void ratio
No.1 LB-100-42	0.55	7.0	1.119	0.9%	0.54
No.2 LB-100-84	0.61	9.0	1.812	0.9%	0.59
No.13 LB-100-84	0.59	9.0	1.807	1.2%	0.58
No.3 LB-100-168	0.56	14.0	2.215	1.9%	0.54
No.4 0.5-15-168	0.63	9.0	3.652	1.3%	0.60
No.5 0.5-15-84	0.58	6.5	2.492	1.3%	0.56
No.6 0.5-15-84	0.59	6.5	2.487	1.3%	0.57
No.7 0.5-15-42	0.59	4.5	1.787	0.9%	0.57
No.8 0.5-15-84	0.60	6.5	2.497	1.3%	0.58
No.9 0.063-15-168	0.43	5.5	5.811	3.1%	0.38
No.10 0.063-15-84	0.44	3.5	4.760	2.4%	0.41
No.11 0.25-15-168	0.61	9.0	3.720	1.9%	0.58
No.12 0.25-15-42	0.57	4.5	1.825	0.9%	0.55
No.14 1.0-20-168	0.58	9.0	3.702	1.9%	0.55
No.15 1.0-20-42	0.56	4.5	1.807	0.9%	0.55
No.16 1.0-15-168	0.61	9.0	3.647	1.9%	0.58
No.17 1.0-15-42	0.63	4.5	1.842	0.9%	0.61
No.18 LB-100-168	0.61	14.0	2.333	1.2%	0.59
No.19 LB-100-42	0.61	7.0	1.178	0.6%	0.60
No.20 1.0-15-168	0.61	9.0	3.647	1.9%	0.58
No.21 1.0-15-42	0.61	4.5	1.796	0.9%	0.59
No.22 0.5-15-168	0.61	9.0	3.651	1.9%	0.58
No.23 0.25-15-168	0.56	9.0	3.720	1.9%	0.53
No.24 0.25-15-42	0.59	4.5	1.851	0.9%	0.57
No.25 0.063-15-168	0.47	5.5	5.998	3.1%	0.43
No.26 0.063-15-42	0.42	2.5	3.167	1.7%	0.40

### 3. Materials, Apparatus and Procedures

the locations for the observed membrane penetrations in the post-dissolution sample for the 0.063, 0.25, 0.5 and 1.0 mm salt tests respectively. Circle sizes were chosen based on the diameter of membrane penetrations as measured using AutoCAD. The membrane penetrations were assumed to be hemispherical in shape and therefore penetration volumes could be calculated taking the circle diameter to equal the hemispherical diameter. The number of membrane penetrations within the 1 cm strip were identified and multiplied by the associated hemispherical volume. The membrane penetration volume was calculated for the 1 cm strip followed by the total membrane surface area in contact with the soil sample. Table 3.9 presents the membrane penetration calculations for the post-dissolution samples.

Table 3.9: Membrane penetration by photographic method

Salt size, mm	Salt (%)	No. of circles	Diameter of hemispherical void, mm	Volume of hemispherical void, mm <sup>3</sup>	MP per 1 cm vertical strip, mm <sup>3</sup>	Total MP, mm <sup>3</sup>	Total MP, ml	Salt % correction	Total MP, ml
0.063	15	354	0.5	0.03	12	182	0.2	-	0.2
0.25	15	225	0.5	0.03	7	116	0.1	-	0.1
0.5	15	134	0.75	0.11	15	232	0.2	-	0.2
1.0	20	78	1.5	0.88	69	1082	1.1	0.75	0.8

The calculated membrane penetration volumes for 15% by weight of 0.063, 0.25, 0.5 and 1.0 mm salt sizes were 0.2, 0.1, 0.2 and 0.8 ml, respectively. The largest membrane penetration correction of 0.8 ml accounted for only 0.4% of the total sample volume. This is in contrast to the total measured volumetric strains of approximately 9% (18 ml) obtained during dissolution for most coarse-sized salt samples. Therefore, accounting for membrane penetration was important but not critical to the analysis of sample volume change with dissolution.

A check to verify membrane penetration based on the previous approach is outlined below. It neglects the thickness of the membrane, and sand and salt particles are taken as equally sized spheres in a simple cubic packing arrangement. Since the mean size of the sand and “0.5 mm” salt size are 0.85 and 0.75 mm respectively, a uniform sphere diameter of 0.85 mm is chosen.

Calculations are as follows:

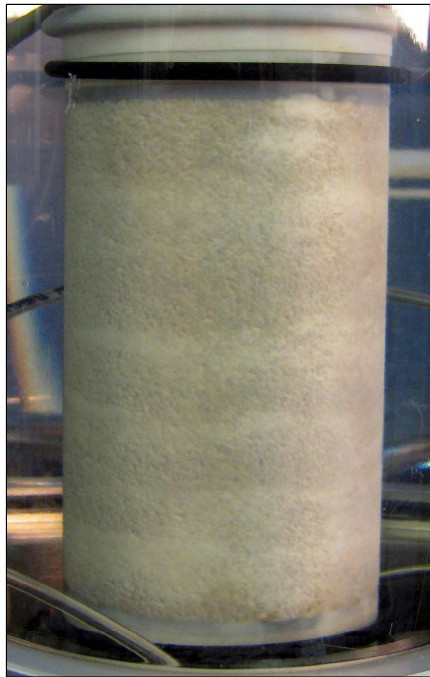
- The volume of salt based on 15% by weight is calculated as 17.8% based on the respective specific gravities. Therefore 17.8% of the particles in contact with the membrane are salt.

- The surface area of the membrane in contact with the sample is calculated based on the side surface area of a 100 mm high cylinder as  $15,708 \text{ mm}^2$ .
- The total number of spherical particles in contact with the membrane based on a sphere diameter of 0.85 mm was  $15,708 \text{ mm}^2 / 0.85 \text{ mm} = 18,480$ . Therefore the number of salt particles in contact with the membrane is 3,289 (17.8% of 18,480).
- Then, assuming membrane penetration to equal the volume of the spheres ( $0.32 \text{ mm}^3 \times 3,289 \text{ no. spheres}$ ), the total volume membrane penetration associated with salt dissolution is 1.05 ml.
- Alternatively, assuming that the membrane filled a cubic void vacated by the particle the total volume membrane penetration is 2.0 ml ( $0.61 \text{ mm}^3 \times 3,289 \text{ no. spheres}$ ).

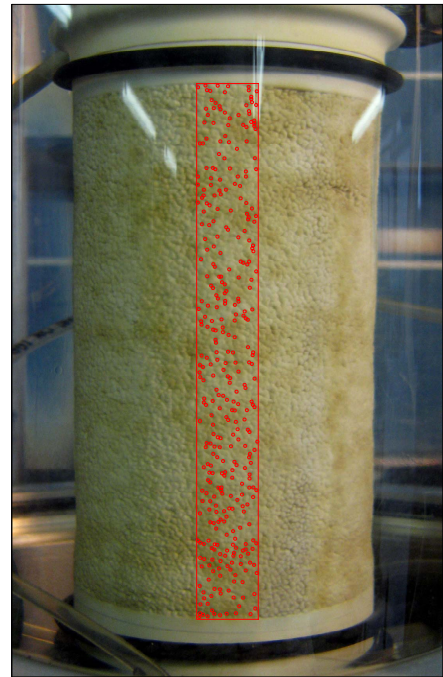
It is likely that the volume predicted using the cubic void assumption is the maximum achievable membrane penetration. However both the spherical and cubic void approach calculations are likely to be much higher than in reality. This is due to the thickness of the membrane (0.4 mm) and the fold thickness (0.8 mm) associated with the penetration of small voids vacated by individual dissolved salt particles (although the membrane thickness would decrease upon extension). Therefore these calculations represent maximum membrane penetration volumes in the dissolution test. The photographic approach calculates significantly less membrane penetration in agreement with the influence of the membrane thickness effects described. Furthermore, the significance of the membrane penetration calculated through any of the approaches described is minimal in terms of the total sample volume or the measured volume changes during dissolution as indicated earlier.

#### **3.5.4 Volume change comparison for each stage of dissolution tests**

The magnitude of volume change associated with each stage of a typical triaxial dissolution test (Test no.7 0.5-15-42) is shown in Figure 3.25. As discussed earlier, the measurement of sample volume changes through cell volume changes during dry compression was not feasible due to complicating factors such as cell distortion and membrane penetration. This is shown when the bulk modulus correction and the membrane penetration correction are applied as there is a discrepancy between



(a) Pre-dissolution

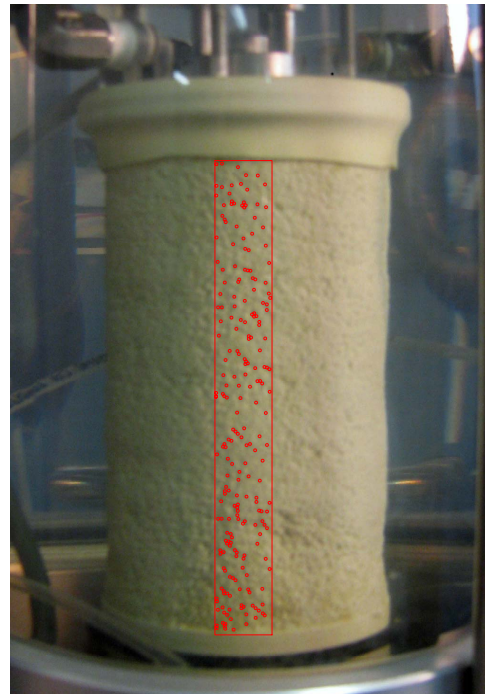


(b) Post-dissolution

Figure 3.21: Pre- and post-dissolution test performed with 0.063 mm salt @ 15% by mass confined at 168 kPa



(a) Pre-dissolution



(b) Post-dissolution

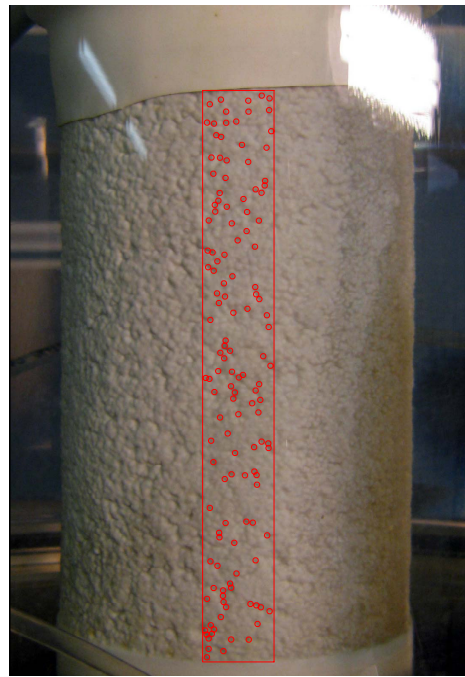
Figure 3.22: Pre- and post-dissolution test performed with 0.25 mm salt @ 15% by mass confined at 168 kPa

### 3. Materials, Apparatus and Procedures

---



(a) Pre-dissolution



(b) Post-dissolution

Figure 3.23: Pre- and post-dissolution test performed with 0.5 mm salt @ 15% by mass confined at 168 kPa



(a) Pre-dissolution



(b) Post-dissolution

Figure 3.24: Pre- and post-dissolution test performed with 1.0 mm salt @ 20% by mass confined at 168 kPa

the remaining volume (2.1 ml) and the cell distortion anticipated through the cell characterisation tests using dummy samples (4.1 ml). However this was unsurprising given the noted variability in cell volume changes with cell pressure application between tests. The membrane penetration for this stage was based on the equation by Nicholson et al. (1993).

The dissolution stage shows by far the greatest total volume change. Sample volume change with dissolution is by far the dominant volume change occurring within the test stages, with corrections minor in comparison. The membrane penetration for this stage was calculated using the photographic technique described earlier.

Lastly, volume changes with shear are small with an initial contractive phase followed by a small amount of dilation. For the sake of clarity, the volume change with ram penetration correction has already been applied. Typically, this resulted in the expulsion of 5.5 ml of cell water during shear.

#### **3.5.5 Sample volume change prior to shearing - calculations example**

The sample volume calculation procedure for a single test is presented in this section. The quantities of sand and salt by weight are known, together with sample dimensions in each test. This data, combined with knowledge of the specific gravity of sand and salt allow the determination of the phase relations. However, the external diameter measurement includes the membrane thickness. Hence, to determine the initial total volume of the soil sample the membrane thickness must be deducted from the diametrical measurement. The associated calculations for test no.16 are presented here.

#### **Sample details - Test no.16 1.0-15-168**

##### **Initial state**

Leighton Buzzard sand (LB): 264.05 g

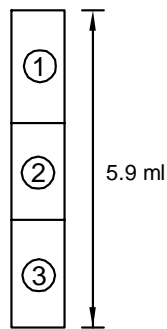
Salt (NaCl): 46.52 g

Sample height  $h_0$ : 99.5 mm



Compression stage

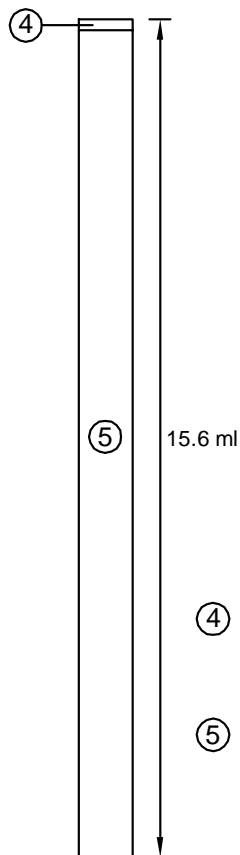
Total measured vol. change  
= 5.9 ml



- ① Cell volume change = 2.1 ml  
(4.1 ml based on dummy sample tests)
- ② Sample volume change - 1.8 ml  
(bulk modulus correction)
- ③ Membrane penetration = 2.0 ml

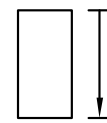
Dissolution stage

Total measured vol. change  
= 15.6 ml

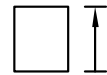


- ④ Membrane penetration = 0.2 ml
- ⑤ Sample volume change = 15.4 ml

Shear stage



Contractive phase = 2.0 ml



Dilative phase = 1.2 ml

Figure 3.25: Total volume changes and their constituents for compression, dissolution and shear stages of a typical triaxial dissolution test (Test no.7 0.5-15-42)

### 3. Materials, Apparatus and Procedures

---

Initial sample diameter  $d_0$ : 50.8 mm

$G_s$  (LB): 2.65

$G_s$  (NaCl): 2.16

LB volume: 99.64 ml

NaCl volume: 21.54 ml

Membrane thickness: 0.4 mm

#### Membrane thickness correction

The membrane thickness correction results in the subtraction of 0.8 mm ( $2 \times 0.4$  mm) from the measured sample diameter. The following provide the measurements and subsequent volumetric calculations for the initially prepared sample prior to cell placement.

Membrane thickness: 0.4 mm

Sample height  $h_0$ : 99.5 mm

Sample diameter  $d_0$ : 50.0 mm

Initial sample volume  $V_0$ : 195.37 ml

Dry density  $\rho$ : 1590 kg/m<sup>3</sup>

Volume of solids  $V_s$ : 121.2 ml

Volume of voids  $V_v$ : 74.19 ml

Void ratio  $e$ : 0.612

Porosity  $n$ : 0.380

$(V_v + V_{soluble})/V_{inert}$ : 0.96

#### **Cell pressure application**

This section outlines two approaches to determine sample volume change with cell pressure application. The bulk modulus method was applied in the tests while the common strains method is presented for comparison.

### 3. Materials, Apparatus and Procedures

---

#### Sample compression with cell pressure application (Bulk modulus method)

This method relies on prior knowledge of the bulk modulus of the material since direct total volume measurements were not feasible during cell pressure application as discussed earlier. In tests subsequent to test no.8, a method for measuring axial displacements was devised. The bulk moduli based on oedometric samples were applied giving the total sample volume change. The sample diameter was then backcalculated. The associated calculations are provided below. All volume data presented in this study is based on this approach.

Bulk modulus  $K$  (see Table 3.3):  $9.0E + 06$  Pa

Cell pressure applied  $\sigma'_3$ : 168000 Pa

Change in sample volume  $\Delta V = V_0(\Delta\sigma'_3/K)$ : 3.647 ml

Sample volume  $V_t$ : 191.721 ml

Volumetric strain  $\varepsilon_{vol}$ : 0.019

Measured axial displacement: 0.2 mm

Sample height  $h$ : 99.3 mm

Sample diameter  $d$  based on known sample height and bulk modulus sample volume calculation:

$$d = \sqrt{\frac{V_t \times 4}{h \times \pi}} = 49.581 \text{ mm}$$

Axial strain: 0.002

Lateral strain: 0.0084

Dry density  $\rho$ : 1620 kg/m<sup>3</sup>

Volume of solids  $V_s$ : 121.2 ml

Volume of voids  $V_v$ : 70.5 ml

e : 0.582

n : 0.368

$(V_v + V_{soluble})/V_{inert}$ : 0.92

#### Sample compression with cell pressure application (Common strains method)

### 3. Materials, Apparatus and Procedures

---

The common strains method of determining sample volume is an alternative to the bulk modulus method. It is based on the assumption that the sample experiences common strains in the axial and lateral dimensions with cell pressure application. This approach was used for comparison with the bulk moduli method only. It did not contribute to the data presented in the dissolution tests since samples are no longer expected to undergo isotropic deformation in accordance with the assumptions made in BS 1377.

Volumetric strain,  $\varepsilon_{vol} = 3 \times \varepsilon_a$ : 0.006

Sample height  $h$ : 99.3 mm

Sample diameter  $d$ : 49.899 mm

$\Delta V = V_0(\Delta\sigma'_3/K)$ : 1.178 ml

Total sample volume  $V_t$ : 194.19 ml

Dry density  $\rho$ : 1599 kg/m<sup>3</sup>

Volume of solids  $V_s$ : 121.2 ml

Volume of voids  $V_v$ : 73.01 ml

Void ratio  $e$ : 0.603

Porosity  $n$ : 0.376

$(V_v + V_{soluble})/V_{inert}$ : 0.95

#### **Dissolution**

Sample total volume and axial strains were available during the dissolution stage. The measured volume change included sample compression and membrane penetration. Therefore membrane penetration was deducted from the total measured volume change to find the sample change during this stage. Example calculations are provided here:

Change in sample height  $\Delta h$ : 1.83 mm

New sample height  $h$ : 97.47 mm

Axial strain  $\varepsilon_a$  : 0.02

Mass undissolved: 0 g

$V_s$ : 99.64 ml

GDS volume change  $\Delta V_{GDS}$ : 17.16 ml

GDS volume change through membrane penetration (see Table 3.7): 0.81 ml

Total sample volume,  $V_t$ : 175.37 ml

#### 3.5.6 Post-dissolution shearing stage - stress-strain relations

Standard triaxial formulae to account for sample strain with shear were applied to test data outputs and are presented here. The axial strain  $\varepsilon_a$  is calculated using:

$$\varepsilon_a = \frac{\Delta l}{l_0} \quad (3.3)$$

where  $\Delta l$  is the change in sample height as measured by the external LVDT and  $l_0$  is the initial sample height. The shear strain  $\varepsilon_s$  is given by:

$$\varepsilon_s = \varepsilon_a - \frac{\varepsilon_v}{3} \quad (3.4)$$

where  $\varepsilon_v$  is the volumetric strain and defined as follows:

$$\varepsilon_v = \frac{\delta V_{sample}}{V_0} \quad (3.5)$$

where  $V_0$  is the sample volume at the beginning of shear and  $\delta V_{sample}$  is the sample volume change as defined as follows:

$$\delta V_{sample} = \Delta V_{GDS} - \delta V_{ram} \quad (3.6)$$

where  $\Delta V_{GDS}$  is the measured cell volume change and  $\delta V_{ram}$  is the volume of cell water displaced by the ram, the calibration of which can be found in Section 3.3.1 and found to be 0.297 ml/mm.

A cross-sectional area correction  $A_c$  was applied to account for sample deformation through barrelling with shear:

$$A_c = A_0 \frac{1 - \varepsilon_v}{1 - \varepsilon_a} \quad (3.7)$$

where  $A_0$  was the cross sectional area at the beginning of shear.

### 3.5.7 Membrane strength correction

Membrane strength corrections for barrelling were assessed in accordance with BS 1377-8:1990 that provides a correction curve for a 38 mm diameter sample fitted with a 0.2 mm thick membrane. An equation allows for the production of correction curves for alternative sample dimensions and membrane thicknesses. Hence a correction curve for the 50 mm samples and 0.3 mm thick membranes used in the experiments was produced and is shown on Figure 3.26. It demonstrates that a membrane strength correction of 2.3 kPa at 20 % axial strain is necessary where barrelling occurs.

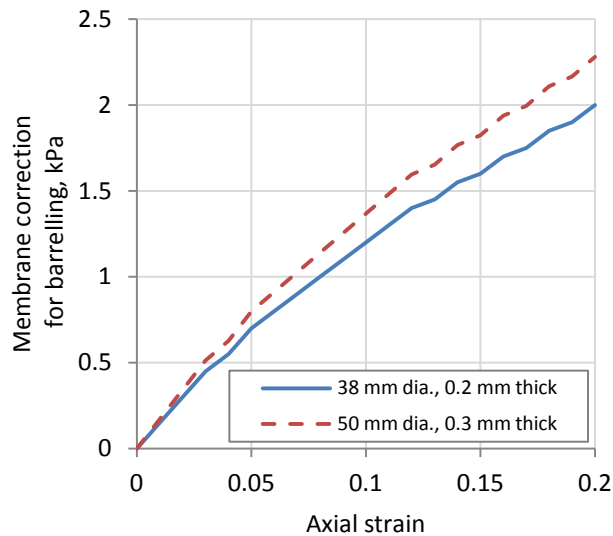


Figure 3.26: Membrane strength correction

The application of the membrane strength correction accounted for 2.7 % of the lowest deviatoric stress measured at the critical state of a shearing test performed at the lowest cell pressure of 42 kPa applied. Therefore the membrane strength correction would account for an even lower percentage of the deviatoric stress required for shearing tests performed under the higher cell pressures applied. Consequently the membrane strength correction for barrelling was overlooked.

## 3.6 Bender element test procedures

Whilst bender elements were used to monitor stiffness changes due to cell pressure application, dissolution and subsequent shearing stages, the focus of the current study was the stiffness changes that accompanied the loss of particles during the dissolution stage. The bender element system (BES) allowed the generation of shear and pressure waves. Shear waves were favoured due to the negligible shear modulus of water meaning that shear wave velocity was not affected by the presence of sample pore fluid.

### 3.6.1 GDS BES Test Wizard

The GDS Bender Element Test Wizard is displayed after the loading of the GDS Bender Element System Software. The BES Test Wizard allowed the hardware setup for the bender element tests, allowing the input of the following:

- Sample height
- Acquisition options
- Source waveform
- Data file acquisition options

These items are discussed in more detail below.

#### **Sample height**

Velocity calculations were made based on sample height that was subject to change with cell pressure application, dissolution and shearing stages. The sample height was available when the loading ram of the submersible load cell was in contact with the sample: pre- and post-cell pressure application, pre- and post-dissolution, and continually through the shearing stage. During the dissolution stage the sample height was estimated based on rate of settlement of identical mixtures measured in oedometric tests.

#### **Acquisition options**

Acquisition options allowed the sample frequency and sampling time of the received wave traces to be set. A sample frequency of 100 thousand samples per second was chosen with a sampling time of 100 milliseconds resulting in 10 thousand samples per wave data file.

#### **Source waveform**

The source waveform options were sinusoidal, square and user defined. Sinusoidal waves were chosen. The period of the sinusoidal waveform was chosen as 0.1 milliseconds to achieve a frequency of 10 kHz. An amplitude of 10 V was used to ensure adequate strength of the received trace as recommended by Jovičić et al. (1996), Arulnathan et al. (1998), and Brignoli et al. (1996).

#### **3.6.2 Bender element test schedule**

A typical test schedule consisted of the following:

- Prior to cell pressure application two shear wave and two pressure wave velocity measurements were taken
- Post cell pressure application, two shear waves and two pressure waves were taken and again after 24 hours prior to the dissolution stage
- During dissolution shear waves were taken at five minute intervals during the first 30 minutes, when the majority of shear wave velocity change occurred, followed by 10 intervals over the remaining 2 hours
- For the shearing stage, shear waves were sent at 30 second intervals for the first 10 of 80 minutes in total. Shear waves were sent at 1, 5 and 10 minute intervals over the remaining 10, 20 and 40 minutes, respectively.

Each shear wave data file was saved for post test analysis where all the shear waves were presented together to allow consistency in the point picking approach and the appropriate sample height was applied to allow the calculation of the shear wave velocities.



## 3.7 Summary

The steps undertaken to obtain a reliable experimental data set on the mechanical consequences of particle loss were described. An experimental programme of sand-salt mixtures subject to a test sequence of triaxial compression-dissolution-shearing posed a number of practical difficulties and unexpected problems, the solutions to which have been presented in this chapter. More specifically:

*Materials:* the constituents of the sand-salt mixtures have been characterised in terms of size distribution, particle strength (i.e. susceptibility to crushing), and bulk stiffness.

*Equipment modification:* changes to a conventional triaxial cell included cell port expansion to allow dual tube flushing circuit and bender elements.

*Equipment additions:* additional equipment such as solution reservoir, peristaltic pump recirculation systems and conductivity measuring were incorporated.

*Equipment calibration:* the requirement to undertake dry initial compression did not allow for volume changes to be measured by sample porewater change. Triaxial cell volumes were used instead, which gave rise to a number of practical complications such as cell distortion, membrane penetration, ram displacement, each of which have been quantified.

*Technical difficulties:* in addition to the planned equipment development, there occurred a number of unexpected technical snags: cell leakage and drifting load cell readings, both of which are described.

The calculation procedure is provided to confirm how the details of the equipment calibration are incorporated.

Finally, the combination of equipment compliance and sample behaviour are placed in context through a quantitative comparison of the volume changes occurring during each stage of the test procedure.

# Chapter 4

## Experimental results

This chapter begins by presenting the volumetric changes that accompanied the dissolution of salt from sand-salt mixtures in triaxial tests, with the influence of size of salt removed a key focus. With dissolution of salt complete, the results of triaxial shearing to determine the strength and stress-strain behaviour of the remaining sand fabric are presented. Comparison with the shearing of intact samples allowed the influence of salt particle removal on the stress-strain behaviour of the soil to be fully assessed. It is argued that particle loss appears to induce a change in soil behaviour. Where a soil may have been originally dense, the volumetric change due to particle loss produces a soil that is apparently loose in its stress-strain behaviour. The results also indicate that the dilatancy commonly observed in laboratory prepared (medium to dense) sand samples is replaced by a more contractant behaviour, although the complete strain response is more complex. In intact sand-salt mixtures, the salt size influences the stress-strain behaviour through grading changes, with implications for the critical state. Throughout, the structural role of the salt in the sand is addressed.

### 4.1 Test programme

A total of 26 tests were performed on samples of (i) sand only, (ii) dry sand with (mostly) 15% added by weight of salt of specified particle size, and (iii) sand-salt mixtures with salt particles dissolved. The mixture characteristics (% salt and size added) and cell pressure for the samples are summarised in Table 4.1. The mnemonic SALt is used to help distinguish these characteristics: S = size (mm), A = amount

(%),  $L$  = load (kPa). Hence, a typical triaxial Test ID appears as follows: “1.0-15-42”. Leighton Buzzard (LB) sand-only tests are named using the following format: “LB-42”. The 26 tests are subdivided into 3 groups, the rationale for which is as follows:

### **Sand**

To establish stress-strain behaviour of the inert as the host fraction. These tests were conducted both dry (Test nos. 18 & 19) and wet (Test nos. 1, 2, 3 & 13).

### **Sand-salt (dry)**

To establish the stress-strain behaviour of the mixtures in the absence of particle loss and identify the influence of added salt on critical states (Test nos. 20-26). These tests also allowed the assessment of the structural role of salt in predominantly sand mixtures.

### **Post-dissolution**

To determine the volumetric state accompanying the loss of a range of particle sizes under triaxial conditions (Test nos. 4-12, 14-17). Subsequently, to establish the effect of particle removal on the stress-strain behaviour of the remaining sand fabric.

An interesting facet of the dissolved mixtures is the formation of loose sand samples and the probing of the associated critical states. A complete index of triaxial test nomenclature is defined in Table 4.1.

## **4.2 Dissolution strains**

Dissolution volumetric strains in triaxial tests with 15% salt by weight, varying with salt particle size and applied stress are presented in Figure 4.1. The first observation is that dissolution strain increases with the salt particle size removed. A second observation relates to the influence of the applied stress. Figure 4.1 presents the results of dissolution tests performed under 42 kPa (3 no.), 84 kPa (2 no.), and 168 kPa (4 no.). Although the applied stress appears to influence the volumetric strain, with higher stresses resulting in slightly higher strains in 0.25, 0.5 and 1.0 mm salt tests, this is minor in the 0.5 and 1.0 mm tests. Furthermore, applied stress effects are not observed for the 0.063 mm salt tests. Based on the presented data, the

#### 4. Experimental results

---

Table 4.1: Triaxial test nomenclature

Test type	Test no.	Test ID	SIZE	AMOUNT	LOAD	
			Salt particle size (mm)	Salt percentage by mass (%)	Cell pressure (kPa)	Shear stage status
Sand	No.1	LB-42	-	-	42	Wet
	No.2	LB-84	-	-	84	Wet
	No.3	LB-168	-	-	168	Wet
	No.13	LB 84	-	-	84	Wet
Sand (dry)	No.18	LB-168	-	-	168	Dry
	No.19	LB-42	-	-	42	Dry
Sand-salt (dry)	No.20	1.0-15-168	1	15	168	Dry
	No.21	1.0-15-42	1	15	42	Dry
	No.22	0.5-15-168	0.5	15	168	Dry
	No.23	0.25-15-168	0.25	15	168	Dry
	No.24	0.25-15-42	0.25	15	42	Dry
	No.25	0.063-15-168	0.063	15	168	Dry
	No.26	0.063-15-42	0.063	15	42	Dry
Dissolution	No.4	0.5-15-168	0.5	15	168	Wet
	No.5	0.5-15-84*	0.5	15	84	Wet
	No.6	0.5-15-84*	0.5	15	84	Wet
	No.7	0.5-15-42	0.5	15	42	Wet
	No.8	0.5-15-84	0.5	15	84	Wet
	No.9	0.063-15-168	0.063	15	168	Wet
	No.10	0.063-15-84	0.063	15	84	Wet
	No.11	0.25-15-168	0.25	15	168	Wet
	No.12	0.25-15-42	0.25	15	42	Wet
	No.14	1.0-20-168	1	20	168	Wet
	No.15	1.0-20-42	1	20	42	Wet
	No.16	1.0-15-168	1	15	168	Wet
	No.17	1.0-15-42	1	15	42	Wet

---

“\*” denotes incomplete dissolution

influence of applied stress is inconclusive but it is suggested that this may play a secondary role in dissolution strain.

As discussed earlier, McGeary (1961) and Lade et al. (1998) demonstrated how fine particles may fill the interparticle voids of the coarse particle matrix without intercepting the coarse particle matrix. McDougall et al. (2013) postulated that the coarse particles constituted the load bearing skeleton of the soil. Then, supposing that the fine 0.063 mm particles did not interfere with the predominant interparticle contacts of the coarse Leighton Buzzard sand, dissolution should result in no rearrangement of sand particles as the strong force network would remain intact. Consequently, no volumetric strain with dissolution would occur. However, it is possible that fine particles participate in the strong force chains of the soil. This helps to explain the relatively low volumetric strain  $\approx 1.0\%$  observed with the dissolution of fine 0.063 mm salt samples in Figure 4.1.

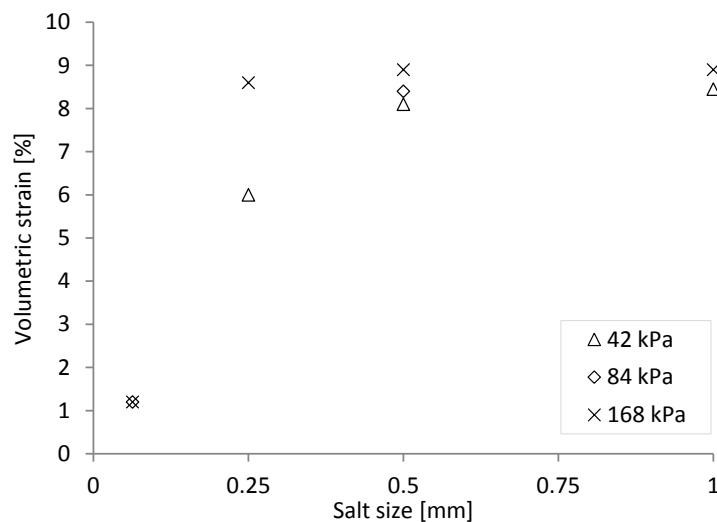


Figure 4.1: Dissolution volumetric strain against salt particle size in triaxial tests

Many DEM studies have demonstrated that load transmission in granular materials is not homogeneous. A strong force network formed by particles carrying loads larger than the average contact force magnitude can be identified (Hunt et al. 2010, Barreto & O’Sullivan 2012). McDougall et al. (2013) stated that for  $D_r < 3.0$ , salt and sand particles were broadly similar in size. This applied to the coarse-salt sizes of 0.25, 0.5 and 1.0 mm used with  $D_r = 2.3, 1.1$  & 0.6, respectively. For these mixtures, it can be expected that salt particles were part of the strong force chain network. It was therefore reasonable to expect that dissolution might result in some disturbance of the load bearing particles causing particle rearrangement and therefore volumetric straining. This is verified by the significantly larger strains accompanying the

dissolution of coarse-sized salt mixtures with  $D_r < 3.0$  as illustrated in Figure 4.1.

Dissolution strain results for 15% by weight of salt oedometer tests investigating the influence of salt particle size are presented in Figure 4.2 (McDougall et al. 2013) allowing comparison with the triaxial test results found here. In that study, it was claimed that particle size was the dominant influence, while no applied stress effects were observed. The same micro-mechanical explanations supported the findings of that study.

Although the trend of increasing dissolution strains with particle size is similar in both triaxial and oedometer tests, strains for fine particle tests were less in triaxial tests, while greater strains were observed for coarse salt sizes. A potential reason may be the difference in sample boundary interfaces in the two test types.

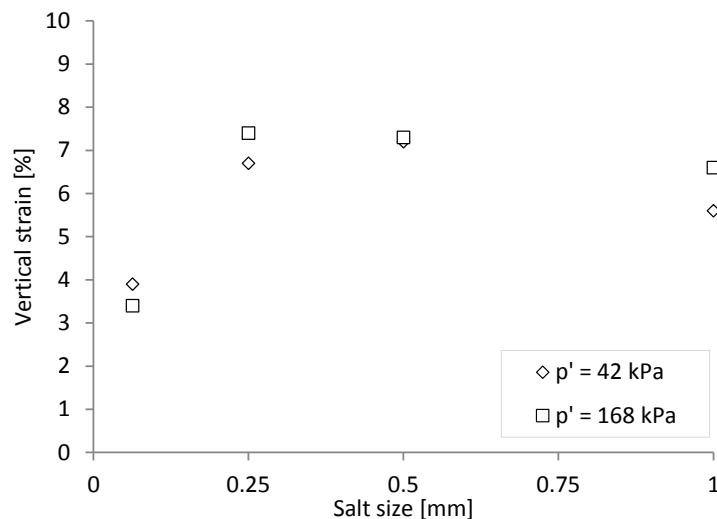


Figure 4.2: Dissolution vertical strain against salt particle size in oedometer tests (after McDougall et al. (2013))

### 4.3 Dissolution void ratio changes

Dissolution void ratio changes for a range of salt particle sizes at 15% by weight are assessed in this section. Triaxial void ratios changes with dissolution from the current study are contrasted with oedometer results based on identical sample mixtures performed by McDougall et al. (2013). Triaxial and oedometric results are presented in 4.3a & 4.3b, respectively. The range of applied stresses in triaxial tests (42-168 kPa) were chosen to represent the mean effective stresses resulting from the vertical stress applications (62-250 kPa) in the oedometer, as discussed in section

3.1.9. Therefore, Figure 4.3a shows the void ratio changes for 42, 84, and 168 kPa triaxial dissolution tests, while Figure 4.3b presents the 62 and 250 kPa oedometer tests. Lines indicating the  $e_{min, LB}$  and  $e_{max, LB}$  are also plotted.

There is considerable agreement between triaxial and oedometric pre- and post-dissolution void ratios. The influence of salt particle size is evident with the 0.063 and 0.125 mm fine-sized salt ( $D_r = 9.1$  and 4.5, respectively) showing pre-dissolution void ratios lower than  $e_{min, LB}$  with 0.25, 0.5 and 1.0 mm coarse-sized salt broadly similar in size ( $D_r = 2.3, 1.1$  and 0.6, respectively) to the Leighton Buzzard sand resulting in pre-dissolution void ratios similar to  $e_{min, LB}$ . Overall, the good agreement between triaxial and oedometric tests in 15 % salt by weight tests (Figure 4.3a) suggests that similar trends would be observed for 2, 5 and 10 % tests in triaxial and oedometer tests.

Minor differences are observed in terms of slightly lower initial (pre-dissolution) void ratios for triaxial samples. Additionally, slightly larger void ratio increases were observed in some triaxial tests. However, these minor differences may be accounted for through slight variances in sample preparation between triaxial and oedometer tests and experimental accuracy. In agreement with the observations made by McDougall et al. (2013), comparison of void ratio changes with dissolution in triaxial and oedometer tests suggest the following:

1. Void ratio was shown to increase in all tests
2. The increase in void ratio was not influenced by:
  - (a) particle size
  - (b) the value of pre-dissolution void ratio
3. The increase in void ratio was insensitive to the applied stresses

While void ratio change with dissolution was unaffected by the salt particle size removed and the applied stress, salt particle size did affect the initial packing density of the sample, e.g. fine salt particle mixtures had lower initial void ratios. Hence, the post-dissolution void ratios for fine salt samples were also lower than coarse salt tests since the magnitude of void ratio increase was common to all 15% salt tests. Consequently, post-dissolution void ratios for fine salt tests were medium in density, while coarse salt tests were loose.

## 4. Experimental results

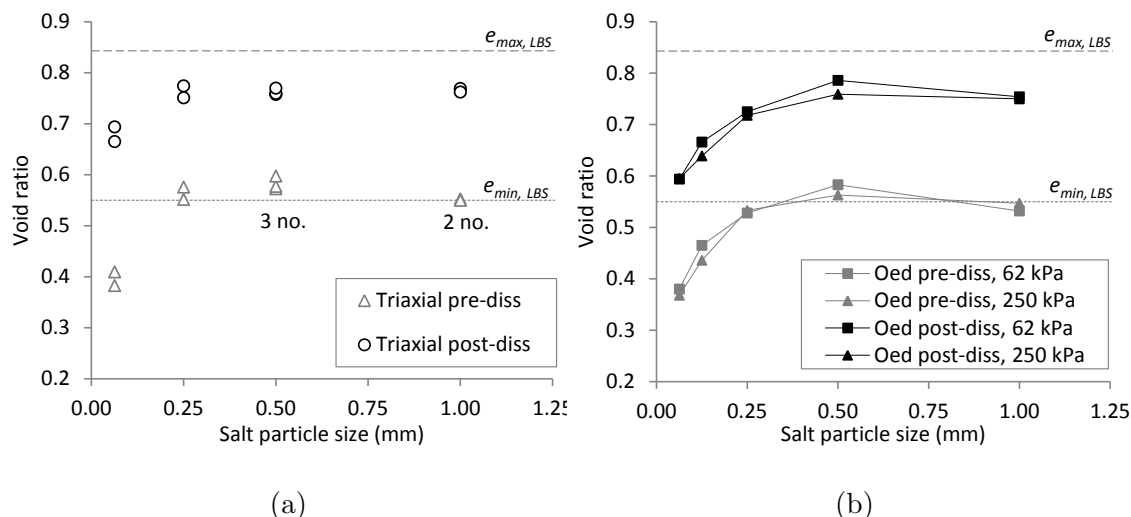


Figure 4.3: Pre- and post-dissolution void ratios for 15 % salt by weight with particle sizes ranging 0.063 to 1.0 mm for (a) triaxial tests (42, 84 and 168 kPa) in the current study, and (b) oedometer tests (62 and 250 kPa) (after McDougall et al. (2013)). Void ratio minimum and maximum for Leighton Buzzard sand also indicated

### 4.4 Dissolution induced lambda values

Dissolution of the fine 0.063 mm salt resulted in relatively little volumetric strain. Therefore it is implicit that salt volume loss in this case contributed mostly to pure void enlargement and void ratio increase, corresponding closely to the condition defined by the decomposition induced lambda parameter  $\Lambda = -1$  by McDougall & Pyrah (2004) (see Figure 4.4).  $\Lambda$  values for the coarse-salt mixtures are not as easily interpreted without a more in-depth analysis of phase volume changes.

### 4.5 Triaxial shear behaviour

This section presents and contrasts the three main types of test in the study known as “sand”, “sand-salt” and “post-dissolution” tests. Only post-dissolution tests having experienced complete dissolution and initially containing 15% of salt by weight are presented in this chapter unless indicated otherwise. A synopsis of the reasons for the three main test types is presented here:

- The effect of particle loss on the shearing behaviour of soil is a primary focus of this thesis and therefore the comparison of identically prepared mixtures, one with salt intact (sand-salt) and the other with the salt having been removed through dissolution (post-dissolution), offer further insight.



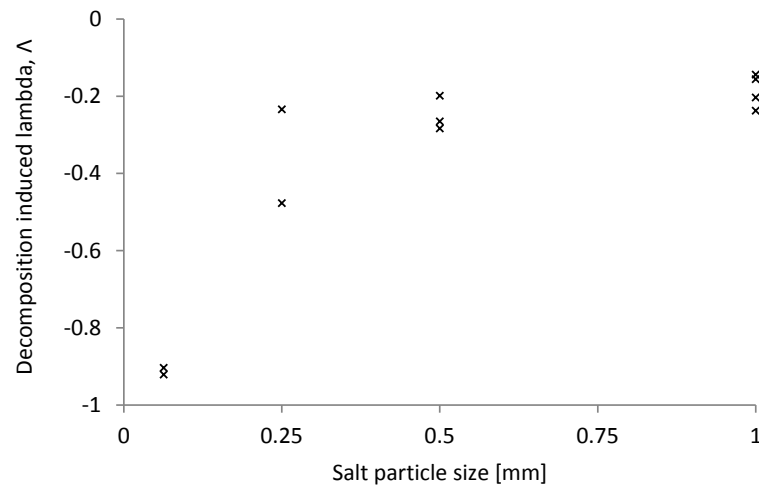


Figure 4.4: Decomposition induced lambda  $\lambda$  against salt particle size used in 15 % salt by weight tests

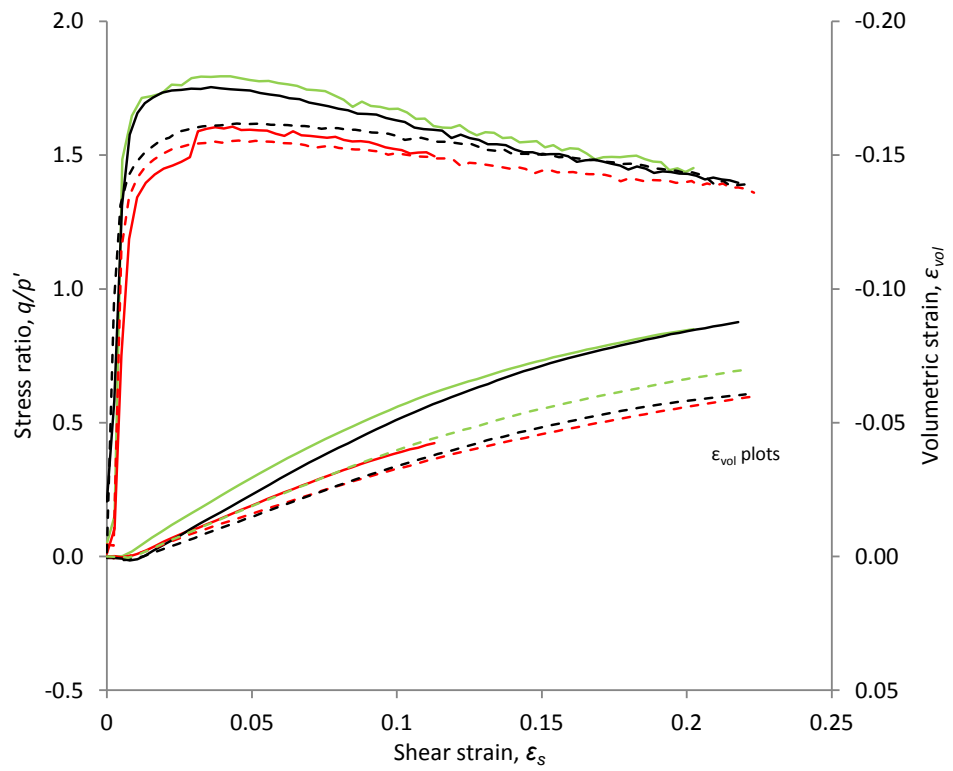
- Leighton Buzzard “sand” tests provided the reference shearing behaviour for dense sand. These allowed comparison with “post-dissolution” samples that also consisted of Leighton Buzzard sand only, having lost the salt fraction.
- The “sand” tests also provided reference for the “sand-salt” tests to allow the assessment of the influence of salt particle size additions to the shearing behaviour of the predominantly sand mixtures.

### 4.5.1 Sand only

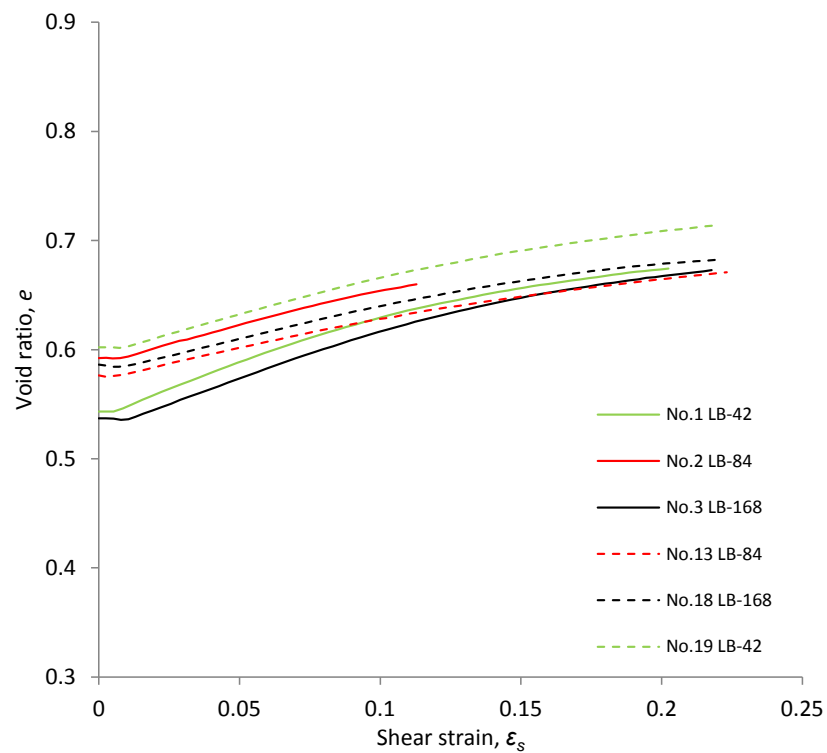
This section compares the stress-strain behaviour of the sand tests. The stress-ratio against shear strain for the sand tests is shown in Figure 4.5. All sand tests show strain-softening with consistently high initial shear stiffness.

The sensitivity of stress-strain behaviour to the initial volumetric state of the soil is illustrated by the sand tests. While all samples were prepared to achieve an initial dense packing arrangement it can be seen that minor variations in the pre-shear void ratios result in noticeable changes in the strength behaviour. A difference of 0.3 in peak stress-ratios was obtained from two samples that differed in initial void ratio by only 0.06 (see Table 4.2).

#### 4. Experimental results



(a)



(b)

Figure 4.5: Shear behaviour of sand (a)  $q/p'$  and  $\varepsilon_{vol}$ , and (b)  $e$  against  $\varepsilon_s$

### 4.5.2 Sand-salt

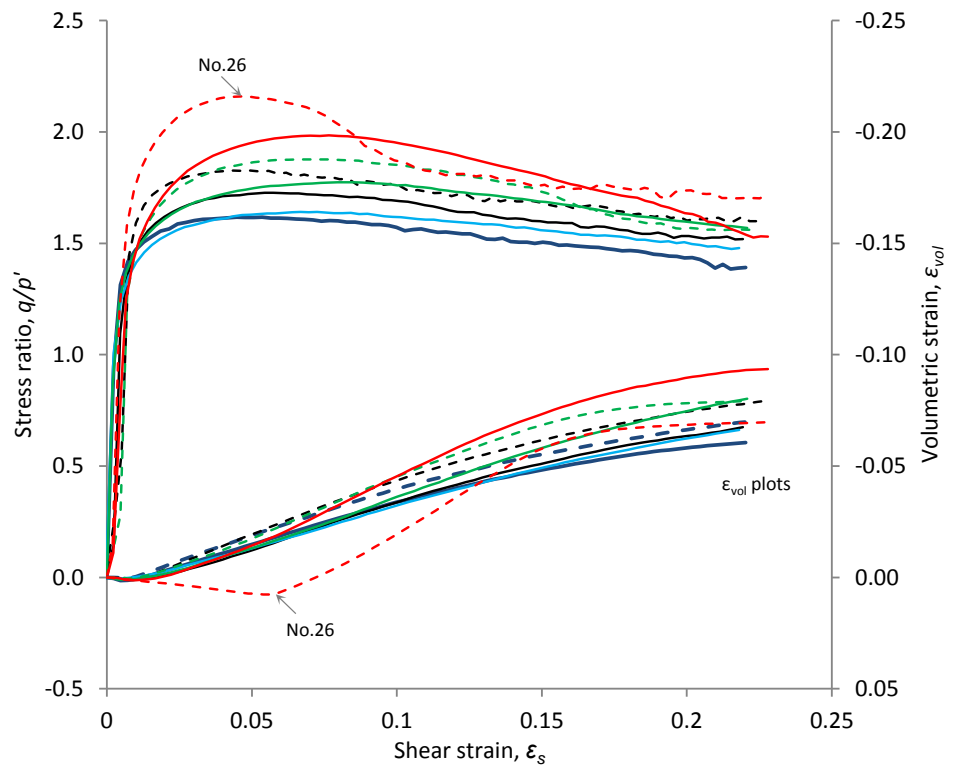
Figure 4.6 allows direct comparison of all the sand-salt tests. As a reference, sand test no.18 is provided along with sand-salt test nos. 20-26. The main points are:

- The 0.063 mm salt test nos. 25 and 26 exhibit the highest peak stress-ratios of the sand-salt mixtures followed by the 0.25, 1.0 and 0.5 mm salt tests
- Initial stress-strain responses of sand-salt mixtures appear similar
- The lowest critical stress-ratio is returned by the sand test
- The critical stress-ratios for the 0.5 mm and 1.0 mm salt tests are most closely related to the sand test since these salt particle sizes are closest in size in relation to the sand meaning the sample gradings are similar

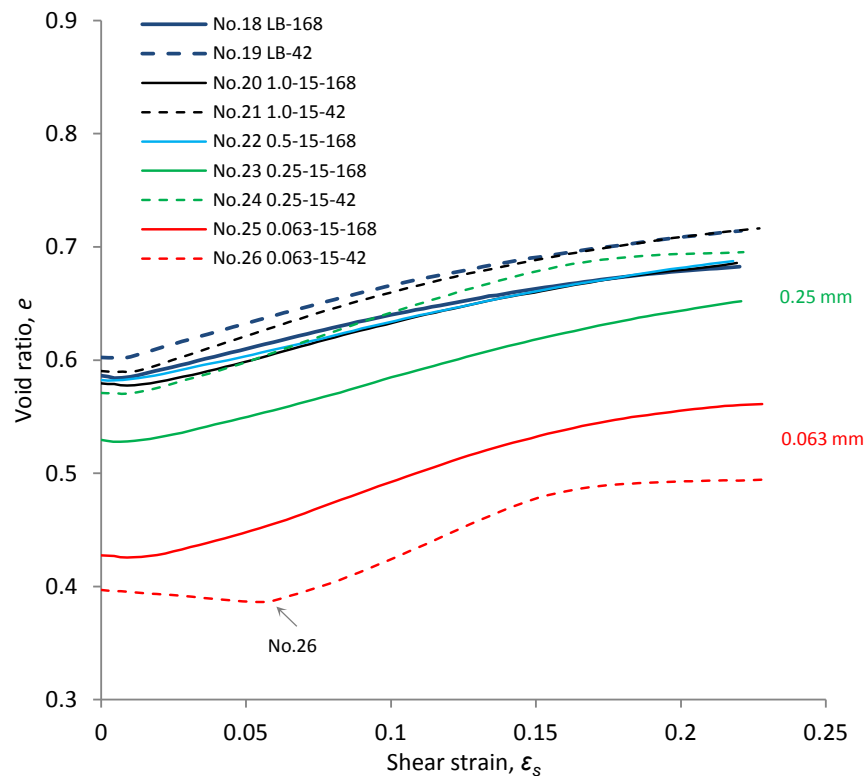
The differences in peak stress-ratio levels can be explained in terms of the grading of the different salt size mixtures. The salt size determines the achievable packing density. Finer salt mixtures have higher initial packing densities and hence lower initial void ratios (Figure 4.6b). For tests with 15 % salt with 0.063 mm salt particles in sand-salt mixtures the sand interstitial voids may not be completely filled. In this scenario, the sand particles should be the primary stress bearers because salt particles ‘nestle’ within the voids. However, it seems apparent that the fine salt performs a structural role due to the higher peak stress-ratios achieved than in sand-only tests. It is possible that the fine salt particles within the interstitial voids of the sand stabilise the sand particles. This increased stability increases the stress required for shear to progress in fine salt mixtures. Experimental studies have shown similar behaviours where additions of silt to clean sand have shown larger shear strengths than sand alone (Carraro et al. 2009, Salgado et al. 2000), similar to findings in DEM studies (Barreto & O’Sullivan 2012).

As salt particle sizes increase above 0.063 mm, they become more equivalent in size to the uniform sand. Therefore they can no longer exist in the sand without constituting part of the strong force network. The  $q/p'$  plots for these mixtures are similar to the sand only tests. Initial void ratios are also similar. The only observable difference based on Figure 4.6 is a softer peak response, i.e. higher shear strains are required for peak development than in sand samples. This suggests that the less stiff salt particles are participating in the load bearing force chains within the soil and influencing the mechanical behaviour overall.

#### 4. Experimental results



(a)



(b)

Figure 4.6: Shear behaviour of sand-salt (a)  $q/p'$  and  $\epsilon_{vol}$ , and (b)  $e$  against  $\epsilon_s$  (dashed lines denote 42 kPa tests), and compared with Leighton Buzzard sand

## 4. Experimental results

---

Test no.26 exhibited the most distinctive stress-strain response. Coincidentally, the sample showed shear plane failure as observed in Figure 4.7a. The volumetric data showed a compressive phase over shear strains of 6% before dilating strongly to a shear strain of 15%, where the critical state appears to have been found. An interesting feature of the test was that the peak strength and maximum rate of dilation were not coincident as might be expected ( $\varepsilon_s \approx 4$  and 10%, respectively). Plane failure was evidenced by the excessive bulge and membrane stretch marks along the failure plane in test no.26. The same mode of failure is evident in test no.25 but the deformation of the sample is not as obvious. This can be explained by the difference in applied cell pressures. Most other tests deformed through barrelling so that a slip plane was not clearly visible externally.

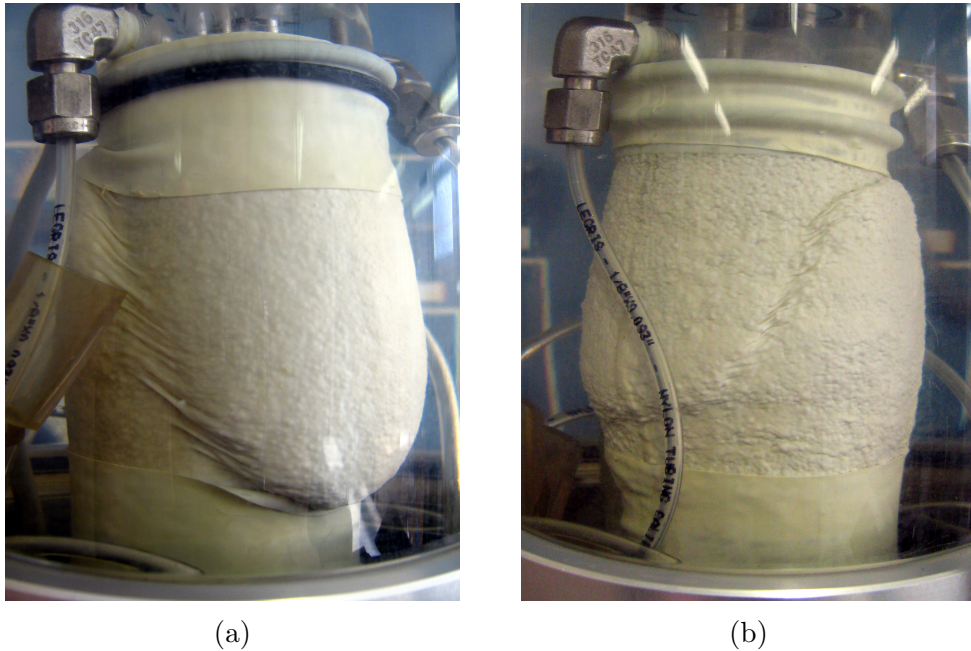


Figure 4.7: Shear plane failure at 20% shear strain for (a) No. 26 (0.063 mm 15% 42 kPa) (b) No. 25 (0.063 mm 15% 168 kPa)

### 4.5.3 Post-dissolution

Figure 4.8 illustrates the post-dissolution strength behaviours of the sand after the complete removal of 15% by weight of salt varying with particle size. As mentioned earlier, notable is the significant change in shearing response of post-dissolution samples in contrast to the dry mixtures presented in Figure 4.6. The post-dissolution shearing response for 15% salt tests tend to exhibit more strain-hardening contractive behaviour.

The size of salt particle removed has influence on shearing behaviour as it has influence on the post-dissolution void ratio of the sand. The post-dissolution void ratios of 0.063 mm salt particle tests were lowest which resulted in the most brittle stress-strain response. Post-dissolution, the larger salt particles of 0.5 or 1.0 mm resulted in the highest void ratios and consequently the most ductile stress-strain response. Since the post-dissolution samples consist solely of Leighton Buzzard sand, the critical stress-ratios were practically the same with values of 1.2-1.3 at 20% shear strain.

## 4.6 Comparison of shear behaviours

### 4.6.1 Sand vs. sand-salt

Distinction between the shear behaviours of sand and sand-salt tests are presented in Figure 4.9. In summary:

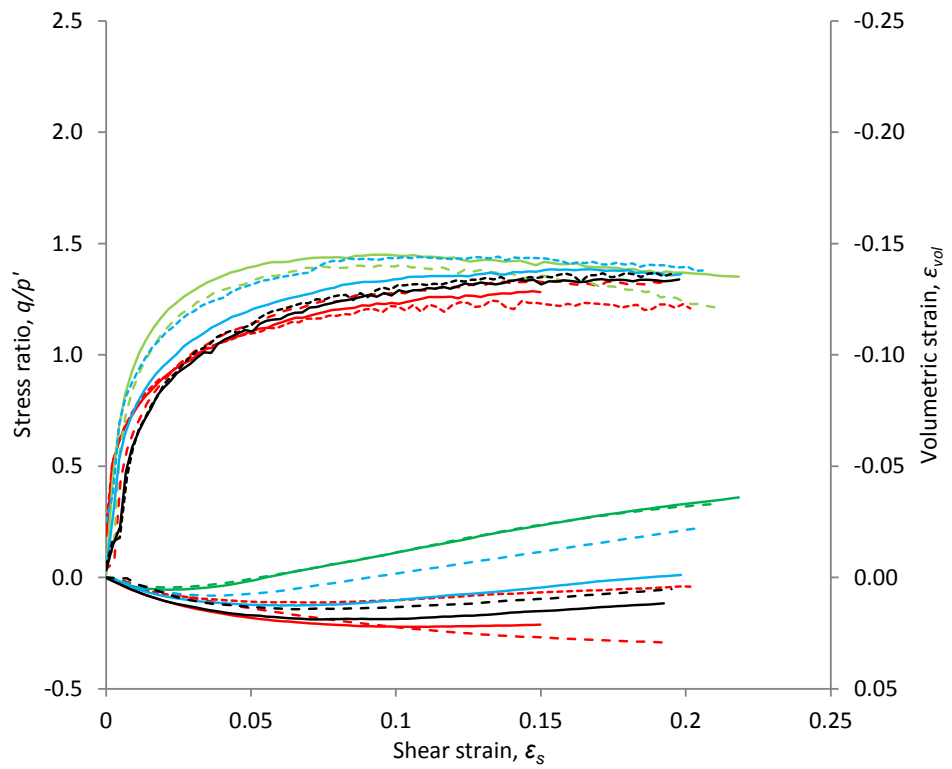
- Sand and sand-salt tests illustrate strain-softening dilative behaviour associated with initially dense soil
- Sand-salt tests show the highest peak stress-ratios, a function of the low void ratios achieved by some sand-salt mixtures
- Both sand and sand-salt tests show higher pre-peak stiffness than post-dissolution tests shown in Figure 4.8a

The convergence of stress-ratio values at the end of shear in sand tests is not shared by the sand-salt tests. The critical stress-ratio values of the sand-salt tests at shear strains of 20% are related to their differing gradings associated with their respective salt particle sizes. This is the reason for the large range of pre-shear void ratios and critical void ratios in Figure 4.9b as discussed later.

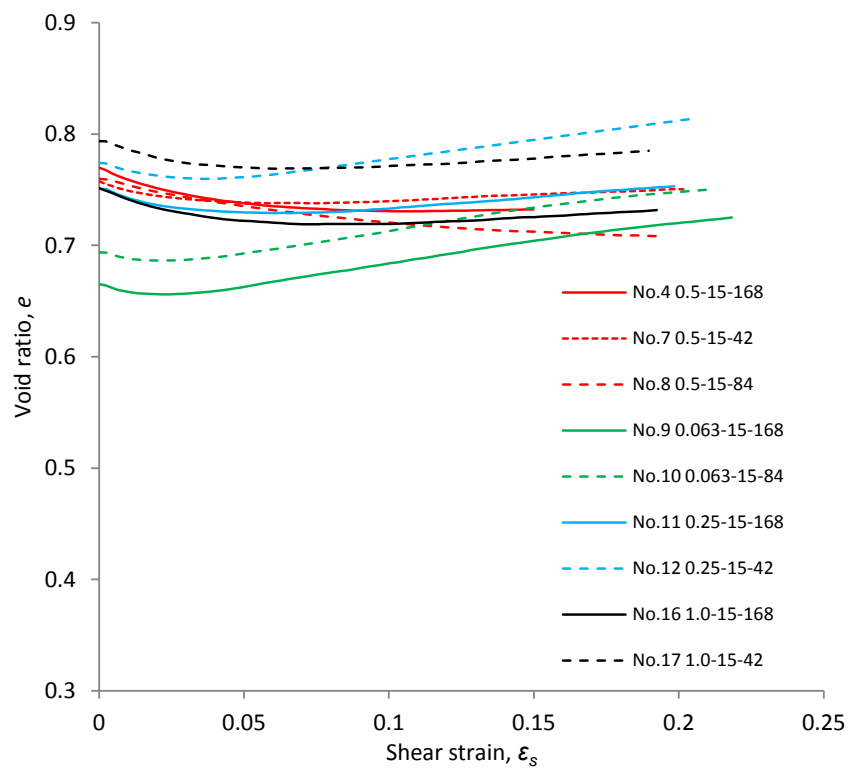
### 4.6.2 Sand-salt vs. post-dissolution

Although the volumetric consequences of particle loss with respect to particle size and percentage by weight lost have been presented in McDougall et al. (2013), the effect of the consequent shearing with respect to particle size lost has received little

#### 4. Experimental results



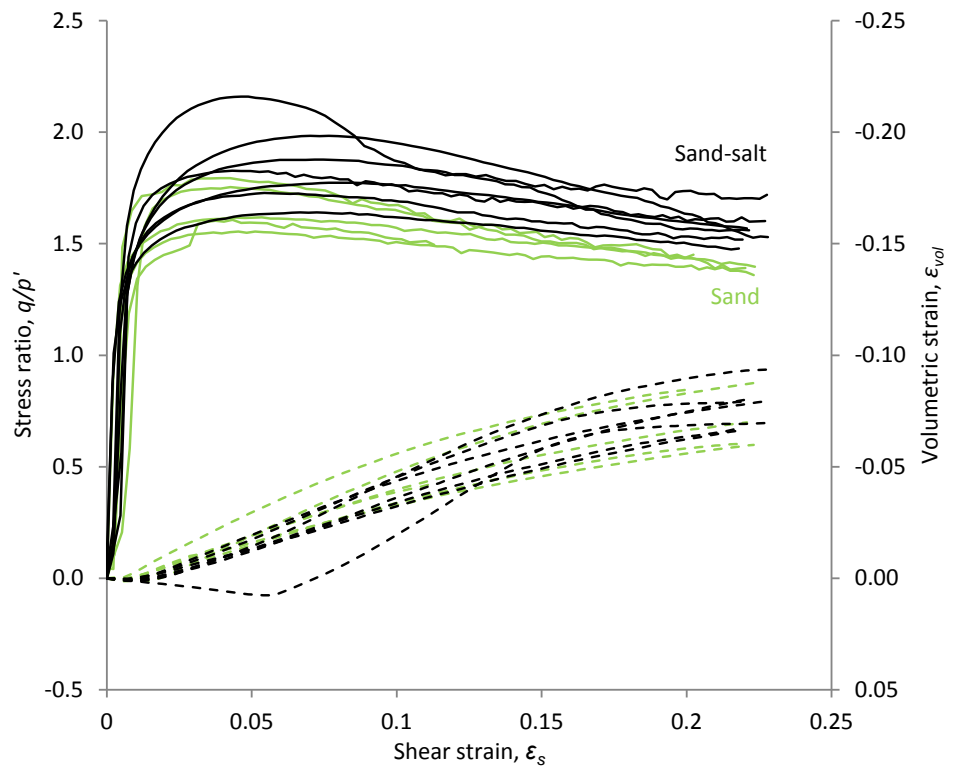
(a)



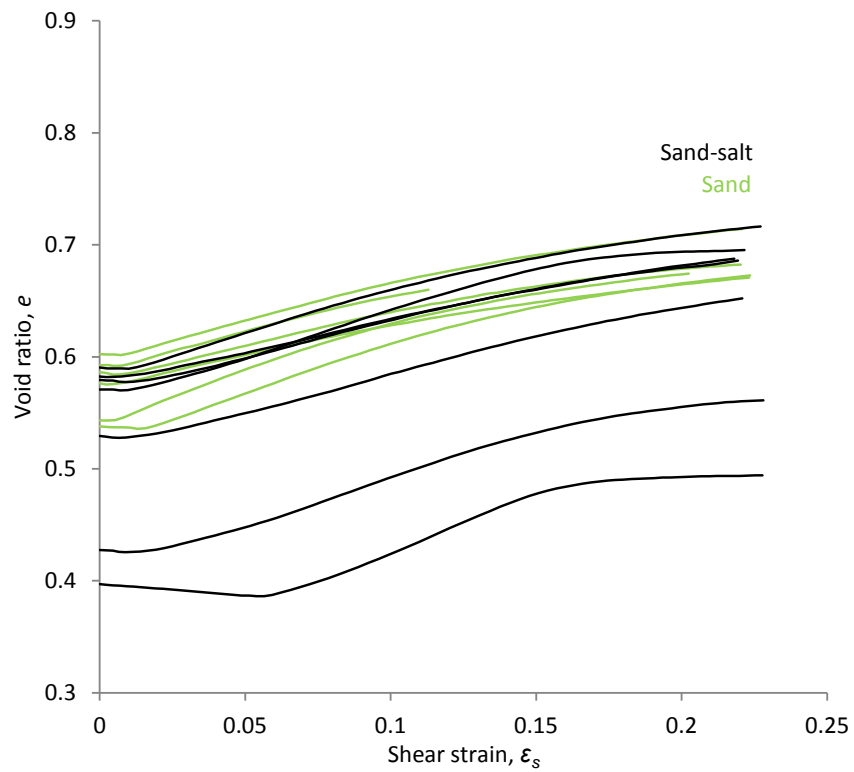
(b)

Figure 4.8: Shear behaviour of post-dissolution tests (a)  $q/p'$  and  $\varepsilon_{vol}$ , and (b)  $e$  against  $\varepsilon_s$

#### 4. Experimental results



(a)



(b)

Figure 4.9: Shear behaviour comparison of sand and sand-salt tests (a)  $q/p'$  and  $\epsilon_{vol}$  (dashed), and (b)  $e$  against  $\epsilon_s$



attention apart from by Fam et al. (2002), Tran et al. (2012) and the publication by Kelly et al. (2012) that was based on dissolution tests performed as part of this study. The general shear behaviours of sand-salt and post-dissolution tests are shown in Figure 4.10. The shearing response of the sand-salt is typically that of a dense sand with a strain-softening dilative behaviour. In contrast, where particle loss has occurred, shearing shows a strain-hardening contractive response. Additionally, the critical state strengths of the sand-salt and sand tests are clearly separated (Figure 4.10a).

Rather than just maintaining a void space during static stress application, or just altering the initial state of the specimens, salt particles seem to be part of or provide support to strong force chains and enhance the shear strength of the soil. The difference in sand-salt and post-dissolution test shear behaviours qualify the role of the salt particles as structural components within the samples, and rather than just maintaining a void space during static stress application, they contribute to the frictional strength of the soil.

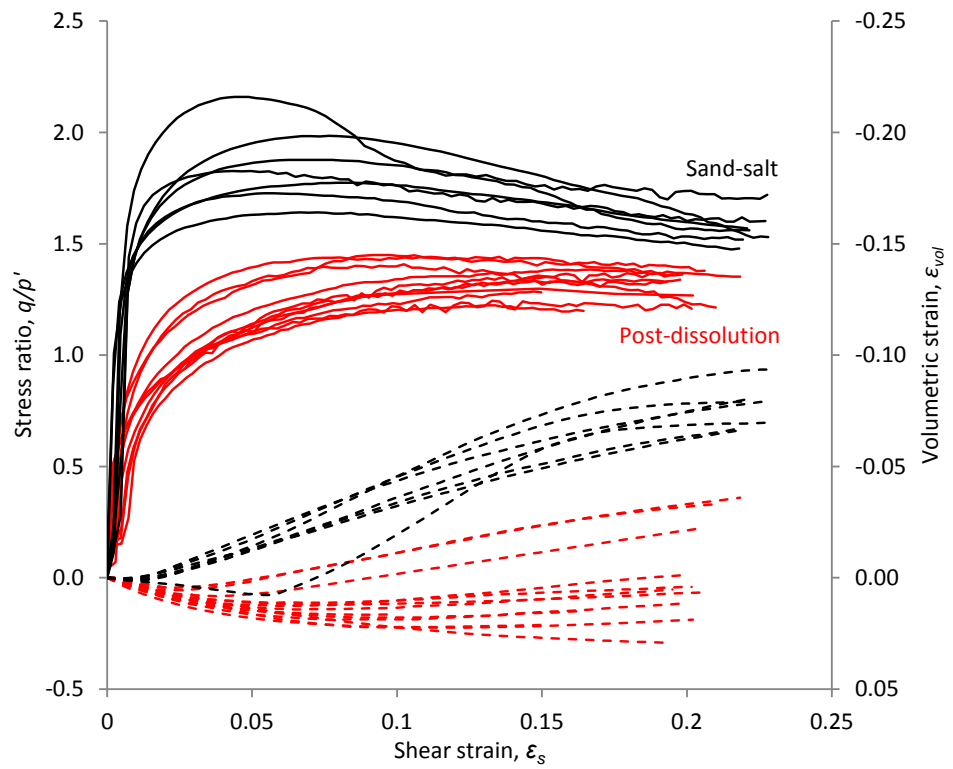
Due to the predominant strain-hardening behaviour in post-dissolution tests, peak stress-ratios are hardly perceptible, and if peaks are perceived, their low values are in contrast to the high peak stress-ratios exhibited by the sand-salt tests. The sand-salt tests demonstrated higher critical (end of shear) stress-ratios than post-dissolution samples. Alternative critical stress-ratios were anticipated due to the various salt particle sizes present in the sand-salt tests resulting in different soil gradings to that of the post-dissolution samples. Further, the presence of salt in the sand-salt tests represent a difference in sample mineralogy to post-dissolution samples. A significant reduction in the critical stress-ratio is evident with dissolution.

However it is the rearrangement of particles within a granular soil that affect the strength behaviour, or stress-ratio evolution, during shear. The micro-scale particle rearrangement during shear is captured by the externally measured volumetric strain. The volumetric strain data shows that large volume increase, or dilation is required to achieve a condition closely resembling the critical state in sand tests ( $\varepsilon_{vol} = 6-9\%$ ) (Figure 4.10a). In contrast, the post-dissolution tests do not reveal significant volume changes ( $\varepsilon_{vol} = +/- 3\%$ ) and are generally contractive.

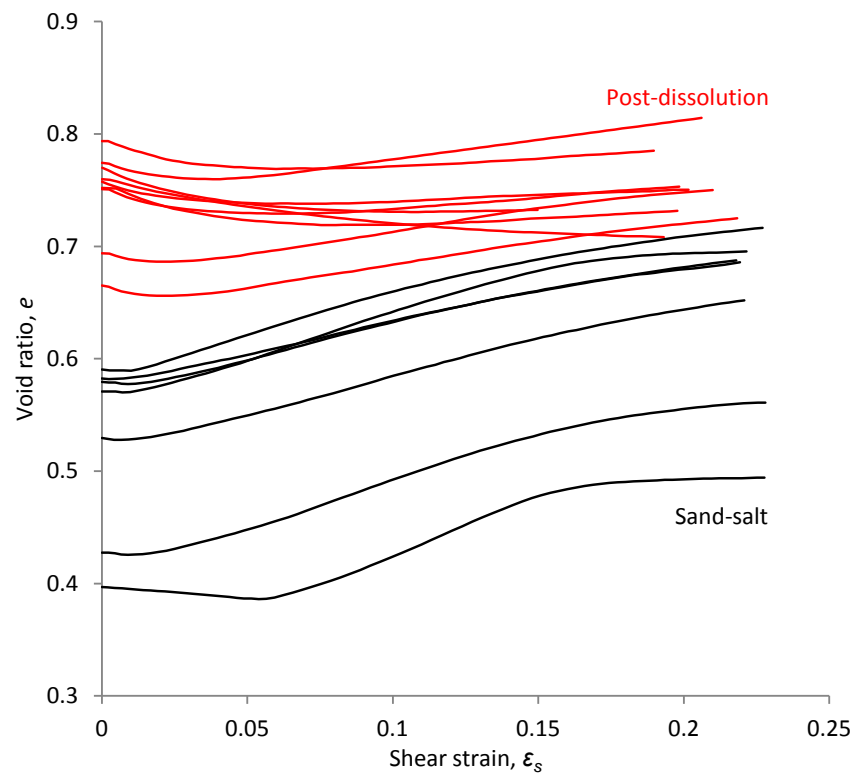
Figure 4.10b shows the range of volumetric behaviour during shear obtained for dry sand-salt and post-dissolution samples in terms of void ratio. Key differences are:

- Pre-shear void ratios in post-dissolution tests are higher, a function of the

#### 4. Experimental results



(a)



(b)

Figure 4.10: Shear behaviour comparison of sand-salt and post-dissolution tests (a)  $q/p'$  and  $\varepsilon_{vol}$  (dashed), and (b)  $e$  against  $\varepsilon_s$

phase relation changes accompanying particle removal

- Pre-shear void ratios in sand-salt tests vary in accordance with the various achievable particle packing in binary mixtures as illustrated by Lade et al. (1998)
- Void ratios at the end of shear in the majority of post-dissolution samples are apparently approaching a common critical state while they vary widely for sand-salt mixtures

Better convergence of void ratios at shear strains of 20% was expected since the cell pressures applied during testing were within a relatively small range of 42 to 168 kPa, remembering that post-dissolution tests consist of sand only. This assumption was based on the expectation that the critical state would be achieved at 20% shear strain. This is not certain based on the data presented although  $q/p'$  and  $e$  each appear to be close to achieving a constant value at shear strains of 20%.

It was anticipated that sand-salt tests would have various void ratios at shear strains of 20% based on their varying grading as a result of the different salt particle sizes. This assumption proved to be correct with a large range of void ratios (Figure 4.10b).

The pre-shear void ratio in both post-dissolution and sand-salt tests is related to the amount and size of salt particles added to the predominantly sand matrix. The pre-shear void ratios for post-dissolution tests are shown to be high; a consequence of particle dissolution as explained earlier. Contractive shearing behaviour was therefore anticipated. Sand-salt tests had much lower initial void ratios and consequently show dilative behaviour.

Previous experimental studies investigating the mechanical effect of dissolution of various percentages of uniform sized salt from uniform sand have also found decreasing peak strength and a change from a dilative to a more contractive shearing response with increasing percentages of salt (Fam et al. 2002, Shin & Santamarina 2009, Tran et al. 2012).

### **4.6.3 Sand-salt vs. post-dissolution shear behaviour with respect to salt size**

A primary research goal was to determine the shearing behaviour of post-dissolution soils. In the previous section behaviours were grouped by test type, i.e. sand,

sand-salt and post-dissolution. Sand-salt and post-dissolution represent pre- and post-particle removal states.

Figure 4.11 shows the shearing behaviour before and after particle removal. Removable particle sizes influenced the initial void ratio in accordance with the achievable packing densities of the mixtures. Salt particle percentage influenced the void ratio change. Therefore the post-dissolution void ratio was a function of the percentage of particles removed and the initial void ratio. The variations between the shearing behaviours with respect to salt particle size may therefore be related to the initial packing density or void ratio. It follows in Figure 4.12 that the initial void ratio in sand-salt tests vary according to the salt particle size while the difference between the pre-shear void ratios of sand-salt and post-dissolution tests are relatively similar.

A possible influence of applied stress may also be observed in Figure 4.12. There are consistently lower initial void ratios for tests loaded to higher cell pressures in sand-salt and post-dissolution tests respectively, but compressive behaviour over larger shear strains. This is indicative of the pressure dependence of soil shearing behaviour even at low cell pressures ranging 42 to 168 kPa. This is illustrated more clearly in Figure 4.12c where three tests performed at cell pressures of 42, 84 and 168 kPa, while sharing identical initial void ratios, demonstrate stress dependent compressive behaviours. The higher pressures of 84 and 168 kPa result in contraction over larger strains.

As salt particle size (0.5 mm salt) increases to resemble that of the sand, the critical void ratio becomes more consistent for the sand-salt and post-dissolution tests (Figure 4.12c). This highlights the structural integrity of the salt particles when sheared at low stresses and their maintained influence on sample grading towards the end of the shearing stage.

### **Sand-salt**

With respect to salt size, the 0.063 mm sand-salt tests showed the highest peak stress-ratios of all the sand-salt tests (Figure 4.11a). This can be explained in terms of the higher soil densities or more compact particle packing arrangements possible with salt sizes smaller than the predominant sand particles.

Sand-salt test no.26 (Figure 4.11a) has a distinctive peak followed by a sudden drop in stress-ratio between shear strains of 7-10%, a feature not evident in any of the other sand-salt tests where the post-peak strain softening is more gradual. This

is possibly related to the occurrence of the failure plane during shear detailed in section 4.5.2.

### **Post-dissolution**

There is an imperceptible difference in maximum stress-ratios for 0.063 mm and 0.25 mm post-dissolution tests. However the shear strains at which the peak stress-ratios occur in 0.25 mm tests are greater than the 0.063 mm tests (Figure 4.11b).

The maximum stress-ratios of larger salt particle tests of 0.5 mm and 1.0 mm are similar but lower than the 0.063 mm and 0.25 mm test values. However the maximum stress-ratios of the 0.5 mm and 1.0 mm tests typically coincide with critical stress-ratios.

The post-dissolution 0.5 mm tests shared an identical pre-shear void ratio of 0.79 resulting in near identical stress-strain behaviours as shown in Figure 4.11c.

For the 1.0 mm tests in Figure 4.11d, post-dissolution void ratios ranged 0.77-0.82, values close to the maximum void ratio for the sand. This indicates that the shearing behaviour for the 0.5 mm and 1.0 mm salt post-dissolution tests represent the weakest strength response for the sand thereby forming the minimum boundary line in the stress-ratio envelope for this sand grading.

### **4.6.4 Sand vs. post-dissolution**

The contrasting shear behaviours of sand and post-dissolution tests are presented in Figure 4.13. Both test types consist of uniformly graded Leighton Buzzard sand only. The sand tests show strain-softening behaviour in contrast to the strain-hardening post-dissolution behaviour noted earlier, and explained by differences in terms of their respective pre-shear void ratios (Figure 4.13). Since the sand in both test types is identical, convergence of stress-ratios and void ratios were expected at the critical state. While convergence is observed for the stress-ratios, convergence of void ratios is less clearly defined.

Performing standard triaxial tests on a uniform, sub-angular to angular Leighton Buzzard sand, ranging 0.75 to 0.212 mm, Klotz & Coop (2002) found similar shearing characteristics, i.e. critical stress-ratio values ranged 1.25-1.45 whereas 1.15-1.4 was achieved using uniform, sub-rounded, Leighton Buzzard with a median diameter of

#### 4. Experimental results

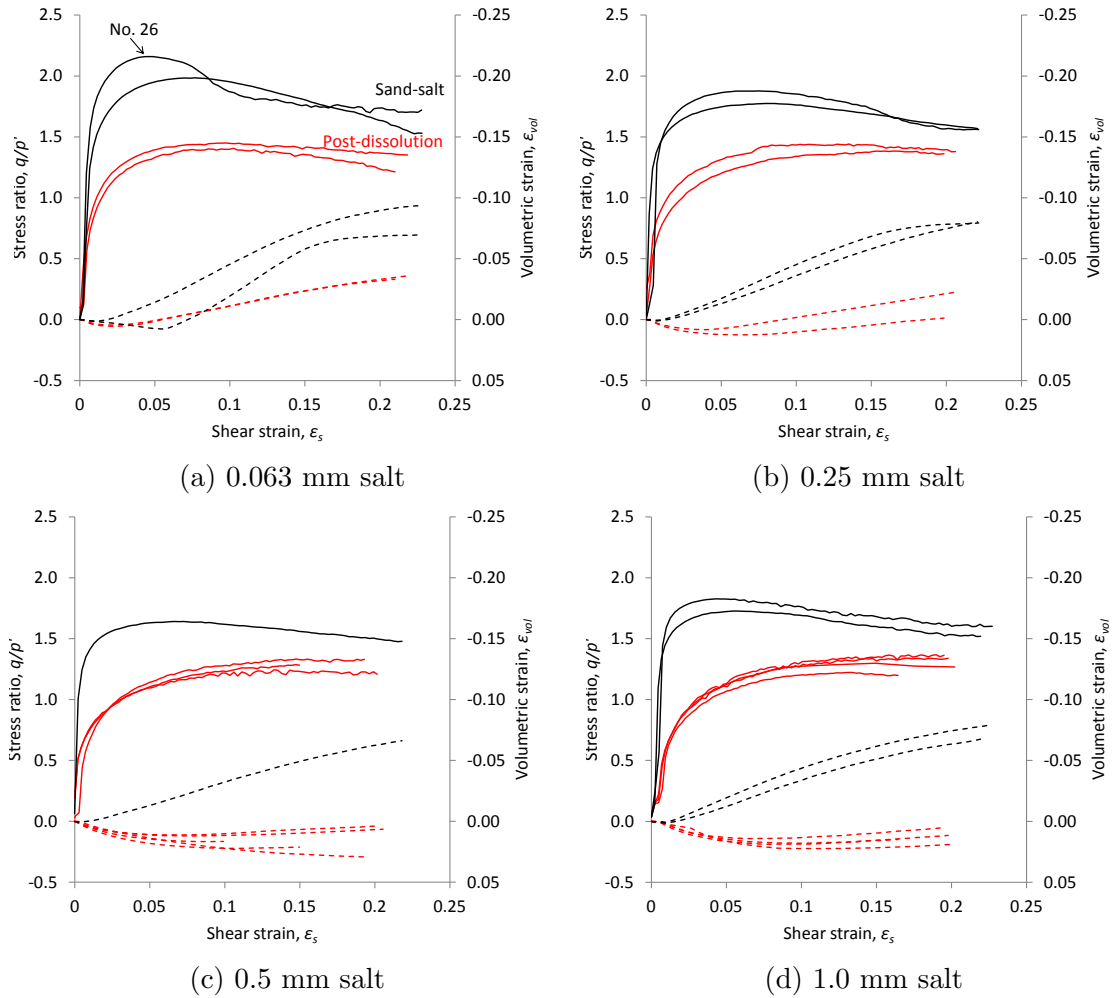


Figure 4.11: Stress-ratio and volumetric strain (dashed) against shear strain for sand-salt and post-dissolution tests (a) 0.063 mm (b) 0.25 mm (c) 0.5 mm and (d) 1.0 mm salt at 15% by weight tests

## 4. Experimental results

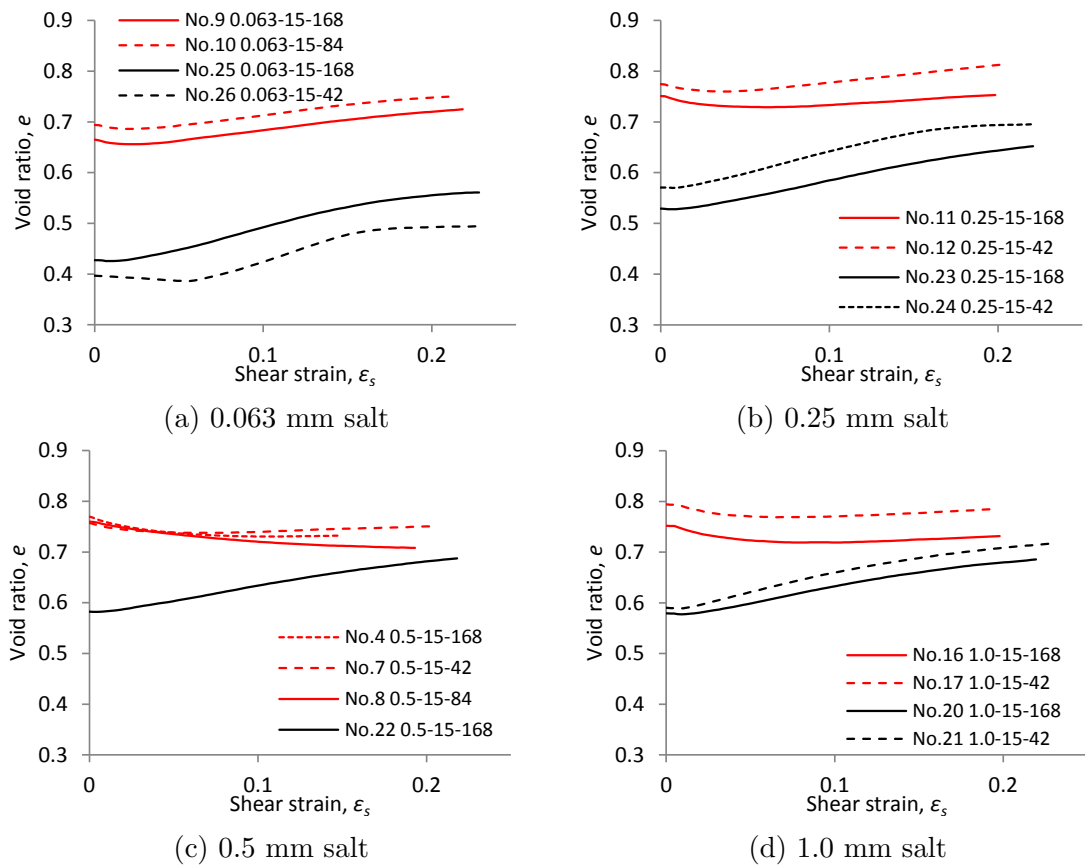


Figure 4.12: Void ratio against shear strain for sand-salt and post-dissolution tests with (a) 0.063 mm (b) 0.25 mm (c) 0.5 mm and (d) 1.0 mm salt at 15% by weight

0.85 mm in this study. In terms of peak stress-ratios, Klotz & Coop (2002) achieved 1.5 for a densely prepared sample under an applied stress of 100 kPa, a value of 1.75 was achieved for densely prepared samples tested under similar stress levels in the current study.

The measurement of volumetric strains in the current study appeared to reach shear strains of approximately 20% without signs of difficulties, allowing the majority of tests to approach the critical state. However, the sand and post-dissolution tests do not converge on a common critical void ratio. Figure 4.13b again affords the opportunity to reflect on the void ratios at the beginning of shear. These range 0.54-0.8, effectively satisfying the range defined by the minimum and maximum void ratios (0.55-0.84).

### **4.6.5 Effect of applied stress in shearing behaviour**

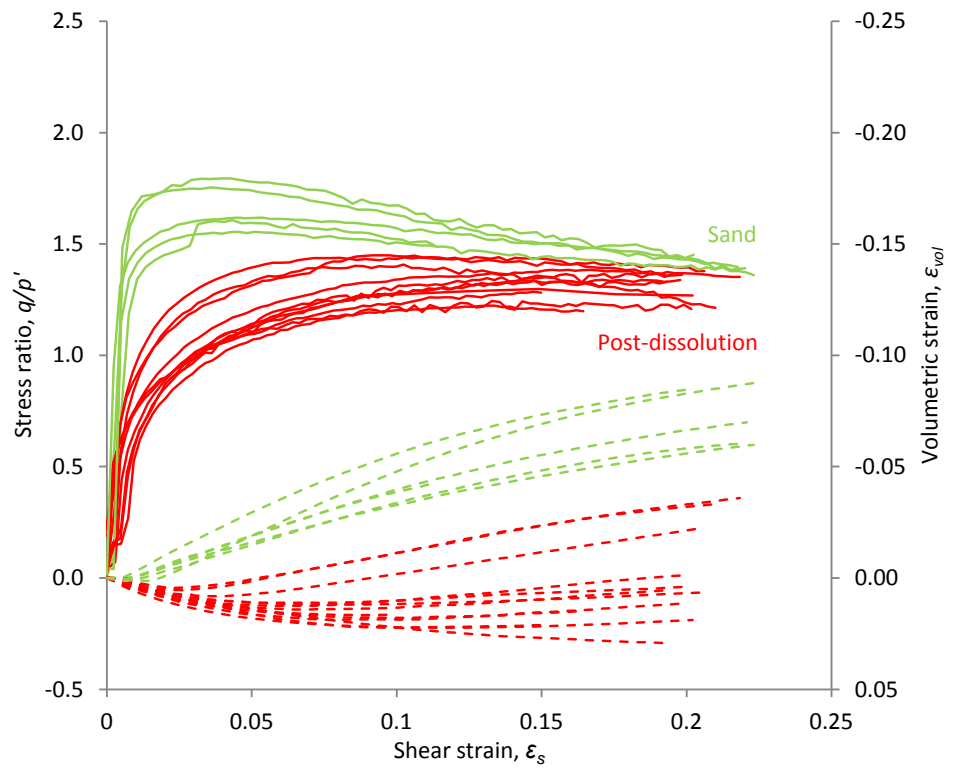
If the void ratios at the end of shear for sand only samples (i.e. post-dissolution and sand tests) are assessed it is clear that there is better convergence as the applied stress increases (Figure 4.14). This is consistent with the results found by (Klotz & Coop 2002) when trying to identify the critical state line. Drained Leighton Buzzard tests performed under an applied stress of 100 kPa had end of shear void ratios ranging 0.175, while as applied stresses increased to 700 kPa the range decreased to 0.075. Similarly, in the current study, tests performed under an applied stress of 42 kPa had end of shear void ratios ranging 0.13, while an increased applied stress of 168 kPa resulted in better convergence with a reduced range of 0.05.

### **4.6.6 Shearing response of sand and sand-salt mixture with identical pre-shear void ratios**

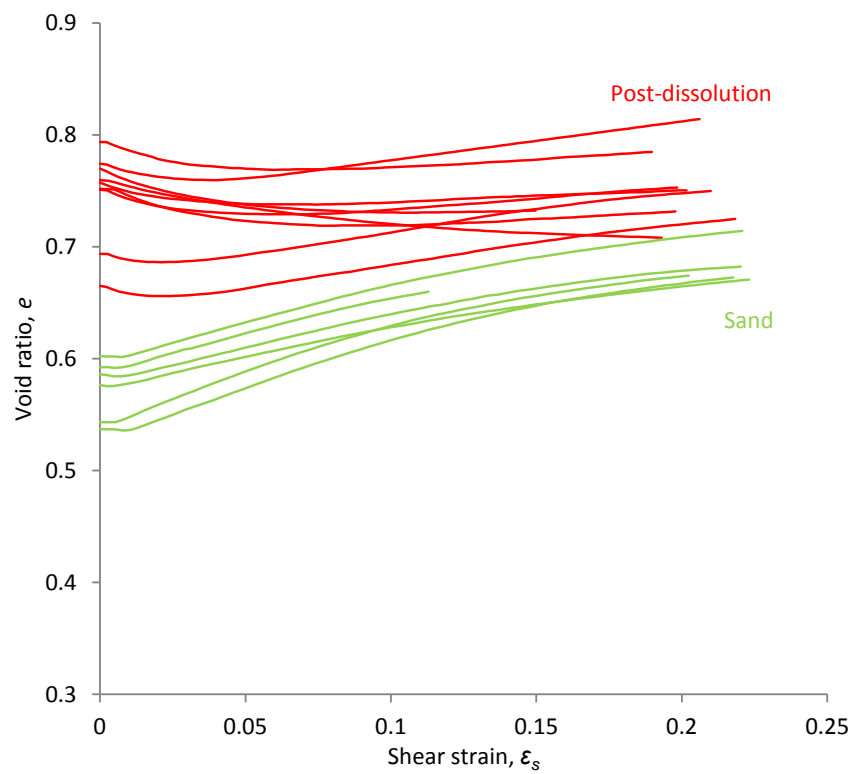
Test nos. 18 (LB-168) and 22 (0.5-15-168) provide the opportunity to assess the influence of salt in the mixture as both share identical gradings and initial void ratios ( $e = 0.59$ ) (Figure 4.15). The two tests show similar shearing behaviour. The exception is the less stiff response of the sand-salt test with the peak stress-ratio developing at a higher shear strain. It is therefore plausible that the less stiff salt particles participate in the strong force chains during shear in the 15% by weight of salt sample (no.22 0.5-15-168).



#### 4. Experimental results



(a)



(b)

Figure 4.13: Shear behaviour comparison of sand-only and post-dissolution tests (a)  $q/p'$  and  $\epsilon_{vol}$  (dashed), and (b)  $e$  against  $\epsilon_s$

#### 4. Experimental results

---

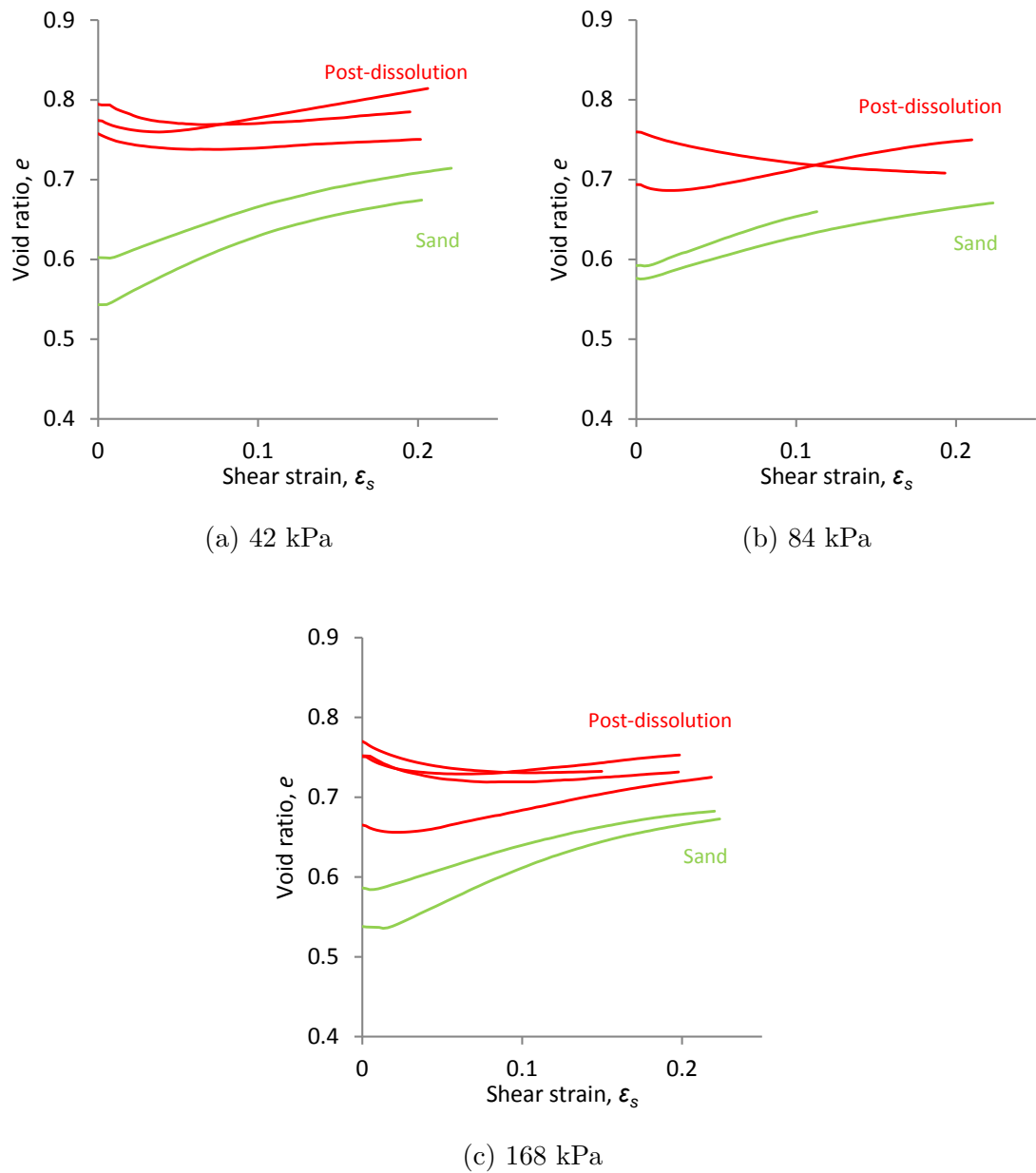


Figure 4.14: Void ratio against shear strain for sand-salt and post-dissolution tests for applied cell pressures of (a) 42 kPa, (b) 84 kPa, and (c) 168 kPa

#### 4. Experimental results

---

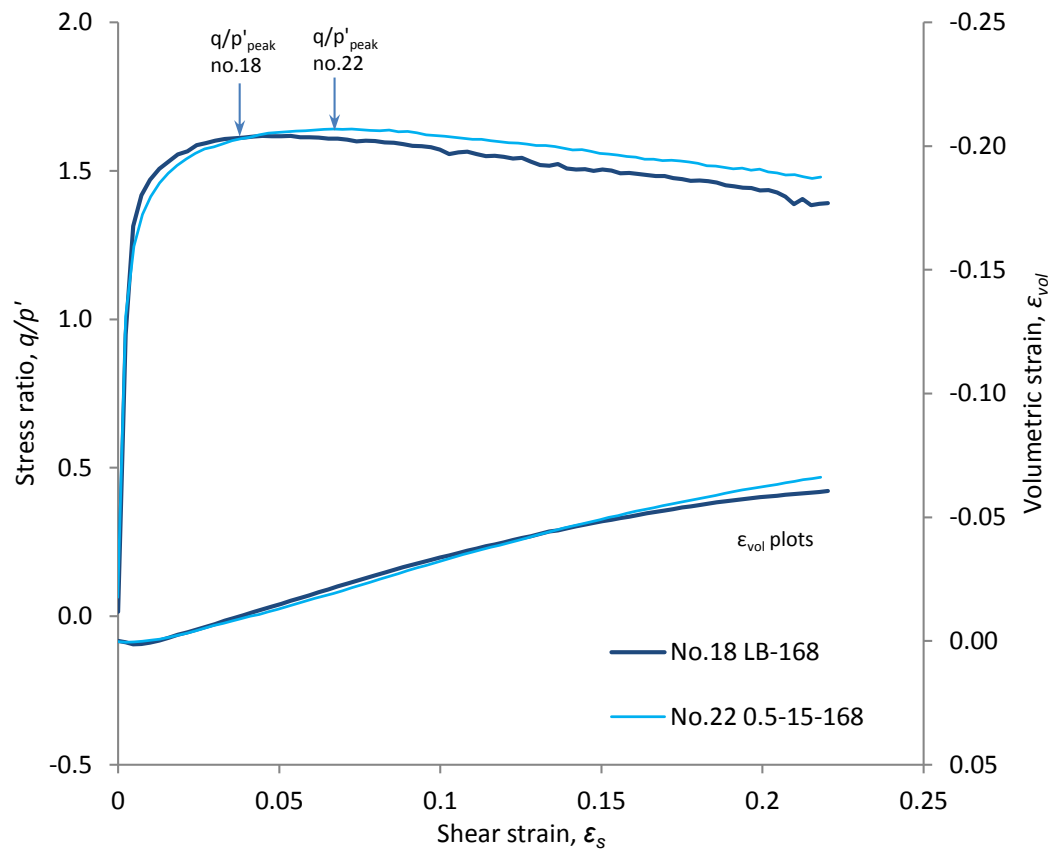


Figure 4.15: Shear behaviour for a sand and sand-salt test with identical pre-shear void ratios and gradings

An interesting observation was made in 20% by weight samples conducted as part of the current study. Test nos. 14 (1.0-20-168) and 15 (1.0-20-42) contained 20% by weight of 1.0 mm salt particles. Under isotropic stress application, the salt particles could be seen protruding through the membrane in the higher stress 168 kPa test. The protruding particles were evidently salt due to their larger size relative to the sand. This suggests that less stiff particles are less likely to form part of strong force chains. At high percentages, such as in test no.22, it is probable that salt particles become part of the load bearing force chains, yet shear behaviour is not altered considerably.

### **4.7 Stress-ratio analysis of sand-salt and post-dissolution tests**

This section analyses the stress-ratios of the sand-salt and post-dissolution tests with focus on the peak stress-ratios and the critical stress-ratios. In this section the critical stress-ratio is taken as the value at shear strains of approximately 20%.

#### **4.7.1 Maximum (peak) stress-ratio against pre-shear void ratio**

The relationship between the peak stress-ratio and the pre-shear void ratio for sand-salt and post-dissolution tests is illustrated in Figure 4.16. It shows:

- The clear difference between pre-shear void ratios for the sand-salt and post-dissolution tests and the consequent peak stress-ratio variability as noted earlier.
- A general linear trend between pre-shear void ratio and peak stress-ratio for the stresses applied.
- The overall trend for the lowest pressure 42 kPa tests shows higher peak stress-ratios but also greater scatter of value. Tests performed at higher pressures show lower peak stress-ratios and also greater linear consistency. This shows the well known pressure dependency of soil behaviour.

#### 4. Experimental results

- Apparent clustering of peak stress-ratios for salt particle sizes of 0.25 mm, 0.5 mm and 1.0 mm in post-dissolution tests with 0.063 mm tests positioned outside. This was mentioned previously where salt sizes near equivalent in size to the sand resulted in similar post-dissolution void ratios.
- A greater range of peak stress-ratios for sand-salt tests according to the pre-shear void ratio which is a function of sample grading.

The wide ranges of critical void ratios for sand-salt and post-dissolution tests presented in Figure 4.16 show that the state parameter cannot reasonably be applied to either test type. For sand-salt tests this wide range is explained in terms of different sample gradings. For post-dissolution tests, the range is large due to the poor convergence of critical void ratios at low stresses. As shown in Figure 4.14 earlier, this range decreases for higher applied stresses suggesting that the application of the state parameter is only meaningful at higher applied stresses when a definitive critical void ratio is obtained. A summary of the void ratios at the beginning of shear for all tests and the resulting maximum (peak) stress-ratios is given in Table 4.2.

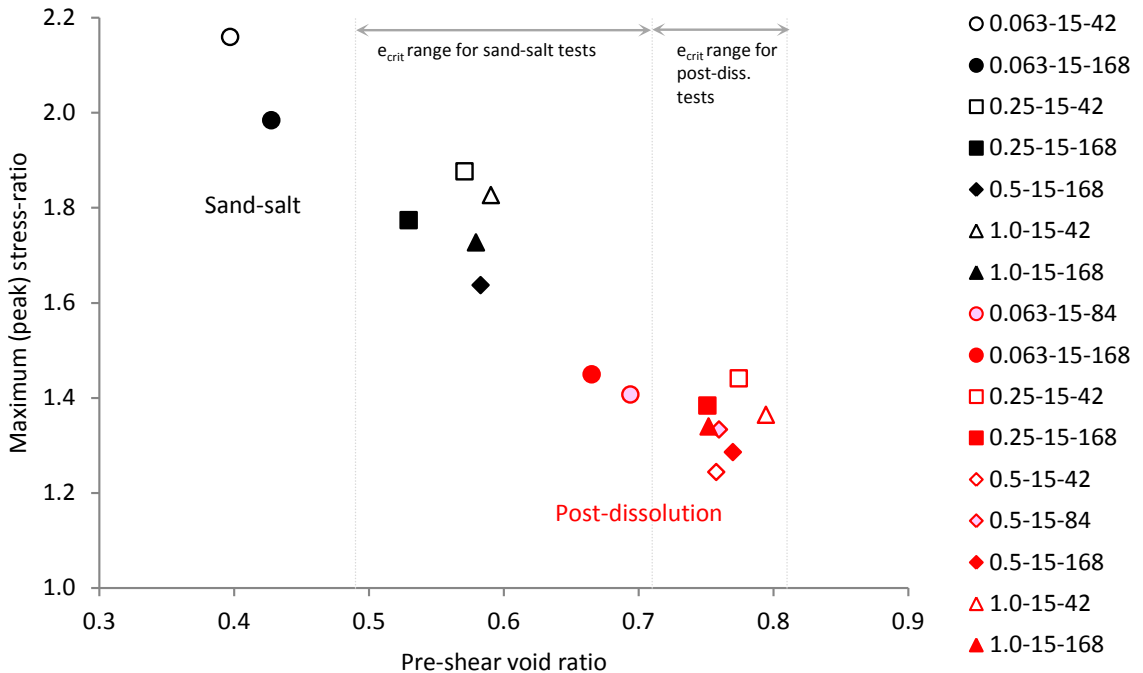


Figure 4.16: Maximum (peak) stress-ratio against pre-shear void ratio for sand-salt and post-dissolution tests

#### 4. Experimental results

---

Table 4.2: Summary of void ratios and peak stress-ratios

Test	Pre-dissolution			Post-dissolution		
	Void ra- tio	Relative density	Peak stress- ratio	Void ra- tio	Relative density	Peak stress- ratio
No.1 LB-100-42	0.55	0.88	1.8	-	-	-
No.2 LB-100-84	0.59	0.76	1.6	-	-	-
No.3 LB-100-168	0.53	0.94	1.7	-	-	-
No.4 0.5-15-168	0.57	0.82	-	0.79	0.15	1.2
No.5 0.5-15-84	0.55	*	-	0.7	-	-
No.6 0.5-15-84	0.57	*	-	0.72	-	-
No.7 0.5-15-42	0.57	0.82	-	0.79	0.15	1.1
No.8 0.5-15-84	0.57	0.82	-	0.79	0.15	1.25
No.9 0.063-15-168	0.38	-	-	0.68	0.48	1.4
No.10 0.063-15-84	0.43	-	-	0.72	0.36	1.35
No.11 0.25-15-168	0.57	-	-	0.76	0.24	1.3
No.12 0.25-15-42	0.56	-	-	0.8	0.12	1.4
No.13 LB-100-84	0.58	0.79	1.5	-	-	-
No.14 1.0-20-168	0.55	-	-	0.78	0.18	1.2
No.15 1.0-20-42	0.56	-	-	0.79	0.15	1.3
No.16 1.0-15-168	0.58	-	-	0.77	0.21	1.3
No.17 1.0-15-42	0.62	-	-	0.82	0.06	1.4
No.18 LB-100-168	0.58	0.79	1.6			
No.19 LB-100-42	0.61	0.7	-			
No.20 1.0-15-168	0.58	-	1.7			
No.21 1.0-15-42	0.6	-	1.8			
No.22 0.5-15-168	0.58	0.79	1.6			
No.23 0.25-15-168	0.53	-	1.7			
No.24 0.25-15-42	0.58	-	1.85			
No.25 0.063-15-168	0.44	-	1.95			
No.26 0.063-15-42	0.41	-	2.1			

---

“\*” denotes incomplete dissolution

### 4.7.2 Peak stress-ratio shear strain

Figure 4.17a shows that maximum (peak) stress-ratios are achieved at lower shear strains in sand-salt tests than post-dissolution tests. Sand-salt peak stress-ratios occur at shear strains of 4-8% while post-dissolution maximum stress-ratios occur at shear strains of 9-20%. As shown earlier, dry sand-salt tests exhibited strain-softening behaviour with peak strengths developing soon after the initiation of shear. However, post-dissolution tests did not develop a distinctive peak and instead exhibited strain-hardening until maximum strength was achieved, coinciding with the critical state condition. Hence, the post-dissolution tests share a relatively common maximum stress-ratio. Void ratios at failure in post-dissolution tests (Figure 4.17b) are relatively consistent since the void ratio at failure coincides with the critical void ratio for these tests.

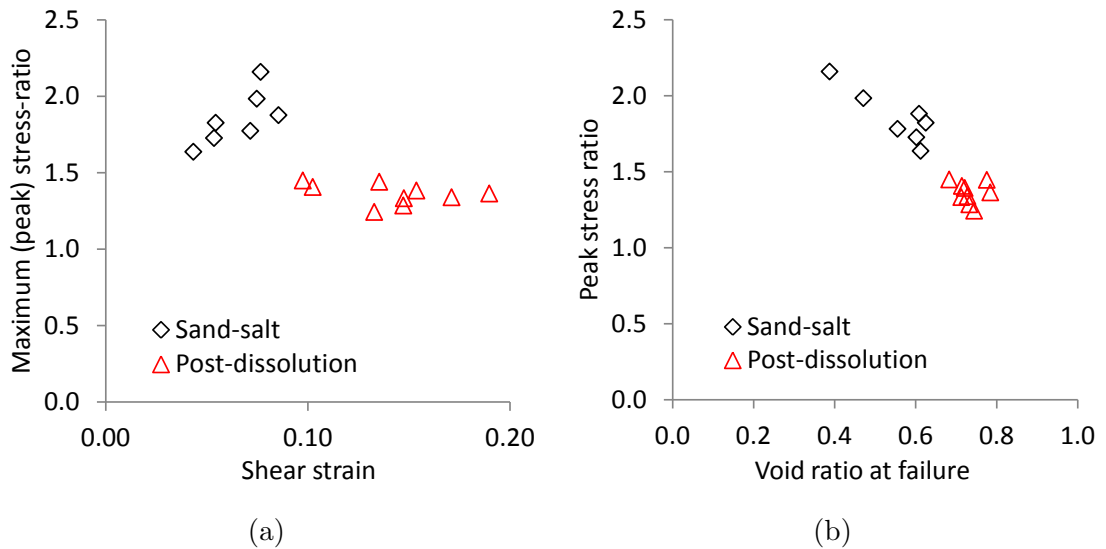


Figure 4.17: Peak stress-ratios against (a) shear strain, and (b) void ratio at failure

### 4.7.3 End of shear stress-ratio with respect to salt particle size

Fine-salt present in sand-salt tests encourages lower void ratios as shown in Figure 4.18b. These fine particles support the strong sand force chains and provide additional shearing resistance to the end of shear as evidenced by the higher end of shear stress-ratios for fine salt particle additions in Figure 4.18a. Post-dissolution tests consist of sand-only samples and therefore end of shear (critical) stress-ratios and void ratios are the same (spread is attributed to tests performed at low stress).

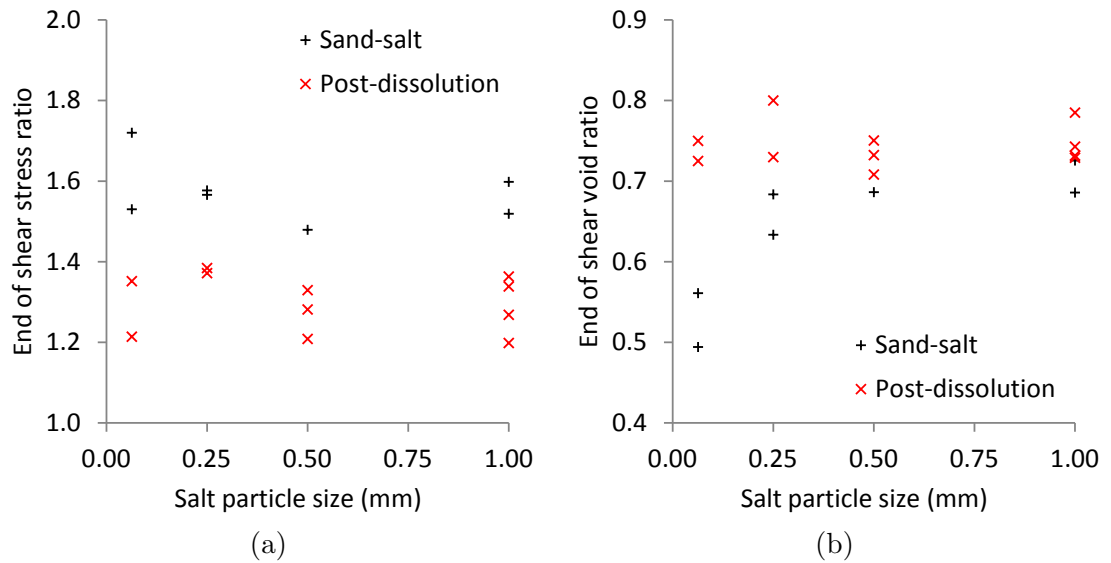


Figure 4.18: End of shear (a) stress-ratio and (b) void ratio against salt particle size

#### 4.7.4 Volumetric shearing response of Leighton Buzzard sand

All samples, including sand tests, were prepared to achieve a dense packing. The high density of the samples is indicated by the low pre-shear void ratios that are close in proximity to  $e_{min, LB}$  as illustrated in Figure 4.19. The volumetric strains at the end of shear for these tests are shown to be highly sensitive to pre-shear void ratios, with slightly lower void ratios resulting in considerably greater end of shear volumetric strains.

#### 4.7.5 Influence of pre-shear void ratio on volumetric behaviour

The ‘dilation commencement’ referred to in Figure 4.20 marks the transition from contractive to dilative behaviour in sand and post-dissolution triaxial tests evident in Figures 4.5b and 4.8b. In the sand tests, an initial contraction at low shear strains was followed by a change to sample volume increase, or dilation. In post-dissolution tests, the contractive stage occurred over much larger strains before the commencement of dilation. Figure 4.20 shows that the pre-shear void ratio has a strong influence on the shear strain that dilation commences. Higher pre-shear void ratios result in contractive phases to larger shear strains prior to the commencement of dilation.



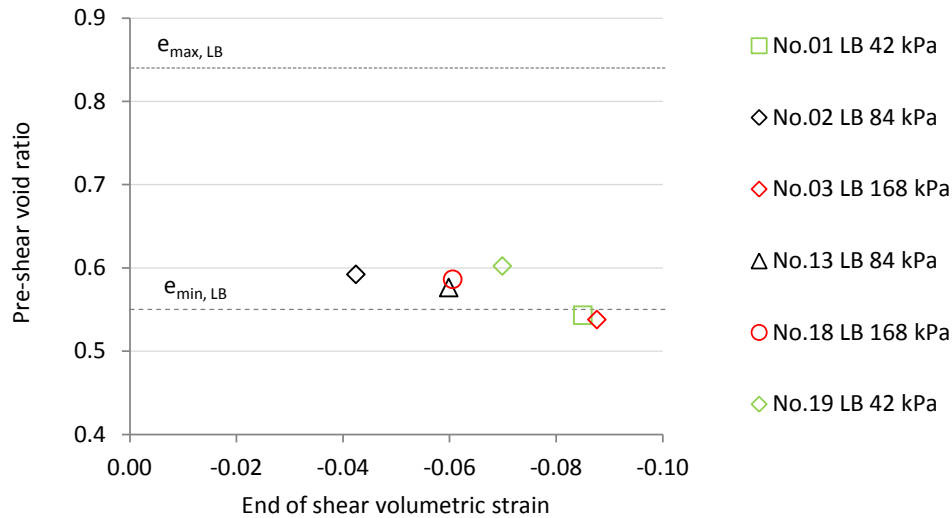


Figure 4.19: Pre-shear void ratio against end of shear volumetric strain for sand tests

For densely prepared sand tests the contraction stage is small or non-existent while the loose post-dissolution sand shows contraction to very large strains. Interestingly for a sand, some post-dissolution tests exhibited contractive behaviour to the end of shear and did not undergo a dilative stage. At large shear strains some post-dissolution tests showed some dilation. This, considering that pre-dissolution sand samples were prepared to achieve a dense packing, shows the effect that particle loss can have on the large-strain volumetric behaviour of soil.

#### 4.7.6 End of shear

Figures 4.21 and 4.22 show void ratio with mean stress paths. Figure 4.21 shows the paths for the sand-salt mixtures where critical states are clearly affected by the addition of salt. All tests show dilatancy, with the magnitude of void ratio increase apparently the same for all mixtures. The presence of fine salt particles resulted in a low initial void ratio and low critical void ratio. Figure 4.22 shows the sand-only and post-dissolution paths. There is much better convergence for the sand-only tests. The post-dissolution tests often reveal an initial contraction followed by dilation. However the overall volumetric change is one of contraction or negligible volume change in 6 of the 9 tests. It is not clear why 3 of the 9 tests are strongly dilatant, but the other 6 tests appear to be converging on a critical void ratio at least as well defined by Klotz & Coop (2002).

#### 4. Experimental results

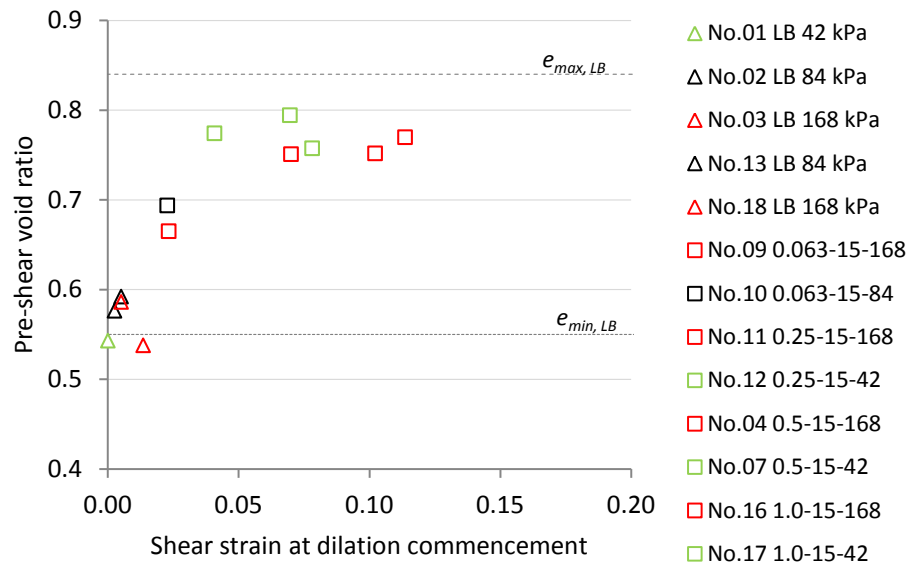


Figure 4.20: Pre-shear void ratio against shear strain at dilation commencement in sand (triangle) and post-dissolution (square) tests

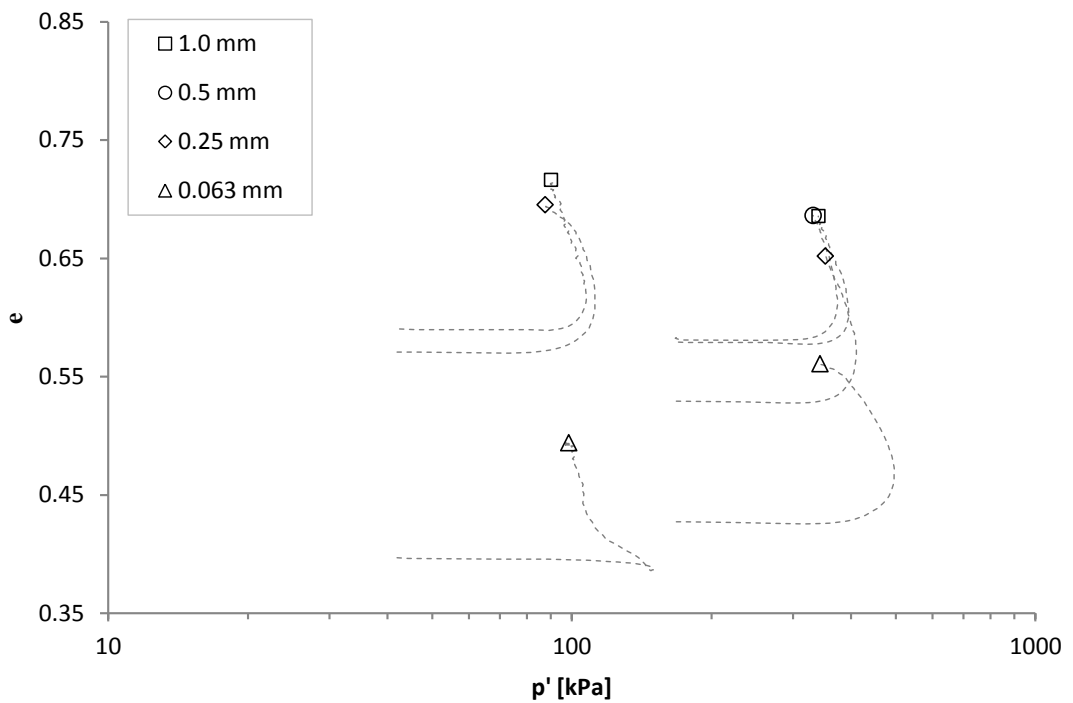


Figure 4.21: End of shear/critical states for sand-salt tests

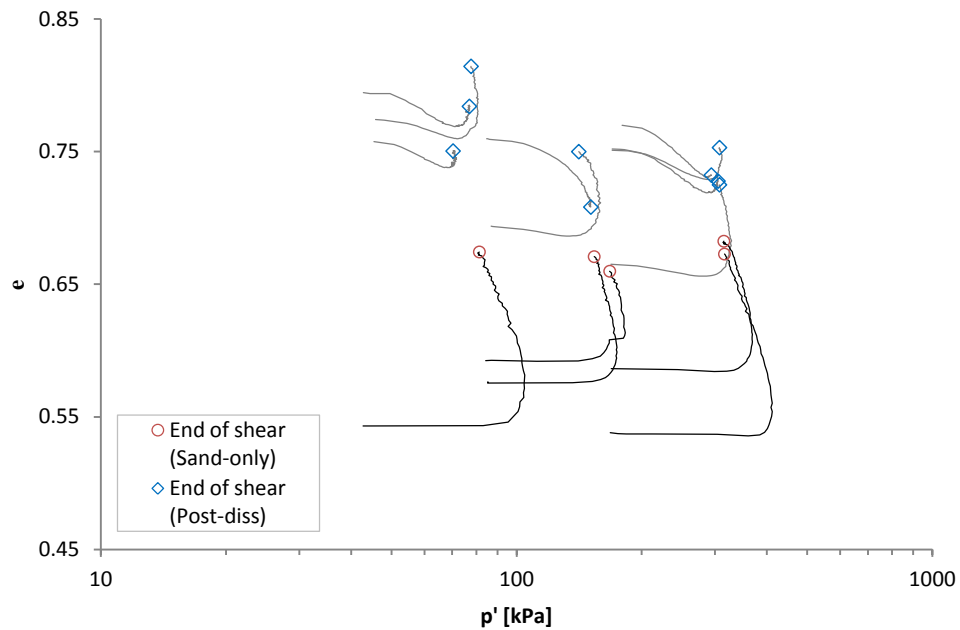


Figure 4.22: End of shear/critical states for sand-only and post-dissolution tests tests

#### 4.7.7 Stiffness evolution

This section presents the large-strain stiffness of the three test types performed as part of the next chapter. In the next chapter the maximum shear modulus of the soil is presented based on bender element measurements. Together, they help define the stiffness-strain curve which is required for the prediction of accurate deformations around geotechnical structures (Jovičić & Coop 1997).

Figure 4.23 presents the tangent stiffness normalised by mean effective stress,  $G/p'$ , for sand, sand-salt and post-dissolution tests. Stiffness calculations are based on increments of  $\approx 0.0025$  shear strain ( $2.5 \times 10^{-1}\%$ ) from triaxial shear data.

Similar stiffness are observed in sand and the sand-salt tests. The post-dissolution tests have notably lower stiffness values.

Figure 4.24 shows the post-dissolution tests. All 1.0 mm tests (nos. 14, 15, 16, and 17) show an early initial stiffness followed by a collapse before regaining stiffness at larger strains. This indicates that the dissolution of 1.0 mm salt particles leads to greater instability in the soil above all other particle sizes tested.

The stiffness of the fine 0.063 mm tests are among the highest. This is consistent with the hypothesis that fine particles “nestle” in the sand voids and can be removed

#### 4. Experimental results

---

without significant impact on the strong force chains of the sand matrix (McDougall et al. 2013).

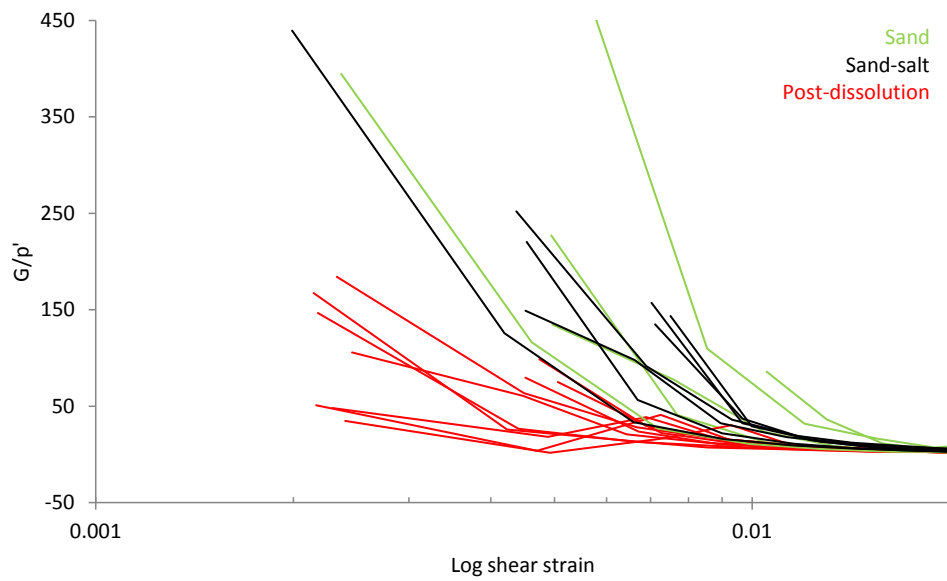


Figure 4.23: Stiffness normalised by mean stress against shear strain

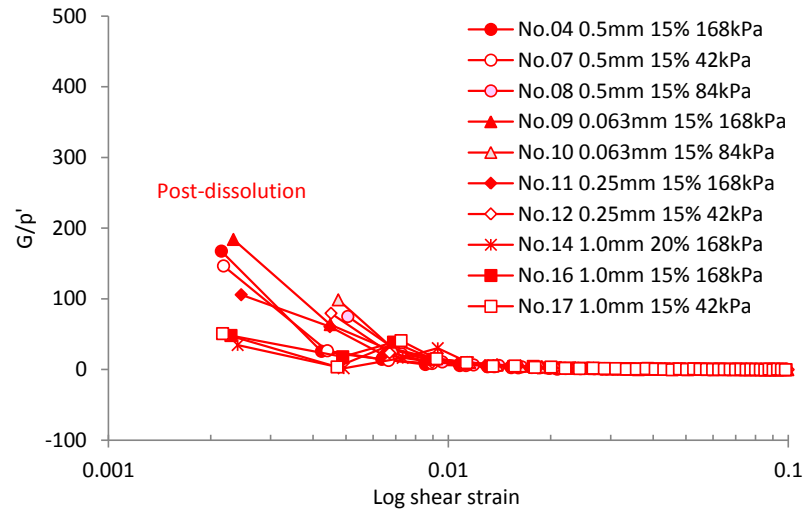


Figure 4.24: Stiffness normalised by mean stress against shear strain in post-dissolution tests

## 4.8 Chapter summary

This chapter presented and analysed the findings from triaxial dissolution tests focusing on the influence of particle size removed, in terms of volumetric change with dissolution, and subsequently, post-dissolution strength and stress-strain behaviour. To illustrate strength and stress-strain changes, comparable intact sand-salt mixtures were sheared. This also permitted the examination of the structural role of salt particles in the sample mixtures, validating their use in this study. Chapter findings are presented below.

### Volumetric changes with dissolution

Volumetric strain was observed with dissolution of salt particles varying in size in all triaxial tests. This indicated that the salt particles performed a structural role within the sand-salt mixtures. However, this role was dependent on the size of the salt particles. Fine salt particle removal resulted in little strain. This was explained using insights from previous studies on particle packing of binary mixtures where fine particles could occupy the interparticle voids of the predominant coarse sized sand. Hence, a minimal amount performed a structural role by intercepting the strong force chains consisting primarily of sand. Increasing salt particle size additions, such that they were near equivalent in size to the sand particles, meant that they were unable to occupy the interparticle voids of the sand. Therefore they provided support to

the strong force chains transmitting load within the sample. Consequently, their removal resulted in buckling or collapse of the strong force chains, as evidenced by the larger dissolution volumetric strain. These results strongly suggest the structural significance of the salt particles in the sand mixtures. It further suggested that, in terms of structural capacity, the salt particles did not merely represent void space in the sand but that they constituted part of the solid phase of the soil.

The complexity of particle loss effects on the volumetric state of the soil was reflected in the void ratio changes that accompanied volumetric strain. In agreement with the findings from all dissolution studies performed in a variety of apparatuses to date, the void ratio was also shown to increase in the triaxial tests performed here. To begin with, salt particle size influenced the initial packing density, or void ratio, of the soil. In samples prepared to achieve a medium-dense packing, fine particle salt additions to coarse sand resulted in initial void ratios lower than the minimum void ratio of the sand, in agreement with the argument referred to above. Coarse salt particles, equivalent in size to the sand, participate structurally in the sand mix. Therefore their initial void ratio were close to the minimum void ratio of the sand. However, void ratio increase in all tests of a given percentage were similar. Therefore the importance of the initial packing density became apparent since the post-dissolution void ratio for fine salt tests was indicated medium density while loose densities were obtained for coarse salt tests.

The combined minor volumetric strain and substantial void ratio increase for dissolution of fine salt particles suggest that these had minor structural influence on the sand structure under static loading. Increasing salt size meant more structural participation, however, with substantial void ratio increase but also significant volumetric strain.

The influence of the applied stress on the total strain and void ratio change was also assessed. Although it appeared that stress may have had a minor influence on the total strain in some sample mixtures, this proved uncertain. Therefore the applied stresses in the current study were not considered to be a major influence. In terms of void ratio change with applied stress, results reflected those of oedometer dissolution tests performed at an earlier stage of the study. That is, void ratio change was independent of the applied stress. However, it appeared to have a slight influence on the initial packing density.

### Large-strain shear

This chapter presents the results of the triaxial strength testing. A total of 26 tests were performed on samples of (i) sand only, (ii) dry sand with (mostly) 15% added by weight of salt of specified particle size, and (iii) sand-salt mixtures with salt particles dissolved. It is this third set that underwent the three stage test procedure: compression-dissolution-shearing. Assessing and comparing each of the three sets of tests:

- Sand only tests showed typical strain softening dilative behaviour
- Dry sand-salt mixtures were also dilatant. Where salt addition produced a wider grading, e.g. 0.063 mm salt particle addition, a tendency to higher critical state strength ratios was observed.
- A strong inverse relationship between maximum strength and pre-shear void ratio was observed.
- In the post-dissolution tests there was a tendency to contract when the initial and final conditions are compared.

Of particular interest was the large strain behaviour of the post-dissolution tests. While there was some convergence in the critical strength between the sand only and post-dissolution sample types, as might have been expected because they are essentially the same soil, the volumetric response did not point to any common critical condition. However, the range of critical volumes measured was within the range of values obtained by other workers in this area.

Particle loss appears to induce a change in soil behaviour. Where a soil may have been originally dense, the volumetric change due to particle loss produces a soil that is apparently loose in its stress-strain behaviour. The dilatancy commonly observed in laboratory prepared (medium to dense) sand samples is replaced by a more contractant behaviour, although the complete strain response is more complex, showing intervals of dilation within an overall contractant response. Accordingly, strength is no longer characterised by a distinct peak but a gradual rise or strain hardening to a critical maximum strength.

The tangent stiffness showed interesting features during the initial shearing of post-dissolution tests initially containing 1.0 mm salt. Initially high stiffness was shown

#### 4. Experimental results

---

to drop followed by a significant recovery with further strain. It would suggest a collapse mechanism occurs shortly after the initiation of shear, analogous to the buckling of poorly supported sand force chains followed by a recovery of stiffness as interparticle voids are reduced.



# Chapter 5

## Bender elements and waves

Bender elements and the waves they generate are discussed in this chapter together with common analytical approaches used to derive wave velocity. Some of the problems associated with wave analysis are outlined, together with the guidelines followed to minimize these. Lastly, methods used in the analysis of wave and small-strain stiffness data are presented.

### 5.1 Shear and pressure waves

In 1828, Poisson showed that when the equilibrium of a solid body is disturbed by a pulse, shock or explosion, two types of elastic waves known as shear (s) and pressure (p) waves are generated (Doyle 1995). Each wave is defined by its propagation with shear wave motion acting perpendicular to the direction of wave travel while pressure waves travel as compression (or sound) waves. The ground motion of a shear wave is perpendicular to the pulse front. The presence of water in a medium further increases the velocity of the pressure wave resulting in larger separation between shear wave and pressure wave arrivals. Interference of shear waves by pressure waves is frequently cited as a source of error in shear wave arrival time. The velocity of shear and pressure waves in soil is used to determine the bulk ( $B_0$ ) and shear ( $G_0$ ) moduli:

$$B_0 = \rho V_p^2 = \rho (L/t)^2 \quad (5.1)$$

$$G_0 = \rho V_s^2 \quad (5.2)$$

where  $\rho$  is the mass density of the soil and  $V_s$  and  $V_p$  is the velocity of the shear and pressure wave.

## 5.2 Bender elements

Pulse wave detection can be obtained using bender elements. These electro-mechanical transducers consist of three sheets; two piezoelectric ceramic strips sandwich a metal shim. A voltage passed through the source bender element causes it to flex in a particular direction depending on the polarisation of the ceramic strips, generating either a shear or pressure wave. The receiving bender element reconverts the received mechanical wave to a voltage that can be recorded and analysed. Researchers in soil mechanics have, until recently, manufactured their own bender elements (Shirley & Hampton 1978, Dyvik & Madshus 1985, Jovičić et al. 1996) and used these in conjunction with signal generators, amplifiers, filters and oscilloscopes to determine the small-strain stiffness ( $G_0$ ) of soil specimens. These studies have suggested many improvements and therefore Santamarina et al. (2001) summarised the critical steps involved in the manufacture and installation of high quality bender elements. These included recommendations for wiring and soldering, water-proofing, electric shielding to avoid electromagnetic cross-talk between the source and receiver bender elements (Dyvik & Madshus 1985), and housing the bender element in epoxy to reduce interference (Jovičić et al. 1996). A modification by Lings (2001) allowed each bender element to send and receive shear and pressure waves. Such is the popularity of bender elements in laboratory testing that commercially produced elements are now available (GDS Instruments, Controls Group), and many of these difficulties have been overcome.

## 5.3 Input wave - frequency

An important consideration is the natural frequency of the system comprising the bender elements, sample and testing device. This is not constant but depends on confining stress Santamarina et al. (2001). They stated that the natural frequency of bender elements coupled with soil in soil cells varied 2 kHz to  $\geq 10$  kHz. So, while

the electrical excitation may be well-defined (i.e. square, sinusoidal wave etc), the mechanical input that enters the sample is a mixture of the response of all intermediate devices between the signal generator and the soil. It follows that the response at the receiver bender element is a mixture of the frequency of the measurement system and the soil element. However, it is the response of the sample alone that is of interest.

### 5.3.1 Influence of input signal period on travel time determination

The influence of the period of the input signal is demonstrated in Figure 5.1. This assessment was performed on test no.8 0.5-15-84 after the application of 84 kPa cell pressure. It shows that while the peak of the source wave changes with input period, the peak of the received wave remains relatively unchanged. Therefore, as the period of the input signal increases, the travel time is shown to decrease dramatically. This has implications for wave travel time determination techniques.

Adopting the common approach of taking the time difference between the peak of the source wave trace to the first major peak of the received trace in the time-domain appears flawed. As the period increases the travel time is reduced dramatically. Santamarina et al. (2001) argued that the input signal is affected by the natural frequencies of the signal generator, wiring and bender element. Therefore the input signal is unlikely to be a true representation of the source wave entering the sample. The data presented in Figure 5.1 also suggests that the frequency of the system masks that of the input signal. Hence, the cross-correlation time determination technique is subject to the same difficulty. The approach relies on the correlation between the input signal and received wave. For the time-domain approach adopted in the current study, the travel time is taken as the time from first deflection of the source wave trace to the first major peak of the received wave. Furthermore, an input signal period of 0.1 milliseconds (ms) was used throughout the study.

## 5.4 Interpretation of wave travel time

The principal objective of shear wave analysis is the determination of shear wave travel time to calculate the shear wave velocity and then the soil shear stiffness. Depending on the approach used, gross errors in the calculation of soil stiffness can be

## 5. Bender elements and waves

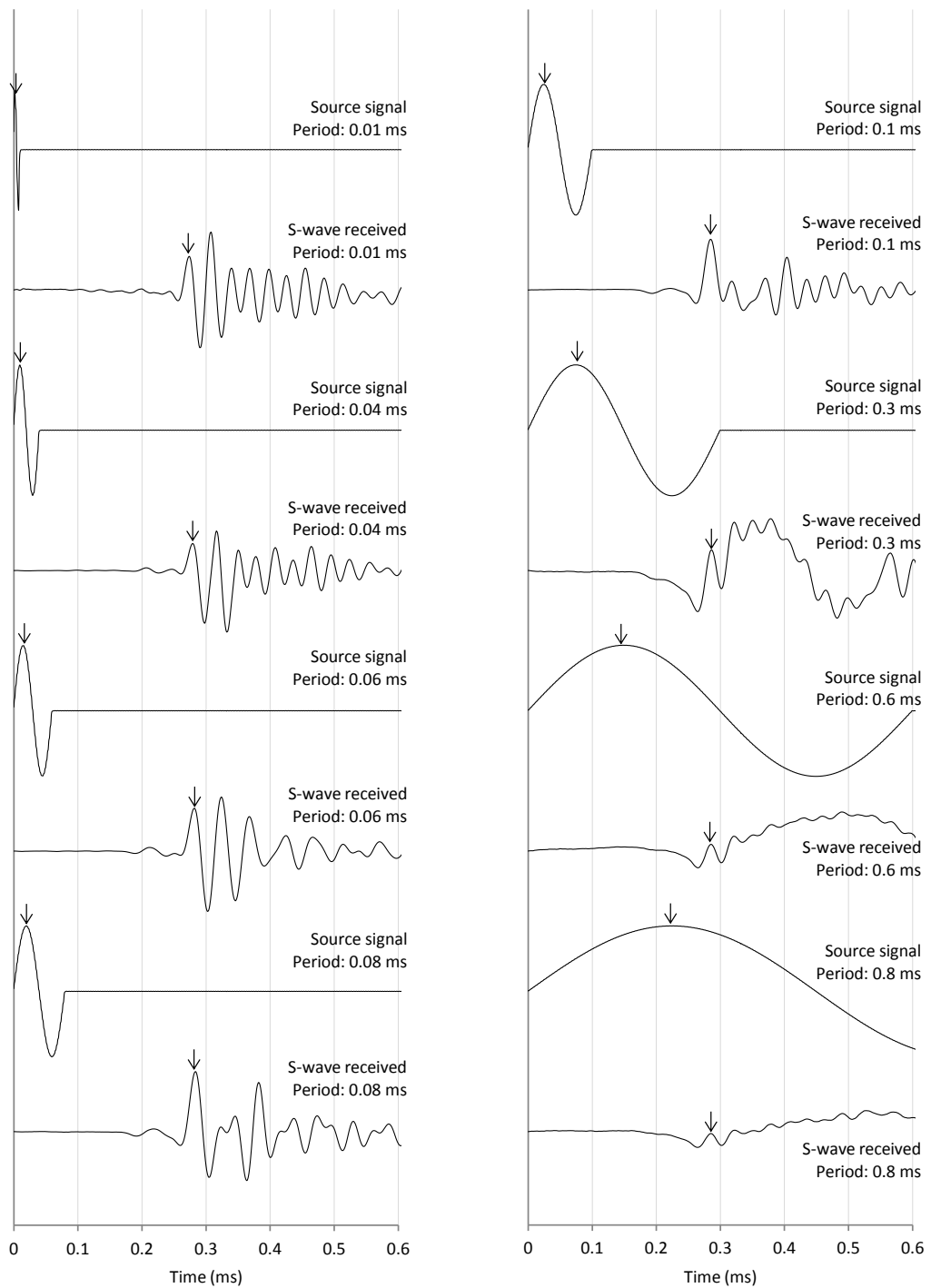


Figure 5.1: Influence of period input on travel-time based on points of similarity. Test no.8 0.5-15-84

made. Bender elements use a transient pulse that generates a wavelet. Santamarina et al. (2001) outlined the phenomena that occur when using a transient pulse in a medium subject to loss and dispersion such as soil. These are:

- Attenuation is the loss of wave energy and is frequency dependent, with high frequencies attenuating more than low frequencies resulting in a shift of the peak to lower frequencies as the travel distance increases
- Dispersion, which is the propagation of different frequencies in different directions in dispersive media such as soil, results in different travel speeds for different frequencies
- A period before the main front has a low amplitude thereby masking the wave arrival time

These phenomena introduce uncertainty in the manual determination of wave travel times. The most appropriate method for the determination of travel times is debatable. Various techniques in the time- and frequency-domains have been developed with those commonly used discussed below.

## 5.5 Near-field effect

Sanchez-Salinerio et al. (1986) showed that the first-arrival often referred to as the near-field effect is actually a compression wave arriving prior to the shear wave. Mancuso & Vinale (1988) found that the near-field effect is reduced when the distance between the source and receiver is in the range of 4 or more wavelengths ( $\lambda$ ). This can be estimated from:

$$\lambda = V_s/f \tag{5.3}$$

where  $f$  is the mean frequency of the received trace. To determine the appropriate input wave frequency, a pilot study can be performed by applying a range of input frequencies over the stresses anticipated to the sample type to be tested. The frequency that satisfies the criteria of  $\lambda \geq 4$  can subsequently be applied in the study.

## **5.6 Time-domain method - shear wave arrival time determination**

Determination of shear wave arrival times in the time-domain consists of assessing plots of the received shear wave trace against time and identifying a characteristic feature to signify the arrival time.

### **5.6.1 First deflection**

A characteristic feature often cited is the first deflection in the received trace (Viggiani & Atkinson (1995), Jovičić et al. (1996), Lings (2001) among others). However, the first-deflection can be difficult to distinguish from background noise and the presence of the near-field effect may lead to a lack of confidence in its selection.

### **5.6.2 First major peak-to-peak**

The first major peak-to-peak method is determined by measuring the time between the crest of the input signal and the first major crest of the received trace. However the peak of the first signal is not necessarily the peak of the input wave since this is affected by the natural frequency of the system (Santamarina et al. 2001). Furthermore, the received waveform does not always resemble the form of the input signal, e.g. stepped peaks, leading to subjectivity in peak selection.

## **5.7 Frequency-domain method - shear wave travel time determination**

Analysis in the frequency-domain involves decomposing the wave into its constituent frequencies.

### **5.7.1 Cross-correlation**

The cross-correlation technique is one method that can be used in conjunction with frequency-domain information. Viggiani & Atkinson (1995) used the cross-

correlation technique in the context of wave analysis in soil. The cross-correlation function  $CC_{xy}(t)$  is a measure of the degree of correlation of sent and received signals;  $X(T)$  and  $Y(T)$ , respectively. The analytical expression of the cross-correlation function is:

$$CC_{xy}(t) = \lim_{T_r \rightarrow \infty} \frac{1}{T_r} \int_{T_r} X(T)Y(T+t)dT \quad (5.4)$$

where  $T_r$  is the total duration of the time record and  $t$  is the time shift between signals. The cross-correlation is calculated in the following way. The time-domain record for the sent and received wave is decomposed into a group of harmonic waves of known frequency and amplitude using the Fast Fourier transform ( $FFT$ ) :  $L_x(f) = FFT[X(t)]$  and  $L_y(f) = FFT[Y(t)]$ . The complex conjugate  $L_y^*(f)$  of  $L_y(f)$  allows the determination of the cross-power spectrum  $G_{xy}(f)$ :

$$G_{yx}(f) = L_x(f) \cdot L_y^*(f) \quad (5.5)$$

Finally the cross-correlation function is determined by applying the Inverse Fast Fourier Transform (IFFT):

$$CC_{yx}(t) = IFFT[G_{yx}(f)] \quad (5.6)$$

The travel time returned by the cross-correlation function is based on the travel time of the whole received waveform. However, the whole waveform is subject to interferences such as the near-field effect.

## 5.8 Effective length of wave travel

The velocity terms in the small-strain bulk and shear moduli calculations (Equations 5.1 & 5.2) rely on the determination of the effective length, or distance, travelled by the wave. Viggiani & Atkinson (1995) demonstrated that the effective length is the tip-to-tip distance between the source and receiver bender elements. Shear wave measurements were taken on samples of different lengths (approx. 40-90 mm) at three confining pressures of 100, 200 and 400 kPa. A linear relationship between travel time and sample length occurred for each confining pressure with the line

intercepting the sample length axis at 6 mm; the cumulative length of the bender element sample intrusions. This indicated that the effective length was the tip-to-tip distance between bender elements in agreement with observations by Brignoli et al. (1996) and Dyvik & Madshus (1985).

## 5.9 Degree of saturation effect on wave velocity

The stiffness of the soil skeleton and the mass density of the soil determine the shear wave velocity (Santamarina et al. 2001). Experimental studies by Cho & Santamarina (2001) have illustrated increasing shear wave velocity with a decreasing degree of saturation for a variety of soils at constant applied stress. This was attributed to increasing contact-level capillary forces. However, as the confining pressure increases the contact level capillary forces are likely to be minor in comparison to contact normal forces. In the dissolution studies presented here, the sample was either dry or fully saturated so capillary forces were not in existence and would not affect shear wave velocity.

Nakazawa et al. (2004) considered shear and pressure wave velocity for degrees of saturation ranging 90-100% (0.05-0.95 in terms of Skempton's  $B$  coefficient) for undisturbed Koshigaya sand with a relative density of 70% and an effective confining stress of 98 kPa. The shear wave velocity was shown to be independent of the  $B$ -value with an average of 180 m/s. On the contrary, pressure waves varied considerably with typical velocities ranging 250-450 m/s at  $B=0$  and 1500-1750 m/s at  $B=1$ . This study showed the high dependency of pressure wave travel time, and consequently velocity, on the degree of saturation to such an extent that interpreting the influence of soil fabric becomes difficult. Therefore shear waves are preferred in the analysis of saturated soils and were used in the current study.

## 5.10 State of stress

Santamarina et al. (2001) presented typical wave velocities for sand and salt in solid and particulate form (Table 5.1). Waves propagate at higher velocities in solid minerals than in particulate form. The stiffness in a solid or continuous medium is not affected greatly by the state of stress. However, in particulate mediums the state of effective stress largely influences the stiffness.



Table 5.1: Pressure wave velocities and densities for solid and particulate salt and quartz

	$V_p$ (m/s)	Density (kg/m <sup>3</sup> )
Solid Minerals		
Salt	4600	2160
Quartz	6100	2650
Particulate Minerals (at 100 kPa confinement)		
Granular salt (dry)	230	1300-1500
Sand (dry)	120-170	1500-1900

## 5.11 Velocity-stress relations

The velocity-stress relationship for granular soil under isotropic loading can be expressed as:

$$V = \alpha \left( \frac{\sigma'_0}{1 \text{ kPa}} \right)^\beta \quad (5.7)$$

where  $\alpha$  and  $\beta$  are experimentally determined (Hardin & Richart 1963). These  $\alpha$  and  $\beta$  coefficients have been used to interpret micromechanical changes that influence shear wave transmission in dissolving soils (Fam et al. 2002, Truong et al. 2010).

### 5.11.1 Interpretation of $\beta$

The mechanical response of the soil to small-strain measurements are controlled by what Santamarina et al. (2001) refer to as ‘contact effects’.  $\beta$  values are presented in Table 5.2. For a cohesionless particulate a  $\beta$  value of 0.167 indicates elastic contacts and a value of 0.25 indicates plastic contacts. The  $\beta$  value has also been shown to increase with particle shape (angularity) and roughness (Santamarina & Cascante 1996).

### 5.11.2 Interpretation of $\alpha$

Santamarina et al. (2001) used shear moduli formulae for isotropically loaded regular packings of monosized spheres to infer that  $\alpha$  is related to particle packing, material properties, contact behaviour and fabric changes. The  $\alpha$  coefficient can be split into

Table 5.2: Theoretical velocity-stress power-law  $\beta$  exponents for solids and particulates

Solid/ contact type	$\beta$
Ideal solid	0
Cemented solid	$\approx 0$
Hertzian contacts (elastic spherical particles)	0.167
Cone-to-plane contacts (rough or angular particles)	0.25
Spherical contacts with contact yield	0.25

two coefficients to assess grain properties ( $A$ ) and packing ( $F(e)$ ) separately (Hardin & Richart 1963) allowing the velocity-stress relation to be re-written as:

$$V = A F(e) \left( \frac{\sigma'_0}{1kPa} \right)^\beta \quad (5.8)$$

where  $F(e)$  is the void ratio function. Many void ratio functions have since been proposed in the literature to take account of different soil types with a variety of these presented in Mitchell & Soga (2005).

## 5.12 Small-strain stiffness empirical relations

Small-strain stiffness is a measure of soil state (Santamarina et al. 2001) without fabric change. Stress changes associated with velocity-stress relation determination do result in fabric change. Therefore velocity-stress relations capture both contact behaviour and fabric change. Empirical equations have been proposed for the small-strain stiffness of soil. For a given soil type under isotropic confinement the following form of equation can be used:

$$G_0 = A F(e) p'^n \quad (5.9)$$

where  $F(e)$  is a void ratio function,  $p'$  is the mean effective stress and  $A$  and  $n$  are material constants (Mitchell & Soga 2005). For a round-grained Ottawa sand

similar in properties to the Leighton Buzzard sand used in the current study, Hardin & Richart (1963) proposed the following void ratio function:

$$F(e) = \frac{(2.17 - e)^2}{(1 + e)} \quad (5.10)$$

in conjunction with material constants  $A = 6900$  and  $n = 0.5$ . Therefore only the mean effective stress and the void ratio of the soil are required to predict the small-strain stiffness. Inserting the minimum and maximum void ratio for Leighton Buzzard sand used in this study resulted in the plots presented in Figure 5.2. Later, this is compared against the small-strain stiffness calculated based on equation  $G_0 = \rho V_s^2$  in post-dissolution and sand-only tests.

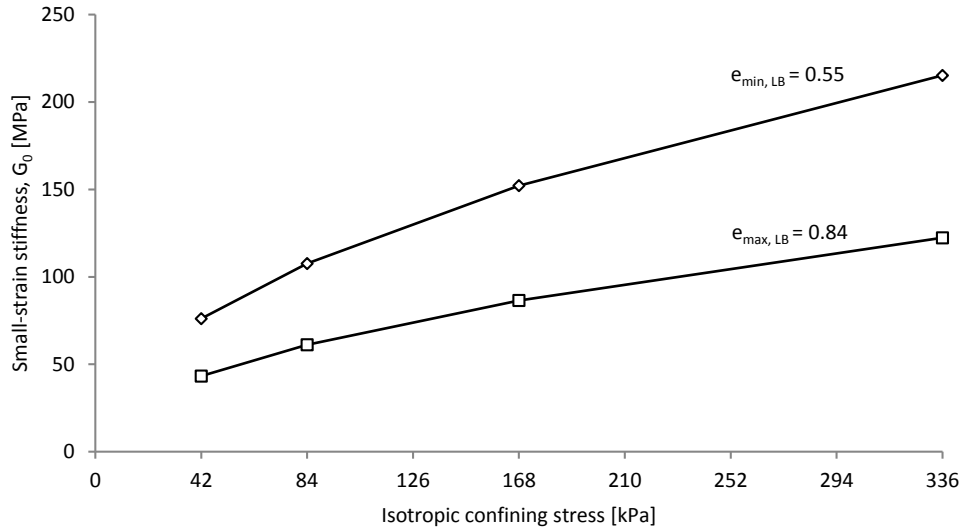


Figure 5.2: Small-strain stiffness based on the empirical formula by Hardin & Richart (1963) for  $e_{min}$  and  $e_{max}$  of Leighton Buzzard sand

As discussed by Mitchell & Soga (2005) the exponent  $n$  for real soil is not the same as that predicted using Hertz-Mindlin contact theory. Values for real soils range 0.4-0.6 as evidenced by the variety of empirical formulae gathered together in Mitchell & Soga (2005) while Hertz-Mindlin contact theory predicts an exponent of 0.33. If the Hertz-Mindlin contact theory is modified to acknowledge that soils are not smooth elastic spheres but consist of rough surfaces, then theoretical exponent values are closer in value to those found in empirical equations (Yimsiri & Soga 2000).

### 5.12.1 Leighton Buzzard sand

Bui (2009) presented small-strain stiffness power relations for Leighton Buzzard sand based on resonant column test data. For coarse sand (Fraction B,  $D_{50} \approx 0.9$  mm) with a void ratio of 0.68 the following relation was found:

$$G_0 = 23.838 \sigma'^{0.428} \quad (5.11)$$

For fine sand (Fraction E,  $D_{50} \approx 0.12$  mm) with a void ratio of 0.64 the following relation was found:

$$G_0 = 22.240 \sigma'^{0.409} \quad (5.12)$$

Both relations are presented in Figure 5.3 showing that fine sand with a similar void ratio to coarse sand resulted in higher small-strain stiffness. This suggests that a higher number of interparticle contacts in fine sand aids wave transmission thereby indicating a higher small-strain stiffness.

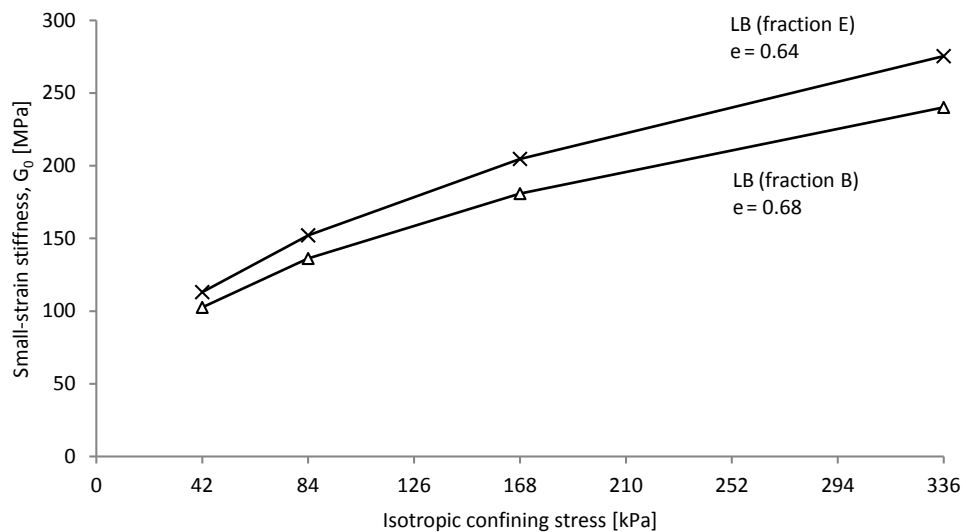


Figure 5.3: Small-strain stiffness based on empirical relations for Leighton Buzzard sand by Bui (2009)

### 5.13 Summary

This chapter considered the various issues associated with the analysis of shear wave velocities measured using bender elements. In particular the following issues can be highlighted:

- The mechanical input that enters the sample in bender element testing is a mixture of the response of all intermediate devices between the signal generator and the soil. Similarly, the response recorded by the receiver is a mixture of the frequency of the measurement system and the soil element. Since the response of the soil element alone is of interest, this raises concerns about shear wave velocity interpretation.
- An increase in the period of the input signal when using the major peak-to-peak point picking method decreases the travel time of shear waves. This makes the interpretation of travel times in bender element testing somewhat subjective.
- Bender element measurements are affected by attenuation, dispersion and near-field effects.
- Travel times for shear waves can be determined by various methods in both the time and frequency domains. Furthermore, all the available methods to determine them have advantages and disadvantages.
- Velocity-stress relations were presented in the context of contact effects (i.e.  $\alpha$  and  $\beta$ ), and void ratio functions. Similar expressions were introduced for the interpretation of shear stiffness in terms of mean effective stress and void ratio functions. These relations and expressions were presented to introduce a framework of comparison (i.e. limiting conditions in terms of maximum and minimum void ratios, as well as isotropic stress conditions) to aid the analysis of bender element tests in the following chapter.

# Chapter 6

## Shear wave and small-strain stiffness results

This chapter presents the shear wave data obtained during the three stages of triaxial testing, i.e. compression, dissolution and shear. The main focus is to assess the shear wave velocity changes that accompany particle loss. These are used in the first study to present small-strain stiffness changes with particulate dissolution in soils.

### 6.1 Wave traces

This section presents the evolution of shear wave velocity during dissolution and shearing stages. The multiple stages encouraged confidence in the use of the first major peak since received traces were sometimes clearer at a particular stage and this facilitated interpretation of poorly defined received traces in other stages. For example, the received shear waves during shear were often more clearly defined due to the higher stresses imposed. The characteristic point of the wave could retrospectively be traced back through the dissolution stage to the start of the test.

#### 6.1.1 Wave traces - loading stage

Figure 6.1 presents typical clearly defined wave data from the pre-dissolution loading stage of a sand-salt test. Shear and pressure wave travel times are shown to decrease with increasing confining stress. The 5 kPa confining stress was supplied through

## 6. Shear wave and small-strain stiffness results

a vacuum pump prior to the application of 168 kPa cell pressure. The near-field effect (n.f.) is present in the received shear wave traces as indicated by the deflection prior to the arrival of the shear wave. The arrows indicate the selected arrival time based on the first major peak method and used to calculate shear wave velocities throughout the study. The travel times for each wave based on the cross-correlation method are also indicated for comparison.

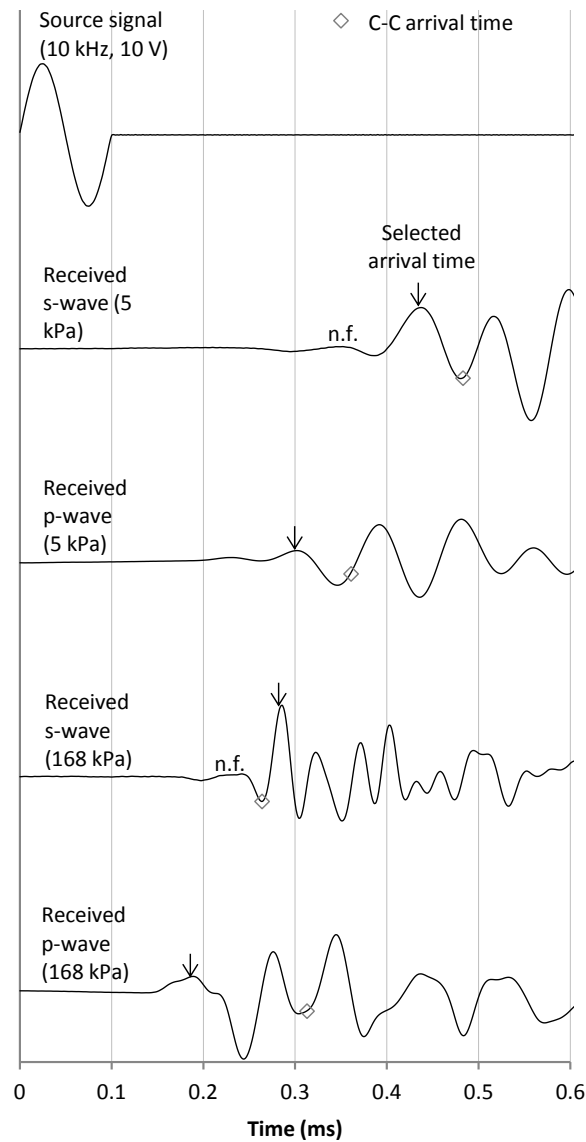


Figure 6.1: Typical source and received pressure and shear waves during pre-dissolution cell pressure application. Arrows indicate the selected arrival time. ‘n.f.’ denotes near-field effect. (Test: No.16 1.0-15-168).

### 6.1.2 Wave traces - dissolution stage

Figure 6.2a shows the shear wave traces obtained at various time intervals throughout the dissolution stage. The plots show a clear increase in shear wave travel time with dissolution. For a sample at constant height (constant wave travel distance), this indicates a decrease in shear wave velocity with dissolution. However, sample height also decreased during dissolution in all tests thereby accentuating changes in terms of the shear wave velocity. The travel time based on the point picking approach and cross-correlation method show qualitative agreement, giving confidence to the use of the point-picking method in the time-domain.

### 6.1.3 Wave traces - shearing stage

Figure 6.2b presents a selection of the shear wave received traces at various axial strains during shear. The selected shear wave arrival times show decreasing travel-time with increasing axial strain.

## 6.2 Shear wave velocity with dissolution and shear

This section presents the key findings from shear wave measurements in the dissolution study. It presents the shear wave velocity changes:

- Throughout the dissolution stage
- During the post-dissolution shearing stage

Travel time determination was based on the point-picking approach in the time-domain outlined in Section 6.1.1. Shear wave travel distance at pre- and post-dissolution stages of triaxial dissolution tests were known. The shear wave travel length during dissolution was not available, as explained earlier, but this was approximated based on vertical strains measured in oedometer dissolution tests performed on equivalent sand-salt mixtures. Figure 6.3 presents the shear wave velocity changes for the 0.063 mm salt tests. The following observations can be made:



6. Shear wave and small-strain stiffness results

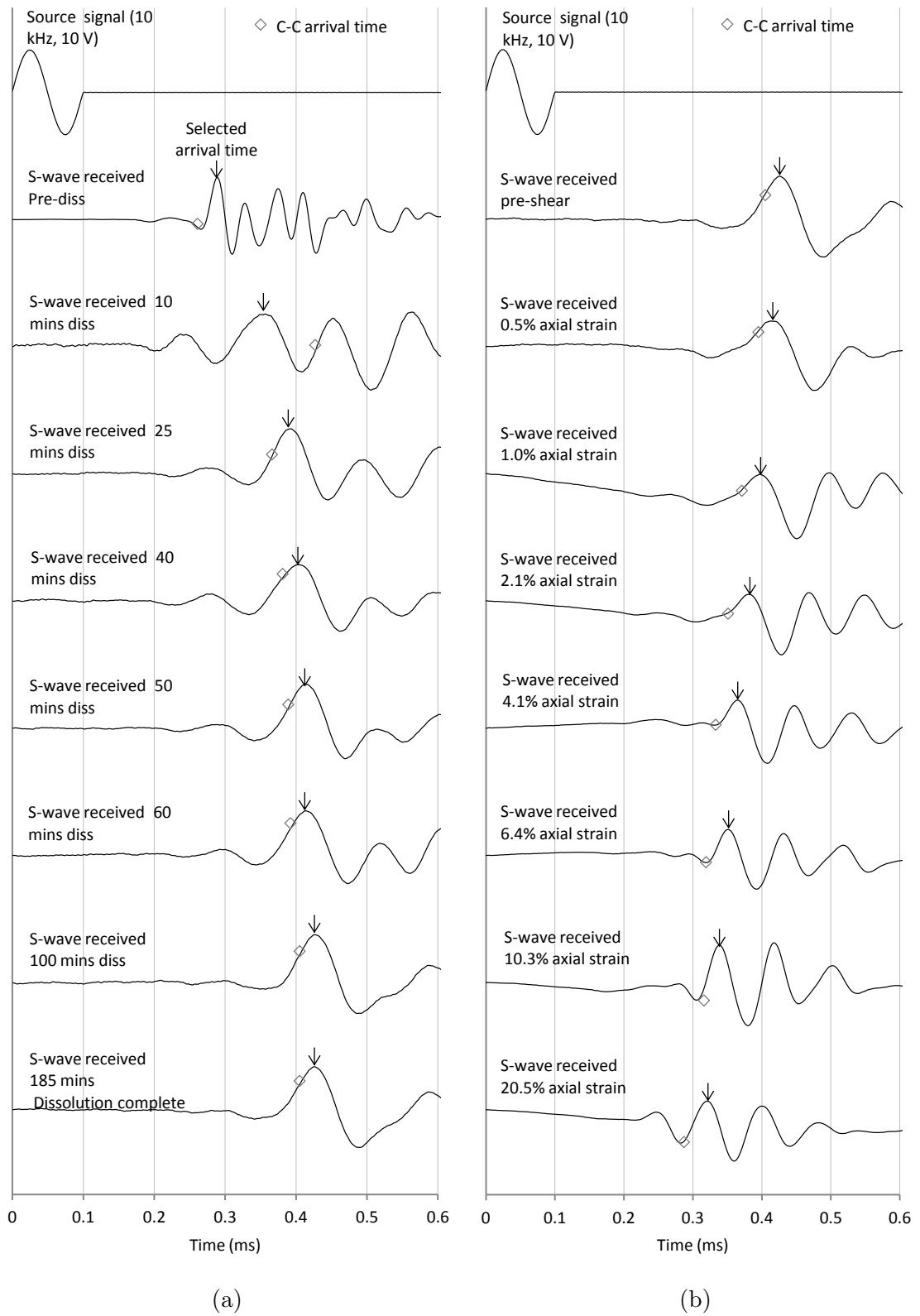


Figure 6.2: Shear wave travel time during (a) dissolution and (b) shear

- Shear wave velocity was greatest at the commencement of the dissolution stage
- Dissolution resulted in substantial shear wave velocity decreases
- The velocity at the beginning of dissolution is never recovered during the application of shear
- Velocity at the beginning of shear is similar to that at the end
- Lastly, the influence of applied stress is apparent with the 168 kPa test showing higher shear wave velocity for tests sharing similar initial void ratios

Similar observations are true for the 0.25, 0.5 and 1.0 mm salt tests presented in Figures 6.4, 6.5 & 6.6, respectively. Subsequent bender element stiffness determination is based on the shear wave velocities presented here.

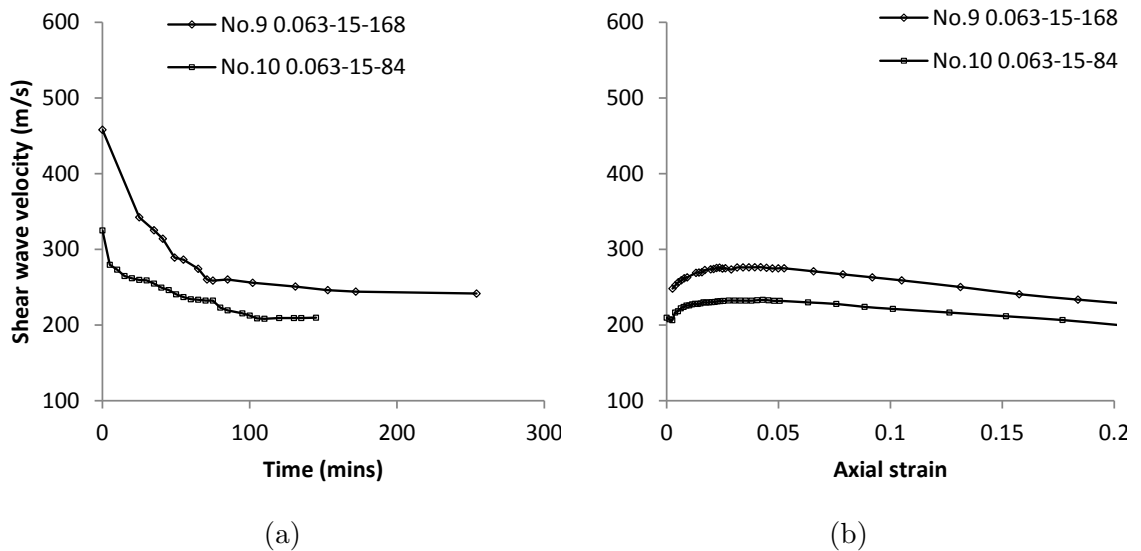


Figure 6.3: Shear wave velocity with (a) time during dissolution and (b) axial strain during triaxial compression for 0.063 mm salt tests

### 6.3 Shear wave velocity with shear of Leighton Buzzard sand

Shear wave velocity with shear of Leighton Buzzard sand is presented in Figure 6.7. The changes are in contrast to those in post-dissolution tests. Notable distinctions are:

## 6. Shear wave and small-strain stiffness results

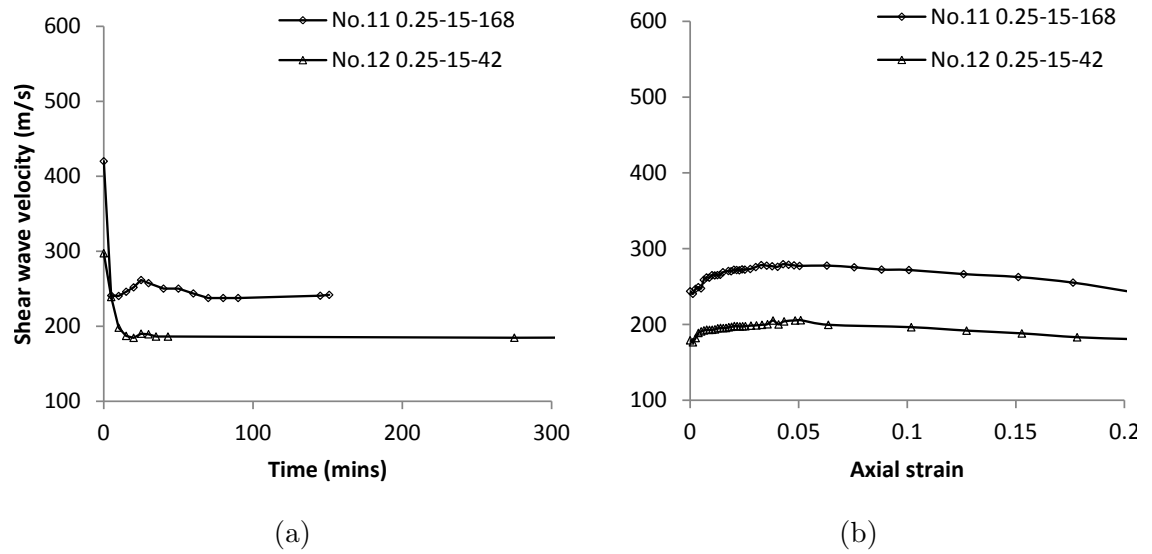


Figure 6.4: Shear wave velocity with (a) time during dissolution and (b) axial strain during triaxial compression for 0.25 mm salt tests

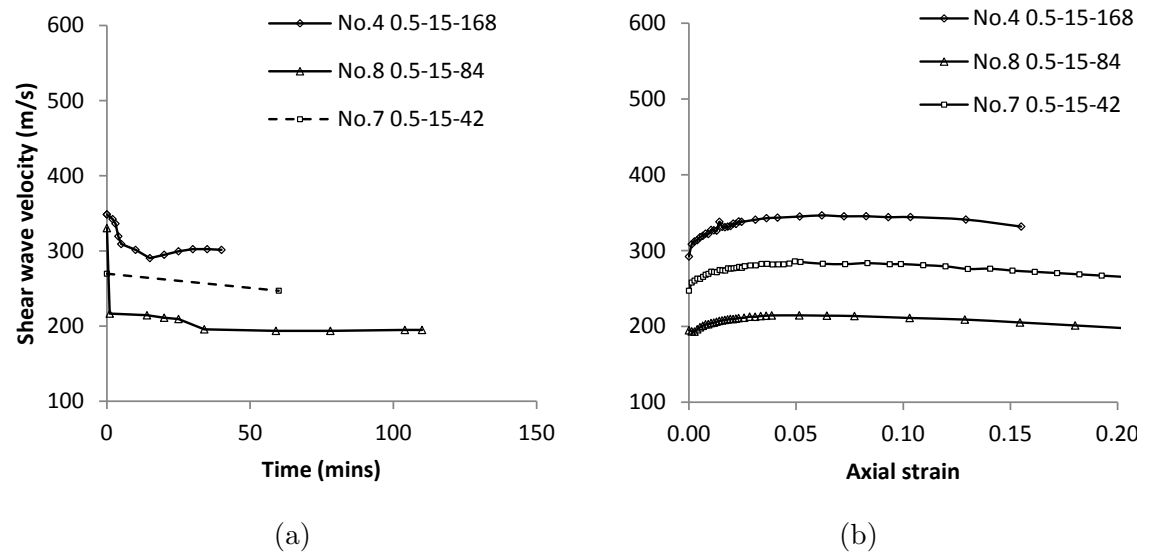


Figure 6.5: Shear wave velocity with (a) time during dissolution and (b) axial strain during triaxial compression for 0.5 mm salt tests

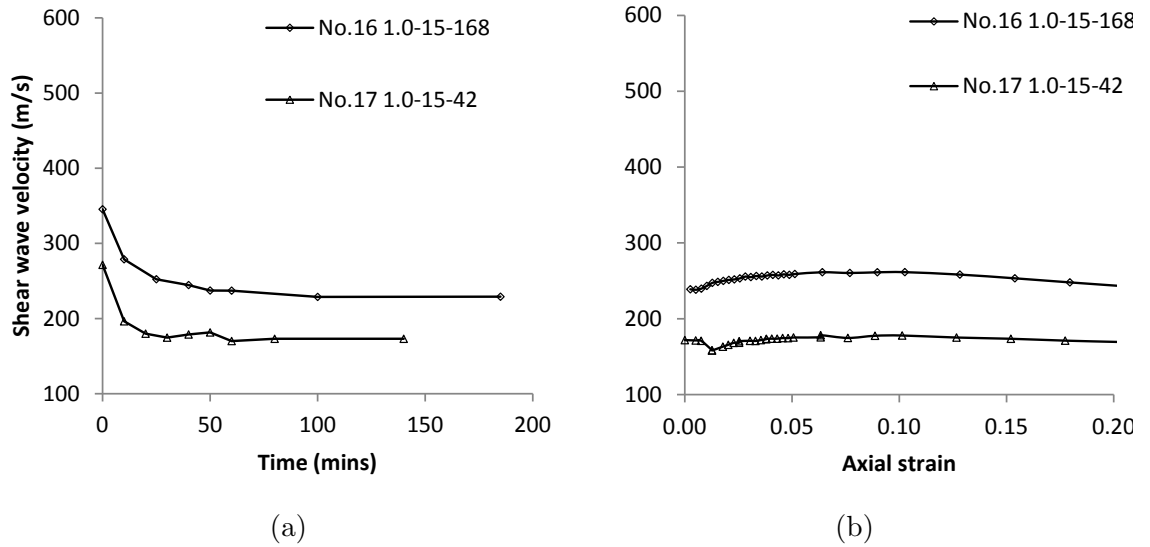


Figure 6.6: Shear wave velocity with (a) time during dissolution and (b) axial strain during triaxial compression for 1.0 mm salt tests

- Velocities are significantly higher at shear commencement than at the end of shear
- There is a brief increase in velocity with the commencement of shear in contrast to the gradual increases in post-dissolution tests

These differences suggest that there is considerable difference between soil fabric in sand-only tests and the sand remaining after salt has been dissolved in post-dissolution tests.

## 6.4 Velocity-stress relations in dissolution testing

Velocity-stress relations have been used to fit experimentally determined shear wave velocities at various stresses in granular soils (Hardin & Richart 1963). More recently, Fam et al. (2002) used a velocity-stress relation to interpret the micromechanical changes that occurred with dissolution of a sand-salt mixture with 5% salt. Truong et al. (2010) also used a velocity-stress relation to show changes associated with sand-salt mixtures with 10% salt. The attainment of a velocity-stress relation for a soil involves a single soil sample that is loaded and unloaded, with shear wave velocity measurements taken at various stress increments.

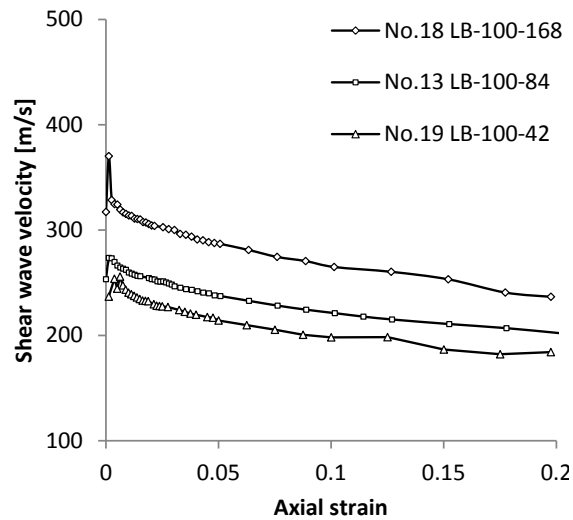


Figure 6.7: Shear wave velocity during shear for dense Leighton Buzzard sand under confining stresses of 42, 84 and 168 kPa

However, the current study did not involve loading and unloading stages. Instead, samples were maintained at a constant confining stress throughout dissolution and shearing stages. Therefore, a single dissolution test contributed only one data point on each of the pre- and post-dissolution velocity-stress relations. Tests performed at confining stresses of 42, 84 and 168 kPa allowed the fitting of velocity-stress relations to the pre- and post-dissolution shear wave velocity data sets.

Considerable consistency between the void ratios of samples used to form each velocity-stress relation is shown later. Although the main objective of shear wave analysis is the determination of stiffness, the application of velocity-stress relations to the results of this study allow comparison with those presented in the literature.

## 6.5 Velocity-stress relation comparison

This section presents the shear wave velocity data points for sand, sand-salt and post-dissolution mixtures used to obtain velocity-stress relations. Although data points are limited, the associated velocity-stress relations show trends relating to salt particle size in sand-salt mixtures, and the subsequent changes associated with dissolution. Furthermore, they allow for comparison with previous dissolution research (Fam et al. 2002) and relations based on data from conventional sand tests (Hardin & Richart 1963).

The velocity-stress relations by Fam et al. (2002) for pre- and post-dissolution stages for a sample with a salt weight percentage of 5% are included for comparison with all dissolution test data presented from the current study. As already stated in the literature review, the relations published by Fam et al. (2002) are based on pre- and post-dissolution measurements taken on a single sample. The relations based on bender element shear wave velocity showed a 10% decrease with dissolution at a confining stress of 100 kPa.

Furthermore, the velocity-stress relations for round-grained Ottawa sand in conventional tests by Hardin & Richart (1963) are included for void ratios representing loose and dense states (0.84 and 0.55 respectively) to represent  $e_{max, LB}$  and  $e_{min, LB}$ . The velocity-stress relations attributed to Hardin & Richart (1963) are based on two velocity-stress relations. For confining pressures  $< 96$  kPa

$$V_s = (119 - 56e) \sigma_0^{0.3} \quad (6.1)$$

was applied and for confining pressures  $> 96$  kPa

$$V_s = (170 - 78.2e) \sigma_0^{0.25} \quad (6.2)$$

was used. These are included in all Figures presented in this section.

### 6.5.1 Sand tests

Figure 6.8 presents the Leighton Buzzard sand velocity data points from the current study together with the associated velocity-stress relation. The “disregarded” data point was omitted from the data set used to generate the velocity-stress relation based on its particularly low value of shear wave velocity. This data point was based on a measurement taken in the first sand-only test of the current study (test no.1). A shear wave input period of 0.4 ms (2.5 kHz) was used for all measurements taken in this test which led to difficulty in the interpretation of shear wave arrival times. In subsequent tests, a shear wave input of 0.1 ms (10 kHz) was used to satisfy the travel distance of greater than 4 wavelengths of the received wave (Mancuso & Vinale 1988, Viggiani & Atkinson 1995), as discussed earlier. This resulted in greater clarity of received wave traces and greater certainty in the determination of wave

arrival times. Data from tests satisfying this guideline were used to fit velocity-stress relations in the following sections.

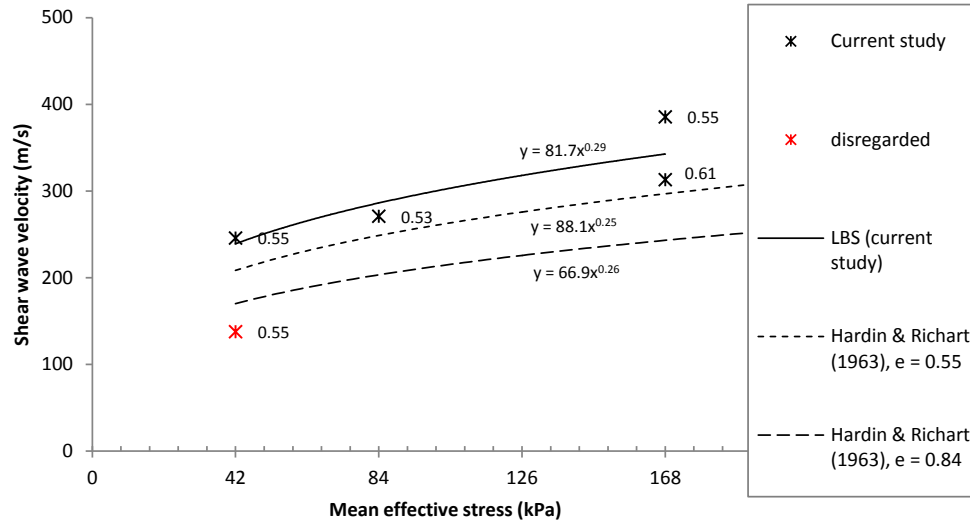


Figure 6.8: Shear wave velocity data and velocity-stress relation for Leighton Buzzard sand samples. Void ratios of samples included. Velocity-stress relations for  $e_{min, LB}$  and  $e_{max, LB}$  based on empirical formulae by Hardin & Richart (1963) included.

No change in shear wave velocity was observed with the introduction and circulation of pore-water to sand-only samples (test nos. 1-3) as anticipated based on the study by Gajo et al. (1997) where decreases of 5 % were observed for a coarse sand. Therefore data from dry sand-only samples (test nos. 18 & 19) are also included to fit the velocity-stress relation in Figure 6.8. This does not lie between the relation proposed by Hardin & Richart (1963) for Ottawa sand at the minimum and maximum void ratios for Leighton Buzzard sand.

However, the general trend is the same and the dense sand-only sample is reasonably close to the 0.55 void ratio velocity-stress relation. Exact agreement was not expected since the Hardin & Richart (1963) velocity-stress relation was generic and based on shear wave velocities calculated using a resonant column apparatus.

### 6.5.2 Sand-salt tests

Change in shear wave velocity with particle loss can be observed through dissolution of salt from sand-salt mixtures. Changes associated with the dissolution of 0.063, 0.25, 0.5 and 1.0 mm salt particles at 15% by weight are presented in this section.

Additional data points were included from dry sand-salt tests (test nos. 20-26) to increase the number of data points and confidence in the fitting of velocity-stress relations to pre-dissolution data.

### **Velocity-stress relations for pre- and post-dissolution tests - 0.063 mm salt**

The pre- and post-dissolution shear wave velocity measurements for the 0.063 mm salt tests are presented in Figure 6.9. Despite limited experimental data, velocity-stress relations were obtained for the 0.063 mm pre- and post-dissolution tests. Based on these the following observations can be made:

- The velocity-stress relation for the pre-dissolution 0.063 mm salt (15% by weight) samples shows much higher shear wave velocities than:
  - the post-dissolution 0.063 mm relation thereby illustrating the significant decrease in shear wave velocity with dissolution for this salt mixture
  - the relations for  $e_{min, LB}$  and  $e_{max, LB}$  based on the empirical relation by Hardin & Richart (1963)
  - The pre-dissolution (5% salt) relation by Fam et al. (2002) and the associated post-dissolution relation. The discrepancy may be due to the salt percentage and size differences

This possibly indicates that the fine salt pre-dissolution mixture had a greater number of interparticle contacts than mixtures described by the other relations.

- Dissolution of 0.063 mm particles results in a decrease in shear wave velocity in each individual test.
- The post-dissolution relation for the 0.063 mm salt tests is similar to the post-dissolution relation presented by Fam et al. (2002) based on bender element measurements
- The relations for the 0.063 mm samples show a 43% decrease with dissolution at 168 kPa confining stress, possibly highlighting a reduction in the numbers of interparticle contacts



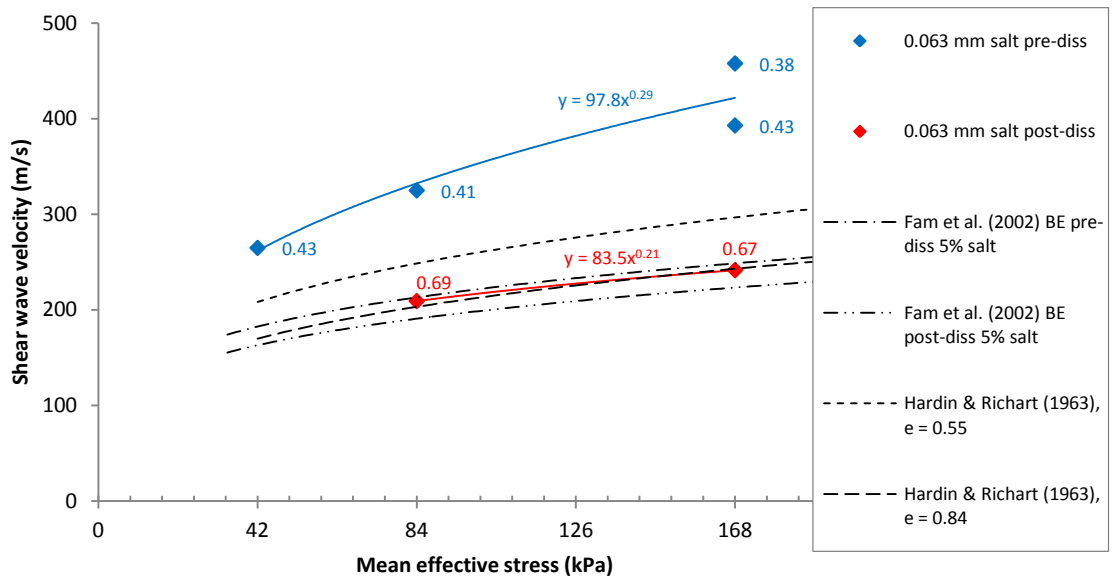


Figure 6.9: Shear wave velocity data and velocity-stress relations for pre- and post-dissolution sand-salt mixtures with 0.063 mm salt. Void ratios for sand-salt mixtures included. Velocity-stress relations for  $e_{min, LB}$  and  $e_{max, LB}$  based on empirical formulae by Hardin & Richart (1963) included.

### Velocity-stress relations for pre- and post-dissolution tests - 0.25 mm salt

The pre- and post-dissolution shear wave velocity measurements for the 0.25 mm salt tests are presented in Figure 6.10. The key observations are similar to those for the 0.063 mm tests in Figure 6.9 and discussed in the previous section:

- Sand-salt pre-dissolution tests show much higher shear wave velocities than sand-only post-dissolution tests
- Dissolution of 0.25 mm particles results in a decrease in shear wave velocity in all tests as expected
- The positioning of the post-dissolution data points are in agreement with the velocity-stress relations by Hardin & Richart (1963) when their relative void ratios are taken into consideration
- The velocity-stress relations show a 42% decrease with dissolution at 168 kPa confining stress. This is a similar reduction to that observed in 0.063 mm tests. That may confirm the influence of the reduction of interparticle contacts

- Again the post-dissolution velocity-stress relation is close in proximity to the post-dissolution relation found by Fam et al. (2002).

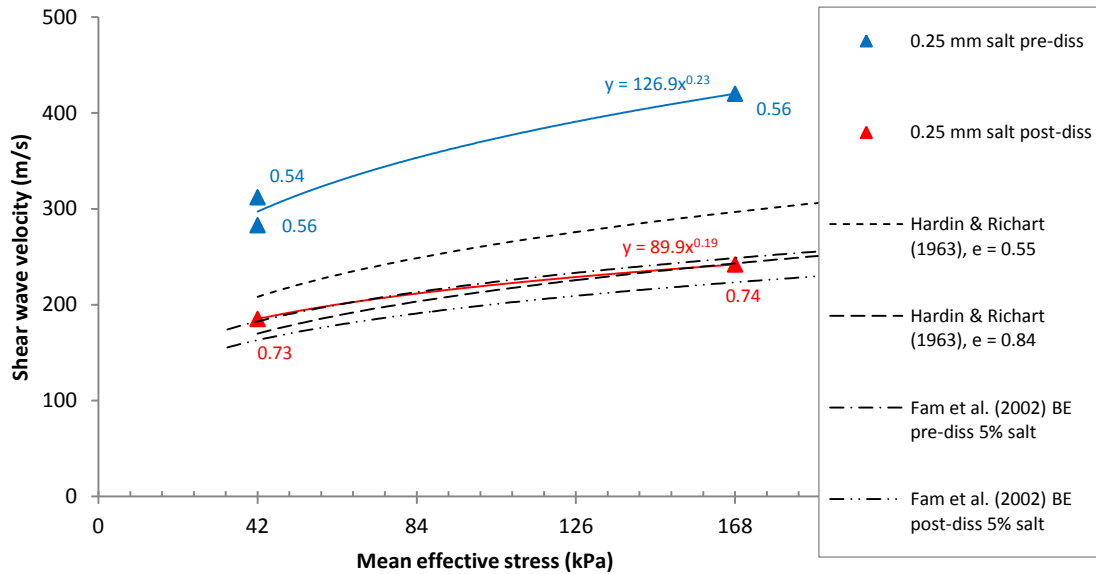


Figure 6.10: Shear wave velocity data and velocity-stress relations for pre- and post-dissolution sand-salt mixtures with 0.25 mm salt. Void ratios for sand-salt mixtures included. Velocity-stress relations for  $e_{min, LB}$  and  $e_{max, LB}$  based on empirical formulae by Hardin & Richart (1963) included.

### Velocity-stress relations for pre- and post-dissolution tests - 0.5 mm salt

The pre- and post-dissolution shear wave velocity measurements for the 0.5 mm salt tests are presented in Figure 6.11. A decrease in shear wave velocity with dissolution is evident in all cases. The velocity-stress relations predict a decrease in velocity of 24.5% at 168 kPa confining stress, about half that for 0.063 and 0.25 mm samples. However, actual data points show decreases from as little as 7% up to 41% even though void ratios for post-dissolution tests are effectively the same. If all other salt particle size tests are assessed, correlation between post-dissolution tests with high void ratios and the relation by Hardin & Richart (1963) is good.

### Velocity-stress relations for pre- and post-dissolution tests - 1.0 mm salt

Figure 6.12 presents the pre- and post-dissolution data for the 1.0 mm salt tests. Key points are:

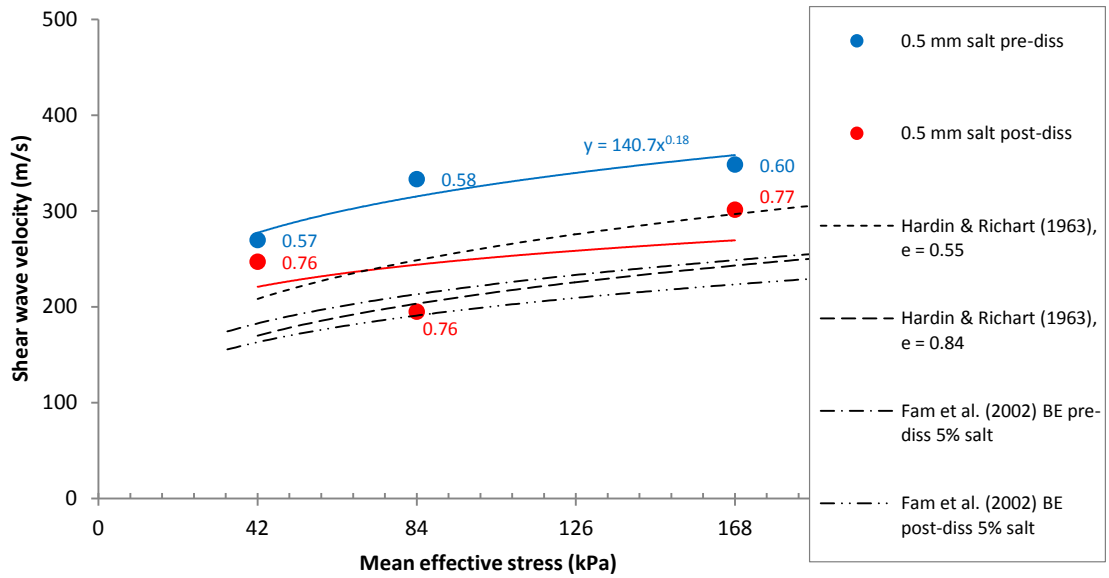


Figure 6.11: Shear wave velocity data and velocity-stress relations for pre- and post-dissolution sand-salt mixtures with 0.5 mm salt. Void ratios for sand-salt mixtures included. Velocity-stress relations for  $e_{min, LB}$  and  $e_{max, LB}$  based on empirical formulae by Hardin & Richart (1963) included.

- The post-dissolution velocity-stress relation is in agreement with the Hardin and Richart relation based on  $e_{max, LB}$  (0.84). This is not surprising since post-dissolution void ratios for the 1.0 mm salt tests are among the highest of all the sand-salt mixtures
- The velocity-stress relations show a 34.7% decrease with dissolution at 168 kPa confining stress, similar to that for 0.063 and 0.25 mm salt samples.

## 6.6 Velocity-stress relations summary

Figure 6.13 shows a notable difference between pre-dissolution and post-dissolution samples performed as part of the current study. Dissolution always resulted in a significant decrease in shear wave velocity.

The post-dissolution samples consist of Leighton Buzzard sand only. It is therefore fitting that this data lies close to relations based on the  $e_{min, LB}$  and  $e_{max, LB}$  as proposed by Hardin & Richart (1963).

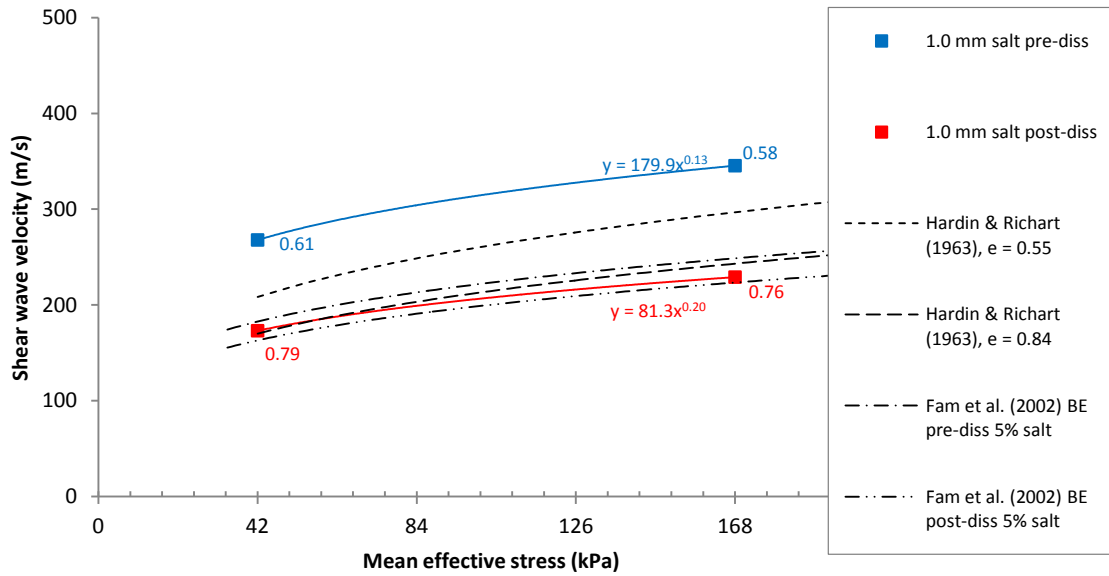


Figure 6.12: Shear wave velocity data and velocity-stress relations for pre- and post-dissolution sand-salt mixtures with 1.0 mm salt. Void ratios for sand-salt mixtures included. Velocity-stress relations for  $e_{min, LB}$  and  $e_{max, LB}$  based on empirical formulae by Hardin & Richart (1963) included.

The change between the 15% salt pre- and post-dissolution tests was much greater than in 5% salt tests performed by Fam et al. (2002). This was expected since Truong et al. (2010) showed that velocity decrease was dependent on the salt percentage lost in oedometer tests.

## 6.7 Velocity-stress relation constants

Table 6.1 summarises the velocity-stress relation constants for sand-only, pre-dissolution and post-dissolution derived from data in the current study. The coefficients for sand-only samples correspond well with those published in the literature by Hardin & Richart (1963). Santamarina et al. (2001) stated that the  $\alpha$  coefficient is an indicator of particle stiffness and packing density; high values indicate high particle stiffness and high packing density. While the  $\alpha$  and  $\beta$  coefficients are inversely proportional, the  $\beta$  value provides additional information on the particle contacts. Theoretical studies have shown  $\beta$  coefficients of 0.167 indicate elastic contacts while values of 0.25 indicate plastic contacts. It has also been found that the

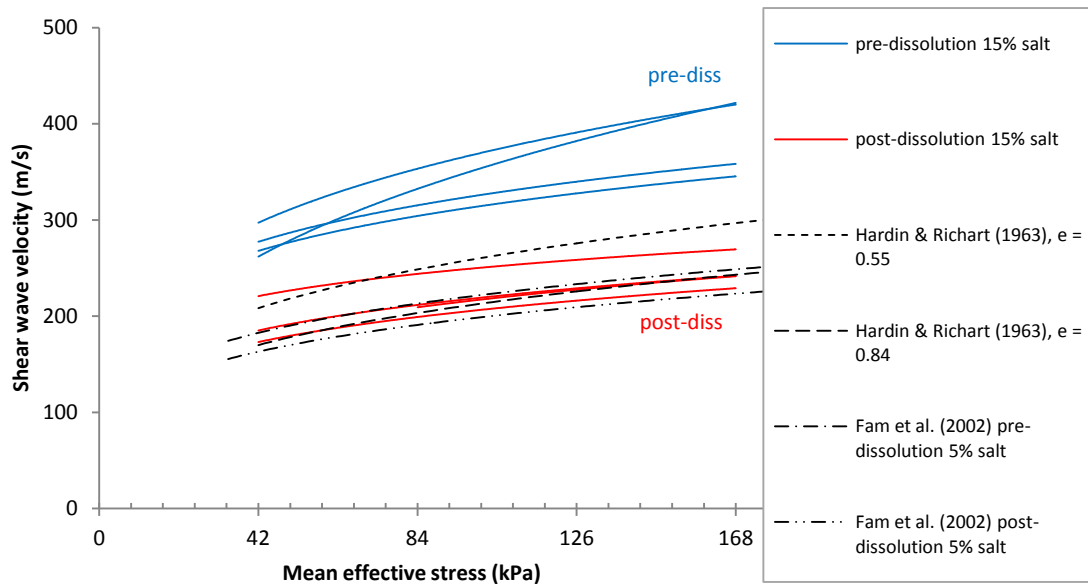


Figure 6.13: Summary of velocity-stress relations for pre- and post-dissolution tests

$\beta$  coefficient increases with particle roughness and angularity (Santamarina & Cascante 1996, Yimsiri & Soga 2000). Aloufi & Santamarina (1995) also showed that fabric breakdown resulted in  $\beta$  values of 0.10.

In pre-dissolution (dry sand-salt) tests, increasing salt size results in increases in  $\alpha$  and decreases in  $\beta$ . In general, this trend indicates a combination of stiffer particles and denser packing. Since particle stiffness is common to all pre-dissolution tests, this suggests that this trend is related to particle packing. This is consistent with earlier data showing denser packing arrangements for fine salt/sand mixtures. The decreasing  $\beta$  with increasing salt particle size indicates a change from plastic to elastic contact stiffness. This is difficult to explain since particle mineral compositions (i.e. sand and salt) were consistent for all tests.

In post-dissolution tests,  $\alpha$  and  $\beta$  values are similar with respect to the salt particle size. Neglecting the 0.5 mm values, the other salt size tests show similar constant values to those found in sand-only tests. This was expected since post-dissolution tests consisted of sand only. It appears that void ratio is linked to any variability.

Further physical interpretation of  $\alpha$  and  $\beta$  parameters were restricted due to the limited data sets on which their associated velocity-stress relations were based. Also, the dynamic changes, in terms of mineralogy, phase-composition and grading accompanying dissolution complicated the analysis using this approach.

## 6. Shear wave and small-strain stiffness results

Test type		Void ratio	Power law constants		Notes
			$\alpha$	$\beta$	
<b>Sand-only</b>	Current study	0.53-0.61	81.7	0.29	Leighton Buzzard sand
	Hardin & Richart (1963)	0.55	88.1	0.25	Ottawa sand
	Hardin & Richart (1963)	0.84	66.9	0.26	Ottawa sand
<b>Pre-dissolution</b>	0.063 mm salt	0.38-0.43	83.5	0.21	Sand-salt $D_r = 9.0$
	0.25 mm salt	0.54-0.56	126.9	0.23	Sand-salt $D_r = 2.3$
	0.5 mm salt	0.57-0.60	140.7	0.18	Sand-salt $D_r = 1.1$
	1.0 mm salt	0.58-0.61	179.9	0.13	Sand-salt $D_r = 0.6$
	Fam et al., (2002)	0.67	79.5	0.22	Angular sand ( $D_{50} = 0.55$ mm) 5% salt ( $D_{50} = 0.35$ mm)
	Truong et al., (2010)	0.74	86	0.21	Jumunjin 40/50 sand: uniform, fine and medium angular sand. 10% salt by volume. $D_r = 1.44$
<b>Post-dissolution</b>	0.063 mm salt	0.69-0.67	83.5	0.21	
	0.25 mm salt	0.73-0.74	89.9	0.19	-
	0.5 mm salt	0.76-0.77	137.1	0.13	Based on data-set with considerable scatter
	1.0 mm salt	0.76-0.79	81.3	0.20	-
	Fam et al., (2002)	0.77	69.8	0.22	Angular sand ( $D_{50} = 0.55$ mm)
	Truong et al., (2010)	0.89	54	0.26	Jumunjin 40/50 sand: uniform, fine and medium angular sand.

Table 6.1: Summary of velocity-stress relation constants

## 6.8 Shear wave velocity versus void ratio in sand-salt mixtures

It is evident that dissolution results in an increase in void ratio, which in turn leads to a decrease in shear wave velocity (Figures 6.9-6.12). For samples sharing similar void ratios, the influence of the confining pressure is evident; lower stresses result in lower shear wave velocities as reported by Hardin & Richart (1963). It would appear that sand-salt tests result in higher shear wave velocities for near identical void ratios. Salt particle size effects for any given void ratio are difficult to ascertain from Figure 6.14. These are assessed with respect to confining stress in Figures 6.15, 6.16 & 6.17.

### 6.8.1 Shear wave velocity versus void ratio - 42 kPa tests

Figure 6.15 presents the shear wave velocity against void ratio for pre- and post-dissolution tests performed under 42 kPa confining stress. Pre-dissolution sand-

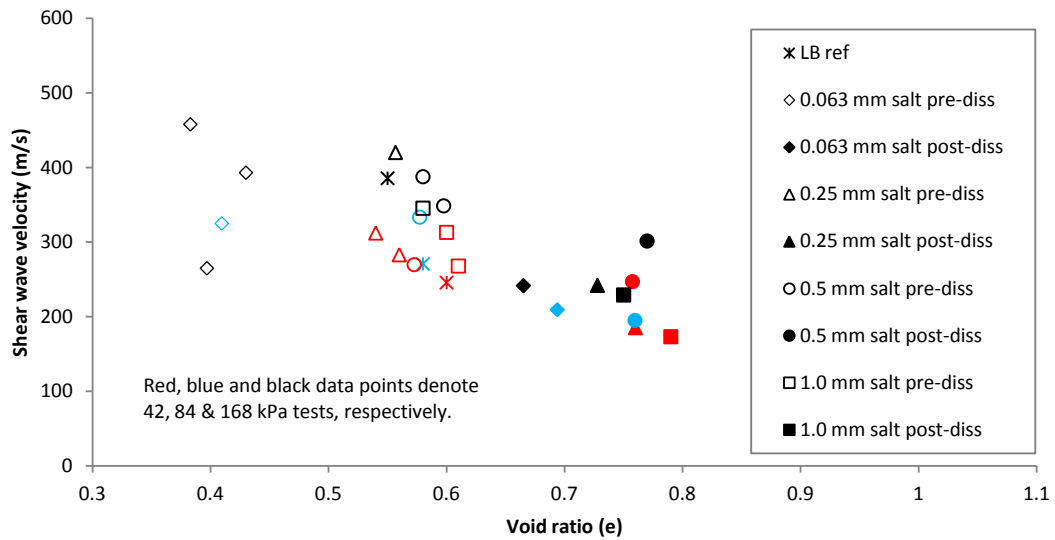


Figure 6.14: Shear wave velocity versus void ratio for confining pressures of 42, 84 & 168 kPa. Hollow and solid symbols denote pre- and post-dissolution tests respectively. Symbol colours of blue, red and black denote confining stresses of 42, 84 and 168 kPa.

salt tests at near identical void ratios to Leighton Buzzard sand-only tests show consistently higher shear wave velocities. This is irrespective of salt particle size indicating that salt particle addition, regardless of size at 15% by weight increases the shear wave velocity.

As stated before, the general trend shows a decrease in shear wave velocity with void ratio increase. However, individual tests indicate that the void ratio is not solely responsible for the shear wave velocity. This is evident where samples of near identical void ratio have widely ranging shear wave velocities, e.g:

- The pre-dissolution 1.0 mm salt tests with void ratios of approximately 0.6 exhibit significantly different shear wave velocities (45 m/s, or 14% greater).
- The post-dissolution 0.25 mm and 0.5 mm salt tests with void ratios of 0.76 have largely different shear wave velocities (66 m/s difference; the 0.25 mm test velocity is 26% lower than the 0.5 mm test).
- The Leighton Buzzard reference sand test shares a similar void ratio to the pre-dissolution 1.0 mm sand tests but has the lowest shear wave velocity. A sand-only test might be expected to show a higher shear wave velocity than sand-salt mixtures primarily because the contact stiffness of sand-to-sand should be higher than that of sand-to-salt. This might be indicative of

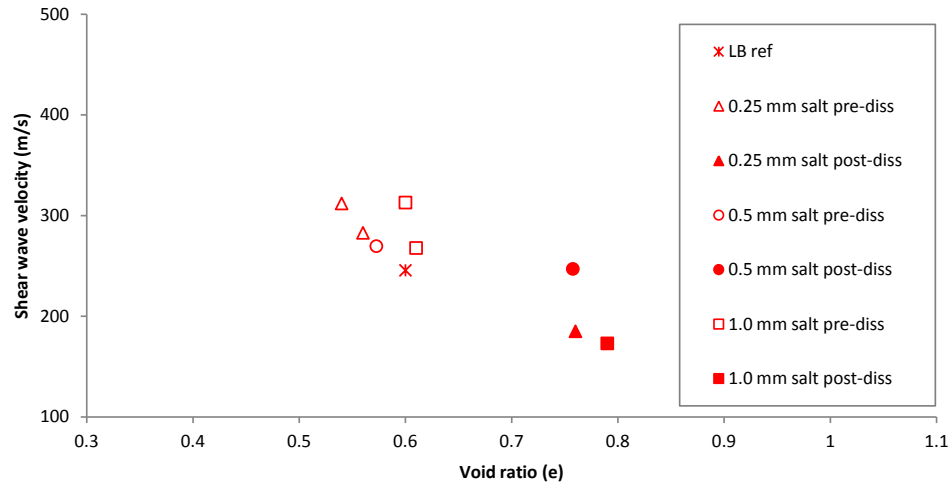


Figure 6.15: Shear wave velocity against void ratio for confining pressures of 42 kPa. Hollow and solid symbols denote pre- and post-dissolution tests respectively.

a mineral hardness effect as the softer salt might increase the contact surface area, therefore enhancing shear wave transmission.

- The Leighton Buzzard sand-only test is comprised of uniform sized sand identical to that in post-dissolution tests. However, the dense Leighton Buzzard sand-only reference test ( $e = 0.6$ ) shares a similar shear wave velocity to a loose 0.5 mm post-dissolution sample ( $e = 0.76$ ).

Differences in soil fabric may be responsible for samples having the same void ratio but large variance in shear wave velocity. However, it is difficult to derive conclusions from the limited data available. The use of velocity-stress relations in the current study helps to identify useful trends and observations.

### 6.8.2 Shear wave velocity versus void ratio - 84 kPa tests

Figure 6.16 presents the shear wave velocity against void ratio for pre- and post-dissolution tests performed under 84 kPa confining stress. Similar to the 42 kPa tests the Leighton Buzzard sand-only reference test has a similar void ratio to the pre-dissolution 0.5 mm salt test, with both samples having similar particle size distributions. However, the shear wave velocity for the 0.5 mm pre-dissolution sand-salt mixture is again higher than that for the sand-only sample.



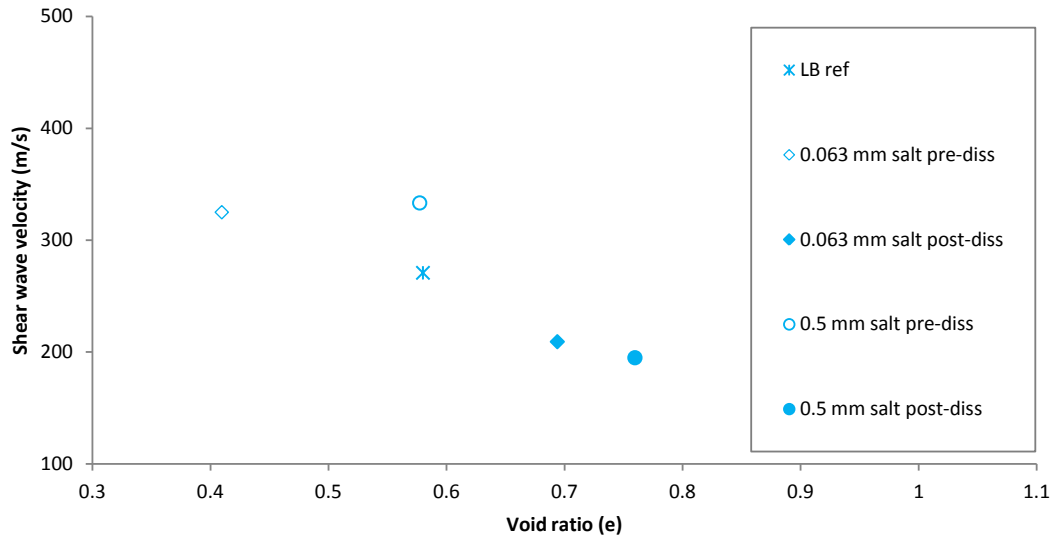


Figure 6.16: Shear wave velocity against void ratio for confining pressures of 84 kPa. Hollow and solid symbols denote pre- and post-dissolution tests respectively.

### 6.8.3 Shear wave velocity versus void ratio - 168 kPa tests

Figure 6.17 presents the shear wave velocity against void ratio for pre- and post-dissolution tests performed under 168 kPa confining stress.

For pre-dissolution data points in the 168 kPa tests, there is another example of two samples sharing the same void ratio but having significantly different shear wave velocities. A 0.5 and 1.0 mm test shares the same void ratio of 0.58 with the shear wave velocity 14% lower for the 1.0 mm tests. The Leighton Buzzard sand-only reference test has a similar void ratio to a 0.25 mm pre-dissolution test. Again it has a lower shear wave velocity that is 8% lower than that of the sand-salt mixture.

## 6.9 Small-strain stiffness

This section presents the small-strain stiffness for pre- and post-dissolution sand-salt samples when sample densities are known. Uncertainty in the quantity of salt dissolved at any point during the dissolution prevent the calculation of small-strain stiffness.

6. Shear wave and small-strain stiffness results

Test	Pre-dissolution (dry)			Post-dissolution (saturated)			G <sub>0</sub> decrease with dissolution [%]
	Dry density [kg/m <sup>3</sup> ]	Shear wave velocity [m/s]	G <sub>0</sub> [MPa]	Bulk density [kg/m <sup>3</sup> ]	Shear wave velocity [m/s]	G <sub>0</sub> [MPa]	
No.1 LB-100-42	1713	138	32	2067	138	39	
No.2 LB-100-84	1657			2032			
No.3 LB-100-168	1713	385	255	2066	385	307	
No.13 LB-100-84	1674	271	123	2042	271	150	
No.4 0.5-15-168	1604	349	195	1932	301	176	10
No.7 0.5-15-42	1630	270	119	1939	247	118	0
No.8 0.5-15-84	1625	333	181	1938	195	74	59
No.9 0.063-15-168	1853	458	388	1991	242	116	70
No.10 0.063-15-84	1818	356	230	1974	209	86	62
No.11 0.25-15-168	1646	420	291	1955	242	114	61
No.12 0.25-15-42	1664	312	162	1937	185	66	59
No.16 1.0-15-168	1620	345	193	1942	229	102	47
No.17 1.0-15-42	1591	268	114	1920	173	58	50
No.18 LB-100-168	1660	327	177				
No.19 LB-100-42	1650	256	108				
No.20 1.0-15-168	1623						
No.21 1.0-15-42	1602	313	157				
No.22 0.5-15-168	1619	388	243				
No.23 0.25-15-168	1697						
No.24 0.25-15-42	1644	283	132				
No.25 0.063-15-168	1802	393	278				
No.26 0.063-15-42	1835	265	129				

Table 6.2: Small-strain stiffness calculations for all triaxial tests

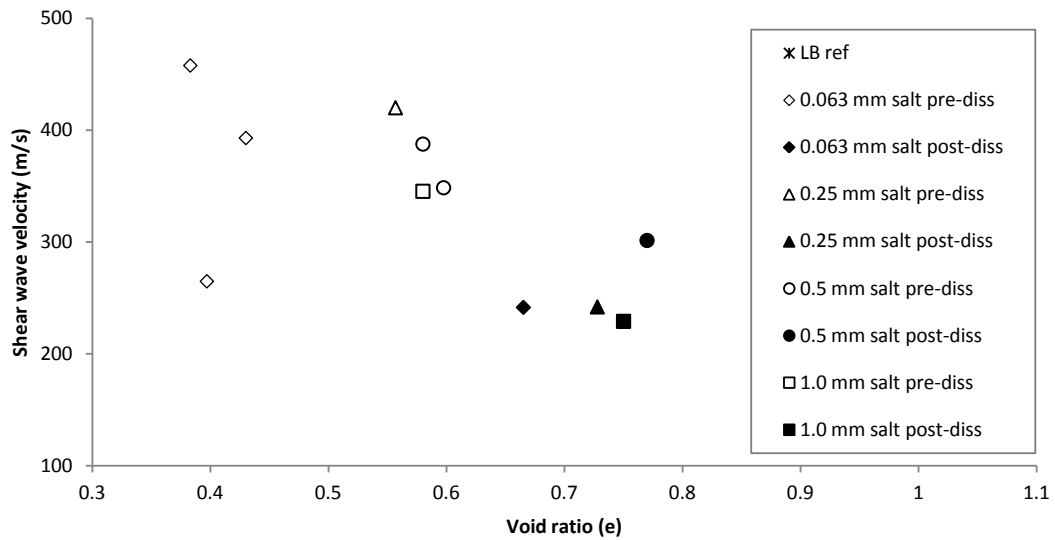


Figure 6.17: Shear wave velocity against void ratio for confining pressures of 168 kPa. Hollow and solid symbols denote pre- and post-dissolution tests respectively.

## 6.10 Stiffness summary and comparison with the literature

Figure 6.18 presents the stiffness from bender element measurements for sand, pre- and post-dissolution sand-salt tests.

Data points form two main groups: pre-dissolution and post-dissolution. Post-dissolution are the most consistent of the two data sets since they consist of Leighton Buzzard sand-only and share relatively similar high void ratios as presented in Table 6.3.

Included in Figure 6.18 are the power-relations found by Bui (2009) for Leighton Buzzard sand fractions B and E with void ratios of 0.68 and 0.64, respectively. As stated earlier, the fraction E Leighton Buzzard sand is near-identical to the sand used in the current study. Here, it is shown Leighton Buzzard sand-only reference tests performed as part of the current study are consistent with the power-relations. This provides confidence in the data especially since the void ratios of the Leighton Buzzard sand-only tests were similar, ranging 0.55-0.6 (see Table 6.3).

## 6. Shear wave and small-strain stiffness results

Test type	Test ID	Descriptor	Salt (%)	Mean effective stress ( $p'$ )	Pre-dissolution void ratio	Post-dissolution void ratio	S-wave velocity (m/s)		Velocity decrease with dissolution (%)
							Pre-dissolution	Post-dissolution	
<b>Saturated sand Tests</b>	No.1	LBS wet	-	42	0.55	n/a	138	n/a	n/a
	No.2	LBS wet	-	84	0.6	n/a	0	n/a	n/a
	No.3	LBS wet	-	168	0.55	n/a	385	n/a	n/a
	No.13	LBS wet	-	84	0.58	n/a	271	n/a	n/a
<b>Dissolution tests</b>	No.4	0.5 mm salt	15	168	0.60	0.77	349	301	14%
	No.7	0.5 mm salt	15	42	0.57	0.76	271	251	7%
	No.8	0.5 mm salt	15	84	0.58	0.76	335	198	41%
	No.9	0.063 mm salt	15	168	0.38	0.67	458	242	47%
	No.10	0.063 mm salt	15	84	0.41	0.69	356	209	41%
	No.11	0.25 mm salt	15	168	0.56	0.73	420	242	42%
	No.12	0.25 mm salt	15	42	0.54	0.76	312	185	41%
	No.16	1.0 mm salt	15	168	0.58	0.75	345	229	34%
	No.17	1.0 mm salt	15	42	0.61	0.79	268	173	35%
<b>Dry sand tests</b>	No.18	LBS	-	168	0.61	n/a	327		
	No.19	LBS wet	-	42	0.60	n/a	256		
<b>Dry sand-salt tests</b>	No.21	1.0 mm salt	15	42	0.6	n/a	313		
	No.22	0.5 mm salt	15	168	0.58	n/a	401		
	No.24	0.25 mm salt	15	42	0.56	n/a	296		
	No.25	0.063 mm salt	15	168	0.43	n/a	414		

Table 6.3: Summary of shear wave velocity and void ratio changes with dissolution

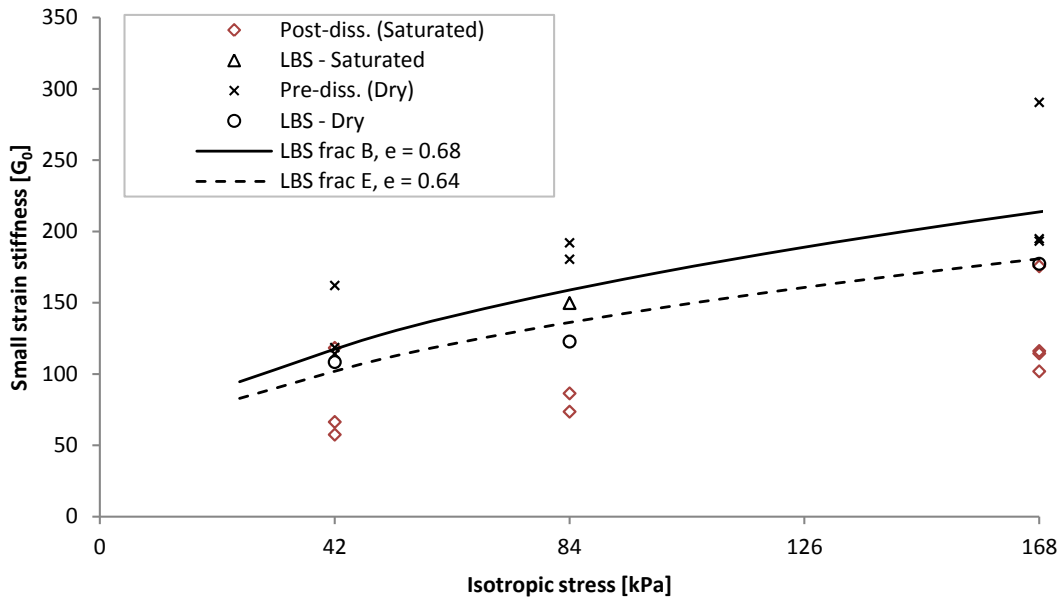


Figure 6.18: Small-strain stiffness for all tests

## 6.11 Chapter summary

This chapter presents the results of the bender element testing. In general it has been shown that during dissolution there is a reduction in shear wave velocity, which is consistent with the observed increase in void ratio.

Shearing of the dissolved samples from the loose dissolved condition shows a small increase in shear wave velocity which becomes constant at axial strains of 0.05 to 0.15 or less, before reducing gradually to values about those at the start of shearing. This echoes the contractant followed by dilatant behaviour within an overall contractant response observed in the volumetric strain data, and highlighted in Chapter 4.

Shearing of the sand only tests, starting from a medium dense condition, shows an initial brief increase followed by a steady and more pronounced decrease in shear wave velocity, consistent with the dilative shearing response.

Shear wave velocities are clearly related to cell pressure. Shear wave velocities are compared with previous work and found to be consistent. Power law constants describing the shear wave velocities with mean stress are obtained and compared.

In addition, shear wave velocities are shown to increase with the addition of fine salt particles. Salt particles of approximately the same size as the sand, when added, have least impact on shear wave velocity.

## 6. Shear wave and small-strain stiffness results

---

A strong inverse relationship is found between shear wave velocities and void ratio, for both pre- and post-dissolution states, reinforcing the influence of particle size, both through the direct impact of particle size on shear wave velocity and the indirect influence on void ratio by dissolution.

# Chapter 7

## Conclusions and recommendations for future work

The study of dissolving soil has the potential to elucidate the mechanical changes in non-conservative soils that are subject to particle loss resulting in complex phase relation changes. The current study has contributed many insights into the mechanisms involved in particle loss phenomena.

### 7.1 Conclusions

#### 7.1.1 From the literature

The decomposition-induced void change parameter  $\Lambda$  was presented as a useful analytical and interpretative tool in the discussion of dissolution studies as an alternative to traditional phase relationships.

The typical volumetric and shear behaviour of coarse-grained materials was presented within the critical state soil mechanics framework.

Following this, a number of dissolution studies relevant to this study were critically reviewed. The following are the key findings of this literature review:

- The mechanical processes occurring during mass loss are not adequately captured by standard phase relationships, due to the dynamic nature of void and

solid phase changes dependent on the amount and size of degradable particulate.

- The complex interaction between soluble and inert particulate is highly dependent on size and relative amounts. Large quantities of small particles may fill or rest within the voids of larger particles. An increase in the amount and size of soluble material results in the increased likelihood of their being part of the load-bearing soil structure. This may be as part of strong force chains or supporting elements. Consequently, different volumetric and stress-strain responses can be expected upon dissolution.
- The complexity of various phase volume changes associated with decomposable or dissolving soils can be captured using the decomposition-induced void change parameter  $\Lambda$ .
- The identification of the CSL is complex due to the following:
  - effect of non-uniform deformations
  - low applied stress levels
  - the difficulty preparing loose samples of granular materials
  - complexities related to the calculation of volumetric changes in experimental tests.
- Previous dissolution studies considered (at most) two different sand/salt diameter ratios with various amounts of salt. The current study investigated a wide range of sand/salt diameter ratios by changing the salt particle size.
- Studies focusing on soil strength changes with particle loss have shown strength decreases in all cases, whether the mechanism of loss is dissolution or erosion, or whether the tests have been performed in the shearbox, triaxial, or as a simulation using DEM.
- A change from strain-softening dilative behaviour tending towards a more strain-hardening contractive response with increasing percentages of material removed was observed. However, the effects of particle size removed was not studied in these tests.
- Analysis of triaxial tests using the state parameter was flawed since void ratio changes with dissolution were based on an assumption of no sample straining. In addition, there was uncertainty about the critical void ratio used.



- Micromechanical insights have been provided by DEM studies investigating the influence of particle loss. As the percentage of material removed increased, the soil fabric was shown to become more anisotropic. This was indicated by contact normals and normal contact forces becoming increasingly aligned in the direction of the major principle axis. This was accompanied by increasing shear contact forces, indicating the development of a less stable fabric. This instability was qualified by the subsequent shearing simulations. Increasing the percentage dissolved resulted in a change from strain-softening dilative to a more strain-hardening contractive behaviour.
- Previous dissolution studies have shown changes in shear wave velocity as measured in bender element testing, but there is a lack of understanding concerning the influence of void ratio and internal fabric/structure.
- Existing studies show that  $K_0$  initially reduces during dissolution only to recover at the end of the dissolution process.

### 7.1.2 Experimental tests and procedures

The steps followed to acquire a reliable experimental data base on the mechanical consequences of particle loss were described. An experimental programme of sand/salt mixtures subject to a test sequence of triaxial compression-dissolution-shearing posed a number of practical difficulties and unexpected problems, the solutions to which have been presented.

More specifically:

- Sample materials and mixtures consisting of sand and salt were characterised in terms of:
  - particle size distributions,
  - particle strength (i.e. susceptibility to crushing),
  - bulk stiffness.
- The standard coefficients of curvature ( $C_c$ ) and uniformity ( $C_u$ ) used to describe particle size distributions are not effective detecting changes in pre- and post-dissolution samples.

- Equipment modification included extension of the triaxial cell using a custom access ring that facilitated the inclusion of a sample pore-water circulation system and bender elements.
- Additional equipment was incorporated such as a pore-water solution reservoir, peristaltic pump recirculation system and conductivity measuring probe.
- Triaxial equipment calibration were performed to allow the use of cell water volume to measure sample volume change during dissolution and shearing stages. This resulted in several practical complications such as:
  - cell distortion,
  - membrane penetration with cell pressure and dissolution,
  - ram displacementeach of which have been quantified.
- Further technical difficulties encountered included
  - cell leakage,
  - sample leakage,
  - drifting load cell readings,
  - replacement of cell pressure and volume change measurement functions.
- A detailed volume calculation procedure was presented to account for all aforementioned practical complications encountered during equipment calibration.
- Finally, the combination of equipment compliance and sample behaviour are placed in context through a quantitative comparison of the volume changes occurring during each stage of the test procedure.

### 7.1.3 Experimental results

Triaxial test results were presented for a total of 26 tests performed on samples of (i) sand only, (ii) dry sand with (mostly) 15% added by weight of salt of specified particle size, and (iii) sand-salt mixtures with salt particles dissolved.

The three stage procedure of compression, dissolution and shearing was applied to the third set of tests.

### **Volumetric aspects in dissolution tests**

#### *Dissolution total volume strains*

In agreement with oedometer dissolution tests performed and published at the preliminary stage of the current study, the size of particles removed had a significant influence on total volume changes. Fine-sized salt removal from coarse Leighton Buzzard sand resulted in minimal strains. More significant strains accompanied the removal of coarse salt particles that were approximately equivalent in size to the Leighton Buzzard sand.

It was argued that the fine salt particles tend to fill the interparticle voids of the coarse sand without intercepting the interparticle contacts of the sand, particularly at the percentages used in this study. Therefore, they could be removed without any significant disruption to the strong force chains formed by the sand.

Incremental salt sizes, however, were argued to perform a greater structural role under static loading by supporting the strong sand force chains. These were too large to fit in the interparticle sand voids without interacting with the sand. It was hypothesized that their dissolution resulted in the buckling or collapse of the strong sand force chains that they initially supported.

Dissolution strains were found to support these hypotheses. Furthermore, the volumetric strains with dissolution helped qualify the structural role of the salt mineral in sand samples under static loading. In this respect the salt particles must constitute part of the solid phase of the soil.

#### *Void ratio: influence of salt on initial packing and post-dissolution states*

In terms of void ratio, the salt particle size affected the initial packing density of the mixtures using the same argument as that for the volumetric strains: fine particles filled the interparticle sand voids without affecting the sand particle matrix significantly. This resulted in initial void ratios below the minimum void ratio of the sand. Coarse salt, near-equivalent in size to the sand, resulted in initial void ratios close to the minimum void ratio of the sand.

Upon dissolution, the void ratio was shown to increase in all tests. This increase was found to be independent of the salt particle size, and the applied stress. The common increase in void ratio meant that the post-dissolution values for coarse salt tests were higher than for fine salt tests; and deemed to be a consequence of their

initial packing. In terms of relative density, this meant that post-dissolution fine salt tests were of a medium density and coarse salt tests were loose.

### *Dissolution effect on decomposition induced parameter*

The decomposition induced parameter  $\Lambda$  value  $\approx -1$  found for fine particle loss was found to accurately describe the observed volumetric changes. This value signifies that solid volume loss contributes to void volume increase only, with no total volume strains. Although  $\Lambda$  accurately captures the volumetric changes for larger salt sizes dissolved, the mechanisms that accompany these changes are not as easily defined.

### **Strength and stress-strain behaviour**

Assessment and comparison of the three sets of triaxial tests outlined above showed:

- Sand-only tests showed typical strain-softening dilative behaviour.
- Dry sand-salt mixtures also showed strain-softening dilative behaviour. Where salt addition produced a wider grading, e.g. 0.063 mm salt particle additions, a tendency to higher critical state strength ratios was observed.
- A strong inverse relationship between maximum strength and pre-shear void ratio was observed.
- In the post-dissolution tests there was a tendency to contract when the initial and final conditions are compared.

The large-strain behaviour of the post-dissolution tests was particularly significant. Despite some convergence in the critical strength between sand and post-dissolution samples of the same composition (i.e. sand only), the volumetric response did not suggest any common critical condition. Nonetheless, the range of critical volumes was within the range of volumes obtained in other studies performed on standard sand samples.

Particle loss appears to induce a change in soil behaviour. Where a soil may have been originally dense, the volumetric change due to particle loss produces a soil that is apparently loose in its stress-strain behaviour. The dilatancy commonly observed in laboratory prepared (medium to dense) sand samples is replaced by a more contractive behaviour, although the complete strain response is more complex,

showing intervals of dilation within an overall contractant response. Accordingly, strength is no longer characterised by a distinct peak but a gradual rise or strain-hardening to a critical maximum strength.

Analysis of the peak strengths for sand-salt and post-dissolution tests using the state parameter was not possible in this study. In both sets of tests, the range of critical void ratios was too great. In sand-salt tests, this was due to grading differences due to the varying salt particle sizes present. In post-dissolution tests, scatter was significant for tests performed at the lowest applied stress. Therefore meaningful analysis using the state parameter was not permitted. Nonetheless, a linear relation is evident between pre-shear void ratios and peak stress-ratios.

Evidence suggests that salt performs a significant structural role in intact sand-salt mixtures during shear as well as under static load. For intact fine-salt mixtures, this was illustrated through the higher peak strengths developed during shear in comparison with sand-only tests. It was further confirmed by the comparison of sand-salt and post-dissolution tests. A significant strength difference was observed, with intact samples showing much higher strengths. Salt particles undoubtedly perform a structural role in the mixtures. However, although peak strengths for sand-salt samples are higher in fine salt mixtures, sand-salt and sand-only mixtures sharing similar initial void ratios show similar peak strengths. In this case sand-salt tests appears to show a less stiff response, i.e. peaks are developed at larger shear strains than in sand-only mixtures. Therefore it appears that the presence of less stiff salt particles, relative to sand, has a minor influence on the stress-strain response.

### 7.1.4 Bender elements

Analytical approaches to determine shear wave velocities were presented. The following issues were acknowledged:

- Shear waves entering the sample in bender element testing respond to all intermediate devices between the signal generator and the soil. Similarly, the response recorded by the receiver is a mixture of the frequency of the measurement system and the soil element. Since the response of the soil element alone is of interest, this raises concerns about shear wave interpretation.
- A common wave travel time approach based on point-picking of characteristic wave feature in the time-domain is the time between the peak of the source

wave and the first major peak of the received wave. It was found that an increase in input period changed the source wave but had little influence on the received wave. Therefore, as the period input increased, travel time was apparently significantly reduced. This might suggest the discrepancy between the input signal and the input wave as discussed in the literature and shows the subjectivity involved in the interpretation of wave travel times.

- Waves generated by bender elements are affected by attenuation, dispersion and near-field effects.
- The guidelines followed to minimise wave interferences that hinder travel time determination were outlined.
- Time- and frequency-domain methods can be used to determine travel times for shear waves. There are advantages and disadvantages to all methods.

### 7.1.5 Shear wave velocity results

The results of the bender element testing have generally shown that there is a reduction in shear wave velocity during dissolution. This is consistent with an observed increase in void ratio.

Shear wave velocity during shearing in dissolved samples showed a small increase before becoming constant at low axial strains, before reducing gradually to values about those at the start of shearing. This resembles the volumetric shearing behaviour for loose post-dissolution samples, where contractive behaviour was followed by some dilation at large axial strains.

In comparison, shearing of initially dense sand only samples showed an immediate increase in shear wave velocity followed by a steady decrease to large axial strains, consistent with the dilative shearing response.

Shear wave velocity during triaxial shear never recovered its high value prior to dissolution suggesting the influence of salt contact effects in intact samples.

Shear wave velocities were clearly related to cell pressure, consistent with other studies. Power law constants describing shear wave velocity with stress were assessed but found to shed little further insight into the micro-mechanical changes accompanying dissolution.

Shear wave velocity was found to increase with fine salt particle addition while coarse salt equivalent in size to the sand showed least impact on wave velocity, although this was still shown to be higher than in sand alone. Increased coordination number in fine-salt mixtures and larger contact surface areas (due to the lower stiffness of salt) in coarse-salt mixtures was suggested to compensate for the lower stiffness of the salt mineral.

A strong inverse relationship was found between shear wave velocities and void ratio, for both pre- and post-dissolution states, reinforcing the influence of particle size, both through the direct impact of particle size on shear wave velocity and the indirect influence on void ratio by dissolution.

Finally, bender element determined stiffness showed substantial decreases with dissolution.

### 7.2 Recommendations for future work

Dissolution sample mixtures tested to date have focused on soil analogues as a first step to understand mechanical changes with particles loss. Effectively binary inert/soluble particle size relations have been used in all studies. The testing of more realistic soil gradings could provide further insights into the mechanics of particle loss.

Further analysis of the experimental results can be done in terms of the dissolution parameter  $\Lambda$ . Qualitative and quantitative measures of phase changes related to dissolution might be useful as input parameters for continuum models used for the prediction of landfill settlement and erosion criteria for granular filters.

Existing experimental evidence related to the effects of mass loss including that discussed in this thesis is limited to one-dimensional loading (oedometer) or standard triaxial conditions. Further investigation should be made under true triaxial conditions to gain further insight on the effect of the intermediate stress ratio on soil response during dissolution. Furthermore, the effects of anisotropic and more generalised stress conditions could also be studied in more detail numerically (DEM) and experimentally (hollow cylinder apparatus).

The pore-water circulation system in the modified triaxial apparatus facilitates the measurement of conductivity allowing the calculation of the dissolved mass. Due

to the high solubility of sodium of chloride in water, dissolution occurs quickly, even when brine solution is used as in the current study. Therefore conductivity measurements taken in the external reservoir do not reflect dissolution progress. This prevents accurate quantification the mass loss at intermediate stages during the dissolution stage. A slower dissolving solute, such as gypsum in water, or limestone in a mild hydrochloric acid, may allow greater control of dissolution progress. This would facilitate the analysis of intermediate volumetric states of dissolving soils, and also allow stiffness measurements based on accurate soil mass densities using bender element waves.

The triaxial apparatus was limited in functionality with cell pressure application and monotonic loading tests the only available options. The application of the  $K_0$  condition during dissolution would be of relevance to situations where soils are laterally confined such as within the core of an embankment dam experiencing erosion, landfill soils and mining tailings. This would necessitate further instrumentation in terms of local strain transducers.

A more complete shear wave velocity data set for pre- and post-dissolution samples together with the sample volume measurement accuracy allowable in the triaxial apparatus could offer further insights into the micromechanical changes with dissolution using a combination of velocity stress relations,  $\alpha$  and  $\beta$  stress relation parameters, and void ratio functions.

Lastly, computed tomography could be used for the assessment of stress localisations in the triaxial sample during dissolution and subsequent shear.



# Appendices

## Appendix A

Particle loss and volume change  
on dissolution: experimental  
results and analysis of particle size  
and amount effects





















## Appendix B

### Volumetric consequences of particle loss by grading entropy













## Appendix C

### Effect of particle loss on soil behaviour



















# References

- Aloufi, M. A. & Santamarina, J. C. (1995), ‘Low and high strain mechanical properties of grain masses - the effect of particle eccentricity’, *Transactions ASAE* **38**(3), 307–314.
- Arulnathan, R., Boulanger, R. W. & Riemer, M. F. (1998), ‘Analysis of bender element tests.’, *Geotechnical Testing Journal* **21**(2), 120–131.
- Atkinson, J. (2007), *The Mechanics of Soils and Foundations, Second Edition*, Spon text, Taylor & Francis.
- Atkinson, J. H. & Bransby, P. L. (1978), *The Mechanics of Soils: An Introduction to Critical State Soil Mechanics*, 2nd edn, McGraw-Hill University Series in Civil Engineering.
- Barreto, D. & O’Sullivan, C. (2012), ‘The influence of inter-particle friction and the intermediate stress ratio on soil response under generalised stress conditions’, *Granular Matter* **14**(4), 505–521.  
**URL:** <http://dx.doi.org/10.1007/s10035-012-0354-z>
- Been, K. & Jefferies, M. G. (1985), ‘A state parameter for sands’, *Géotechnique* **35**(2), 99–112.
- Been, K., Jefferies, M. G. & Hachey, J. (1991), ‘The critical state of sands’, *Géotechnique* **41**, 365–381.
- Bishop, A. W. & Henkel, D. J. (1962), *Test measurement of soil properties in the triaxial test*, 2nd edn, Arnold.
- Bolton, M. (1986), ‘The strength and dilatancy of sands’, *Géotechnique* **36**(1), 65–78.
- Brignoli, E. G. M., Gotti, M. & Stokoe, K. H. (1996), ‘Measurement of shear waves in laboratory specimens by means of piezoelectric transducers’, *Geotechnical Testing Journal* **19**(4), 384–397.

## REFERENCES

---

- Bui, M. T. (2009), Influence of some particle characteristics on the small strain response of granular materials, PhD thesis, University of Southampton.
- Carraro, J., Prezzi, M. & Salgado, R. (2009), 'Shear strength and stiffness of sands containing plastic or nonplastic fines', *Journal of Geotechnical and Geoenvironmental Engineering* **135**(9), 1167–1178.
- Casagrande, A. (1936), *Characteristics of Cohesionless Soils Affecting the Stability of Slopes and Earth Fills*, Harvard University.
- Case studies on evaluation of liquefaction resistance of imperfectly saturated soil deposits* (2004), Germany.
- Castellanza, R. & Nova, R. (2004), 'Oedometric tests on artificially weathered carbonatic soft rocks', *Journal of Geotechnical and Geoenvironmental Engineering* **130**(7), 728–739.
- Chang, C. S., Misra, A. & Sundaram, S. S. (1991), 'Properties of granular packings under low amplitude cyclic loading', *Soil Dynamics and Earthquake Engineering* **10**(4), 201 – 211.
- Chang, D. S. & Zhang, L. M. (2011), 'A stress-controlled erosion apparatus for studying internal erosion in soils', *ASTM Geotechnical Testing Journal* **34**(6), 579–589.
- Cho, G. C. & Santamarina, J. C. (2001), 'Unsaturated particulate materials-particle-level studies', *Journal of geotechnical and geoenvironmental engineering* **127**(1), 84–96.
- Cooper, A. (1998), Subsidence hazards caused by the dissolution of permian gypsum in england : geology, investigation and remediation, *in* J. Maund & M. Eddleston, eds, 'Geohazards in engineering geology', number 15 *in* 'Special Publications in Engineering Geology', Geological Society of London, London, UK, pp. 265–275.
- Doyle, H. (1995), *Seismology*, Wiley.
- Dyvik, R. & Madshus, C. (1985), 'Lab measurements of  $g_{max}$  using bender elements', *Proc. ASCE Annual Convention on Advances in the Art of Testing Soils under Cyclic Conditions, Detroit, Michigan* pp. 186–196.
- Fam, M., Cascante, G. & Dusseault, M. (2002), 'Large and small strain properties of sands subjected to local void increase', *Journal of Geotechnical and Geoenvironmental Engineering* **128**(12), 1018 – 1025.

## REFERENCES

---

- Fell, R. & Fry, J. J., eds (2007), *Internal erosion of dams and their foundations - selected and reviewed papers from the workshop on Internal Erosion and Piping of Dams and their Foundations, Aussois, France, 25-27 April 2005*, Taylor & Francis Group, London, UK.
- Gajo, A., Fedel, A. & Mongiov, L. (1997), 'Experimental analysis of the effects of fluid-solid coupling on the velocity of elastic waves in saturated porous media', *Géotechnique* **47**, 993–1008.
- Grabco, D., Palistrant, N., Shikimaka, O., Zhitaru, R., Rahvalov, R. & Zugravescu, D. (2002), Hardness and brittleness of rocks studied by microindentation method in combination with the registration of acoustic emission signals, in 'Proc. 8th European Conference on Nondestructive Testing (ECNDT), Barcelona, Spain, June 17-21 2002', Vol. 8.
- Gribble, C. & McLean, A. (2003), *Geology for Civil Engineers, Second Edition*, Taylor & Francis.
- Gudehus, G. (1996), 'A comprehensive constitutive equation for granular materials', *Journal of the Japanese Geotechnical Society : Soils and Foundations* **36**(1), 1–12.
- Hardin, B. O. (1978), 'The nature of stress-strain behaviour of soils', *Earthquake engineering and soil mechanics* **1**, 3–90.
- Hardin, B. O. & Drnevich, V. P. (1972), 'Shear modulus and damping in soils: Measurement and parameter effects.', *ASCE J Soil Mech Found Div* **98**(SM6), 603–624.
- Hardin, B. O. & Richart, F. E. (1963), 'Elastic wave velocities in granular soils', *Journal of Soil Mechanics & Foundations Div* **3407**(SM1), 33–65.
- Head, K. (1982), *Manual of soil laboratory testing*, number v. 2, Pentech Press.
- Head, K. (1986), *Manual of soil laboratory testing*, Vol. 3, Pentech Press.
- Herle, I. (1997), Hypoplastizität und Granulometrie einfacher Korngerüste, PhD thesis, Karlsruhe University.
- Hester, R. E. & Harrison, R. M., eds (1995), *Waste Treatment and Disposal*, The Royal Society of Chemistry.
- Hunt, G., Tordesillas, A., Green, S. & Shi, J. (2010), 'Force-chain buckling in granular media: a structural mechanics perspective', *Phil. Trans. R. Soc. A* **368**(1910), 249–262.

## REFERENCES

---

- Jovičić, V. & Coop, M. R. (1997), 'Stiffness of coarse-grained soils at small strains', *Géotechnique* **47**, 545–561.
- Jovičić, V., Coop, M. R. & Simic, M. (1996), 'Objective criteria for determining  $g_{max}$  from bender element tests', *Géotechnique* **46**(2), 357–362.
- Kelly, D., McDougall, J. & Barreto, D. (2012), Effect of particle loss on soil behaviour, *in* '6<sup>th</sup> International Conference on Scour and Erosion, Paris, August 27-31, 2012', pp. 639–646.
- Kenney, T. & Lau, D. (1985), 'Internal stability of granular filters.', *Canadian geotechnical journal* **22**(2), 215 – 225.
- Khan, I. H. & Hasnain, S. I. (1981), 'Engineering properties of sabkha soils in the benghazi plain and construction problems', *Engineering Geology* **17**(3), 175–183.
- Klotz, E. & Coop, M. (2002), 'On the identification of critical state lines for sands', *Geotechnical Testing Journal* **25**(3), 289 – 302.
- Knappett, J. & Craig, R. F. (2012), *Craig's Soil Mechanics*, Spon Press.
- Lade, P., Liggio, C. & Yamamuro, J. (1998), 'Effects of non-plastic fines on minimum and maximum void ratios of sand', *Geotechnical Testing Journal* **21**(4), 336–347.
- Lambe, T. & Whitman, R. (1969), *Soil Mechanics*, Series in soil engineering, Wiley.
- Lee, K. L. & Seed, H. B. (1967), 'Drained strength characteristics of sands', *J. Soil Mech. Fdns Div. Am. Soc. Civ. Engrs* **93**(SM6), 117–141.
- Lőrincz, J., Imre, E., Gálos, M., Trang, Q., Rajkai, K., Fityus, S. & Telekes, G. (2005), 'Grading entropy variation due to soil crushing', *International Journal of Geomechanics* **5**(4), 311–319.  
**URL:** [http://dx.doi.org/10.1061/\(ASCE\)1532-3641\(2005\)5:4\(311\)](http://dx.doi.org/10.1061/(ASCE)1532-3641(2005)5:4(311))
- Lings, M. L. (2001), 'Drained and undrained anisotropic elastic stiffness parameters', *Géotechnique* **51**(6), 555–565.
- Mancuso, C. & Vinale, F. (1988), Propagazione delle onde sismiche: teoria e misura insito, *in* 'Atti del Convegno del Gruppo Nazionale di Coordinamento per gli Studi di Ingegneria Geotecnica, Monselice', Rome: Consiglio Nazionale delle Ricerche, pp. 115–138.

## REFERENCES

---

- McDougall, J., Kelly, D. & Barreto, D. (2013), 'Particle loss and volume change on dissolution: experimental results and analysis of particle size and amount effects', *Acta Geotechnica* **8**(6), 619–627.
- McDougall, J. R. & Pyrah, I. C. (2004), 'Phase relations for decomposable soils', *Géotechnique* **54**, 487–493.
- McGeary, R. K. (1961), 'Mechanical packing of spherical particles', *Journal of the American Ceramic Society* **44**(10), 513–522.
- Menaa, M., Meguid, M. & Assaf, G. (2009), 'On the effects of subgrade erosion on the contact pressure distribution under rigid surface structures', *Journal of Geotechnical and Geoenvironmental Engineering* **135**(10), 1538–1542.
- Mitchell, J. K. & Soga, K. (2005), *Fundamentals of soil behavior*, John Wiley & Sons.
- Muir Wood, D. (2007), 'The magic of sands the 20th Bjerrum lecture presented in oslo, 25 november 2005', *Canadian Geotechnical Journal* **44**(11), 1329–1350.
- Muir Wood, D. & Maeda, K. (2008), 'Changing grading of soil: effect on critical states', *Acta Geotechnica* **3**(1), 3–14.
- Nicholson, P., Seed, R. & Anwar, H. (1993), 'Elimination of membrane compliance in undrained triaxial testing. ii. mitigation by injection compensation', *Canadian geotechnical journal* **30**(5), 739–746.
- Ovando-Shelley, E. & Perez, B. (1997), 'Undrained behaviour of clayey sands in load controlled triaxial tests', *Géotechnique* **47**(1), 97–111.
- Powrie, W. (2014), *Soil Mechanics: Concepts and Applications, Third Edition*, Taylor & Francis.
- Roscoe, K. H., Schofield, A. N. & Wroth, C. P. (1958), 'On the yielding of soils', *Géotechnique* **8**, 22–53.
- Rothenburg, L. & Bathurst, R. J. (1989), 'Analytical study of induced anisotropy in idealized granular materials', *Géotechnique* **39**, 601–614.
- Russell, A. R. & Khalili, N. (2004), 'A bounding surface plasticity model for sands exhibiting particle crushing', *Canadian Geotechnical Journal* **41**(6), 1179–1192.

## REFERENCES

---

- Salgado, R., Bandini, P. & Karim, A. (2000), 'Shear strength and stiffness of silty sand', *Journal of Geotechnical and Geoenvironmental Engineering* **126**(5), 451–462.
- Sanchez-Salinerio, I., Roesset, J. M. & Stokoe, K. H. (1986), 'Analytical studies of body wave propagation and attenuation. report gr 86-15, university of texas, austin'.
- Santamarina, J. C. & Cascante, G. (1996), 'Stress anisotropy and wave propagation: a micromechanical view', *Canadian Geotechnical Journal* **33**(5), 770–782.
- Santamarina, J., Klein, K. & Fam, M. (2001), *Soils and waves*, J. Wiley & Sons.
- Sharma, H. & De, A. (2007), 'Municipal solid waste landfill settlement: Postclosure perspectives', *Journal of Geotechnical and Geoenvironmental Engineering* **133**(6), 619–629.
- Shin, H. & Santamarina, J. (2009), 'Mineral dissolution and the evolution of  $k_0$ ', *Journal of Geotechnical and Geoenvironmental Engineering* **135**(8), 1141–1147.
- Shirley, D. J. & Hampton, L. D. (1978), 'Shearwave measurements in laboratory sediments', *The Journal of the Acoustical Society of America* **63**(2), 607–613.
- Tchobanoglous, G., Theisen, H. & Vigil, S. A. (1993), *Integrated Solid Waste Management: Engineering Principles and Management Issues*, McGraw-Hill Higher Education.
- Thevanayagam, S. (1998), 'Effect of fines and confining stress on undrained shear strength of silty sands', *Journal of Geotechnical and Geoenvironmental Engineering* **124**(6), 479–491.
- Thevanayagam, S. & Mohan, S. (2000), 'Intergranular state variables and stress-strain behaviour of silty sands', *Géotechnique* **50**(1), 1–23.
- Thornton, C. (2000), 'Numerical simulations of deviatoric shear deformation of granular media', *Géotechnique* **50**(1), 43–53.
- Tran, M. K., Shin, H., Byun, Y. H. & Lee, J. S. (2012), 'Mineral dissolution effects on mechanical strength', *Engineering Geology* **125**, 26 – 34.
- Truong, Q., Eom, Y. & Lee, J. (2010), 'Stiffness characteristics of soluble mixtures', *Géotechnique* **60**(4), 293 – 297.
- Vanders, I. & Kerr, P. (1967), *Mineral Recognition*, John Wiley & Sons Inc.



## REFERENCES

---

- Verdugo, R. & Ishihara, K. (1996), 'The steady state of sandy soils', *Journal of the Japanese Geotechnical Society : Soils and Foundations* **36**(2), 81–91.
- Vesic, A. S. & Clough, G. W. (1968), 'Behaviour of granular materials under high stresses', *J. Soil Mech. Fdns Div. Am. Soc. Civ. Engrs* **94**(SM3), 661–688.
- Viggiani, G. & Atkinson, J. H. (1995), 'Stiffness of fine-grained soil at very small strains', *Géotechnique* **45**, 249–265.
- Wheeler, S. J. (1988), 'Undrained shear strength of soils containing large gas bubbles', *Géotechnique* **38**(3), 399–413.
- White, H. E. & Walton, S. F. (1937), 'Particle packing and particle shape', *Journal of the American Ceramic Society* **20**(1-12), 155–166.
- Yimsiri, S. & Soga, K. (2000), 'Micromechanics-based stress-strain behaviour of soils at small strains', *Géotechnique* **50**, 559–571.